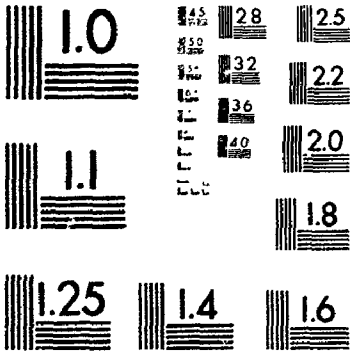

MICROCOPY RESOLUTION TEST CHART
NATIONAL BUREAU OF STANDARDS
STANDARD REFERENCE MATERIAL 1010a
(ANSI and ISO TEST CHART No 2)

A Study of the Mechanics of Faulting and Earthquakes

by

Zhaomin Yin, B.Sc.(Hons.), M.Sc.

A thesis submitted to the Faculty of Graduate Studies and Research
in partial fulfillment of the requirements for the
degree of Doctor of Philosophy

Department of Earth Sciences
Carleton University
Ottawa, Ontario, Canada
September, 1993

ISBN 0-315-89763-5

Name ZHAOMIN YIN

Dissertation Abstracts International is arranged by broad, general subject categories. Please select the one subject which most nearly describes the content of your dissertation. Enter the corresponding four-digit code in the spaces provided.

Geophysics — SUBJECT TERM

0373 — SUBJECT CODE

U·M·I

Subject Categories

THE HUMANITIES AND SOCIAL SCIENCES

COMMUNICATIONS AND THE ARTS
Architecture 0729
Art History 0377
Cinema 0900
Dance 0378
Fine Arts 0357
Information Science 0723
Journalism 0391
Library Science 0399
Mass Communications 0708
Music 0413
Speech Communication 0459
Theater 0465

EDUCATION
General 0515
Administration 0514
Adult and Continuing 0516
Agricultural 0517
Art 0273
Bilingual and Multicultural 0282
Business 0688
Community College 0275
Curriculum and Instruction 0727
Early Childhood 0518
Elementary 0524
Finance 0277
Guidance and Counseling 0519
Health 0680
Higher 0745
History of 0520
Home Economics 0278
Industrial 0521
Language and Literature 0279
Mathematics 0280
Music 0522
Philosophy of 0998
Physical 0523
Psychology 0525
Reading 0535
Religious 0527
Sciences 0714
Secondary 0533
Social Sciences 0534
Sociology of 0340
Special 0529
Teacher Training 0530
Technology 0710
Tests and Measurements 0288
Vocational 0747

LANGUAGE, LITERATURE AND LINGUISTICS
Language
- General 0679
- Ancient 0289
- Linguistics 0290
- Modern 0291

Literature
- General 0401
- Classical 0294
- Comparative 0295
- Medieval 0297
- Modern 0298
- African 0316
- American 0591
- Asian 0305
- Canadian (English) 0352
- Canadian (French) 0355
- English 0593
- Germanic 0311
- Latin American 0312
- Middle Eastern 0315
- Romance 0313
- Slavic and East European 0314

PHILOSOPHY, RELIGION AND THEOLOGY
Philosophy 0422
Religion
- General 0318
- Biblical Studies 0321
- Clergy 0319
- History of 0320
- Philosophy of 0322

Theology 0469

SOCIAL SCIENCES
American Studies 0323
Anthropology
- Archaeology 0324
- Cultural 0326
- Physical 0327

Business Administration
- General 0310
- Accounting 0272
- Banking 0770
- Management 0454
- Marketing 0338

Canadian Studies 0385
Economics
- General 0501
- Agricultural 0503
- Commerce-Business 0505
- Finance 0508
- History 0509
- Labor 0510
- Theory 0511

Folklore 0358
Geography 0366
Gerontology 0351
History
- General 0578
- Ancient 0579
- Medieval 0581
- Modern 0582
- Black 0328
- African 0331
- Asia, Australia and Oceania 0332
- Canadian 0334
- European 0335
- Latin American 0336
- Middle Eastern 0333
- United States 0337

History of Science 0585
Law 0398
Political Science
- General 0615
- International Law and Relations 0616
- Public Administration 0617

Recreation 0814
Social Work 0452
Sociology
- General 0626
- Criminology and Penology 0627
- Demography 0938
- Ethnic and Racial Studies 0631
- Individual and Family Studies 0628
- Industrial and Labor Relations 0629
- Public and Social Welfare 0630
- Social Structure and Development 0700
- Theory and Methods 0344

Transportation 0709
Urban and Regional Planning 0999
Women's Studies 0453

THE SCIENCES AND ENGINEERING

BIOLOGICAL SCIENCES
Agriculture
- General 0473
- Agronomy 0285
- Animal Culture and Nutrition 0475
- Animal Pathology 0476
- Food Science and Technology 0359
- Forestry and Wildlife 0478
- Plant Culture 0479
- Plant Pathology 0480
- Plant Physiology 0817
- Range Management 0777
- Wood Technology 0746

Biology
- General 0306
- Anatomy 0287
- Biostatistics 0308
- Botany 0309
- Cell 0379
- Ecology 0329
- Entomology 0353
- Genetics 0369
- Limnology 0793
- Microbiology 0410
- Molecular 0307
- Neuroscience 0317
- Oceanography 0416
- Physiology 0433
- Radiation 0821
- Veterinary Science 0778
- Zoology 0472

Biophysics
- General 0786
- Medical 0760

EARTH SCIENCES
Biogeochemistry 0425
Geochemistry 0996
Geodesy 0370
Geology 0372
Geophysics 0373
Hydrology 0388
Mineralogy 0411
Paleobotany 0345
Paleoecology 0426
Paleontology 0418
Paleozoology 0985
Palynology 0427
Physical Geography 0368
Physical Oceanography 0415

HEALTH AND ENVIRONMENTAL SCIENCES
Environmental Sciences 0768
Health Sciences
- General 0566
- Audiology 0300
- Chemotherapy 0992
- Dentistry 0567
- Education 0350
- Hospital Management 0769
- Human Development 0758
- Immunology 0982
- Medicine and Surgery 0564
- Mental Health 0347
- Nursing 0569
- Nutrition 0570
- Obstetrics and Gynecology 0380
- Occupational Health and Therapy 0354
- Ophthalmology 0381
- Pathology 0571
- Pharmacology 0419
- Pharmacy 0572
- Physical Therapy 0382
- Public Health 0573
- Radiology 0574
- Recreation 0575
- Speech Pathology 0460
- Toxicology 0383

Home Economics 0386

PHYSICAL SCIENCES

Pure Sciences
Chemistry
- General 0485
- Agricultural 0749
- Analytical 0486
- Biochemistry 0487
- Inorganic 0488
- Nuclear 0738
- Organic 0490
- Pharmaceutical 0491
- Physical 0494
- Polymer 0495
- Radiation 0754

Mathematics 0405
Physics
- General 0605
- Acoustics 0986
- Astronomy and Astrophysics 0606
- Atmospheric Science 0608
- Atomic 0748
- Electronics and Electricity 0607
- Elementary Particles and High Energy 0798
- Fluid and Plasma 0759
- Molecular 0609
- Nuclear 0610
- Optics 0752
- Radiation 0756
- Solid State 0611

Statistics 0463

Applied Sciences
Applied Mechanics 0346
Computer Science 0984
Engineering
- General 0537
- Aerospace 0538
- Agricultural 0539
- Automotive 0540
- Biomedical 0541
- Chemical 0542
- Civil 0543
- Electronics and Electrical 0544
- Heat and Thermodynamics 0348
- Hydraulic 0545
- Industrial 0546
- Marine 0547
- Materials Science 0794
- Mechanical 0548
- Metallurgy 0743
- Mining 0551
- Nuclear 0552
- Packaging 0549
- Petroleum 0765
- Sanitary and Municipal 0554
- System Science 0790

Geotechnology 0428
Operations Research 0796
Plastics Technology 0795
Textile Technology 0994

PSYCHOLOGY
General 0621
Behavioral 0384
Clinical 0622
Developmental 0620
Experimental 0623
Industrial 0624
Personality 0625
Physiological 0989
Psychobiology 0349
Psychometrics 0632
Social 0451

The undersigned hereby recommend to the Faculty of Graduate Studies and Research acceptance of the thesis entitled "A study of the mechanics of faulting and earthquakes", submitted by Zhaomin Yin, in partial fulfillment of the requirements for the degree of Doctor of Philosophy.

Chairman, Department of Earth Sciences

Thesis Supervisor

External Examiner

Carleton University
October, 1993

ABSTRACT

This thesis deals with the mechanics of faulting and earthquakes. The following topics are studied through analytical and numerical methods:

(1) The Coulomb-Navier failure criterion is applied to tectonic faulting in the two dimensional case and/or the general three-dimensional case of rocks containing arbitrarily oriented preexisting strength anisotropies and subject to both Andersonian stress systems (one of the principal stress axes is vertical) and non-Andersonian stress systems (the principal stress axes are arbitrarily oriented). General expressions for the normal stress, the shear stress and its direction, and the critical stress difference necessary to cause failure are derived as a function of depth, material parameters, pore fluid pressure, orientation of the stress field and orientation of the strength anisotropy. The limiting range of orientations, for which slip occurs along the preexisting strength anisotropy rather than along a new fault, is given as a function of material parameters, orientation of the stress field, and depth for different stress regimes. When the stress field is non-Andersonian and/or strength anisotropies are not parallel to the intermediate stress direction, faulting is generally oblique-slip. A kinematic classification of faulting is given on the basis of the angle between the strike direction and the slip direction on the fault plane. Triangular diagrams, analogous to those used in petrology, are introduced to describe the type of faulting in terms of the principal stress directions and the fault plane orientation.

(2) Probability theory and spherical statistics are introduced in the stress inversion problem. A new model is developed to determine the tectonic stress field from inversion of a population of faults of measured orientation and slip direction, in which three aspects neglected in previous inversion methods are taken into account: (i) By treating the measured slip direction and fault plane orientation as random variables, following the von Mises and the Fisher distribution, respectively, the probability distribution of the predicted maximum shear stress and the distribution of the misfit angle between the measured slip and the predicted maximum shear stress direction are evaluated by a numerical method, and both are found to follow approximately the von Mises distribution with mean zero and variance varying from zero to infinity. Two new inversion criteria are proposed that take both measurement errors simultaneously into account. (ii) The statistical basis and physical implications of the previous inversion criteria are clarified in terms of the maximum likelihood function, which shows that all the previous methods were based on empirical criteria and did not take both kinds of measurement errors simultaneously into account. The previous methods are proven to be special cases of the new method. (iii) A procedure is proposed to test the hypothesis that the stress field is spatially and temporally

uniform against the hypothesis that the stress is inhomogeneous. The new method is applied to inversion of the stress field in three areas, with a comparison with the results of previous methods.

(3) The Coulomb-Navier failure criterion is applied to stress inversion. According to the Coulomb-Navier failure criterion, the normalized critical stress difference (i.e., the critical stress difference divided by the effective overburden pressure) is the same for each fault if the stress field is uniform. Based of the normalized critical stress difference, a new method is proposed to determine the average friction coefficient of faults and the normalized magnitudes of the principal stresses from inversion of a population of faults of measured orientations and slip directions. This method has been applied to four fault-slip sets of data. For three of the four examples, an average friction coefficient $\bar{\mu}_0$=0.64, 0.70, and 0.88 is obtained. One example shows a relatively low average friction coefficient $\bar{\mu}_0$=0.22, but this value is of poor quality due to the effect of possibly non-uniform stresses. These results are in agreement with the average value of the friction coefficient (μ_0=0.75) determined from laboratory experiments. Because the new method is based on the assumption of uniform stress field, the reliability of inversion results decreases with increases in heterogeneity both in the principal directions and in the magnitudes of the principal stresses. The pore fluid pressure cannot be determined from inversion of fault-slip data and must be determined by other independent methods. The results suggest that the long-lasting controversy of whether the stress level in the upper crust is of the order of tens or hundreds of megapascals is mainly due to uncertainty about the pore fluid pressure.

(4) The effects on earthquake rupturing of heterogeneities both in stress and in strength along a large fault zone are incorporated in the potential dynamic stress drop, defined as the difference between the tectonic shear stress and the dynamic frictional strength according to a slip-weakening model. The distribution of the potential dynamic stress drop along the strike of the fault plane, denoted by $\Delta\tau_d(x)$, is modelled as a one-dimensional stochastic process. Under a dynamic fracture criterion, a relation is established between earthquake rupturing and $\Delta\tau_d(x)$. Thus, any earthquake rupture process can be regarded as a segment of a realization of the process $\Delta\tau_d(x)$. Three independent earthquake observations, i.e., the constant average stress drop, the Gutenberg-Richter relationship, and the measured surface slip of earthquake faults, are used to infer the distribution function of $\Delta\tau_d(x)$, with the following results. (i) Based on the observation of constant earthquake stress drop, an analytical solution has been derived for the distribution function of $\Delta\tau_d(x)$, which shows that among all known stochastic models, only the fractional Brownian process with index $H \rightarrow 0$ (fractal dimension D=2 in the one-dimensional case) can give rise to an approximately constant earthquake stress drop. (ii) The probability distribution of the size of zerosets of the fractional Brownian process shows a power law relation between the

cumulative number and the size of zerosets, which resembles the frequency-seismic moment relation. Using an average b-value of 1.0 for small earthquakes, an index $H \rightarrow 0$ of the fractional Brownian process is obtained. (iii) The surface slip data of two strike-slip dominated earthquake faults with rupture length of more than 100 km are inverted using the method of power spectral analysis. Both data sets display a power-law relationship between the sample power spectrum and the spatial frequency, characteristic of the fractional Brownian distribution. The index H is obtained to be approximately zero for both earthquake faults. All three independent lines of evidence suggest that earthquake rupturing possesses some properties of a stochastic process, which can be modelled by the fractional Brownian motion with index $H \rightarrow 0$, i.e. with fractal dimension $D=2$ in the one-dimensional case.

ACKNOWLEDGMENTS

I would like to express my deepest gratitude to Prof. G. Ranalli for accepting me as his Ph.D. student, and to the Department of Earth Sciences for providing a learning and research environment that was both challenging and supportive.

This thesis was completed under the supervision of Prof. G. Ranalli, who suggested, supported, and patiently supervised all aspects of the thesis. The energy and time invested by Prof. G. Ranalli in this thesis were enormous. I hope that his investment has been rewarded.

Several people deserve recognition for their special support for my thesis work and for various forms of help for other aspects involved in my Ph.D. study and research. I have benefited from a graduate course given by Prof. R. L. Brown; a suggestion from Dr. F. P. Agterberg of the Geological Survey of Canada helped me solve a statistical problem; Dr. S. Chen of the Department of Mathematics and Statistics suggested useful reference books and provided technical support when I had a difficulty in studying the fractional Brownian function; H. Wilson corrected the written English of several term papers I wrote during my first year at Carleton. I have also benefited from discussion with J. Liu, Z. Deng, Dr. C. Lowe, and Dr. Z. Yue (a former Ph.D. student of the Department of Civil Engineering). The departmental technicians J. Hogg and E. de Kemp, and secretaries E. Lambton, S. Hill, and S. Thayer provided help during my five years in the department.

This thesis work was partly supported by NSERC grants to Prof. G. Ranalli. I gratefully acknowledge Carleton University scholarships and an Ontario Graduate Scholarship.

I appreciate all the love and patience of my wife, X. Zhang, who took over nearly all the tedious work of house-keeping and baby-raising in order to support my research. Also, I would like to thank my father and brothers and sisters for their persistent moral support during the long separation of five years.

TABLE OF CONTENTS

LIST OF FIGURES

LIST OF TABLES

LIST OF SYMBOLS

Symbol	Description
α, β, γ	Euler angles
α_1	significance level for hypothesis testing
α_2	a factor used for estimation of confidence intervals: $1-\alpha_2$ is the confidence level
δ	stress ratio defined as $\delta=(\sigma_2-\sigma_3)/(\sigma_1-\sigma_3)$
E	random variable denoting the angle between the maximum shear stress direction and the strike of the fault
ε	the value of E
ε_0	mean direction of E
(Θ, Φ)	random variables denoting the plunge and the trend of the normal to the fault plane
κ	concentration parameter for measurement errors in slip direction
κ'	concentration parameter for measurement errors in fault plane orientation
$\hat{\kappa}$	the estimate of κ
κ_ε	concentration parameter of random variable E
κ_ω	concentration parameter of random variable Ω
κ_s	concentration parameter of random variable S
λ	pore fluid factor, defined as λ=(pore fluid pressure)/(ρgz)
μ	coefficient of friction in homogeneous, isotropic rocks
μ_0	coefficient of friction along preexisting faults
$\overline{\mu}_0$	average friction coefficient of faults
ξ_1, ξ_2, ξ_3	angles between the normal to the fault plane and the σ_1, σ_2, σ_3-axis, respectively
ρ	average density of overlying rocks
σ	normal stress acting on the fault plane
σ_1	the maximum principal stress
$\sigma_{1(n)}$	normalized maximum principal stress, defined as the ratio of σ_1 to the effective overburden pressure
$\overline{\sigma}_{1(n)}$	average normalized maximum principal stress
σ_2	the intermediate principal stress

$\sigma_{2(n)}$	normalized intermediate principal stress, defined as the ratio of σ_2 to the effective overburden pressure
$\overline{\sigma}_{2(n)}$	average normalized intermediate principal stress
σ_3	the minimum principal stress
$\sigma_{3(n)}$	normalized minimum principal stress, defined as the ratio of σ_3 to the effective overburden pressure
$\overline{\sigma}_{3(n)}$	average normalized minimum principal stress
σ_v	vertical stress or effective overburden pressure; $\sigma_v=\rho gz(1-\lambda)$
$(\sigma_1-\sigma_3)$	critical stress difference
$(\sigma_{1(n)}-\sigma_{3(n)})$	normalized critical stress difference, defined as the ratio of the critical stress difference to the effective overburden pressure
$(\overline{\sigma}_{1(n)}-\overline{\sigma}_{3(n)})$	average normalized critical stress difference
$\Delta(\sigma_{1(n)}-\sigma_{3(n)})$	misfit stress difference, defined as the difference between normalized critical stress difference and average normalized critical stress difference
$\Delta\sigma$	misfit ratio, defined as the ratio of misfit stress difference to average normalized critical stress difference
τ	shear stress acting on the fault plane
τ_h	the horizontal component of τ on the fault plane
τ_d	the dip component of τ on the fault plane
$\tau_f(x,y)$	static frictional strength along the fault plane as a function of position
$\tau_s(x,y)$	static shear stress on the fault plane as a function of position
$\tau_d(x,y)$	dynamic frictional strength along the fault plane as a function of position
$\Delta\tau_d(x)$	potential dynamic stress drop along the fault plane as a function of position
$\overline{\Delta\tau}_d$	average stress drop
ϕ_0	frictional angle defined as $\phi_0=\tan^{-1}(\mu_0)$
ψ	angle between the σ_1-axis and the fault plane
ψ_{min}	minimum limiting angle for faulting along strength anisotropies
ψ_{max}	maximum limiting angle for faulting along strength anisotropies
Ω	random variable denoting the pitch angle between the slip and the strike direction
ω	the value of Ω
ω_0	mean direction of Ω
a_i	a factor associated with the ith fault, defined as $a_i=\hat{\kappa}/\kappa_{si}$

b	b-value in the Gutenberg-Richter law
D	fractal dimension
f	spatial frequency
g	acceleration of gravity
h(k)	power spectral density function
$\hat{h}(k)$	sample power spectral density
h	unit vector coinciding with the direction of the strike of the fault
H	the index in the fractional Brownian motion
$\hat{H}$	the estimated index
i	the ith fault
k	wave number
l	unit vector coinciding with the direction of the maximum shear stress on the fault plane
L	seismic rupture length
m_τ	mean of the stochastic process $\Delta\tau_d(x)$
$\hat{m}_\tau$	sample mean of $\Delta\tau_d(x)$
m	unit vector coinciding with the vertical direction
n	total number of faults
n	unit vector coinciding with the direction of the normal to the fault plane
N	cumulative number of seismic events
p	unit vector coinciding with the slip direction
$\mathbf{P}^*$, $\mathbf{B}^*$, $\mathbf{T}^*$	the principal stress directions of ideal local stress field
R	the principal stress ratio; $R=\sigma_1/\sigma_3$
R(s)	autocovariance function
rv	abbreviate of random variable
S	random variable denoting the misfit angle between predicted maximum shear stress direction and slip direction
s	the value of S
s_0	mean direction of S
S_0	cohesive strength along preexisting strength anisotropies
S^*	random variable denoting normalized misfit angle
s^*	the value of S^*
t	vector denoting the traction force acting on the fault plane
u_i, v_i, w_i (i=1, 2, 3)	cosines of the angles between y_1 and x_i, y_2 and x_i, and y_3 and x_i,

	respectively
$\Delta u_d(x)$	dynamic slip as a function of position
$\overline{\Delta u_d}$	average dynamic slip
v	variance for the measurement errors both in slip direction and in fault plane orientation
$\hat{v}$	the estimate of v
$v^{1/2}$	standard deviation for the measurement errors both in slip direction and in fault plane orientation
x_i (i=1, 2, 3)	geographical coordinate system; x_1, x_2, and x_3 coincide with the vertical, the east, and the north, respectively
y_i (i=1, 2, 3)	stress coordinate system; y_1, y_2, and y_3 coincide with the σ_1, σ_2, and σ_3-axis, respectively
z	depth

Chapter 1

Foreword

Faulting, one of the important deformation modes in the upper crust, is the product of the interaction between tectonic stress and brittle rocks, which is often manifested by earthquakes. The mechanical properties of rocks and the state of stress of the crust are difficult to quantify. This is because rocks in the crust are heterogeneous and anisotropic at all scales, and the stresses not only have various sources but also vary spatially and temporally. In recent years, these heterogeneities both in rock strength and in stress have increasingly drawn Earth scientists' attention, and various observations (geological, seismological, and experimental) and analyses (quantitative and qualitative) have been made. Although a significant advance has been achieved in the description of fault geometry and kinematics, and in the dynamics of faulting and earthquakes, there are still many problems which are imperfectly understood. This thesis deals with three topics in the area of mechanics of faulting and earthquakes: (1) faulting in rocks containing preexisting strength anisotropies; (2) inversion of the tectonic stress field; and (3) modelling of earthquake rupturing as a stochastic process. These three topics are studied quantitatively, from both a continuum mechanics and a stochastic approach.

Chapters 2 and 3 deal with the problem of faulting in rocks containing preexisting strength anisotropies. Chapter 2 studies the two-dimensional case: the strength anisotropies are parallel to the intermediate principal stress axis and subject to Andersonian stress systems (one of the principal stresses is vertical). Chapter 3 extends the analysis to the general three-dimensional case (i.e., the strength anisotropies have arbitrary orientation with respect to the principal stress axes, and are subject to arbitrary orientations of the stress field). Under the

assumption that the Coulomb-Navier failure criterion is adequate to describe geological faulting, Anderson's faulting theory is extended to include faulting along preexisting strength anisotropies subject to an arbitrarily oriented stress field. Quantitative expressions are derived for the critical stress difference and the magnitude and direction of the maximum shear stress on the fault plane in terms of principal stress directions, orientation of strength anisotropy, material parameters, and depth. In addition, the orientation constraints on reactivation of preexisting faults are studied and explicit expressions are derived. These expressions are useful for stress analysis of faulting and fault reactivation under a variety of tectonic environments.

The stress inversion problem is dealt in Chapters 4 and 5. In Chapter 4, probability theory and spherical statistics are introduced into the analysis of stress inversion. This helps to clarify several aspects left unsolved in the previous methods, such as the probability distribution of the misfit angle, which is important for devising an inversion algorithm, and the hypothesis testing procedure to check whether a given data set represents a uniform stress field. A new method comprising two inversion algorithms is proposed, grounded in probability theory. Most previous methods are shown to be particular cases of the new method. In Chapter 5, a new method is developed to determine the average friction coefficient of preexisting faults from inversion of a population of faults with measured orientations and slip directions. The new method can be used to study the in situ frictional strength of faults, to complement the results derived from laboratory experiments.

Chapter 6 studies the effects of heterogeneities both in tectonic stress and in fault strength on earthquake rupturing along a single fault. The concepts of fractals, stochastic processes, and power spectral analysis are used to infer the distribution function of the dynamic stress drop from earthquake observations. The analysis consistently suggests that the earthquake rupturing process

can be modelled by a special stationary process, the fractional Brownian motion with index $H \approx 0$. On the one hand, these results confirm the hypothesis made by previous workers that the distribution of earthquakes is fractal. On the other hand, the results clarify the controversy whether different earthquake sequences are characterized by different fractal dimension D (or index H). The new theory has potential application to earthquake prediction, since it predicts different frequency distributions for small and large earthquakes.

The appendices list the FORTRAN programs for the new methods of inversion of tectonic stress field and average coefficient of friction.

Although the thesis is mainly theoretical, applications of the proposed new models and methods are also emphasized. In each chapter, some geological and seismological examples are illustrated. In Chapter 3, triangular diagrams, of the type commonly used in petrology, are introduced to present the results for different types of faulting. Chapters 4 and 5 give four examples of application of the new techniques of stress inversion to field fault measurement data. In Chapter 6, the surface slip data of two large earthquake faults are used to infer the distribution function of the dynamic stress drop.

The thesis is presented as a series of papers, some of which have been published in modified form, while others are still in preparation. Chapter 2 is an expansion of a paper published in *Journal of Structural Geology* by Ranalli and Yin (1990, Vol. 12, pp. 1067-1071). Chapters 3 and 4 were published in *Journal of Structural Geology* (Yin and Ranalli, 1992, Vol. 14, pp. 237-244) and in *Journal of Geophysical Research* (Yin and Ranalli, 1993, Vol. 98, pp. 12165-12176), respectively. The material in Chapters 3 and 4 presents essentially the results of the author's work with Ranalli's guidance. The material in Chapter 2 initially came from a project shared approximately evenly with Ranalli, but has been completely rewritten by the author.

Chapter 2

Critical Stress Difference and Orientation of Faults in Rocks with Strength Anisotropies: the Two-Dimensional Case

ABSTRACT

Based on the Coulomb-Navier failure criterion, quantitative expressions are derived for the critical stress difference on thrust, normal, and strike-slip faults, both in homogeneous, isotropic rocks, and along preexisting strength anisotropies with different cohesion and friction coefficient, subject to the limitation that the plane of anisotropy contains the intermediate principal stress axis. The range of orientations for which rupturing occurs along preexisting planes of weakness rather than along a new fault is given as a function of depth, pore fluid pressure, and material parameters. Given the principal stress directions, these expressions allow the estimation of the stress and orientation limiting conditions for the reactivation of preexisting faults in the three faulting regimes, and to infer the variation of the strength of the upper and middle crust with depth.

INTRODUCTION

The Coulomb-Navier criterion is an empirical failure criterion derived from rock experiments. On the assumption that this criterion adequately describes geological faulting, it is possible to predict the orientation of fracture planes and the critical stress state for faulting in the upper crust (see e.g. Jaeger and Cook, 1969; Ranalli, 1987; Mandl, 1988). Anderson (1905, 1951) first applied the Coulomb-Navier failure criterion to the brittle deformation of the upper crust. He proposed a mechanical model for tectonic faulting, in which the conjugate normal, strike-slip, and thrust faults are interpreted as the products of the brittle shear failure of homogeneous and isotropic rocks under a state of stress where one of the three principal stress axes is vertical with respect to the surface of the Earth and the intermediate stress axis is parallel to the fault plane. Anderson's model establishes the relationship between tectonic faulting and stress field and makes it possible to analyze the stress state associated with faulting, so that, given the orientations of conjugate faults, the principal stress directions and the friction coefficient can be determined; conversely, given the stresses and material parameters, the orientation and type of faults can be predicted.

The critical stress difference required for faulting, which represents the strength of rocks and/or faults (according to whether a new fracture plane is formed or slip is along a preexisting fault), is an important parameter to describe the mechanical properties of the upper crust, and it is often used to estimate the variation with depth of the strength of the upper crust in the construction of rheological profiles (Ranalli and Murphy, 1987; Lowe and Ranalli, 1993). Although, on the basis of Anderson's model, the critical stress difference can be read off the Mohr stress circle, the graphic method is cumbersome and inaccurate in the calculation of the

critical stress difference. Sibson (1974) derived quantitative expressions for the critical stress difference required for slip along preexisting normal, strike-slip, and thrust faults which are cohesionless and most favourably oriented with respect to the stress field, i.e., making an angle $\psi=(1/2)\tan^{-1}(1/\mu_0)$ with the σ_1-axis and paralleling the σ_2-axis, where μ_0 is the coefficient of friction. (Compressive stresses are taken as positive, and the principal stresses are $\sigma_1>\sigma_2>\sigma_3$.)

In this chapter, I extend Sibson's analysis to include fault planes with finite cohesive strength and arbitrary orientation with respect to the σ_1-axis. I also analyze orientation constraints on the reactivation (or activation) of preexisting strength anisotropies. A strength anisotropy is defined as a surface with smaller cohesion and/or friction coefficient (S_0, μ_0) than the corresponding quantities in the surrounding homogeneous and isotropic rocks (S, μ). Strength anisotropies may include different types of planes of weakness, such as preexisting faults and joints, layering, and fabric. Although similar problems have been considered before (Jaeger, 1960; Jaeger and Cook, 1969; Sibson, 1985; Nur et al., 1986; Ivins et al., 1990), no unified quantitative treatment in terms of the three tectonic faulting regimes is available. The present analysis is limited to the two-dimensional case where one of the principal stress axes is vertical and the plane of anisotropy parallels the σ_2-axis. Extension of the analysis to the general three-dimensional case introduces further complexities and will be addressed in the next chapter.

CRITICAL STRESS DIFFERENCE ON NEW AND MOST FAVOURABLY ORIENTED PREEXISTING FAULTS

The Coulomb-Navier shear failure criterion can be expressed as

$$\tau = S + \mu\sigma \tag{2.1}$$

where τ, σ are shear and normal stress acting on the fault plane, and S, μ denote the cohesion and friction coefficient (denoted as S_0, μ_0 if referring to a strength anisotropy). In equation (2.1), the absolute sign is not applied to the shear stress since the occurrence of fracture depends only on the magnitude of the shear stress and my attention is restricted to its positive value. The normal stress is the effective normal stress, i.e., corrected for pore fluid pressure if a fluid phase is present (Jaeger and Cook, 1969).

Assuming S_0=0, Sibson (1974) derived expressions for the critical stress difference on preexisting fracture planes with most favourable orientation, that is, making an angle $\psi=(1/2)\tan^{-1}(1/\mu_0)$ with the σ_1-axis. Sibson's formulation (1974) is summarized as follows. With reference to Figure 2.1, the shear and the normal stress acting on the most favourably oriented fault plane are, respectively (see e.g. Jaeger and Cook, 1969, pp. 87-91)

$$\begin{aligned} \tau &= \frac{1}{2}(\sigma_1 - \sigma_3)\sin 2\psi \\ \sigma &= \frac{1}{2}(\sigma_1 + \sigma_3) - \frac{1}{2}(\sigma_1 - \sigma_3)\cos 2\psi \end{aligned} \tag{2.2}$$

Thus, assuming S_0=0, the Coulomb-Navier criterion can be written as

$$\frac{1}{2}(\sigma_1 - \sigma_3)\sin 2\psi = \mu_0[\frac{1}{2}(\sigma_1 + \sigma_3) - \frac{1}{2}(\sigma_1 - \sigma_3)\cos 2\psi] \tag{2.3}$$

Introducing a parameter $R=\sigma_1/\sigma_3$ termed the principal stress ratio into equation (2.3) yields

$$(R-1)\sin 2\psi = \mu_0[(R+1) - (R-1)\cos 2\psi] \tag{2.4}$$

Substituting $\psi=(1/2)\tan^{-1}(1/\mu_0)$ in equation (2.4), the principal stress ratio R can be written as

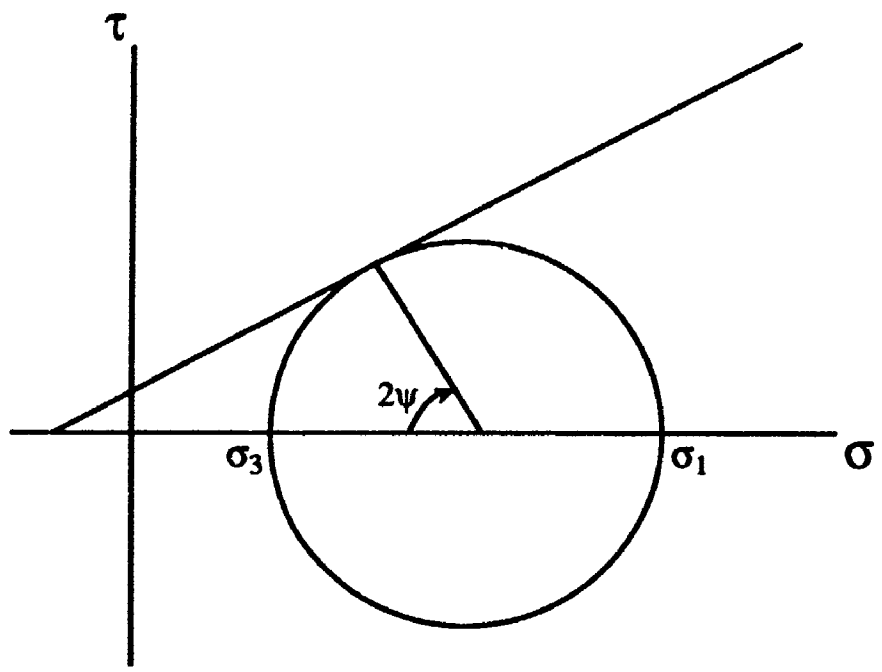

Figure 2.1. Mohr circle and failure envelope for homogeneous, isotropic rock and/or a most favourably oriented plane of weakness with finite cohesion. $\psi=(1/2)\tan^{-1}(1/\mu)$ when referring to the homogeneous rock, and $\psi=(1/2)\tan^{-1}(1/\mu_0)$ when referring to the most favourably oriented plane of weakness.

$$R = [(\mu_0^2 + 1)^{1/2} + \mu_0]^2 \tag{2.5}$$

In the case of thrust faulting, where $\sigma_3=\rho gz(1-\lambda)$ (effective overburden pressure; λ is the pore fluid factor, defined as the ratio of pore fluid pressure to overburden pressure), the critical stress difference can be derived from the relation $R=\sigma_1/\sigma_3$

$$(\sigma_1 - \sigma_3) = (R-1)\rho gz(1-\lambda) \tag{2.6}$$

where ρ is the average density of overlying rock, g the acceleration of gravity, and z depth.

In the case of strike-slip faulting, where $\sigma_2=\rho gz(1-\lambda)$, the critical stress difference is

$$(\sigma_1 - \sigma_3) = \frac{R-1}{1+\delta(R-1)}\rho gz(1-\lambda) \tag{2.7}$$

where $\delta=(\sigma_2-\sigma_3)/(\sigma_1-\sigma_3)$ is the ratio of stress differences (coming from writing the intermediate principal stress as $\sigma_2=\sigma_3+\delta(\sigma_1-\sigma_3)$).

Finally, in the case of normal faulting, where $\sigma_1=\rho gz(1-\lambda)$, the critical stress difference becomes

$$(\sigma_1 - \sigma_3) = \frac{R-1}{R}\rho gz(1-\lambda) \tag{2.8}$$

Equations (2.6), (2.7), and (2.8) are Sibson's formulations. They allow the direct calculation of the critical stress difference for the three different faulting regimes along preexisting, most favourably oriented, cohesionless planes of weakness. The critical stress difference, which increases with depth, is larger for thrust faults than for strike-slip and normal faults (in that order).

The assumption $S_0=0$ restricts the applicability of equations (2.6) - (2.8) to preexisting strength anisotropies that have zero or negligible cohesion. However, the analysis can be readily

extended to new faults in homogeneous, isotropic rocks and/or preexisting anisotropies with cohesive strength. With reference to Figure 2.1, the Coulomb-Navier criterion for the general case of a new fracture with parameters S and μ can be written as

$$\frac{1}{2}(\sigma_1 - \sigma_3)\sin 2\psi = S + \mu[\frac{1}{2}(\sigma_1 + \sigma_3) - \frac{1}{2}(\sigma_1 - \sigma_3)\cos 2\psi] \tag{2.9}$$

Equation (2.9) can also be expressed in terms of the principal stress ratio

$$(R-1)\sin 2\psi = \frac{2S}{\sigma_3} + \mu[(R+1) - (R-1)\cos 2\psi] \tag{2.10}$$

Substituting $\psi=(1/2)\tan^{-1}(1/\mu)$ in equation (2.10) and solving for R gives

$$R = \frac{2S}{\sigma_3}[(\mu^2+1)^{1/2} + \mu] + [(\mu^2+1)^{1/2} + \mu]^2 \tag{2.11}$$

The variation of R with the coefficient of friction for various values of the ratio between cohesive strength and minimum principal stress is shown in Figure 2.2. By eliminating σ_3, the principal stress ratio R in equation (2.11) can be expressed as a function of the material parameters (S and μ) and the effective overburden pressure ($\rho gz(1-\lambda)$). In the case of thrust faulting, where $\sigma_3=\rho gz(1-\lambda)$, equation (2.11) becomes

$$R = \frac{2S}{\rho gz(1-\lambda)}[(\mu^2+1)^{1/2} + \mu] + [(\mu^2+1)^{1/2} + \mu]^2 \tag{2.12}$$

In the case of strike-slip faulting, where $\sigma_3=\rho gz(1-\lambda)/[1+\delta(R-1)]$, equation (2.11) can be rewritten as

$$R = \frac{2S(1-\delta)[(\mu^2+1)^{1/2} + \mu] + \rho gz(1-\lambda)[(\mu^2+1)^{1/2} + \mu]^2}{\rho gz(1-\lambda) - 2\delta S[(\mu^2+1)^{1/2} + \mu]} \tag{2.13}$$

In the case of normal faulting, where $\sigma_3=\rho gz(1-\lambda)/R$, the principal stress ratio is

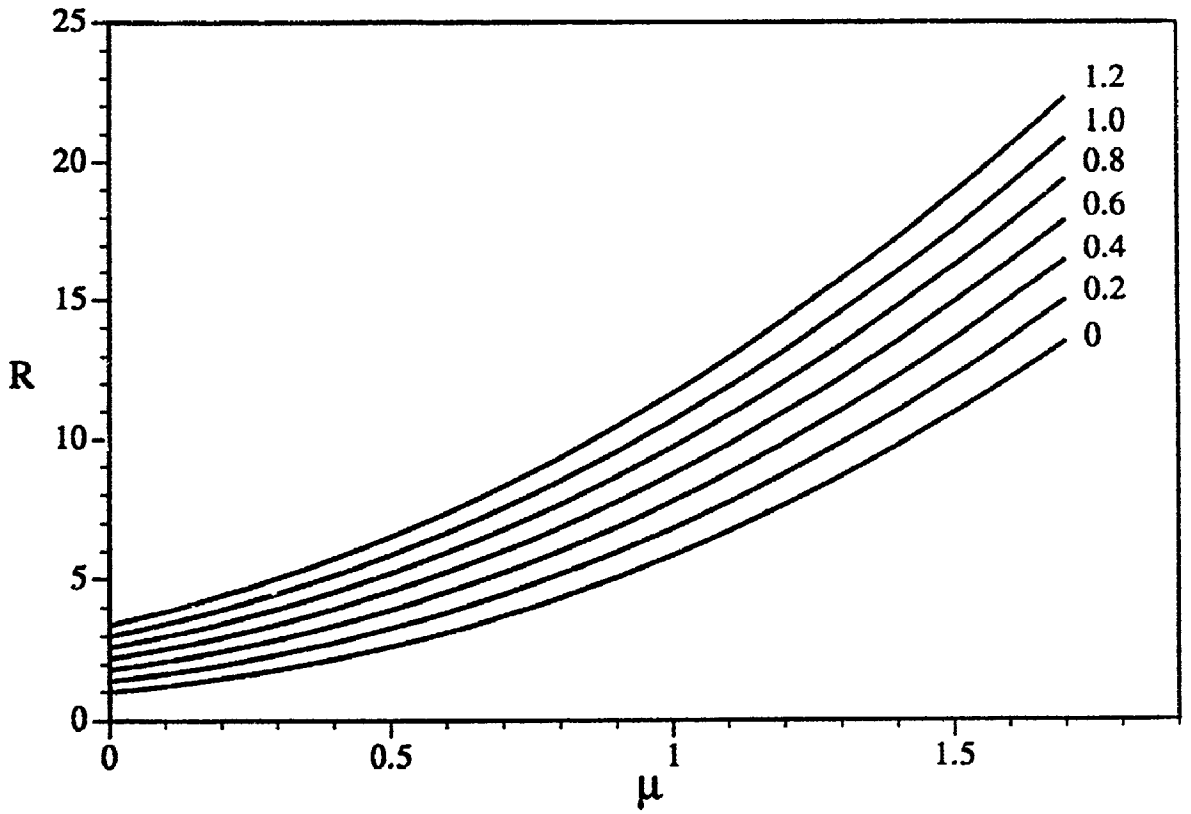

Figure 2.2. Principal stress ratio $R=\sigma_1/\sigma_3$ at failure as a function of the friction coefficient μ. Numbers on curves denote values of S/σ_3.

$$R = \frac{\rho g z(1-\lambda)\left[(\mu^2+1)^{1/2}+\mu\right]^2}{\rho g z(1-\lambda) - 2S\left[(\mu^2+1)^{1/2}+\mu\right]} \tag{2.14}$$

Equations (2.12), (2.13), and (2.14) are valid both for new faults in homogeneous, isotropic rocks and for strength anisotropies with most favourable orientation with respect to the σ_1-axis (when applied to the latter case, the material parameters S and μ have to be replaced by S_0 and μ_0, the cohesion and friction coefficient along the plane of weakness). The critical stress difference for thrust, strike-slip, and normal faulting along new fracture planes and/or along strength anisotropies with non-zero cohesion are formally identical to equations (2.6), (2.7), and (2.8) respectively, with R given by equations (2.12), (2.13), and (2.14) rather than equation (2.5). The critical state of stress at faulting for the three different faulting regimes is shown in Figure 2.3. When S=0 and $\mu=\mu_0$, equations (2.12), (2.13), and (2.14) reduce to equation (2.5), i.e., to Sibson's expressions for the special case of cohesionless, most favourably oriented fracture planes. For cohesionless fracture planes, the principal stress ratio R is independent of depth and is identical for all three standard faulting regimes. Finite cohesion has the effect of making R depth-dependent as well as faulting regime-dependent.

In the above analysis, I have followed Sibson's procedure to derive the critical stress difference in terms of the principal stress ratio R. Alternatively, the critical stress difference can be expressed directly as a function of the material parameters and depth without resort to R, so as to make the expressions more concise. I rewrite the Coulomb-Navier criterion given by equation (2.9) as

$$(\sigma_1-\sigma_3)\sin 2\psi = 2S + \mu\left[(\sigma_1-\sigma_3)+2\sigma_3-(\sigma_1-\sigma_3)\cos 2\psi\right] \tag{2.15}$$

Substituting $\psi=(1/2)\tan^{-1}(1/\mu)$ in equation (2.15) and solving the equation for $(\sigma_1-\sigma_3)$ yields

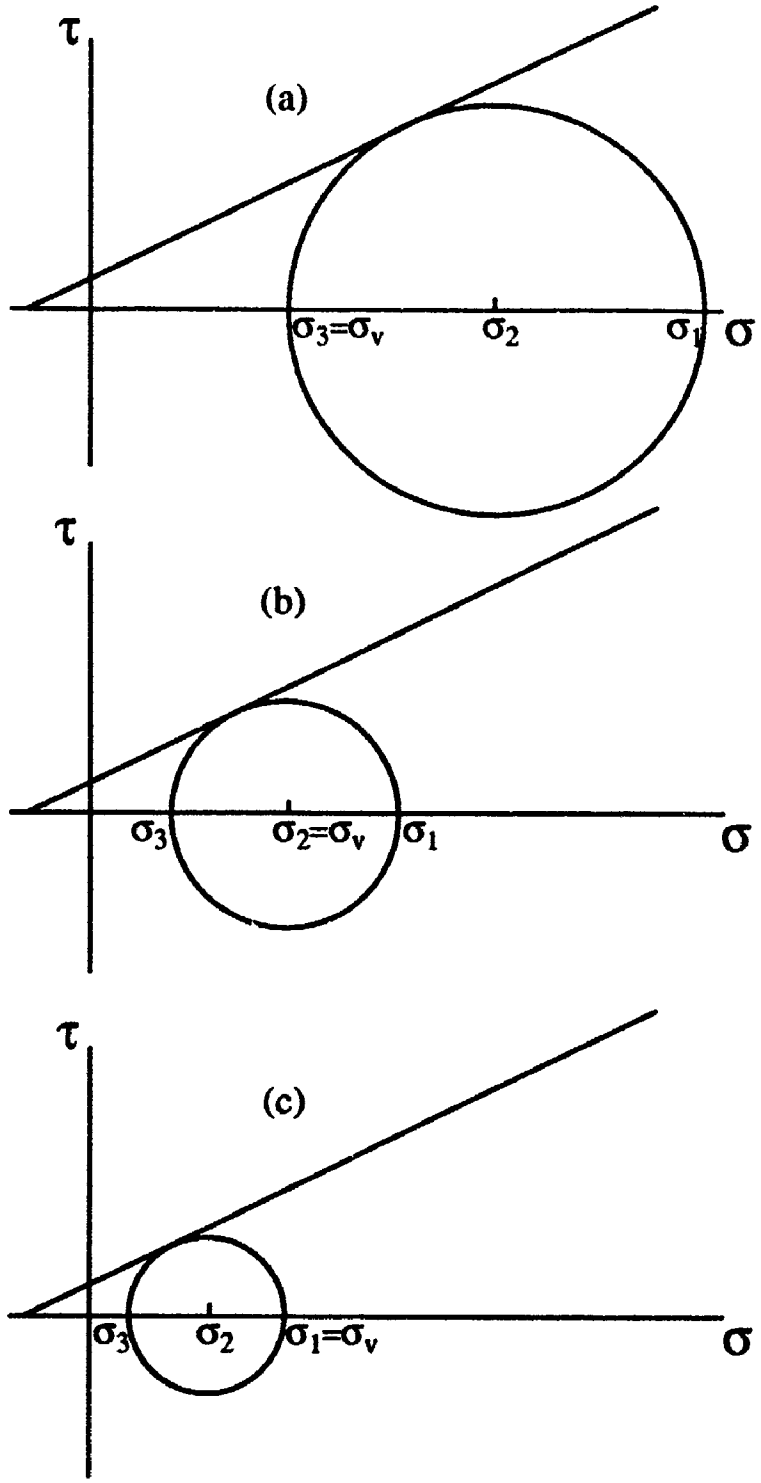

Figure 2.3. The critical stress state for three different types of faulting both in homogeneous, isotropic rocks and along most favourably oriented preexisting strength anisotropies with finite cohesive strength. Overburden pressure denoted by σ_v; δ=1/2. (a) Thrust faulting, (b) strike-slip faulting, and (c) normal faulting.

$$(\sigma_1 - \sigma_3) = \frac{2\mu\sigma_3 + 2S}{(\mu^2+1)^{1/2} - \mu} \tag{2.16}$$

In the case of thrust faulting, where $\sigma_3=\rho gz(1-\lambda)$, equation (2.16) becomes

$$(\sigma_1 - \sigma_3) = \frac{2\mu\rho gz(1-\lambda) + 2S}{(\mu^2+1)^{1/2} - \mu} \tag{2.17}$$

In the case of strike-slip faulting, the minimum principal stress can be expressed as $\sigma_3=\rho gz(1-\lambda)-\delta(\sigma_1-\sigma_3)$, and the critical stress difference becomes

$$(\sigma_1 - \sigma_3) = \frac{2\mu\rho gz(1-\lambda) + 2S}{(\mu^2+1)^{1/2} + \mu(2\delta - 1)} \tag{2.18}$$

In the case of normal faulting, the minimum principal stress can be expressed as $\sigma_3=\rho gz(1-\lambda)-(\sigma_1-\sigma_3)$ and equation (2.16) can be rewritten as

$$(\sigma_1 - \sigma_3) = \frac{2\mu\rho gz(1-\lambda) + 2S}{(\mu^2+1)^{1/2} + \mu} \tag{2.19}$$

To calculate the critical stress difference for preexisting strength anisotropies, the material parameters S and μ in equations (2.17), (2.18), and (2.19) have to be replaced by S_0 and μ_0, respectively. In comparison with the previous expressions (equations (2.12), (2.13), and (2.14) together with equations (2.6), (2.7), and (2.8)), equations (2.17), (2.18), and (2.19) are formally more concise and make the calculation of the critical stress difference easier. Furthermore, they yield the critical stress difference directly in terms of material parameters and depth.

Let $(\sigma_1-\sigma_3)_N$ and $(\sigma_1-\sigma_3)_F$ denote the critical stress difference for formation of a new fault and the critical stress difference for faulting along a most favourably oriented preexisting strength anisotropy, respectively. The relations between $(\sigma_1-\sigma_3)_N$ and $(\sigma_1-\sigma_3)_F$ can be derived from equations (2.17), (2.18), and (2.19). Since the effective overburden pressure $\rho gz(1-\lambda)$ is the same

for both the formation of a new fault and for faulting along a most favourably oriented strength anisotropy, solving each of equations (2.17), (2.18) and (2.19) for $\rho gz(1-\lambda)$ twice, once in terms of S, μ and $(\sigma_1-\sigma_3)_N$, and once in terms of S_0, μ_0 and $(\sigma_1-\sigma_3)_F$, and equating the two effective overburden pressures, I obtain the relation between $(\sigma_1-\sigma_3)_N$ and $(\sigma_1-\sigma_3)_F$. For thrust faults,

$$(\sigma_1-\sigma_3)_N=\frac{\mu[(\mu_0^2+1)^{1/2}-\mu_0](\sigma_1-\sigma_3)_F+2(S\mu_0-S_0\mu)}{\mu_0[(\mu^2+1)^{1/2}-\mu]} \tag{2.20}$$

For strike-slip faults,

$$(\sigma_1-\sigma_3)_N=\frac{\mu[(\mu_0^2+1)^{1/2}+\mu_0(2\delta-1)](\sigma_1-\sigma_3)_F+2(S\mu_0-S_0\mu)}{\mu_0[(\mu^2+1)^{1/2}+\mu(2\delta-1)]} \tag{2.21}$$

For normal faults,

$$(\sigma_1-\sigma_3)_N=\frac{\mu[(\mu_0^2+1)^{1/2}+\mu_0](\sigma_1-\sigma_3)_F+2(S\mu_0-S_0\mu)}{\mu_0[(\mu^2+1)^{1/2}+\mu]} \tag{2.22}$$

Equations (2.20), (2.21), and (2.22) show that the critical stress difference $(\sigma_1-\sigma_3)_N$ (for formation of a new fault) has a linear relation with $(\sigma_1-\sigma_3)_F$ (for slip along a most favourably oriented preexisting strength anisotropy). When $\mu=\mu_0$, the slope in the linear relation becomes unity.

Figure 2.4 shows some examples of the critical stress differences as a function of depth for both homogeneous, isotropic rocks and most favourably oriented preexisting strength anisotropies in the three different faulting regimes. Two different pore-fluid pressures, corresponding to dry rock ($\lambda=0$) and to approximately hydrostatic ($\lambda=0.4$) water pressure, are chosen. The critical stress difference for faulting along new planes in homogeneous, isotropic rock is larger than that for faulting along most favourably oriented strength anisotropies, by an amount (constant in the particular case $\mu=\mu_0$) which depends on material parameters and faulting

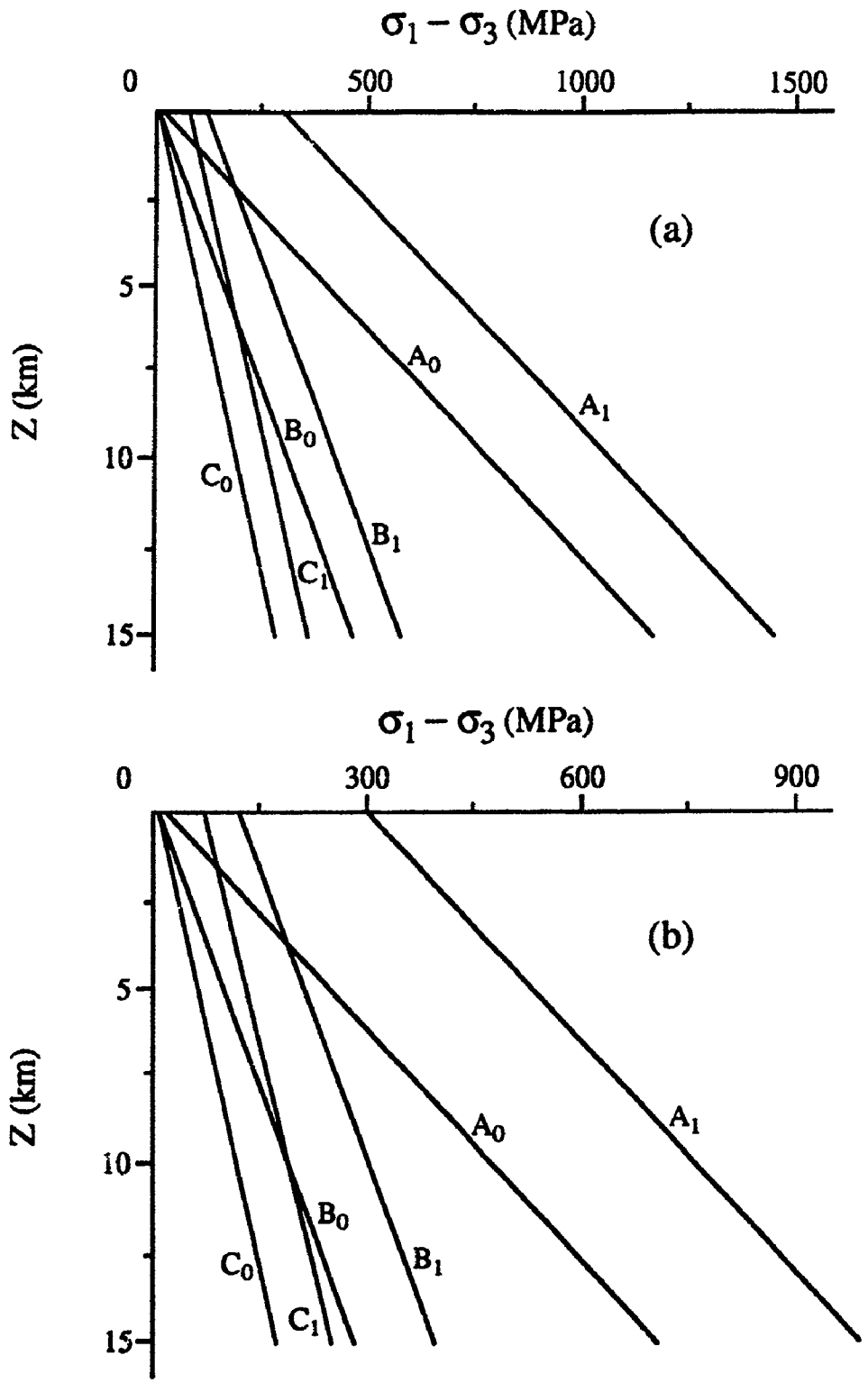

Figure 2.4. Critical stress difference ($\sigma_1 - \sigma_3$) versus depth (z) for homogeneous, isotropic rock (A_1, B_1, C_1) and for most favourably oriented preexisting strength anisotropies (A_0, B_0, C_0) in thrust, strike-slip, and normal faulting regimes, respectively. Two cases are presented: (a) no pore fluid pressure λ=0,; and (b) ratio of pore fluid to overburden pressure λ=0.4. Parameters are: S=75 MPa, S_0=5 MPa, $\mu=\mu_0$=0.75, δ=1/2, and ρ=2600 kg m^{-3}.

regimes. In the calculation of the critical stress differences, I have used average values of the material parameters (S=75 MPa, S_0=5 MPa, $\mu=\mu_0=0.75$, ρ=2600 kg m^{-3}). Because these parameters are independent of depth, the critical stress differences increase linearly with depth. In reality, however, the material parameters may change with depth, for example, due to the variations of lithology, and the critical stress difference may show variations from linearity.

CRITICAL STRESS DIFFERENCE FOR FAULTING ALONG ARBITRARILY ORIENTED PREEXISTING STRENGTH ANISOTROPIES

In rocks anisotropic with respect to strength, faulting often occurs along preexisting strength anisotropies because they have lower cohesive and/or frictional strength than the surrounding rocks; for instance, the majority of earthquakes in the world are distributed along preexisting fault zones. Usually, the preexisting strength anisotropies are not necessarily most favourably oriented, i.e., they make an angle $\psi\neq(1/2)\tan^{-1}(1/\mu_0)$ with the σ_1–axis. In the previous section, I have derived expressions for the critical stress difference on the most favourably oriented fracture planes. Now, I extend the analysis to preexisting strength anisotropies which have arbitrary orientation with respect to the σ_1-axis.

Figure 2.5 shows the critical state of stress on the plane of a preexisting strength anisotropy which makes an angle ψ with the maximum principal stress axis. The shear and the normal stress on the plane of the strength anisotropy are formally identical to equation (2.2), but with $\psi\neq(1/2)\tan^{-1}(1/\mu_0)$. Therefore, the Coulomb-Navier criterion can be written as

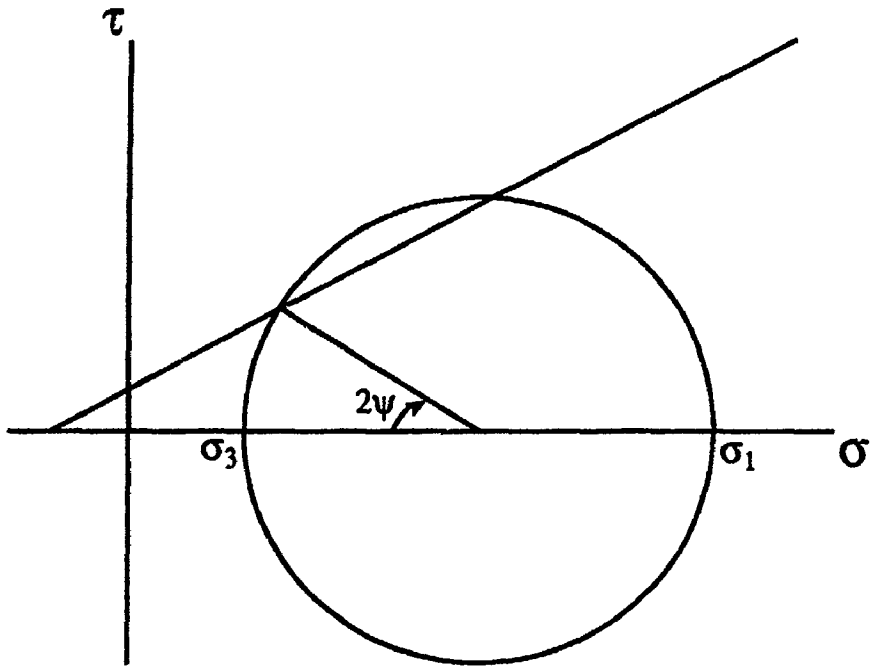

Figure 2.5. The critical stress state at failure for a preexisting strength anisotropy which makes an angle $\psi \neq 1/2\tan^{-1}(1/\mu_0)$ with the σ_1–axis.

$$\frac{1}{2}(\sigma_1-\sigma_3)\sin 2\psi = S_0 + \mu_0[\frac{1}{2}(\sigma_1+\sigma_3) - \frac{1}{2}(\sigma_1-\sigma_3)\cos 2\psi] \tag{2.23}$$

which, by solving for $(\sigma_1-\sigma_3)$, becomes

$$(\sigma_1-\sigma_3) = \frac{2\mu_0\sigma_3 + 2S_0}{\sin 2\psi + \mu_0(\cos 2\psi - 1)} \tag{2.24}$$

In the thrust faulting regime, where $\sigma_3=\rho gz(1-\lambda)$, equation (2.24) becomes

$$(\sigma_1-\sigma_3) = \frac{2\mu_0\rho gz(1-\lambda) + 2S_0}{\sin 2\psi + \mu_0(\cos 2\psi - 1)} \tag{2.25}$$

In the strike-slip faulting regime, where $\sigma_3=\rho gz(1-\lambda)-\delta(\sigma_1-\sigma_3)$, the critical stress difference can be expressed as

$$(\sigma_1-\sigma_3) = \frac{2\mu_0\rho gz(1-\lambda) + 2S_0}{\sin 2\psi + \mu_0(\cos 2\psi - 1 + 2\delta)} \tag{2.26}$$

In the normal faulting regime, where $\sigma_3=\rho gz(1-\lambda)-(\sigma_1-\sigma_3)$, equation (2.24) can be rewritten as

$$(\sigma_1-\sigma_3) = \frac{2\mu_0\rho gz(1-\lambda) + 2S_0}{\sin 2\psi + \mu_0(\cos 2\psi + 1)} \tag{2.27}$$

When $\psi=(1/2)\tan^{-1}(1/\mu_0)$, equations (2.25), (2.26), and (2.27) reduce to equations (2.17), (2.18), and (2.19), respectively, i.e., reduce to the case of most favourably oriented fractures.

Let $(\sigma_1-\sigma_3)_A$ denote the critical stress difference for slip along an arbitrarily oriented preexisting strength anisotropy paralleling the σ_2-axis. A linear relation between $(\sigma_1-\sigma_3)_A$ and $(\sigma_1-\sigma_3)_N$ (for formation of a new fault) can be derived by equating the effective overburden pressure in equations (2.25), (2.26), and (2.27) with the same quantity in equations (2.17), (2.18), and (2.19), respectively. For thrust faults, I obtain

$$(\sigma_1 - \sigma_3)_A = \frac{\mu_0[(\mu^2+1)^{1/2} - \mu](\sigma_1 - \sigma_3)_N + 2(S_0\mu - S\mu_0)}{\mu[\sin 2\psi + \mu_0(\cos 2\psi - 1)]} \tag{2.28}$$

For strike-slip faults,

$$(\sigma_1 - \sigma_3)_A = \frac{\mu_0[(\mu^2+1)^{1/2} + \mu(2\delta - 1)](\sigma_1 - \sigma_3)_N + 2(S_0\mu - S\mu_0)}{\mu[\sin 2\psi + \mu_0(\cos 2\psi - 1 + 2\delta)]} \tag{2.29}$$

For normal faults,

$$(\sigma_1 - \sigma_3)_A = \frac{\mu_0[(\mu^2+1)^{1/2} + \mu](\sigma_1 - \sigma_3)_N + 2(S_0\mu - S\mu_0)}{\mu[\sin 2\psi + \mu_0(\cos 2\psi + 1)]} \tag{2.30}$$

The critical stress differences in the thrust faulting regime for strength anisotropies of various orientations are compared in Figure 2.6 with the critical stress differences for the formation of a new fault and for slippage along a most favourably oriented anisotropy.

ORIENTATION CONSTRAINTS ON (RE)ACTIVATION OF PREEXISTING STRENGTH ANISOTROPIES

For a given stress regime, failure along a strength anisotropy, rather than formation of a new fault, occurs only if the critical stress difference for the anisotropy is less than that for the new fault. The orientation constraint problem has been considered before (see e.g. Jaeger and Cook, 1969, Sibson, 1985; Nur et al., 1986; Ivins et al., 1990). However, here I give new explicit expressions for each of the three faulting regimes. The orientation conditions for faulting along a strength anisotropy are shown in Figure 2.7. The angles ψ_{min} and ψ_{max} define the lower and upper limits within which sliding occurs along the anisotropy. Outside this range, a new fault

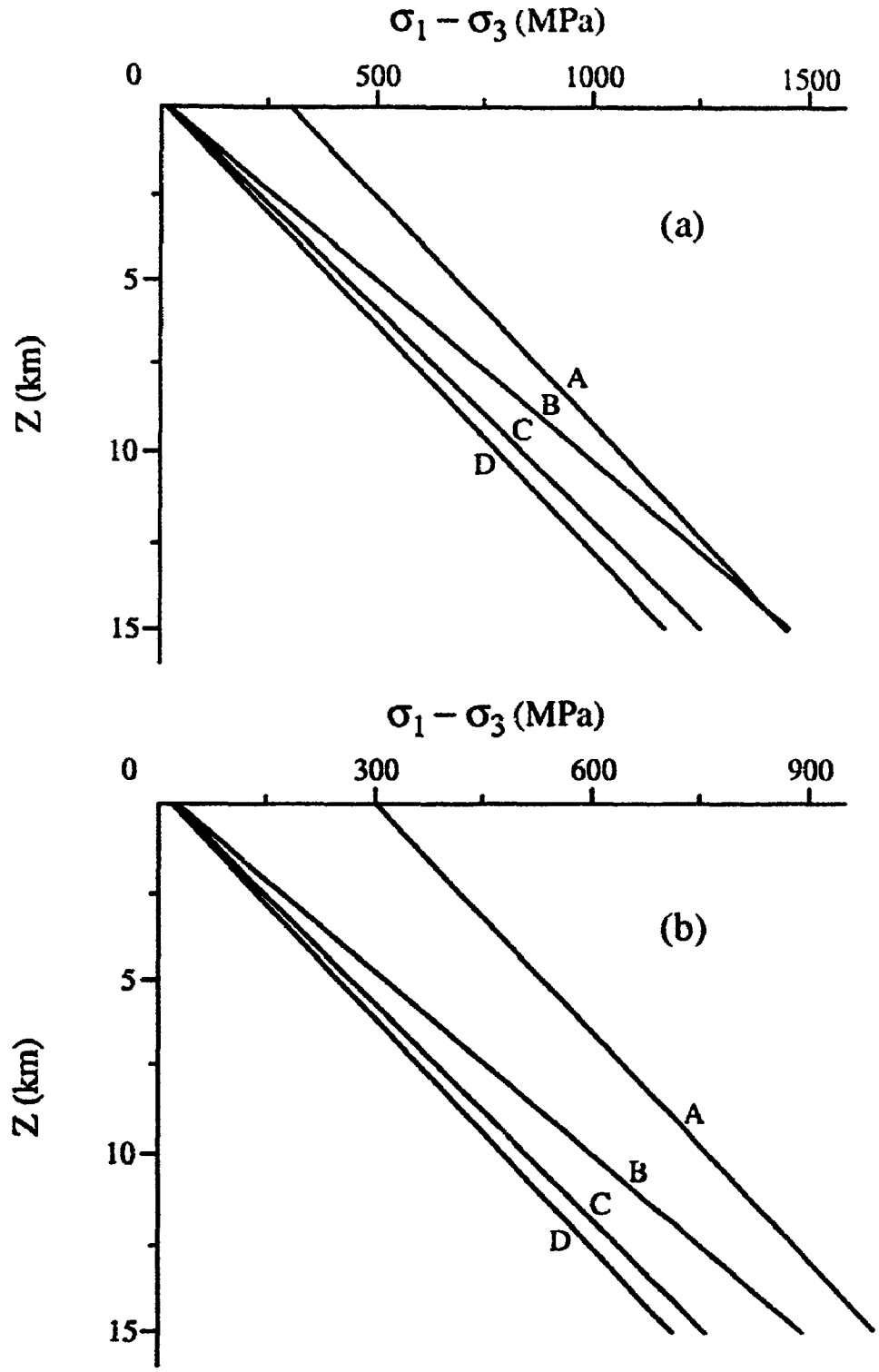

Figure 2.6. Critical stress difference ($\sigma_1 - \sigma_3$) versus depth (z) for thrust faulting: (A) new fault in homogeneous, isotropic rock; (B) strength anisotropy at an angle ψ=15° or 38° with σ_1–axis; (C) strength anisotropy at an angle ψ=20° or 33° with σ_1–axis; (D) strength anisotropy with most favourable orientation $\psi=1/2\tan^{-1}(1/\mu_0)$. The two anisotropies in each case are symmetric with respect to the most favourably oriented anisotropy plane. Material parameters are the same as for Figure 2.4, and pore fluid pressures are: (a) λ=0; (b) λ=0.4.

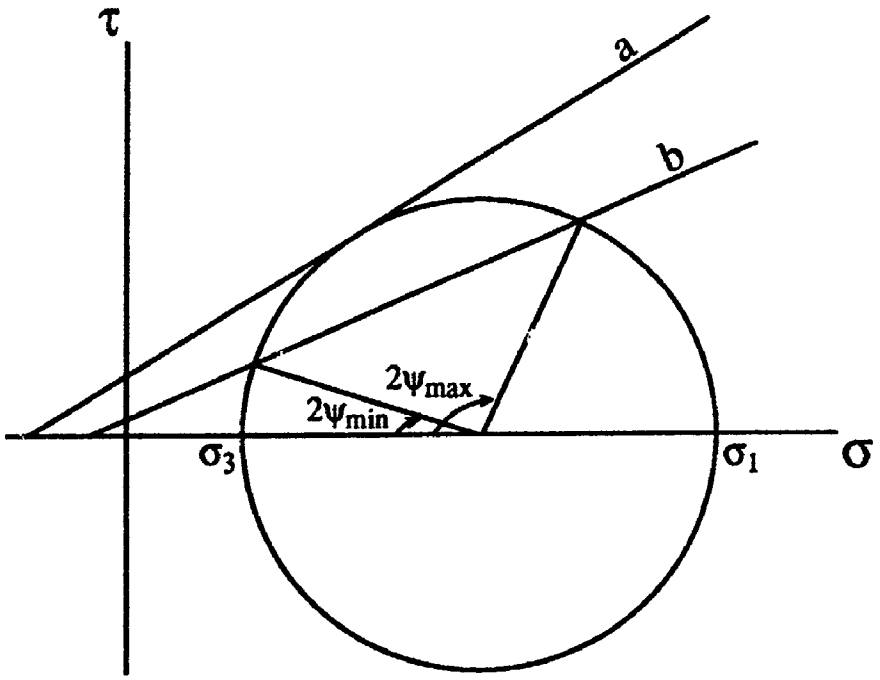

Figure 2.7. Mohr circle for failure in homogeneous, isotropic rock (a) and along preexisting strength anisotropy (b). Faulting occurs along the strength anisotropy for orientations $\psi_{min} \leq \psi \leq \psi_{max}$ with respect to the σ_1–axis.

forms with orientation $\psi=(1/2)\tan^{-1}(1/\mu)$ with respect to the σ_1-axis. For a given faulting regime, therefore, the minimum and maximum limiting angles (ψ_{min} and ψ_{max}) can be derived by equating the critical stress difference for the strength anisotropy with that for the formation of a new fault.

In the case of thrust faulting, equating equations (2.25) and (2.17) gives

$$\sin 2\psi + \mu_0(\cos 2\psi - 1) = \frac{[(\mu^2+1)^{1/2} - \mu][2\mu_0 \rho g z(1-\lambda) + 2S_0]}{2\mu\rho g z(1-\lambda) + 2S} \tag{2.31}$$

Introducing the angle of friction $\phi_0=\tan^{-1}(\mu_0)$ and solving equation (2.31), two solutions can be obtained, one for the minimum limiting angle (ψ_{min}) and the other for the maximum limiting angle (ψ_{max})

$$\begin{aligned} \psi_{min} &= \frac{1}{2}\{\sin^{-1}[\frac{(\mu^2+1)[\mu_0\rho g z(1-\lambda)+S_0]+(S\mu_0 - S_0\mu)}{(\mu_0^2+1)[\mu\rho g z(1-\lambda)+S]}] - \phi_0\} \\ \psi_{max} &= \frac{1}{2}\{\pi - \sin^{-1}[\frac{(\mu^2+1)[\mu_0\rho g z(1-\lambda)+S_0]+(S\mu_0 - S_0\mu)}{(\mu_0^2+1)[\mu\rho g z(1-\lambda)+S]}] - \phi_0\} \end{aligned} \tag{2.32}$$

Following the same procedure, the limiting angles for strike-slip and normal faulting can be derived by equating equation (2.26) with (2.18) and (2.27) with (2.19), respectively. It follows that for strike-slip faulting the limiting angles are

$$\begin{aligned} \psi_{min} &= \frac{1}{2}\{\sin^{-1}[\frac{(\mu^2+1)[\mu_0\rho g z(1-\lambda)+S_0]-(S\mu_0 - S_0\mu)(2\delta-1)}{(\mu_0^2+1)[\mu\rho g z(1-\lambda)+S]}] - \phi_0\} \\ \psi_{max} &= \frac{1}{2}\{\pi - \sin^{-1}[\frac{(\mu^2+1)[\mu_0\rho g z(1-\lambda)+S_0]-(S\mu_0 - S_0\mu)(2\delta-1)}{(\mu_0^2+1)[\mu\rho g z(1-\lambda)+S]}] - \phi_0\} \end{aligned} \tag{2.33}$$

and for normal faulting

$$\psi_{min} = \frac{1}{2}\{\sin^{-1}[\frac{(\mu^2+1)[\mu_0\rho gz(1-\lambda)+S_0]-(S\mu_0-S_0\mu)}{(\mu_0^2+1)[\mu\rho gz(1-\lambda)+S]}] - \phi_0\}$$

$$\psi_{max} = \frac{1}{2}\{\pi - \sin^{-1}[\frac{(\mu^2+1)[\mu_0\rho gz(1-\lambda)+S_0]-(S\mu_0-S_0\mu)}{(\mu_0^2+1)[\mu\rho gz(1-\lambda)+S]}] - \phi_0\} \tag{2.34}$$

Equations (2.32), (2.33), and (2.34) give the limiting ranges of orientation (with respect to the σ_1-axis) for the (re)activation of preexisting anisotropies containing the σ_2-axis under Andersonian stress systems (one principal stress axis vertical) as a function of material parameters and depth. Even in the case of independence of material parameters on depth, the limiting angles are a function of depth. They also depend on the faulting regime. Figure 2.8 gives ψ_{min} and ψ_{max} as functions of depth and faulting regime for two representative values of pore-fluid pressure. The orientation range within which faulting occurs along preexisting planes of weakness at any depth is larger for normal faults than for thrust faults, with strike-slip faults constituting an intermediate case. Therefore, reactivation of preexisting faults is more likely in a normal faulting regime. For any given faulting regime and pore-fluid pressure, the limiting range of orientation decreases with increasing depth. The results of this analysis can be compared with the particular case of reactivation of preexisting cohesionless faults (Sibson, 1985). The three-dimensional case for extensional reactivation of preexisting thrust faults has been treated by Ivins et al. (1990): their limiting angle can be proven to be equivalent to ψ_{max} given by equation (2.34).

DISCUSSION AND CONCLUSIONS

The results given in this chapter are valid for new faults and preexisting strength anisotropies containing the σ_2-axis under Andersonian stress systems. They can be summarized

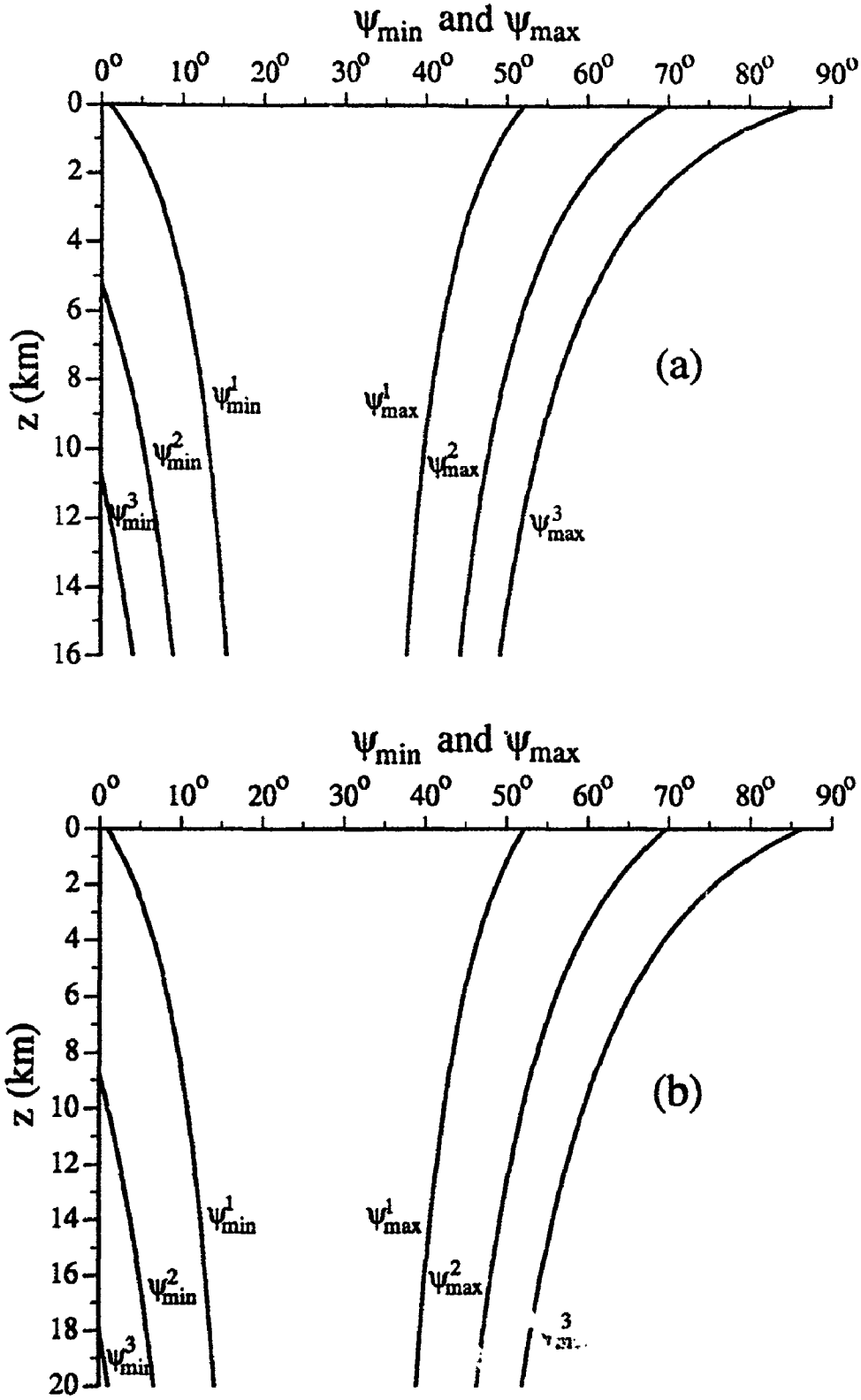

Figure 2.8. Limiting angles ψ_{min} and ψ_{max} for failure along preexisting anisotropies versus depth for thrust (ψ^1_{min}, ψ^1_{max}), strike-slip (ψ^2_{min}, ψ^2_{max}), and normal faulting (ψ^3_{min}, ψ^3_{max}), in the case of (a) no pore fluid pressure λ=0 and (b) ratio of pore fluid pressure to overburden pressure λ=0.4. Material parameters are the same as for Figure 2.4.

as follows.

(1) Sibson's (1974) expressions for the critical stress difference for sliding on most favourably oriented preexisting thrust, strike-slip, and normal faults with S_0=0 have been extended to the formation of new faults in homogeneous, isotropic rocks and/or most favourably oriented strength anisotropies with finite cohesion (equations (2.12), (2.13), and (2.14)). More concise expressions for the critical stress differences have been derived in terms of material parameters and depth (equations (2.17), (2.18), and (2.19)). A linear relation between the critical stress difference for formation of a new fault and that for faulting along a preexisting strength anisotropy has been given for the three different faulting regimes (equations (2.20), (2.21), and (2.22)).

(2) Expressions for the critical stress difference on arbitrarily oriented preexisting strength anisotropies in the thrust, strike-slip, and normal faulting regimes have been obtained in terms of material parameters, depth, and anisotropy orientation (equations (2.25), (2.26), and (2.27)). A linear relation has been derived between the critical stress difference on arbitrarily oriented preexisting strength anisotropies and the critical stress difference for formation of new faults in the thrust, strike-slip, and normal faulting regimes (equations (2.28), (2.29), and (2.30)).

(3) In each of the three faulting regimes, the limiting range of orientations for which faulting occurs along a preexisting strength anisotropy rather than along a fresh plane in homogeneous, isotropic rocks has been derived as a function of material parameters and depth (equations (2.32), (2.33), and (2.34)).

Although the discussion of detailed case histories is beyond the scope of this work, it is worth pointing out that, given the complex geometry of faults and fault systems (see e.g. Ranalli, 1980; Okubo and Aki, 1987; Walsh and Watterson. 1988) and the presence of strength

anisotropies at all scales, the relation between tectonic stress field and fault orientation must be interpreted with care. For instance, low-angle normal faults under certain conditions may be reactivated thrust faults under an Andersonian extensional regime, although they may of course be the result of new fracturing in more complex stress fields (A. Yin, 1989). Also, it is commonly assumed in seismicity studies that seismic risk along different segments of a large fault depends in part on variations of frictional and cohesive properties along the fault. While this is certainly valid in well-documented cases, it is highly likely that variations in fault orientation also play an important role, since the critical stress difference required for sliding depends on the orientation of the fracture plane with respect to the stress field (see Tajima and Célérier, 1989 for an example of three-dimensional seismological analysis of fault reactivation).

The present approach has two major limitations: it is essentially two-dimensional (the plane of anisotropy contains the intermediate principal stress axis), and it assumes an Andersonian stress systems (one principal stress direction is vertical). It nevertheless represents a systematic generalization of the two-dimensional shear failure criterion as applied to geological faulting. Faulting in the three-dimensional case under non-Andersonian stress systems will be considered in the next chapter.

REFERENCES

Anderson, E. M., The dynamics of faulting, *Trans. Geol. Soc. Edin., 8*, 393-402, 1905.

Anderson, E. M., *The Dynamics of Faulting and Dyke Formation* (2nd edn), Oliver and Boyd, Edinburgh, 1951.

Ivins, E. R., T. H. Dixon, and M. P. Golombek, Extensional reactivation of an abandoned thrust: a bound on shallowing in the brittle regime, *J. Struct. Geol., 12*, 303-314, 1990.

Jaeger, J. C., Shear fracture of anisotropic rocks, *Geol. Mag., 97*, 65-72, 1960.

Jaeger, J. C. and N. G. W. Cook, *Fundamentals of Rock Mechanics* (3rd edn), Chapman and Hall, London, 1969.

Lowe, C., and G. Ranalli, Density, temperature, and rheological models for the southeastern Canadian Cordillera: implications for its geodynamic evolution, *Can. J. Earth Sci., 30*, 77-93, 1993.

Mandl, G., *Mechanics of Tectonic Faulting*, Elsevier, Amsterdam, 1988.

Nur, A., H. Ron, and O. Scotti, Fault mechanics and the kinematics of block rotation, *Geology, 14*, 746-749, 1986.

Okubo, P., and K. Aki, Fractal geometry in the San Andreas fault system, *J. Geophys. Res., 92*, 345-355, 1987.

Ranalli, G., A stochastic model for strike-slip faulting, *Math. Geol., 12*, 399-412, 1980.

Ranalli, G., *Rheology of the Earth*, Allen and Unwin, London, 1987.

Ranalli, G., and D. C. Murphy, Rheological stratification of the lithosphere, *Tectonophysics, 132*, 281-295, 1987.

Sibson, R. H., Frictional constraints on thrust, wrench, and normal faults, *Nature, 249*, 542-

544, 1974.

Sibson, R. H., A note on fault reactivation, *J. Struct. Geol.*, *7*, 751-754, 1985.

Tajima, F., and B. Célérier, Possible focal mechanism change during reactivation of a previously ruptured subduction zone and stress tensor implications, *Geophys. J. Int.*, *98*, 301-316, 1989.

Walsh, J. J., and J. Watterson, Analysis of the relationship between displacements and dimensions of faults, *J. Struct. Geol.*, *10*, 239-247, 1988.

Yin, A., Origin of regional, rooted low-angle normal faults: a mechanical model and its tectonic implications, *Tectonics*, *8*, 469-482, 1989.

Chapter 3

Critical Stress Difference, Fault Orientation, and Slip Direction in Anisotropic Rocks Under Non-Andersonian Stress Systems: the Three-Dimensional Case

ABSTRACT

The Coulomb-Navier failure criterion is applied to geological faulting in the general three-dimensional case of rocks containing arbitrarily oriented strength anisotropies and subject to non-Andersonian stress systems (i.e., with none of the principal stresses acting in the vertical direction). General expressions for the critical stress difference necessary to cause failure as a function of depth are given in terms of material parameters, pore fluid pressure, orientation of the stress field, and orientation of the strength anisotropy. The limiting range of orientation of planes of anisotropy with respect to the stress field, for which faulting occurs along the preexisting anisotropy rather than along a new fault, is calculated as a function of depth for different stress regimes.

When the stress field is non-Andersonian and/or strength anisotropies not containing the intermediate stress axis occur in the rock, faulting generally is oblique-slip. A kinematic classification of faulting is given on the basis of the angle between the strike direction and the slip direction on the fault plane. Triangular diagrams, analogous to those used in petrology, are introduced to describe (i) faulting in isotropic rock subject to arbitrarily oriented stress fields, and (ii) faulting along preexisting strength anisotropies subject to stress fields with one principal axis

oriented vertically. The type of faulting as a function of stress field and anisotropy orientation can be read off directly from these diagrams.

INTRODUCTION

Faulting in the upper lithosphere is usually described in terms of the Coulomb-Navier brittle failure criterion (see e.g. Jaeger & Cook, 1969; Ranalli, 1987; Mandl, 1988). Assuming one principal stress direction to be vertical, Anderson (1905, 1951) used this criterion to account for the orientation of normal, strike-slip, and thrust faults. Sibson (1974) derived expressions for the critical stress difference in the three standard faulting regimes on planes with negligible cohesion most favourably oriented for failure. In Chapter 2, I have extended Sibson's analysis to faulting in homogeneous, isotropic rocks and along preexisting strength anisotropies with finite cohesion, and derived expressions for the critical stress difference and the limiting range of orientation for (re)activation of strength anisotropies in the two-dimensional case (i.e. planes of anisotropy parallel to the σ_2-axis) and under Andersonian stress systems (i.e. vertical orientation of one of the principal stress axes).

Often, however, none of the three principal stress directions is vertical, i.e. the stress state is non-Andersonian, and planes of anisotropy are arbitrarily oriented with respect to the principal stress axes (see e.g. the analyses of stress distributions in crustal blocks by Hafner (1951), Sanford (1959), A. Yin (1989), and the general discussion by Mandl (1988)). Consequently, the problem arises of determining, given the orientation of the stress field, the critical stress difference necessary for faulting in both isotropic and anisotropic rocks in the general case when the planes of weakness are not parallel to the direction of intermediate stress, and the limiting range of orientations (with respect to the principal stress system) for which faulting occurs on strength anisotropies rather than on new fault planes. This problem is addressed in this chapter. The aim is to provide a simple extension of the Coulomb-Navier failure criterion which may be

useful in the analysis of fault reactivation. A classification is also given of oblique-slip faulting in terms of the orientation of principal stresses, strength anisotropies, and slip directions.

FORMATION OF NEW FAULTS IN HOMOGENEOUS, ISOTROPIC ROCKS

In a Cartesian coordinate system y_1, y_2, y_3 (corresponding to the direction of principal stresses σ_1, σ_2, σ_3, respectively), let **m** be a unit vector denoting the normal to the horizontal plane (i.e. the surface of the Earth), where its components m_i (i = 1, 2, 3) are the directional cosines of **m** in the y_i-coordinate system, i.e., the cosines of the angles between **m** and the y_i-axis (Figure 3.1). The traction vector **t** on the horizontal plane has components (Jaeger & Cook, 1969, p. 20; Mandl, 1988, p. 204).

$$t_1 = -\sigma_1 m_1, \quad t_2 = -\sigma_2 m_2, \quad t_3 = -\sigma_3 m_3 \tag{3.1}$$

where signs have been chosen such that compressive stresses are positive, and the traction vector components are negative when pointing in the negative direction of the coordinate axes. The traction vector can be resolved into a normal and a shear component (σ_v and τ, respectively). The normal component is the overburden pressure

$$\sigma_v = \rho g z(1-\lambda) \tag{3.2}$$

where ρ is density, g acceleration of gravity, z depth, and λ the pore fluid factor (ratio of pore fluid pressure to overburden pressure). This component can also be obtained from

$$\begin{aligned} \sigma_v &= \mathbf{t}\cdot(-\mathbf{m}) \\ &= \sigma_1 m_1^2 + \sigma_2 m_2^2 + \sigma_3 m_3^2 \end{aligned} \tag{3.3}$$

which, writing $\sigma_2 = \sigma_3 + \delta(\sigma_1 - \sigma_3)$ $(0<\delta<1)$ and noting that **m** is a unit vector, becomes

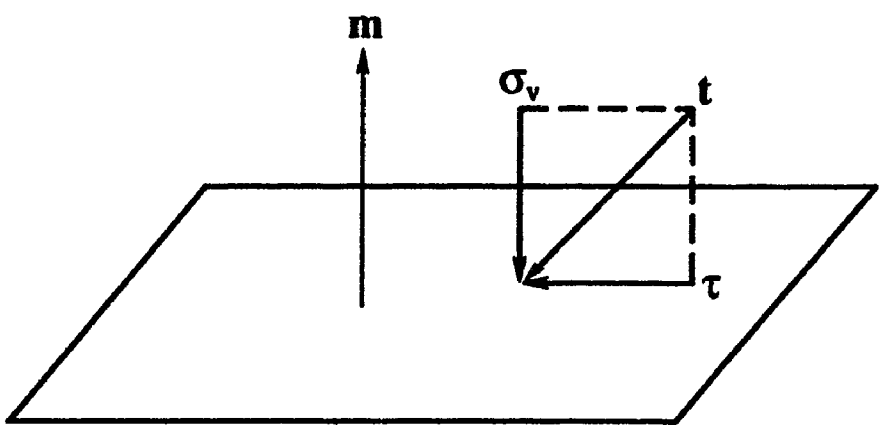

Figure 3.1. Traction vector **t** with its normal (σ_v) and shear (τ) components on the horizontal plane of unit normal **m** with respect to the principal stress directions.

$$\sigma_v = (m_1^2 + \delta m_2^2)(\sigma_1 - \sigma_3) + \sigma_3 \tag{3.4}$$

Comparing equations (3.2) and (3.4), I obtain for the maximum stress difference

$$(\sigma_1 - \sigma_3) = \frac{\rho g z(1-\lambda) - \sigma_3}{m_1^2 + \delta m_2^2} \tag{3.5}$$

When the stresses reach the critical state, i.e., the shear stress on the fault plane equals the fault strength, the maximum stress difference in equation (3.5) becomes the critical stress difference, and shear fracture will occur on planes paralleling the σ_2-axis and making an angle $\psi=(1/2)\tan^{-1}(1/\mu)$ with the σ_1-axis, where μ is the coefficient of internal friction.

The Coulomb-Navier failure criterion can be written as (Jaeger & Cook 1969, p. 87-91)

$$\frac{1}{2}(\sigma_1 - \sigma_3)\sin 2\psi = S + \mu\left[\frac{1}{2}(\sigma_1 - \sigma_3) + \sigma_3 - \frac{1}{2}(\sigma_1 - \sigma_3)\cos 2\psi\right] \tag{3.6}$$

where S is cohesion and ψ the angle between the plane of failure (containing the σ_2-axis) and the σ_1-axis. From equation (3.5), the minimum principal stress σ_3 can be expressed as

$$\sigma_3 = \rho g z(1-\lambda) - (\sigma_1 - \sigma_3)(m_1^2 + \delta m_2^2) \tag{3.7}$$

Substituting equation (3.7) in (3.6), and using the relation $\psi=(1/2)\tan^{-1}(1/\mu)$, I obtain the following relation that holds at failure

$$(\sigma_1 - \sigma_3) = \frac{2\mu\rho g z(1-\lambda) + 2S}{(\mu^2+1)^{1/2} - \mu + 2\mu(m_1^2 + \delta m_2^2)} \tag{3.8}$$

Equation (3.8) gives the critical stress difference for Coulomb-Navier shear fracture in homogeneous, isotropic rocks as a function of material parameters, depth, and orientation of the tectonic stress field. Given values of the material parameters and the principal stress directions, equation (3.8) allows us to calculate the critical stress difference (i.e. the fault strength) at failure

as a function of depth. Some examples are shown in Figure 3.2 for various orientations of the stress field.

In the particular case when one of the principal stress directions is vertical (Andersonian stress states), one obtains: for thrust faulting, $\sigma_3=\sigma_v$, $m_1=m_2=0$, $m_3=1$; for strike-slip faulting, $\sigma_2=\sigma_v$, $m_1=m_3=0$, $m_2=1$; for normal faulting, $\sigma_1=\sigma_v$, $m_1=1$, $m_2=m_3=1$ (σ_v is vertical stress). Substituting these values in equation (3.8), equation (3.8) reduces to equations (2.17), (2.18), and (2.19) derived in Chapter 2 for the two-dimensional case under Andersonian stress systems.

In many two-dimensional analyses of faulting (Hafner, 1951; Sanford, 1959; A. Yin, 1989), it is assumed that the σ_2-axis is horizontal, and the σ_1, σ_3 axes vary with position (this is the case, for instance, that leads to listric normal and thrust faults; see also Mandl (1988)). For such a stress state ($m_2=0$, $m_1\neq0$, $m_3\neq0$) equation (3.8) reduces to

$$(\sigma_1-\sigma_3)=\frac{2\mu\rho g z(1-\lambda)+2S}{(\mu^2+1)^{1/2}+\mu(2m_1^2-1)} \tag{3.9}$$

The critical stress difference required for failure depends on the orientation of the principal stress axes, as the latter affects the normal stress on potential fracture planes. For a complete analysis of faulting, therefore, the determination of principal stress trajectories has to be followed by the determination of the critical stress difference as a function of position (see the discussion by Buck (1990) and A. Yin (1990)).

SLIP ALONG PREEXISTING STRENGTH ANISOTROPIES

Now I assume that the rock contains arbitrarily oriented planes of weakness. Let **n** be a unit vector denoting the normal to such a plane. The directional cosines of **n** in the Cartesian

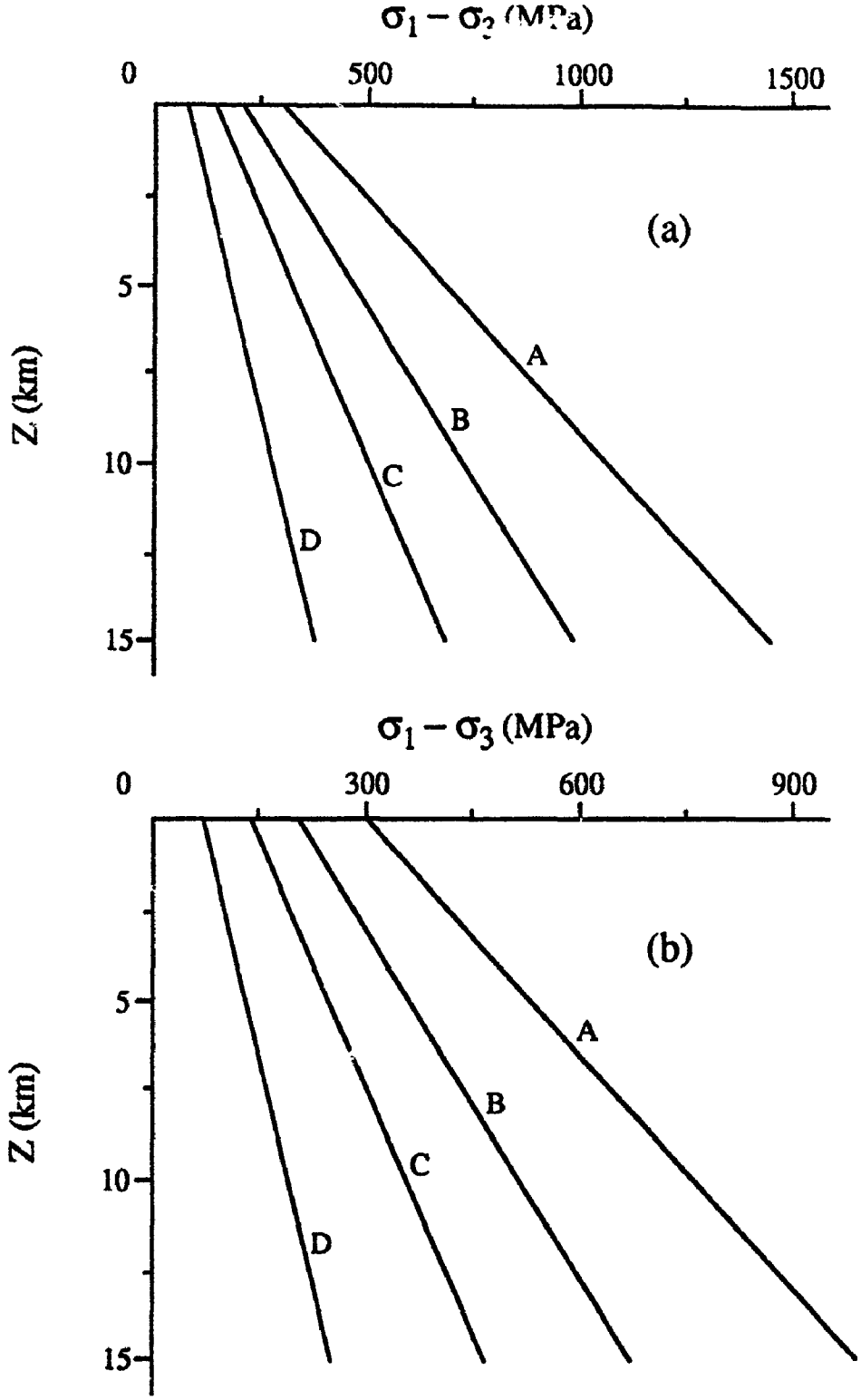

Figure 3.2. Critical stress difference ($\sigma_1 - \sigma_3$) versus depth (z) for faulting in isotropic rock in the case of (a) no pore fluid pressure (λ=0) and (b) hydrostatic pore fluid pressure (λ=0.4). Orientations of the stress field are: (A) σ_3 is vertical (thrust faulting); (B) σ_1, σ_2, and σ_3–axis make an angle 80°, 60°, and 32° with the vertical unit vector **m**, respectively; (C) the σ_1, σ_2, and σ_3–axis make an angle 60°, 60°, and 45° with **m**; (D) σ_1 is vertical (normal faulting). Material parameters are: S=75 MPa, μ=0.75, ρ=2600 kg m^{-3}, and δ=1/2.

coordinate system y_1, y_2, and y_3 (representing the directions of the principal stresses σ_1, σ_2, and σ_3) are $n_i=\cos\xi_i$ (i=1, 2, 3), where ξ_i is the angle between **n** and the y_i–axis (Figure 3.3). The traction vector **t** acting on the plane of weakness has components $t_1=-n_1\sigma_1$, $t_2=-n_2\sigma_2$, $t_3=-n_3\sigma_3$, and its magnitude is

$$t^2 = n_1^2\sigma_1^2 + n_2^2\sigma_2^2 + n_3^2\sigma_3^2 \tag{3.10}$$

The traction vector **t** can be resolved into a normal and a shear component. The normal component, in a manner analogous to equation (3.4), can be written as

$$\begin{aligned}\sigma &= \mathbf{t}\cdot(-\mathbf{n}) \\ &= n_1^2\sigma_1 + n_2^2\sigma_2 + n_3^3\sigma_3 \\ &= (n_1^2 + \delta n_2^2)(\sigma_1 - \sigma_3) + \sigma_3\end{aligned} \tag{3.11}$$

The shear component can be obtained from the relation $\tau^2=t^2-\sigma^2$,

$$\tau^2 = n_1^2\sigma_1^2 + n_2^2\sigma_2^2 + n_3^2\sigma_3^2 - [(n_1^2 + \delta n_2^2)(\sigma_1 - \sigma_3)^2 + \sigma_3]^2 \tag{3.12}$$

Substituting $n_3^2=1-n_1^2-n_2^2$ in equation (3.12), expanding the last term on the left side, and noting that $\sigma_2-\sigma_3=\delta(\sigma_1-\sigma_3)$, it follows that

$$\tau = (\sigma_1 - \sigma_3)[(n_1^2 + \delta^2 n_2^2) - (n_1^2 + \delta n_2^2)^2]^{1/2} \tag{3.13}$$

Thus the Coulomb-Navier criterion can be written as

$$(\sigma_1 - \sigma_3)\left[(n_1^2 + \delta^2 n_2^2) - (n_1^2 + \delta n_2^2)^2\right]^{1/2} = S_0 + \mu_o\left[(n_1^2 + \delta n_2^2)(\sigma_1 - \sigma_3) + \sigma_3\right] \tag{3.14}$$

where S_0, μ_0 are cohesion and friction coefficient of the preexisting strength anisotropy (in general, S_0 is much less than S, and μ_0 is about equal to μ (Scholz (1992)). Substituting the minimum principal stress σ_3 given by equation (3.7) in equation (3.14) and solving for $(\sigma_1-\sigma_3)$ yields

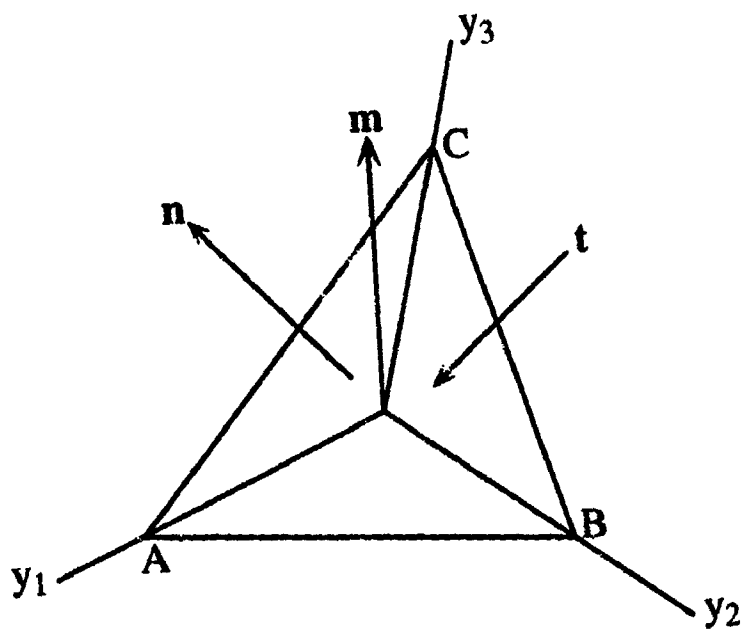

Figure 3.3. Preexisting strength anisotropy (plane ABC) with unit normal **n** in the principal stress system with axes (y_1, y_2, y_3). The unit vector **m** and vector **t** denote the direction of the normal to the horizontal plane and the traction acting on the anisotropy, respectively.

$$(\sigma_1 - \sigma_3) = \frac{\mu_0 \rho g z(1-\lambda) + S_0}{\left[(n_1^2 + \delta^2 n_2^2) - (n_1^2 + \delta n_2^2)^2\right]^{1/2} + \mu_0\left[(m_1^2 + \delta m_2^2) - (n_1^2 + \delta n_2^2)\right]} \tag{3.15}$$

Equation (3.15), which reduces to equations (2.25), (2.26), and (2.27) derived in Chapter 2 if the plane of weakness contains the σ_2-axis and one of the principal stress directions is vertical, gives the critical stress difference for faulting along a strength anisotropy as a function of depth, material parameters, and orientation of stress field and anisotropy. Some examples are given in Figure 3.4 for various orientations of the anisotropy and different material parameters.

At a given depth and for a given orientation of the stress field, faulting will occur along a plane of weakness only for a range of orientations, i.e. those for which the critical stress difference given by equation (3.15) is less than that given by equation (3.8). Outside this range, a new fault forms at an angle $\psi=(1/2)\tan^{-1}(1/\mu)$ with respect to the σ_1-axis and containing the σ_2-axis. Therefore, the limiting range of the orientation of strength anisotropies can be obtained by equating equations (3.15) and (3.8)

$$[(n_1^2 + \delta^2 n_2^2) - (n_1^2 + \delta n_2^2)^2]^{1/2} - \mu_0(n_1^2 + \delta n_2^2) = \frac{\mu_0[(1+\mu^2)^{1/2} - \mu]}{2\mu} + \frac{\mu S_0 - \mu_0 S}{\mu(\sigma_1 - \sigma_3)} \tag{3.16}$$

where the critical stress difference $(\sigma_1 - \sigma_3)$ is given by equation (3.8). For a given component n_i (i=1, 2, 3), equation (3.16) allows calculation of the ranges in the other two components consistent with faulting along pre-existing anisotropies. These reduce to the limiting angles given by equations (2.32), (2.33), and (2.34) for anisotropies containing the σ_2-axis and vertical orientation of one of the principal stresses.

A graphic representation of the limiting range of orientations of strength anisotropies can be obtained by using the three-dimensional Mohr circle (see e.g. Jaeger & Cook 1969, pp. 27-29).

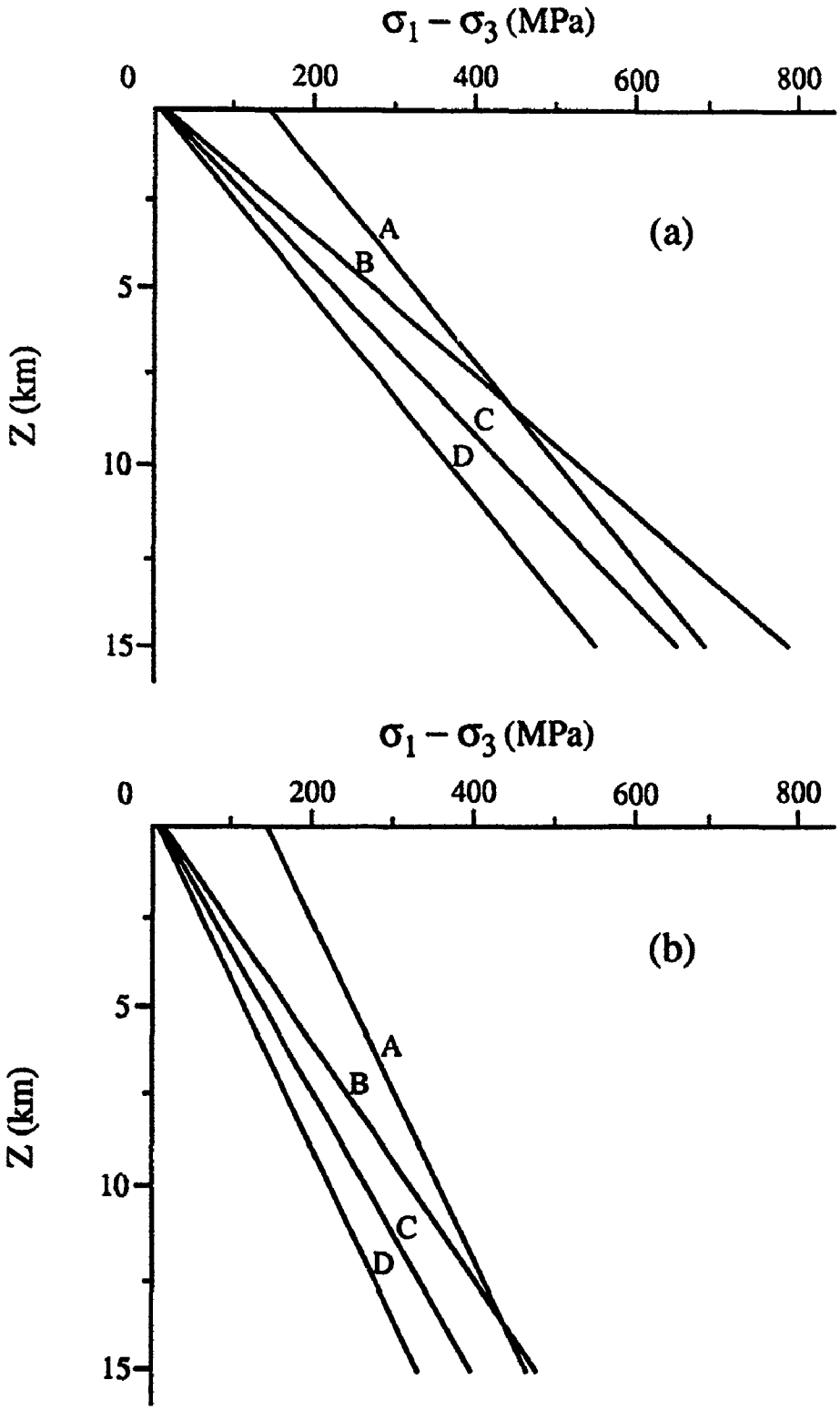

Figure 3.4. Critical stress difference ($\sigma_1 - \sigma_3$) versus depth (z) for faulting under a stress system with orientations of 60°, 60°, and 45° between **m** and σ_1, σ_2, and σ_3–axis, respectively, in the case of (a) no pore fluid pressure (λ=0) and (b) hydrostatic pore fluid pressure (λ=0.4). (A) New fault in isotropic rock; (B) anisotropy with orientation ξ_1=55°, ξ_2=60°, ξ_3=50°; (C) anisopy with orientation ξ_1=70°, ξ_2=60°, ξ_3=37°; (D) most favourably oriented strength anisotropy (ξ_1=90°-1/2tan^{-1}(1/μ_0), ξ_2=90°, ξ_3=1/2tan^{-1}(1/μ_0)). Material parameters are the same as for Figure 3.2, with S_0=5 MPa and μ_0=μ.

With reference to Figure 3.5, the three circles of radii $(\sigma_2-\sigma_3)/2$, $(\sigma_1-\sigma_3)/2$, and $(\sigma_1-\sigma_2)/2$ represent the stress states on planes parallel to σ_1-axis ($n_1=0$), σ_2-axis ($n_2=0$), and σ_3-axis ($n_3=0$), respectively; the planes are arbitrarily oriented with respect to the other two stress axes in each case. Concentric circles (of which only two families are shown in the figure, for simplicity) represent stress states on planes on which a component $n_i=\cos\xi_i$ (i=1, 2, 3) is fixed. The two failure envelopes shown apply to intact rock (parameters S, μ) and strength anisotropies (S_0, μ_0). If for instance ξ_2 (angle between the normal to the plane of weakness and the σ_2-axis) is given, one can immediately read off the range in ξ_1 for which a plane of weakness fails. The range in ξ_3 can be calculated from the condition that **n** is a unit vector, or read off from a three-dimensional Mohr diagram on which all three families of circles are drawn. Figure 3.6 gives some examples of limiting angles for failure along strength anisotropies as a function of depth for various values of material parameters and orientation of the stress field. Note that the limiting angle shown in Figure 3.6 is the angle ψ between the plane of weakness and the σ_1-axis, while ξ_1 above is the angle between the normal to the plane of weakness and the σ_1-axis; $\psi=90°-\xi_1$.

OBLIQUE-SLIP FAULTING

When the stress field is Andersonian and the fracture plane is parallel to the intermediate stress axis, faulting is of necessity either purely dip-slip or purely strike-slip, and oblique-slip faulting (that is, with the slip on the fault plane not being perpendicular or parallel to the strike direction) does not occur. However, when the above restrictions on the orientation of both stress field and strength anisotropies are dropped, oblique-slip faulting becomes possible. On the assumption that the direction of maximum shearing stress and the direction of slip on the fault

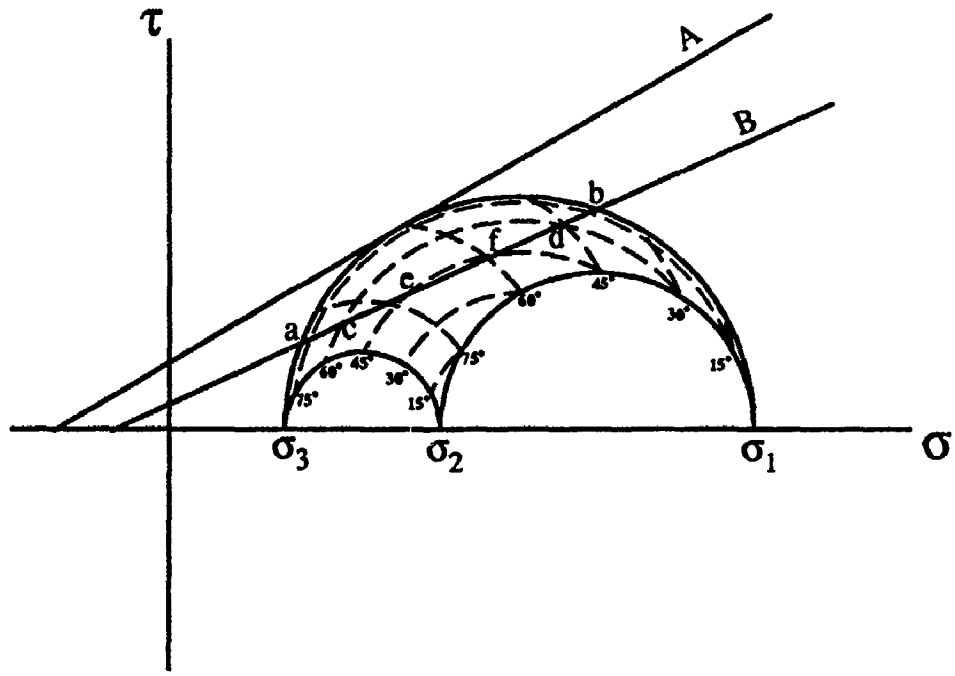

Figure 3.5. Three-dimensional Mohr circle for failure in isotropic rock (envelope A) and along strength anisotropy (envelope B). Dashed circles concentric with full circle with diameter $\sigma_1-\sigma_3$ represent stress states on planes with fixed ξ_2; the other family represents stress states on planes with fixed ξ_1. For a given ξ_2, the range of ξ_1 for which failure occurs along the anisotropy can be read from envelope B. For instance, for $\xi_2=90°$, the limiting range is $a \geq \xi_1 \geq b$; for $\xi_2=60°$, $c \geq \xi_1 \geq d$; and for $\xi_2=45°$, $e \geq \xi_1 \geq f$.

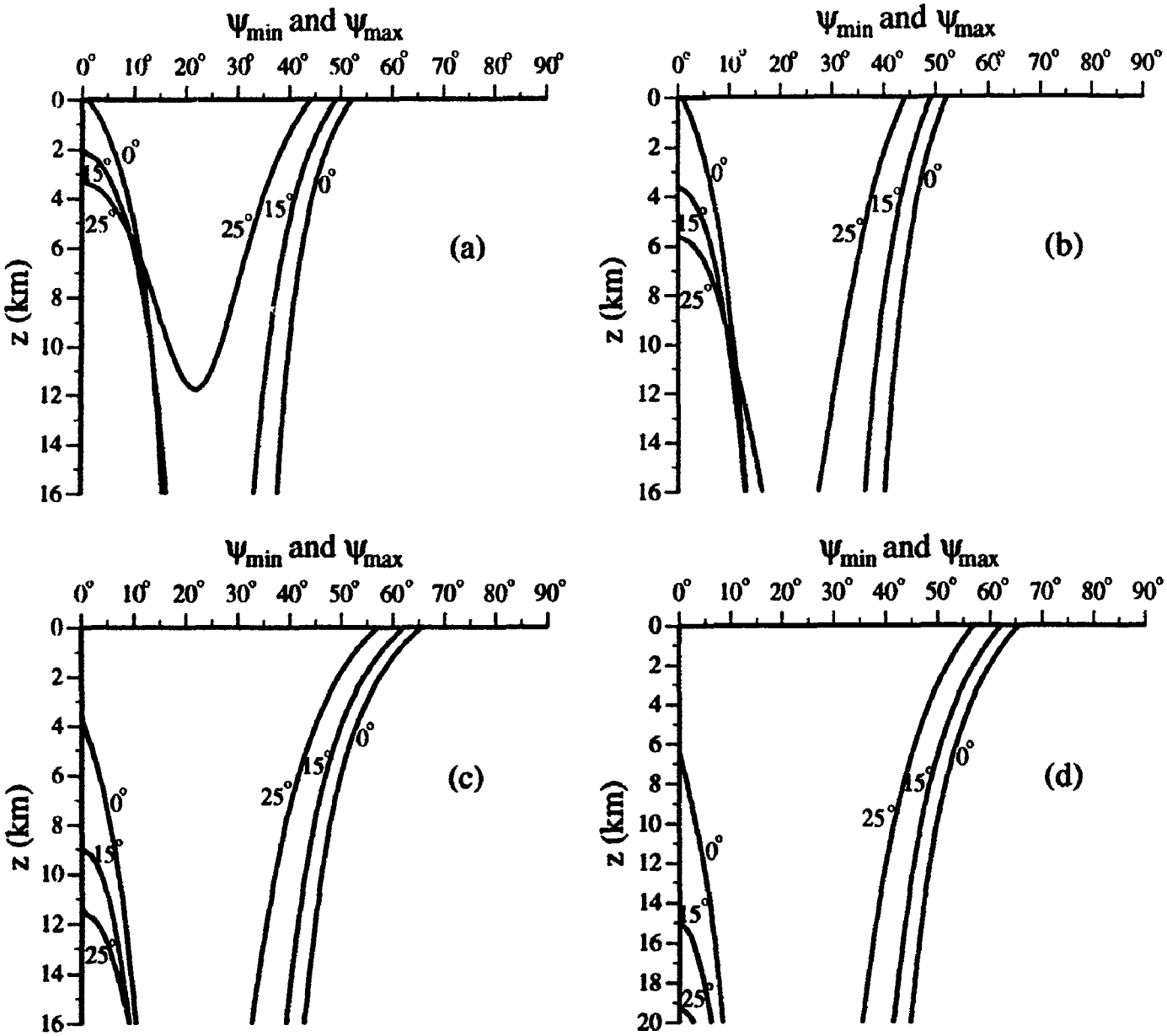

Figure 3.6. The minimum and maximum limiting angles ψ_{min} and ψ_{max} between plane of strength anisotropy and σ_1-axis versus depth for slip along the anisotropy. Values on the curves denote the angle between the plane of anisotropy and σ_2-axis. (a) σ_3 is vertical, λ=0; (b) σ_3 is vertical, λ=0.4; (c) σ_1, σ_2, σ_3-axis oriented 60°, 60°, 45° with respect to the vertical direction (**m**), λ=0; (d) σ_1, σ_2, σ_3-axis oriented 60°, 60°, 45° with respect to **m**, λ=0.4.

plane coincide (Bott, 1959), I analyze in this section the general non-Andersonian case for anisotropic rocks (the Andersonian case has been considered by Bott, 1959; see also Mandl, 1988, pp. 203-206).

With reference to Figure 3.7, let **h** be the unit strike vector in the horizontal direction on the fault plane referred to the Cartesian coordinates y_i (i = 1, 2, 3) coinciding with the principal stress directions. The maximum shear stress on the fault plane and its strike and dip components are denoted by τ, τ_h, and τ_d, respectively. The angle ω (measured clockwise on the fault plane) giving the direction of τ, and therefore the slip direction, with respect to strike, is the quantity that must be expressed in terms of the orientation of the stress system (defined by the unit vector **m**) and the orientation of the fault plane (defined by the unit vector **n**). I call ω the "pitch angle" of slip. Assuming that the unit vector **n** is upward, i.e., considering the case of the stresses acting on the foot-wall, the signs of τ_h and τ_d are defined so that the rightward direction of τ_h and the downward direction of τ_d are positive (Figure 3.7). It follows that $0 \le n_i \le 1$ and $-1 \le m_i \le 1$ in each case.

Since the unit vector **h** is perpendicular to both **n** and **m**, one can write

$$h_1 n_1 + h_2 n_2 + h_3 n_3 = 0 \tag{3.17a}$$

$$h_1 m_1 + h_2 m_2 + h_3 m_3 = 0 \tag{3.17b}$$

$$h_1^2 + h_2^2 + h_3^2 = 1 \tag{3.17c}$$

From equations (3.17a) and (3.17b), we have

$$\frac{h_1}{m_2 n_3 - m_3 n_2} = \frac{h_2}{m_3 n_1 - m_1 n_3} = \frac{h_3}{m_1 n_2 - m_2 n_1} \tag{3.18}$$

Substituting equation (3.18) in equation (3.17c) yields

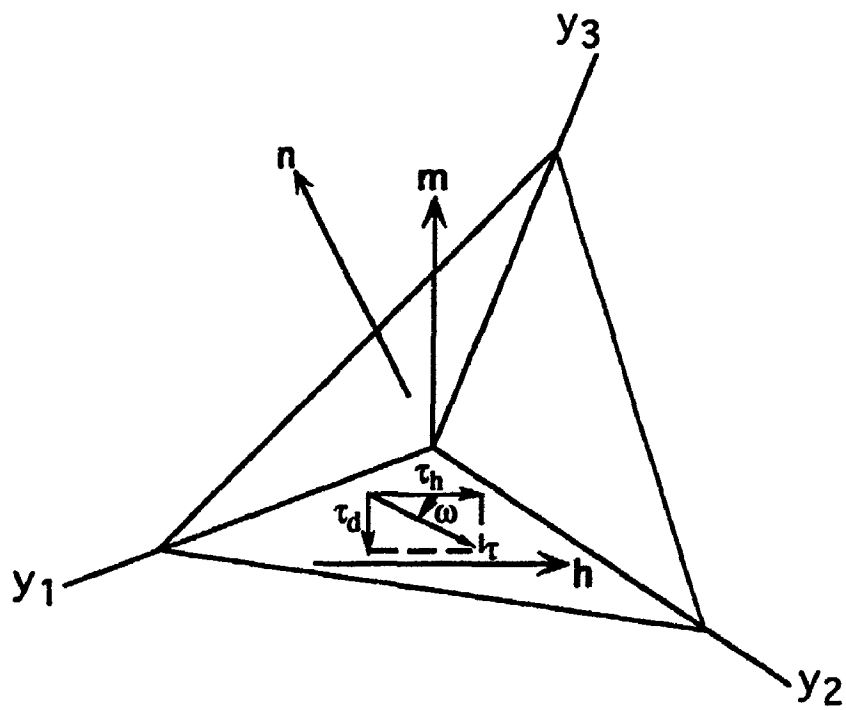

Figure 3.7. Resolution of shear stress τ on fracture plane with normal **n** in the principal stress system with axes (y_1, y_2, y_3) with respect to the vertical **m**. The horizontal unit vector (along the strike) is **h**. The strike and dip component of shear stress are τ_h and τ_d, respectively. The pitch angle ω gives the direction of τ (and consequently of slip) with respect to the horizontal.

$$h_1 = \frac{m_2n_3 - m_3n_2}{\left[(m_2n_3 - m_3n_2)^2 + (m_3n_1 - m_1n_3)^2 + (m_1n_2 - m_2n_1)^2\right]^{1/2}}$$

$$h_2 = \frac{m_3n_1 - m_1n_3}{\left[(m_2n_3 - m_3n_2)^2 + (m_3n_1 - m_1n_3)^2 + (m_1n_2 - m_2n_1)^2\right]^{1/2}} \tag{3.19}$$

$$h_3 = \frac{m_1n_2 - m_2n_1}{\left[(m_2n_3 - m_3n_2)^2 + (m_3n_1 - m_1n_3)^2 + (m_1n_2 - m_2n_1)^2\right]^{1/2}}$$

The strike component of the maximum shear stress is given by $\tau_h = \mathbf{t} \cdot \mathbf{h}$, where $\mathbf{t}$ is the traction vector acting on the fracture plane; that is

$$\tau_h = -\sigma_1 n_1 h_1 - \sigma_2 n_2 h_2 - \sigma_3 n_3 h_3 \tag{3.20}$$

and, using equations (3.19) and the identity $\sigma_2 = \sigma_3 + \delta(\sigma_1 - \sigma_3)$, it follows that

$$\tau_h = \frac{(\sigma_1 - \sigma_3)[(m_3n_1n_2 - m_2n_1n_3) - \delta(m_3n_1n_2 - m_1n_2n_3)]}{[(m_2n_3 - m_3n_2)^2 + (m_3n_1 - m_1n_3)^2 + (m_1n_2 - m_2n_1)^2]^{1/2}} \tag{3.21}$$

The dip component is related to maximum shear stress and strike component by the relation $\tau_d^2 = \tau^2 - \tau_h^2$. Recalling equation (3.13) one can write

$$\tau_d = \pm(\sigma_1 - \sigma_3)\left\{(n_1^2 + \delta^2 n_2^2) - (n_1^2 + \delta n_2^2)^2 - \frac{[(m_3n_1n_2 - m_2n_1n_3) - \delta(m_3n_1n_2 - m_1n_2n_3)]^2}{(m_2n_3 - m_3n_2)^2 + (m_3n_1 - m_1n_3)^2 + (m_1n_2 - m_2n_1)^2}\right\}^{1/2} \tag{3.22}$$

Unlike equation (3.21), which gives both the magnitude and the sign of τ_h, equation (3.22) gives only the magnitude of τ_d. The sign of τ_d can be determined by the product of the cosine of the angle between τ and $\mathbf{m}$, i.e.

$$\cos(\tau,\mathbf{m}) = \frac{(n_1^2+\delta n_2^2)(n_1m_1+n_2m_2+n_3m_3) - (n_1m_1+\delta n_2m_2)}{[(n_1^2+\delta^2 n_2^2)-(n_1^2+\delta n_2^2)^2]^{1/2}} \tag{3.23}$$

If $\cos(\tau, \mathbf{m})\cos(\mathbf{n}, \mathbf{m})\leq 0$, τ_d in equation (3.23) takes the plus sign; otherwise it takes the minus sign.

The pitch angle is therefore given by

$$\tan\omega = \frac{\tau_d}{\tau_h}$$

$$= \pm\left\{\frac{[(n_1^2+\delta^2 n_2^2)-(n_1^2+\delta n_2^2)^2][(m_2n_3-m_3n_2)^2+(m_3n_1-m_1n_3)^2+(m_1n_2-m_2n_1)^2]}{[(m_3n_1n_2-m_2n_1n_3-\delta(m_3n_1n_2-m_1n_2n_3)]^2}-1\right\}^{1/2} \tag{3.24}$$

The value of the pitch angle depends on the signs of τ_h and τ_d. For $\tau_h>0$, $\tau_d\geq 0$, $0°\leq\omega<90°$; for $\tau_h\leq 0$, $\tau_d>0$, $90°\leq\omega<180°$; for $\tau_h<0$, $\tau_d\leq 0$, $180°\leq\omega<270°$; and for $\tau_h\geq 0$, $\tau_d<0$, $270°\leq\omega<360°$.

Equations (3.21), (3.22), and (3.24) give the strike component, the dip component, and the pitch angle of the maximum shear stress (and consequently the motion direction) on the fault plane, for any orientation of stress field and fault plane. Pure dip-slip and pure strike-slip faulting are particular cases, depending for their occurrence on the vertical orientation of one principal stress axis and either the absence or a particular orientation (containing the σ_2-axis) of strength anisotropies. In all other cases, faulting is oblique-slip.

A kinematic classification of faults, based on the value of the angle ω, is shown in Figure 3.8. A similar classification, for the special case of Andersonian stress systems, has been given by Bott (1959), based on the relative values of principal stresses.

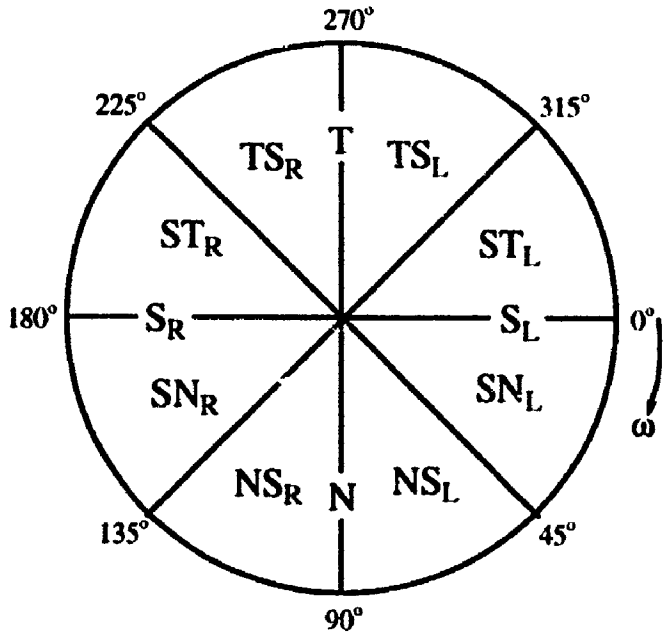

Figure 3.8. Kinematic classification of faults based on the angle ω between the direction of slip and the horizontal. Purely normal, thrust, and strike-slip faults are denoted by N, T, and S, respectively. Combinations of letters denote oblique-slip faulting, with the first letter referring to the predominant component of slip. Subscripts L and R denote left-lateral and right-lateral slip, respectively.

EXAMPLES

In order to predict the possible types of faulting under given conditions, I consider different cases separately. For the *formation of new faults in non-Andersonian stress systems*, the fracture plane contains the intermediate stress direction (n_2=0), and $n_1^2+n_3^2=1$. Under these conditions, equations (3.21), (3.22), and (3.24) reduce to

$$\tau_h = \frac{-m_2 n_1 n_3(\sigma_1 - \sigma_3)}{[(m_3 n_1 - m_1 n_3)^2 + m_2^2]^{1/2}} \tag{3.25a}$$

$$\tau_d = \pm \frac{(m_3 n_1 - m_1 n_3) n_1 n_3(\sigma_1 - \sigma_3)}{[(m_3 n_1 - m_1 n_3)^2 + m_2^2]^{1/2}} \tag{3.25b}$$

$$\tan\omega = \pm \frac{m_3 n_1 - m_1 n_3}{m_2} \tag{3.25c}$$

where the sign of τ_d is determined by equation (3.23). By substituting the critical stress difference (equation (3.8)), the strike and dip components of the maximum shear stress on the fault plane can be expressed in terms of material parameters, depth, and orientation of the stress field, that is

$$\tau_h = \frac{-m_2 n_1 n_3[2\mu\rho g z(1-\lambda) + 2S]}{[(m_3 n_1 - m_1 n_3)^2 + m_2^2]^{1/2}[(\mu^2+1)^{1/2} - \mu + 2\mu(m_1^2 + \delta m_2^2)]} \tag{3.26a}$$

$$\tau_d = \pm \frac{[(m_3 n_1 - m_1 n_3) n_1 n_3][2\mu\rho g z(1-\lambda) + 2S]}{[(m_3 n_1 - m_1 n_3)^2 + m_2^2]^{1/2}[(\mu^2+1)^{1/2} - \mu + 2\mu(m_1^2 + \delta m_2^2)]} \tag{3.26b}$$

The type of faulting along new fracture planes as a function of the orientation of the stress

field can be determined from equations (3.26a), (3.26b), and (3.25c). As $m_1^2+m_2^2+m_3^2=1$, it is convenient to display the results on a triangular diagram, similar to the construction used in petrology, where the coordinates m_i^2 of any point are given by the distance from the side opposite to the vertex where $m_i^2=1$. Figure 3.9 shows the different types of faulting in terms of the orientation of the stress system. Each point in the diagram represents two potential conjugate fault planes, containing the intermediate stress axis and making an angle $\psi=(1/2)\tan^{-1}(1/\mu)$ with the σ_1-axis. Results are presented for the case where, on a stereographic projection, the principal stress axes, σ_1, σ_2, σ_3, are arranged in anticlockwise order; if they are arranged in clockwise order the type of faulting does not change, but the sense of slip is reversed. Naturally, oblique-slip faulting is the rule, unless one principal stress direction is vertical or the σ_2-axis is horizontal. In the exceptional case where σ_2-axis is horizontal ($m_2=0$) and values of m_1 and m_3 are in the middle-range, thrust and normal faults can coexist in conjugate sets. Also, pure strike-slip along dipping planes is possible. In situations where the orientation of the stress field is known and the rock is isotropic, diagrams such as the one shown in Figure 3.9, together with equations (3.26a), (3.26b), and (3.25c) allow the prediction of the fault plane orientation and slip direction.

Next I examine the case of *Andersonian stress systems in rocks containing strength anisotropies* (also considered by Mandl 1988, pp. 203-206). Under these conditions, new faults are always pure dip-slip or strike-slip, but faulting along preexisting strength anisotropies are commonly oblique-slip. Three different stress systems are possible.

If σ_1 is vertical ($m_1=\pm1$, $m_2=m_3=0$), equations (3.21), (3.22), and (3.24) become

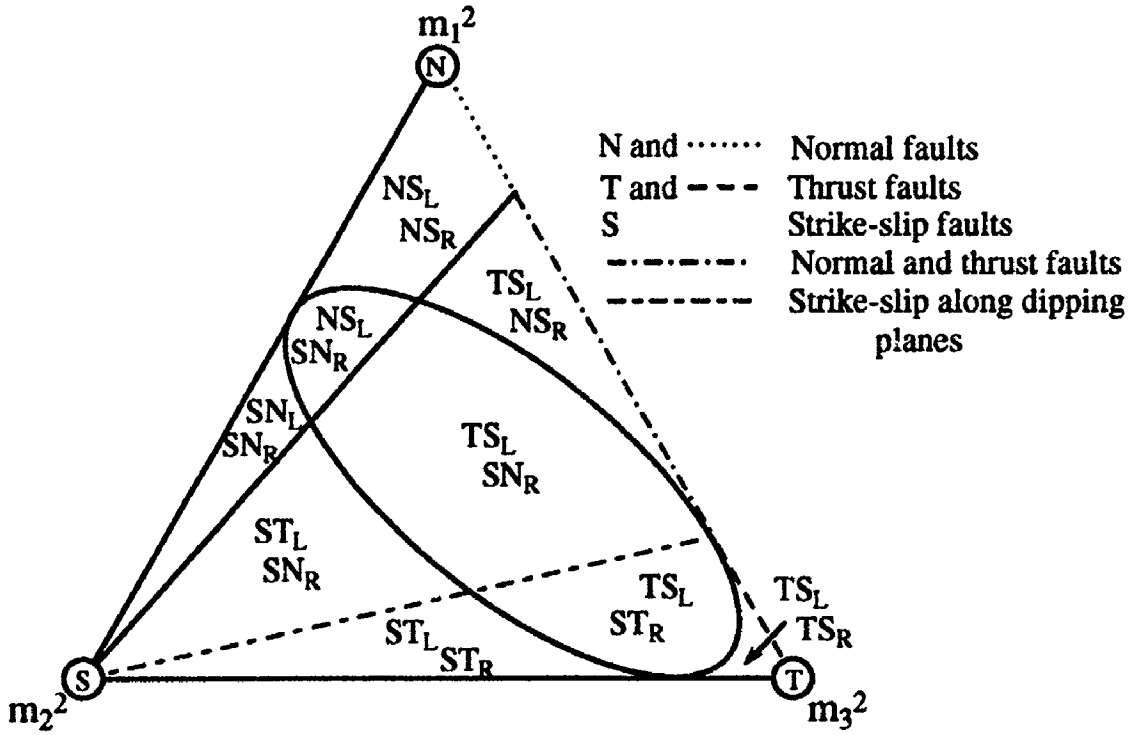

Figure 3.9. Faulting regimes in isotropic rock as a function of the orientations of the three principal stress axes with respect to the vertical unit vector **m**. In each field within the triangle, two conjugate sets of faults are predicted. Normal, thrust, and strike-slip faults of Andersonian type occur only at the vertices. For m_2=0 (horizontal intermediate stress direction) and middle-range values of m_1 and m_3, normal and thrust faults can coexist in conjugate sets. Strike-slip along dipping planes can occur for a fixed m_1/m_3 ratio. In other cases, faulting is generally oblique-slip.

$$\tau_h = \frac{\delta m_1 n_2 n_3 (\sigma_1 - \sigma_3)}{(n_2^2 + n_3^2)^{1/2}} \tag{3.27a}$$

$$\tau_d = \pm \frac{n_1 [n_2^2 (1-\delta) + n_3^2](\sigma_1 - \sigma_3)}{(n_2^2 + n_3^2)^{1/2}} \tag{3.27b}$$

$$\tan\omega = \pm \frac{n_1 [n_2^2 (1-\delta) + n_3^2]}{\delta n_2 n_3} \tag{3.27c}$$

If σ_2 is vertical ($m_1=m_3=0$, $m_2=\pm 1$), we have

$$\tau_h = -\frac{m_2 n_1 n_3 (\sigma_1 - \sigma_3)}{(n_1^2 + n_3^2)^{1/2}} \tag{3.28a}$$

$$\tau_d = \pm \frac{n_2 [n_1^2 (1-\delta) - \delta n_3^2](\sigma_1 - \sigma_3)}{(n_1^2 + n_3^2)^{1/2}} \tag{3.28b}$$

$$\tan\omega = \pm \frac{n_2 [n_1^2 (1-\delta) - \delta n_3^2]}{n_1 n_3} \tag{3.28c}$$

Finally, if σ_3 is vertical ($m_1=m_2=0$, $m_3=\pm 1$)

$$\tau_h = \frac{m_3 n_1 n_2 (1-\delta)(\sigma_1 - \sigma_3)}{(n_1^2 + n_2^2)^{1/2}} \tag{3.29a}$$

$$\tau_d = \pm \frac{n_3 (n_1^2 + \delta n_2^2)(\sigma_1 - \sigma_3)}{(n_1^2 + n_2^2)^{1/2}} \tag{3.29b}$$

$$\tan\omega = \pm\frac{n_3(n_1^2+\delta n_2^2)}{n_1 n_2(\delta-1)} \tag{3.29c}$$

In equations (3.27)-(3.29), the sign of τ_d is determined by equation (3.23) and the critical stress difference (σ_1-σ_3) is given (3.15). Substituting the appropriate value of (σ_1-σ_3), τ_h and τ_d for the three special cases (Andersonian stress systems) can be expressed as functions of material parameters, depth, and orientation of strength anisotropy. For instance, if σ_3 is vertical, equations (3.27a) and (3.27b) can be rewritten as

$$\tau_h = \frac{m_3 n_1 n_2(1-\delta)[\mu_0\rho gz(1-\lambda)+S_0]}{(n_1^2+n_2^2)^{1/2}\{[(n_1^2+\delta^2 n_2^2)-(n_1^2+\delta n_2^2)^2]^{1/2}-\mu_0(n_1^2+\delta n_2^2)\}} \tag{3.30a}$$

$$\tau_d = \pm\frac{n_3(n_1^2+\delta n_2^2)[\mu_0\rho gz(1-\lambda)+S_0]}{(n_1^2+n_2^2)^{1/2}\{[(n_1^2+\delta^2 n_2^2)-(n_1^2+\delta n_2^2)^2]^{1/2}-\mu_0(n_1^2+\delta n_2^2)\}} \tag{3.30b}$$

The above relations reduce to those for normal, strike-slip, and thrust faults, respectively, if faulting occurs along a new fracture plane (n_2=0). However, oblique-slip faulting takes place if favourably oriented planes of weakness are present. The results can be presented on triangular diagrams with coordinates n_i^2. Figure 3.10 illustrates both the limiting angles for faulting along strength anisotropies and the faulting regimes. The limiting angles are a function of depth (see equation (3.16)); z=10 km is the case shown. Faulting along strength anisotropies does not occur in the shaded areas where new faults form (normal, strike-slip, or thrust according to which principal stress direction is vertical). Pure dip-slip and pure strike-slip faulting can occur along strength anisotropies which contain the σ_1 or σ_2-axis. In all other cases, faulting is oblique-slip.

Faulting in the most general case of non-Andersonian stress systems in rocks containing strength anisotropies can be predicted using the general equations (3.21), (3.22), and (3.24).

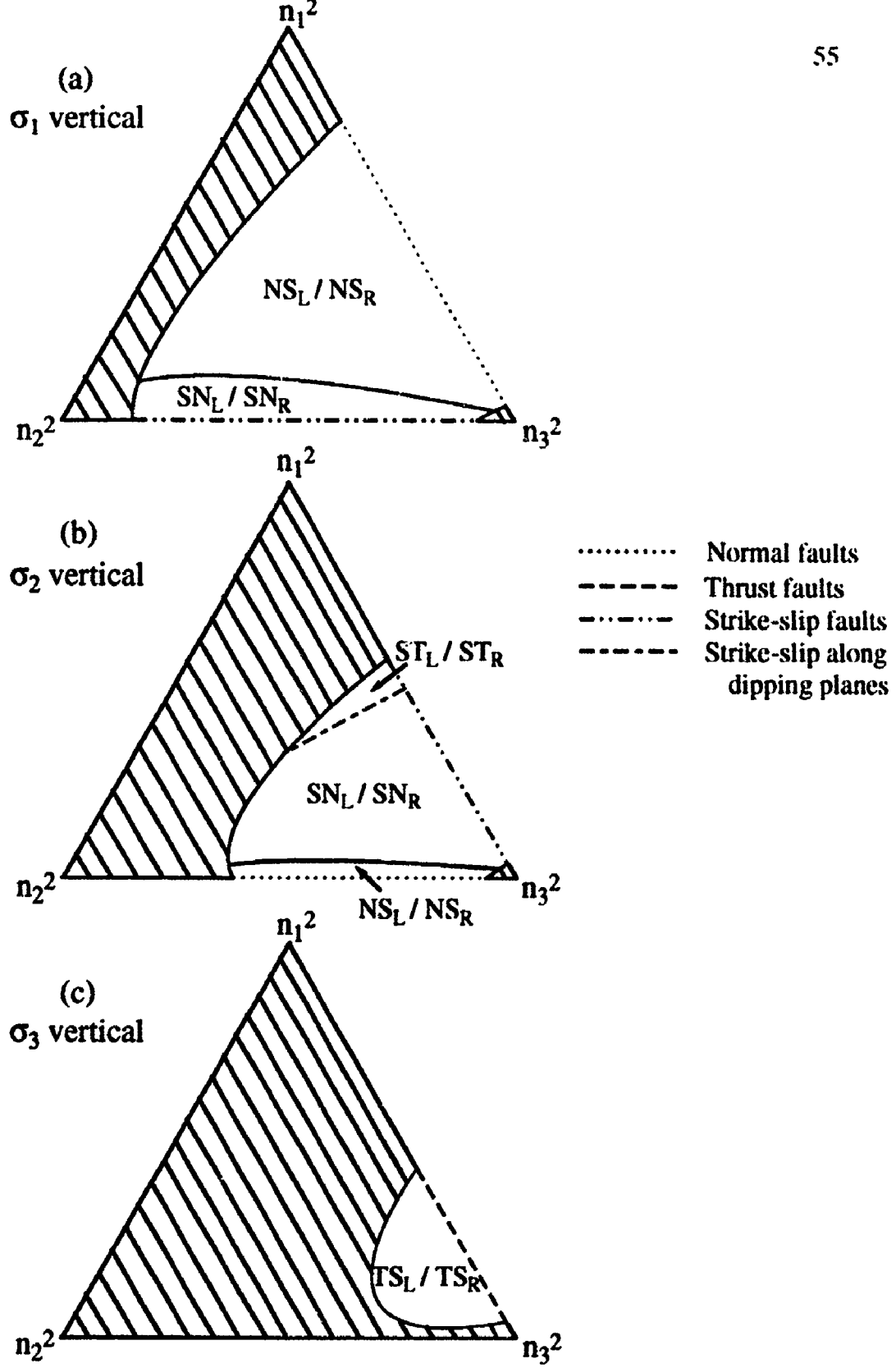

Figure 3.10. Faulting regimes in rocks containing strength anisotropies under Andersonian stress system as a function of the orientation **n** of the anisotropy. (a)-(c) refer to different vertical principal stress. Calculations are for z=10 km, S=75 MPa, S_0=5 MPa, $\mu=\mu_0=0.75$, ρ=2600 kg m^{-3}, λ=0.4, and δ=1/2. The shaded areas denote values of **n** for which new faults (of the type appropriate to the vertical principal stress) form. Faulting along preexisting planes of weakness, with slip as shown, occurs in the unshaded areas.

However, the results cannot be simply presented on triangular diagrams.

CONCLUSIONS

The common occurrence of oblique-slip faults and of faults having dip angles other than those predicted for "standard" stress states are indications of the existence of non-Andersonian stress systems and of fault reactivation. However, a general theory of faulting in anisotropic rocks under non-Andersonian stress systems has not been formulated so far. In this chapter, I have provided simple expressions for the critical stress difference for Coulomb-Navier shear fracture in both isotropic rock and anisotropic rock as a function of material parameters, pore fluid pressure, depth, orientation of the stress field and orientation of anisotropies. The expressions can be used in stress analyses, to complement the calculation of stress magnitude and trajectories, in order to assess the likelihood of faulting in a given tectonic environment (see e.g. A. Yin 1989, and the discussion by Buck 1990 and A. Yin 1990). They are also useful for calculation of the upper crust strength under a variety of tectonic environments (Ranalli and Murphy, 1987; Lowe and Ranalli, 1993).

An expression has been given for calculating the limiting range of orientations of strength anisotropies (within which faulting occurs along preexisting strength anisotropies rather than along fresh planes in homogeneous, isotropic rocks) as a function of material parameters, pore fluid pressure, depth, and orientation of the stress field. This extends the previous two-dimensional treatment in Chapter 1, and makes it possible to extend to three dimensions two-dimensional analyses of fault reactivation and rotation (see e.g. Sibson, 1985; Nur et al., 1986; 1989; Ivins et al., 1990).

With respect to oblique-slip faulting resulting from non-Andersonian stress systems, strength anisotropies not being parallel to the intermediate stress axis, or both, explicit expressions have been given for dip and strike components of the maximum shear stress and the slip direction on the fault plane, in terms of critical stress difference (that is, material parameters and depth) and orientations of stress system and strength anisotropy, thereby extending previous analyses by Bott (1959) and Mandl (1988).

These results have been synthesized graphically by means of triangular diagrams, where expected type of faulting is given as a function of stress orientations (for new faults), or as a function of anisotropy orientation (for slip along preexisting faults). A variety of tectonic environments, with their relevant faulting patterns, are thus amenable to analysis on the basis of a simple direct application of the Coulomb-Navier criterion.

REFERENCES

Anderson, E. M., The dynamics of Faulting, *Trans. Geol. Soc. Edin., 8*, 393-402, 1905.

Anderson, E. M., *The Dynamics of Faulting and Dyke Formation*, 2nd edn, Oliver & Boyd, Edinburgh, 1951.

Bott, M. H. P., The mechanics of oblique slip faulting, *Geol. Mag., 96*, 109-117, 1959.

Buck, W. R., Comment on "Origin of regional, rooted low-angle normal faults: a mechanical model and its tectonic implications" by An Yin, *Tectonics, 9*, 545-546, 1990.

Hafner, W., Stress distribution and faulting, *Geol. Soc. Am. Bull., 62*, 373-398, 1951.

Ivins, E. R., T. H. Dixon, and M. P. Golombek, Extensional reactivation of an abandoned thrust: a bound on shallowing in the brittle regime, *J. Struct. Geol. 12*, 303-314, 1990.

Jaeger, J. C. and N. G. W. Cook, *Fundamentals of Rock Mechanics*, 3rd edn, Chapman and hall, London, 1969.

Lowe, C., and G. Ranalli, Density, temperature, and rheological models for the southeastern Canadian Cordillera: implications for its geodynamic evolution, *Can. J. Earth Sci., 30*, 77-93, 1993.

Mandl, G., *Mechanics of Tectonic Faulting*, Elsevier, Amsterdam, 1988.

Nur, A., H. Ron, and O. Scotti, Fault mechanics and the kinematics of block rotations, *Geology, 14*, 746-749, 1986.

Nur, A., H. Ron, and O. Scotti, Kinematics and mechanics of tectonic block rotation, *American Geophysical Union. Geophysical Monograph, 49*, 31-46, 1989.

Ranalli, G., *Rheology of the Earth*, Allen and Unwin, London, 1987.

Ranalli, G., and D. C. Murphy, Rheological stratification of the lithosphere, *Tectonophysics,*

132, 281-295, 1987.

Sanford, A. R., Analytical and experimental study of simple geological structure, *Bull. Geolo. Soc. Am.*, *70*, 19-51, 1959.

Scholz, C. H., *The Mechanics of Earthquake and Faulting*, Cambridge University Press, Cambridge, 1990.

Sibson, R. H., Frictional constraints on thrust, wrench, and normal faults, *Nature*, *249*, 542-544, 1974.

Sibson, R. H., A note on fault reactivation, *J. Strut. Geol.*, *7*, 751-754, 1985.

Yin, A., Origin of regional, rooted low-angle normal faults: a mechanical model and its tectonic implications, *Tectonics*, *8*, 469-482, 1989.

Yin, A., Reply, *Tectonics*, *9*, 547-549, 1990.

Chapter 4

Determination of Tectonic Stress Field from Fault-Slip Data: a New Probabilistic Model

ABSTRACT

Probability theory and spherical statistics are introduced to the inversion of the tectonic stress field from fault slip and earthquake focal mechanism data. On the assumptions that (1) slip and shear stress direction on the fault plane coincide, and (2) measured slip direction and fault plane orientation are random variables following the von Mises and the Fisher distribution, respectively, the effects of measurement errors in both variables on stress field inversion are considered. Both probabilistic distribution of the predicted shear stress direction on the fault plane and distribution of the misfit angle between the predicted shear stress and the measured slip direction are evaluated by a numerical method and are found to follow approximately the von Mises distribution, with the concentration parameter varying from infinity to zero according to the orientation of the fault plane, the direction of the principal stress axes and the stress shape parameter.

Measurement errors in both slip direction and fault plane orientation give rise to misfit angles between the predicted shear stress and the measured slip direction even if the tectonic stress field is uniform. A new inversion method is proposed that takes both measurement errors simultaneously into account. It is proven that several existing methods are special cases of this inversion method. The new procedure makes it possible to evaluate statistically the extent and

significance of the deviations of the stress field from uniformity, i.e., the likelihood that a given fault population originates from a uniform tectonic stress field. For sufficiently large sample size, the misfit angles should belong to a von Mises family if the stress field is uniform. A significant deviation from a von Mises distribution implies that the tectonic stress field is not uniform.

Three examples of application of the new inversion method are presented, using field fault data from Greece and Japan available in the literature. The results are compared with those obtained from previous methods, and the uncertainties in the inverted stress field are assessed. Although these examples are taken from field fault measurements, the same method can be applied to focal mechanism data.

INTRODUCTION

The determination of the tectonic stress field is one of the major concerns in tectonics and seismology. Geological and seismological evidence demonstrate that faulting in anisotropic rocks is often kinematically controlled by preexisting zones of weakness. Consequently, different fault mechanisms in a given region may result from a uniform stress field. Following the assumption that the slip direction coincides with the maximum shear stress direction on the fault plane (Bott, 1959), Carey and Brunier (1974) made the first attempt to determine the tectonic stress field from inversion of a population of faults of measured orientations and slip directions. Since then, various methods have been proposed to determine the paleostress field, using fault orientations and slip directions, and the contemporary stress field, using earthquake focal mechanisms (Angelier, 1979; Etchecopar et al., 1981; Angelier et al., 1982; Angelier, 1984; Gephart and Forsyth, 1984; Michael, 1984; Gephart, 1985; Reches, 1987; Angelier, 1990). These methods have been applied to many areas with different tectonic settings (Vasseur et al., 1983; Gephart and Forsyth, 1985; Carey-Gailhardis and Mercier, 1987; Lana and Correig, 1987; Michael, 1987; Angelier, 1989; Huang and Angelier, 1989; Bergerat et al., 1990; Caldentey and Lana, 1990; Vetter, 1990; Fleischmann and Nemcok, 1991; Will and Powell, 1991).

The direction of maximum shear stress on a fault plane can be expressed as a function of the principal stress directions, the ratio of stress differences and the orientation of fault plane (Bott, 1959; Angelier, 1979; Célérier, 1988; also see Chapter 3 of this thesis). On the assumption that the direction of slip coincides with the shear stress direction, the direction of slip on a fault plane can then be obtained immediately provided the stress field is known (direct problem). In the inversion problem, the aim is to find a stress field under which the predicted shear stress

directions are compatible with the measured slip directions on a set of faults of measured orientation. Therefore, the central theme of stress inversion deals with the treatment of the misfit angle between the predicted maximum shear stress and the measured slip direction on each fault. Although a number of inversion methods have been devised, there are still some problems which have not been satisfactorily dealt with. This is reflected in the fact that application of different methods to the same data set yields significantly different stress solutions (Angelier, 1990; Gephart, 1990). Furthermore, the probabilistic basis and implications of different methods are unclear. All methods (except that proposed by Angelier et al. (1982)) take into account separately either the uncertainty in slip direction or the uncertainty in fault plane orientation, although it has been realized that both kinds of measurement errors give rise to misfit angles, since errors in fault plane orientation induce errors in predicted shear stress direction (Angelier et al., 1984; Gephart and Forsyth, 1984; Gephart, 1990). A model is needed to take simultaneously into account effects of both uncertainties on stress inversion. In addition, all previous methods assume a uniform stress field. No statistical approaches are available to test this hypothesis.

In this chapter, I propose a new model through which probability theory and spherical statistics are introduced to stress inversion. The basic idea is the treatment of both measurement errors in slip direction and fault plane orientation as random variables, and the assumption that their probability distributions are known and of general nature in spherical statistics. The new method allows not only to take simultaneously into account both slip and fault plane uncertainties, but also to evaluate statistically the extent and significance of the deviation of the resolved stress field from uniformity. I consider here only the geometric constraint (i.e., the constraint posed by the slip direction on the stress field). The inversion problem dealing with the mechanical constraint (i.e., the constraint posed by the magnitude of shear and normal stress on

the stress field; Reches, 1987; Célérier, 1988) will be treated in the next chapter.

GENERAL ASSUMPTIONS

Fault plane orientation (denoted by azimuth and dip angle of the plane, or by trend and plunge of the normal to the plane) is measured in space (on the sphere), and can be modeled as a bivariate distribution. Directions or directional measurement errors on the sphere are most generally modeled in terms of the Fisher distribution (Mardia, 1972, pp. 228-230; Fisher et al., 1987, pp. 86-88) which is analogous to the isotropic bivariate normal distribution on the plane. Slip direction (usually denoted by the pitch angle between the striation and the strike direction) is measured on the fault plane, and is therefore a one-dimensional random variable. The von Mises distribution, much as the normal (Gaussian) distribution models measurement errors on the line, serves as a probability model for directions or directional measurement errors on a plane (i.e., on the circle) (Mardia, 1972, pp. 57-68; Fisher et al., 1987, pp. 81-83). Alternatively, slip direction can also be measured in space and modeled by the Fisher distribution, such as in the case of earthquake focal mechanism data for which the slip direction is the normal to the auxiliary plane. However, it can be proven that this reduces to the von Mises distribution if the direction of slip is described in terms of the pitch angle (Fisher et al., 1987, p. 86). That is to say, slip direction on the fault plane can be modelled by the von Mises distribution no matter how it is measured.

All the previous methods of stress inversion are based on the following two assumptions (1) the slip direction coincides with the shear stress direction on any fault plane; (2) the stress field in a region is spatially and temporally uniform. In this chapter, I keep the first assumption

and drop the second. I also assume that the measured slip direction and fault plane orientation are random variables, obeying the von Mises and the Fisher distribution respectively. Whether or not the stress field is uniform depends on the data measured. Hereafter, the notation rv denotes random variable, and VM, F, N denote the von Mises, the Fisher, and the normal distribution respectively. Following the conventional notation, a random variable is written in upper case and its value in lower case.

Let Ω be a rv, representing the pitch angle of striation on a given fault (Figure 4.1). Its distribution is $VM(\omega_0, \kappa)$, and the probability density can be written as (Mardia, 1972, p. 57; Fisher et al., 1987, pp. 81-82)

$$f(\omega) = \frac{1}{2\pi I_0(\kappa)} \exp[\kappa \cos(\omega - \omega_0)], \qquad 0 \le \omega < 2\pi \tag{4.1}$$

where ω is measured in radians. The modified Bessel function $I_0(\kappa)$ is given by

$$I_0(\kappa) = 1 + \frac{(\frac{\kappa}{2})^2}{(1!)^2} + \frac{(\frac{\kappa}{2})^4}{(2!)^2} + \frac{(\frac{\kappa}{2})^6}{(3!)^2} \quad \cdots\cdots \tag{4.2}$$

The parameters ω_0 and κ, related to location and shape, are the mean direction and concentration parameter respectively; ω_0 and $1/\kappa$ behave like the mean and the variance in distributions on the line.

The von Mises distribution has a close relationship with the normal distribution. Substituting $v=1/\kappa$ in the normal distribution, where v is the variance, $N(\omega_0, 1/\kappa)$ and $VM(\omega_0, \kappa)$ agree very closely subject to the condition that κ is large (say, $\kappa>3$, corresponding to the standard deviation $v^{1/2}<33°$) (Mardia, 1972, p. 68; Fisher et al., 1987, p. 82). Figure 4.2 shows some examples of the comparison of the two distributions for different κ. This implies that rv Ω can also be modeled by the normal distribution because the standard deviation of measurement

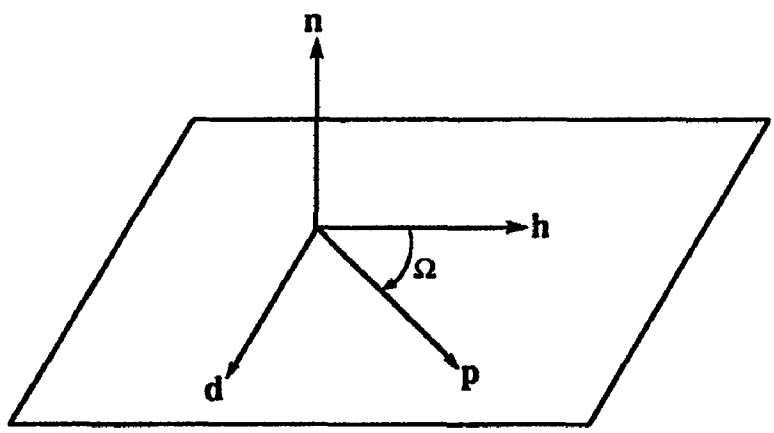

Figure 4.1. On a fault plane with unit normal **n**, the pitch angle Ω is measured clockwise from the strike denoted by unit vector **h**. The dip and slip directions are denoted by the unit vectors **d** and **p**, respectively.

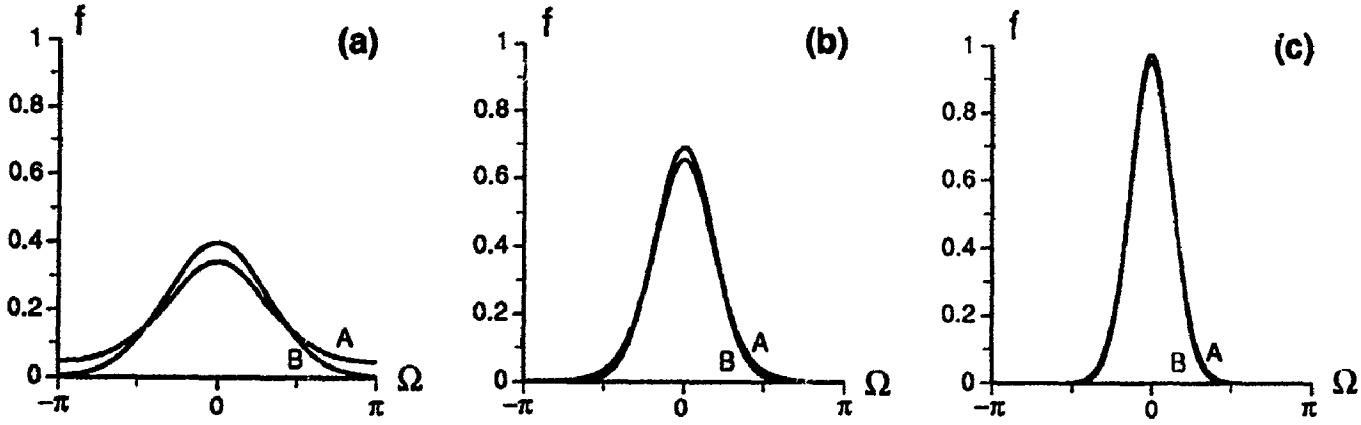

Figure 4.2. Comparison between the von Mises distribution (A) with zero mean direction and the normal distribution (B) with zero mean. (a) concentration parameter $\kappa=1$; (b) $\kappa=3$; (c) $\kappa=6$.

errors, although unknown, is not expected to surpass 33°.

The orientation of fault plane is usually denoted by its dip and dip azimuth, or alternatively by the plunge and the trend of its normal. Let Θ, Φ denote the plunge and the trend of the normal to the fault plane. Then rv's (Θ, Φ) are two-dimensional and follow $F\{(\theta_0, \phi_0), \kappa'\}$. The density function is (Fisher et al., 1987, p. 86)

$$f(\theta,\phi) = \frac{\kappa'}{2\pi[\exp(\kappa') - \exp(-\kappa')]} \exp[\kappa'(\sin\theta \sin\theta_0 \cos(\phi - \phi_0) + \cos\theta \cos\theta_0)] \sin\theta, \qquad (0 \le \theta \le \pi, 0 \le \phi < 2\pi) \tag{4.3}$$

where θ, ϕ are measured in radians, and (θ_0, ϕ_0) and κ' are the mean direction and concentration parameter, respectively.

The Fisher distribution is very close to the isotropic bivariate normal distribution if κ' is large (i.e. the dispersion is small), just as in the relationship between the von Mises and the normal distribution. This implies that the isotropic bivariate normal distribution can also serve as a probability model for the fault plane orientation since the dispersion of measurement errors in fault plane orientation, although unknown, are not anticipated to be very large. The random variables Θ and Φ are not independent in the Fisher distribution. Nevertheless, when the mean direction (θ_0, ϕ_0) lies on the equatorial plane, Θ and Φ can be considered as approximately independent if the dispersion of rv's (Θ, Φ) is small. In analogy with the orthogonal coordinate system on the plane, a local coordinate system Θ^*, Φ^* can be defined on the sphere (Figure 4.3), where Θ^* is measured along the longitude (A) which contains the mean direction (θ_0, ϕ_0), and Φ^* is measured along the great circle (B) which is perpendicular to and intersects the longitude at mean direction (θ_0, ϕ_0); rv's (Θ^*, Φ^*) can then be modeled by the independent bivariate normal distribution. Numerical results demonstrate that $F\{(\theta_0, \phi_0), \kappa'\}$ has much the same dispersion as

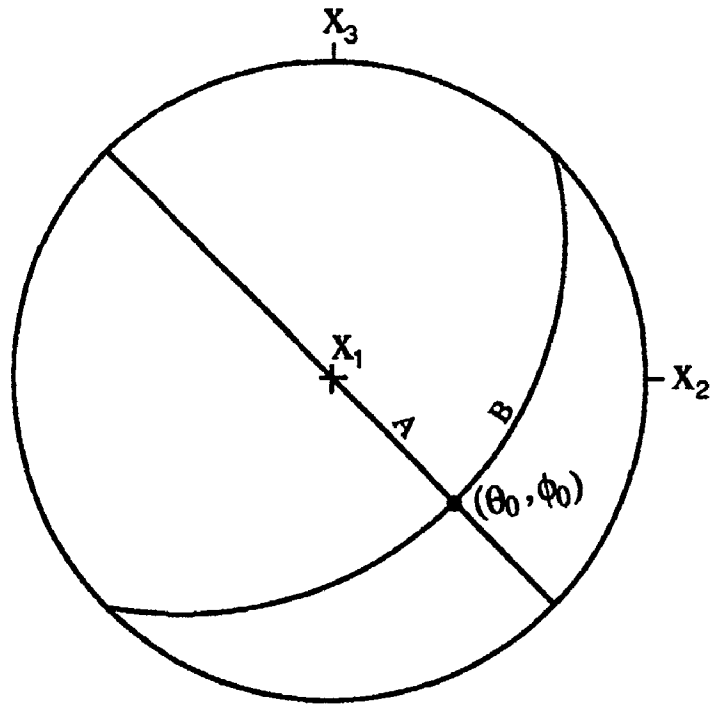

Figure 4.3. Definition of local orthogonal coordinate system (A, B). The mean direction (θ_0, ϕ_0) refers to the normal to the fault plane. The geographical coordinate system is x_i (i=1, 2, 3). Upper hemisphere Schmidt's projection.

$N(\theta_0^*, \phi_0^*, 1/\kappa', 1/\kappa')$ when κ' is large.

Equations (4.1) and (4.3) are of general validity for slip directions and fault plane orientations, respectively. In the rest of this chapter, I assume that the rv's Ω and (Θ, Φ) for each fault have constant concentration parameters κ and κ', respectively. This is the most natural assumption, and appears to be borne out by measurements on given fault populations.

SHEAR STRESS DIRECTION AND MISFIT ANGLE AS RANDOM VARIABLES

As the direction of predicted maximum shear stress on each fault is a function of rv's (Θ, Φ), it is also a random variable. The maximum shear stress direction can be treated as a one-dimensional rv because it is constrained to lie on the fault plane. I first derive the distribution of shear stress direction on any fault plane from the known distribution $F\{(\theta_0, \phi_0), \kappa'\}$ and a given stress field; then I consider the probability distribution of the misfit angle between predicted shear stress and measured slip direction.

The derivation of the shear stress as a function of stress field and fault plane orientation proceeds by vector analysis, rather than tensor analysis as in previous authors (Angelier et al., 1982; Célérier, 1988). Let x_i be a Cartesian coordinate system coincident with the geographical coordinate system (i.e., x_1, x_2, and x_3 coincide with the vertical, the east, and the north directions respectively), and y_i another Cartesian coordinate system with y_1, y_2, and y_3 coinciding with the directions of the principal stresses σ_1, σ_2, and σ_3, respectively (Figure 4.4). Corresponding to these two Cartesian coordinates system, I define two spherical coordinate systems, x-sphere and y-sphere, in which x_1 and y_1 are the polar axes and the azimuth is counted clockwise from x_3 and y_3, respectively. The transformation between x_i and y_i can be achieved by three successive

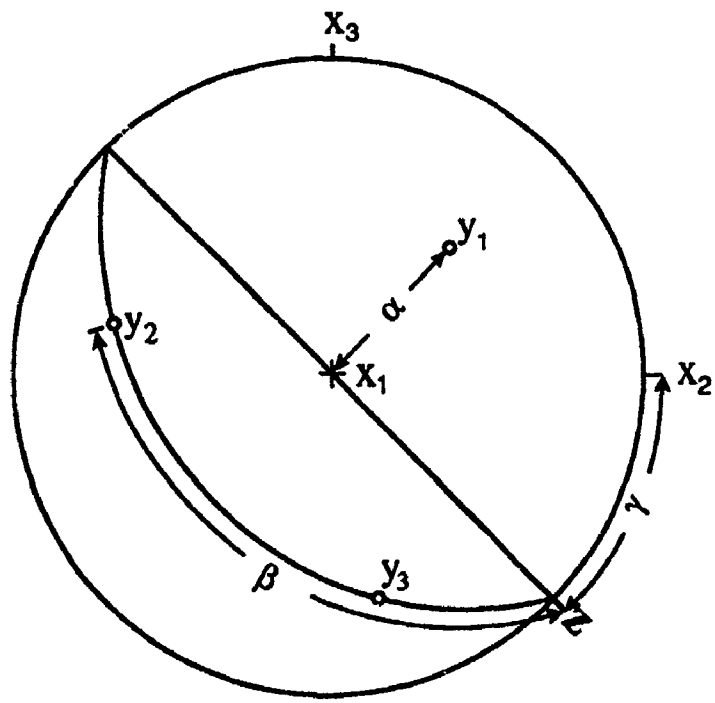

Figure 4.4. Cartesian coordinate system y_i coinciding with principal stress directions σ_1, σ_2, σ_3. Geographical coordinate system x_i as in Figure 4.3. Unit vector **z** denoting the direction of the intersection between the y_2-y_3 plane and the x_2-x_3 plane plots at point **z**; α, β, and γ are the Euler angles. Upper hemisphere Schmidt's projection.

rotations of the Euler angles α, β, γ (refer to Figure 4.4). Assuming $\mathbf{z}=y_1 \times x_1$ be a unit vector indicating the direction of the intersection line between the y_2-y_3 plane and the x_2-x_3 plane, α is defined as the angle between y_1 and x_1 ($0 \le \alpha \le \pi$); β as the angle between y_2 and $\mathbf{z}$, measured anticlockwise on the y_2-y_3 plane starting from y_2 ($0 \le \beta \le 2\pi$); and γ as the angle between x_2 and $\mathbf{z}$, measured clockwise from x_2 on the x_2-x_3 plane ($0 \le \gamma \le 2\pi$). Consequently, the transformation matrix is

$$\begin{pmatrix} u_1 & u_2 & u_3 \\ v_1 & v_2 & v_3 \\ w_1 & w_2 & w_3 \end{pmatrix} = \begin{pmatrix} \cos\alpha & \sin\alpha\sin\gamma & \sin\alpha\cos\gamma \\ \sin\alpha\sin\beta & \cos\beta\cos\gamma - \cos\alpha\sin\beta\sin\gamma & -\cos\beta\sin\gamma - \cos\alpha\sin\beta\cos\gamma \\ -\sin\alpha\cos\beta & \sin\beta\cos\gamma + \cos\alpha\cos\beta\sin\gamma & -\sin\beta\sin\gamma + \cos\alpha\cos\beta\cos\gamma \end{pmatrix} \tag{4.4}$$

where u_i, v_i, w_i (i=1, 2, 3) are cosines of the angles between y_1 and x_i, y_2 and x_i, and y_3 and x_i, respectively.

Let $\mathbf{n}$ be a unit vector denoting the direction of the normal to the fault plane, where $n_{1x}=\cos(\pi/2-\Theta)$; $n_{2x}=\sin(\pi/2-\Theta)\sin(\Phi-\pi)$; $n_{3x}=\sin(\pi/2-\Theta)\cos(\Phi-\pi)$ (the subscript x denotes the x_i-coordinate system). The direction cosines of $\mathbf{n}$ in the y_i-coordinate system can be obtained from the transformation matrix

$$\begin{pmatrix} n_{1y} \\ n_{2y} \\ n_{3y} \end{pmatrix} = \begin{pmatrix} u_1 & u_2 & u_3 \\ v_1 & v_2 & v_3 \\ w_1 & w_2 & w_3 \end{pmatrix} \begin{pmatrix} n_{1x} \\ n_{2x} \\ n_{3x} \end{pmatrix} \tag{4.5}$$

The traction vector $\mathbf{t}$ on the fault plane has components in stress coordinates (Jaeger & Cook, 1979, p. 20; Mandl, 1988, p. 204)

$$t_1 = -\sigma_1 n_{1y}, \quad t_2 = -\sigma_2 n_{2y}, \quad t_3 = -\sigma_3 n_{3y} \tag{4.6}$$

The traction can be resolved into a normal and a shear component (σ and τ, respectively) (Figure

4.5). The normal component σ has a sense opposite to the vector **n** and a magnitude equal to

$$\sigma = \mathbf{t} \cdot (-\mathbf{n}) = \sigma_1 n_{1y}^2 + \sigma_2 n_{2y}^2 + \sigma_3 n_{3y}^2 \tag{4.7}$$

This component can also be expressed as

$$\sigma_{(1)} = -\sigma n_{1y}, \quad \sigma_{(2)} = -\sigma n_{2y}, \quad \sigma_{(3)} = -\sigma n_{3y} \tag{4.8}$$

where $\sigma_{(1)}$, $\sigma_{(2)}$, $\sigma_{(3)}$ are three components of σ. The shear stress can be obtained from

$$\tau = \mathbf{t} - \sigma \tag{4.9}$$

Substituting equations (4.6) and (4.8) into equation (4.9), we have

$$\begin{aligned}
\tau_1 &= \sigma n_{1y} - \sigma_1 n_{1y} = n_{1y}(\sigma_1 n_{1y}^2 + \sigma_2 n_{2y}^2 + \sigma_3 n_{3y}^3 - \sigma_1) \\
\tau_2 &= \sigma n_{2y} - \sigma_2 n_{2y} = n_{2y}(\sigma_1 n_{1y}^2 + \sigma_2 n_{2y}^2 + \sigma_3 n_{3y}^2 - \sigma_2) \\
\tau_3 &= \sigma n_{3y} - \sigma_3 n_{3y} = n_{3y}(\sigma_1 n_{1y}^2 + \sigma_2 n_{2y}^2 + \sigma_3 n_{3y}^2 - \sigma_3)
\end{aligned} \tag{4.10}$$

which, by putting $n_{3y}^2 = 1 - n_{1y}^2 - n_{2y}^2$ and writing $\sigma_2 - \sigma_3 = \delta(\sigma_1 - \sigma_3)$, where δ is the ratio of stress differences, becomes

$$\begin{aligned}
\tau_1 &= (\sigma_1 - \sigma_3) n_{1y}(n_{1y}^2 + \delta n_{2y}^2 - 1) \\
\tau_2 &= (\sigma_1 - \sigma_3) n_{2y}(n_{1y}^2 + \delta n_{2y}^2 - \delta) \\
\tau_3 &= (\sigma_1 - \sigma_3) n_{3y}(n_{1y}^2 + \delta n_{2y}^2)
\end{aligned} \tag{4.11}$$

The magnitude of τ is

$$\tau = (\tau_1^2 + \tau_2^2 + \tau_3^2)^{1/2} = (\sigma_1 - \sigma_3)[(n_{1y}^2 + \delta^2 n_{2y}^2) - (n_{1y}^2 + \delta n_{2y}^2)^2]^{1/2} \tag{4.12}$$

Suppose **l** be a unit vector coincident with the shear stress direction. The direction cosines of the shear stress in the y_i-coordinate system can be expressed as

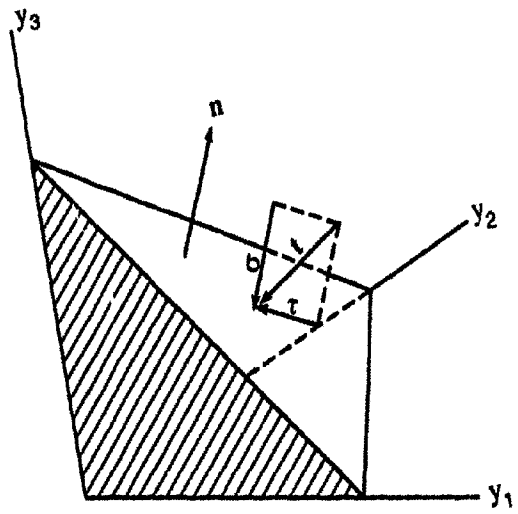

Figure 4.5. Resolution of traction **t** into normal (σ) and shear (τ) components on the fault plane with normal **n** in the principal stress system y_i (i=1, 2, 3).

$$
\begin{aligned}
l_{1y} &= \frac{\tau_1}{\tau} = \frac{n_{1y}(n_{1y}^2 + \delta n_{2y}^2 - 1)}{[(n_{1y}^2 + \delta^2 n_{2y}^2) - (n_{1y}^2 + \delta n_{2y}^2)^2]^{1/2}} \\
l_{2y} &= \frac{\tau_2}{\tau} = \frac{n_{2y}(n_{1y}^2 + \delta n_{2y}^2 - \delta)}{[(n_{1y}^2 + \delta^2 n_{2y}^2) - (n_{1y}^2 + \delta n_{2y}^2)^2]^{1/2}} \\
l_{3y} &= \frac{\tau_3}{\tau} = \frac{n_{3y}(n_{1y}^2 + \delta n_{2y}^2)}{[(n_{1y}^2 + \delta^2 n_{2y}^2) - (n_{1y}^2 + \delta n_{2y}^2)^2]^{1/2}}
\end{aligned}
\tag{4.13}
$$

In analogy to the slip direction (pitch angle) which is measured with respect to the strike of the fault, it is adequate to define the direction of the maximum shear stress on the fault plane by the angle E between the unit shear vector **l** and the fault strike, defined by unit vector $\mathbf{h}=\mathbf{x}_1 \times \mathbf{n}$. From the relationship between **h** and **n**, it follows that

$$
h_{1x} = 0, \quad h_{2x} = \cos\Phi, \quad h_{3x} = -\sin\Phi \tag{4.14}
$$

where h_{1x}, h_{2x}, h_{3x} are the cosines of the angles between **h** and x_i (i=1, 2, 3) respectively. Using the transformation matrix, the coordinates of **h** in the stress coordinate system can be expressed as

$$
\begin{pmatrix} h_{1y} \\ h_{2y} \\ h_{3y} \end{pmatrix} = \begin{pmatrix} u_1 & u_2 & u_3 \\ v_1 & v_2 & v_3 \\ w_1 & w_2 & w_3 \end{pmatrix} \begin{pmatrix} h_{1x} \\ h_{2x} \\ h_{3x} \end{pmatrix} \tag{4.15}
$$

The angle E between the predicted shear stress on the fault plane and the strike can be derived from

$$
\cos(E) = \mathbf{l} \cdot \mathbf{h} = \frac{-(n_{1y} h_{1y} + \delta n_{2y} h_{2y})}{[(n_{1y}^2 + \delta^2 n_{2y}^2) - (n_{1y}^2 + \delta n_{2y}^2)^2]^{1/2}} \tag{4.16}
$$

Equation (4.16) gives rv E as a function of rv's (Θ, Φ) and the unknown stress field.

There is no simple solution to the distribution of the maximum shear stress direction (E). I study it by a numerical method in which the continuous random variables (Θ, Φ) and E are simulated by discrete random variables. For given principal stress directions and stress ratio δ, the probability $P(\Theta=\theta_j, \Phi=\phi_j)$ is approximately equal to $g(\Theta=\theta_j, \Phi=\phi_j)ds$, where g is the probability density element function defined as the density function $f(\theta, \phi)$ in equation (4.3) divided by $\sin(\theta)$ (Fisher et al., 1987, p. 86), and ds is a finite area. Consequently, the probability $P(E=\varepsilon_k)$ $(k=1, 2, 3, \cdots)$ can be obtained by summing the probabilities $P(\Theta=\theta_j, \Phi=\phi_j)$ $(j=1, 2, 3, 4, \cdots)$, where (θ_j, ϕ_j) satisfy the function $\varepsilon_k=f(\theta_j, \phi_j)$ given by equation (4.16). This yields

$$P(E=\varepsilon_k) = \sum_{\varepsilon_k=f(\theta_j,\phi_j)} g(\Theta=\theta_j, \Phi=\phi_j)\,ds \tag{4.17}$$

and the density $f(E=\varepsilon_k)$ is

$$f(E=\varepsilon_k) = \frac{1}{d\varepsilon} \sum_{\varepsilon_k=f(\theta_j,\phi_j)} g(\Theta=\theta_j, \Phi=\phi_j)\,ds \tag{4.18}$$

where $d\varepsilon$ is a finite angle.

Numerical simulation shows that in most cases the distribution of E can be approximated by the von Mises distribution, that is $E \sim VM(\varepsilon_0, \kappa_\varepsilon)$. The mean direction ε_0 is approximately equal to $f(\theta_0, \phi_0)$, where (θ_0, ϕ_0) is the mean direction of rv's (Θ, Φ) and f is the function given in equation (4.16). In spite of the constant concentration parameter κ' of rv's (Θ, Φ), the concentration parameter κ_ε of E varies from infinity (point distribution) to zero (uniform distribution) according to the orientation of principal stresses, the ratio of stress differences, and the mean direction of the fault plane orientation. Figure 4.6 shows some examples.

Let rv S be the angle between the slip (Ω) and the predicted shear stress direction (Ξ) on a fault

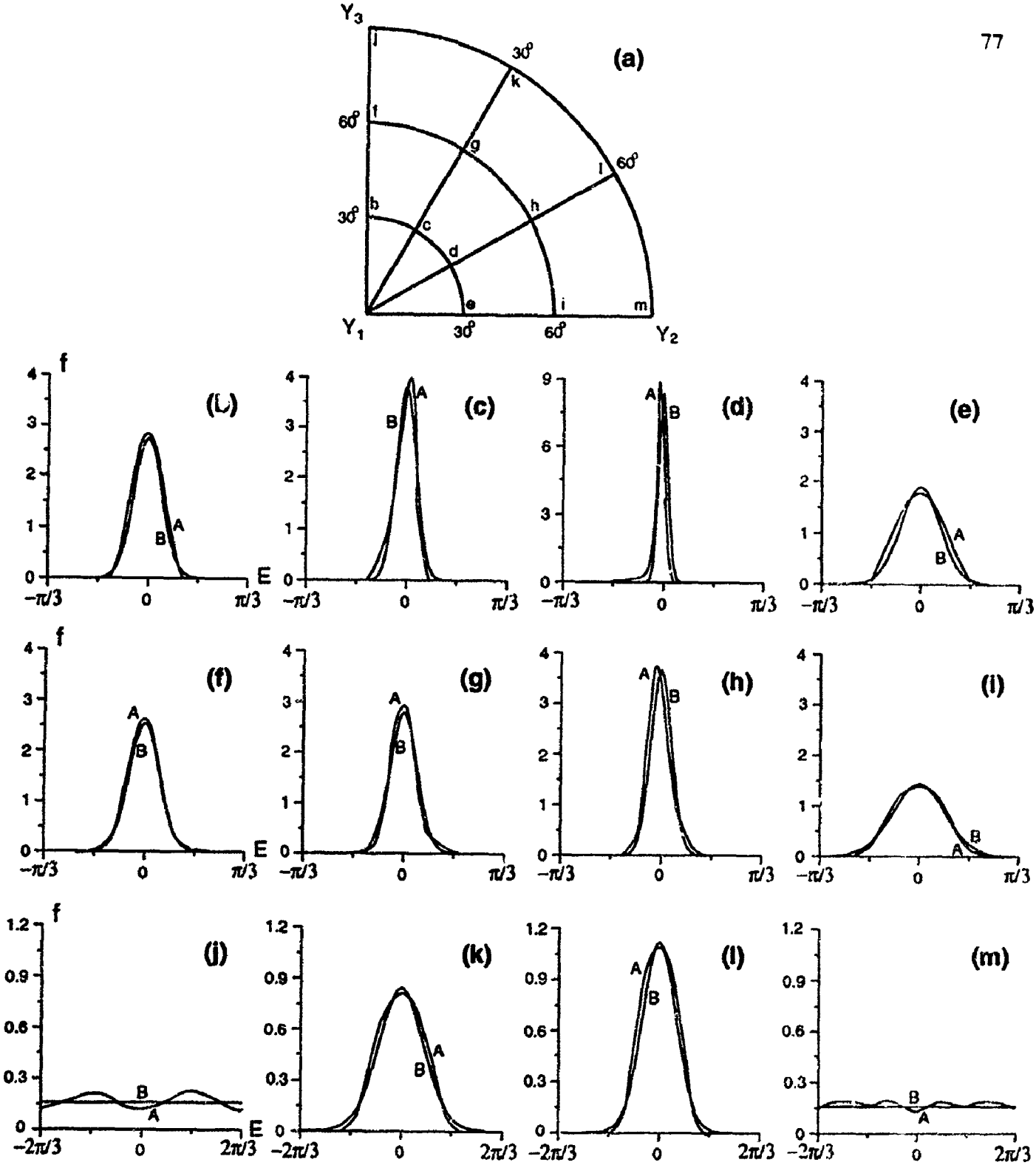

Figure 4.6. Comparison between the distribution of rv E (curve A, calculated from equation (4.16)) and von Mises distribution (curve B). (a) upper hemisphere polar projection denoting positions of the mean direction of the normal to fault plane; (b)-(m) distributions referring to position b, c, ..., m of the mean direction, with mean of E shifted to zero for comparison purposes. Principal stress axes and geographic axes are assumed to coincide; parameters are δ=0.5, κ=67 (i.e., standard deviation about 7°).

2

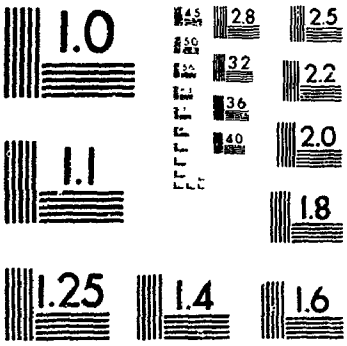

MICROCOPY RESOLUTION TEST CHART
NATIONAL BUREAU OF STANDARDS
STANDARD REFERENCE MATERIAL 1010a
(ANSI and ISO TEST CHART No 2)

$$S = \Omega - E \tag{4.19}$$

where Ω and E are independent and $\Omega \sim VM(\omega_0, \kappa)$, $E \sim VM(\varepsilon_0, \kappa_r)$. The distribution of the difference of two independent von Mises variables is approximately von Mises (Mardia, 1972, pp. 67-68). The distribution of the misfit angle S is therefore approximately $VM(s_0, \kappa_s)$, where the mean direction is $s_0=\omega_0-\varepsilon_0$ and the concentration parameter κ_s is related to κ and κ_r as

$$A(\kappa_s) = A(\kappa)\,A(\kappa_r) \tag{4.20}$$

where $A(\kappa)=I_1(\kappa)/I_0(\kappa)$ is the ratio of modified Bessel functions (Mardia, 1972, pp. 67-68, p. 122). Since the slip is assumed to coincide with the shear stress direction, the mean direction ω_0 of rv Ω should be equal to the mean direction ε_0 of rv E, and $s_0=0$. Consequently, the density function of rv S can be written as

$$f(s) = \frac{1}{2\pi I_0(\kappa_s)} \exp[\kappa_s \cos(s)], \qquad 0 \le s < 2\pi \tag{4.21}$$

It should be noted that κ_s is not constant but a function of stress field and the mean direction of the fault plane orientation.

TWO NEW CRITERIA FOR STRESS INVERSION

Determination of the stress field involves computation of the misfit angle between the predicted maximum shear stress and the measured slip direction. In the previous section, the shear stress and the slip direction have been considered separately, which simplifies the derivation of the distribution of rv S (the misfit angle). However, equations (4.16) and (4.19) are not convenient for calculation of the misfit angles, which can also be obtained by scalar

multiplication between two unit vectors (slip and maximum shear stress direction). If **p** is a unit vector indicating the slip direction, its coordinates in the y_i-coordinate system are

$$\begin{pmatrix} p_{1y} \\ p_{2y} \\ p_{3y} \end{pmatrix} = \begin{pmatrix} u_1 & u_2 & u_3 \\ v_1 & v_2 & v_3 \\ w_1 & w_2 & w_3 \end{pmatrix} \begin{pmatrix} p_{1x} \\ p_{2x} \\ p_{3x} \end{pmatrix} \tag{4.22}$$

where p_{1x}, p_{2x}, p_{3x} are the coordinates of **p** in the x_i-coordinate system. Consequently, the misfit angle can be expressed in terms of the principal stress directions, the ratio of stress differences, the measured slip direction, and fault plane orientation, as follows

$$\cos(s) = \mathbf{l} \cdot \mathbf{p} = \frac{-(n_{1y}p_{1y} + \delta n_{2y}p_{2y})}{[(n_{1y}^2 + \delta^2 n_{2y}^2) - (n_{1y}^2 + \delta n_{2y}^2)^2]^{1/2}} \tag{4.23}$$

As mentioned before, the determination of tectonic stress field, given a set of fault planes and associated slips, consists in searching for a stress field which is most consistent with the data. If there are no measurement errors, the ideal solution for a uniform stress field would satisfy the condition

$$\sum_{i=1}^{n} |s_i| = 0 \tag{4.24}$$

where s is the misfit angle and the subscript i (i=1, 2,···, n) denotes the ith fault. The fact that equation (4.23) is usually not satisfied does not necessarily imply that the stress field is nonuniform, since measurement errors both in fault plane orientations and in slip directions may give rise to considerable misfits. Because of the lack of a probabilistic model to account for the misfits, the various existing inversion methods are based on empirical criteria. Of these methods, the following four are representative. Other methods which assign artificial values to the

unconstrained elements of the stress tensor and/or are based on other assumptions (for instance, taking the magnitude of the shear stress as the same on any fault plane (Michael, 1984; 1987)) are not considered here.

Criterion 1 is based on the minimization of the sum of squares of misfit angles (Carey, 1976; Angelier, 1979; Angelier, 1984; Angelier, 1990)

$$C_1 = \sum_{i=1}^{n} s_i^2 \tag{4.25}$$

Criterion 2 maximizes the sum of cosines of misfit angles (Angelier, 1984; Angelier, 1990)

$$C_2 = \sum_{i=1}^{n} \cos(s_i) \tag{4.26}$$

The criterion based on minimization of the sum of squares of tangents of misfit angles (Angelier, 1984; 1990) can be considered as a fast and approximate algorithm for criterion 2. Criterion 3 minimizes the sum of absolute values of misfit angles (Gephart and Forsyth, 1984; Gephart, 1990)

$$C_3 = \sum_{i=1}^{n} |s_i| \tag{4.27}$$

Criterion 4, quite different from the above three, consists in minimizing the sum of the rotation angles (ζ_i) of each fault plane about its measured normal, necessary to make the predicted shear stress and the measured slip direction coincide (Gephart and Forsyth, 1984; Gephart, 1990)

$$C_4 = \sum_{i=1}^{n} \zeta_i \tag{4.28}$$

The statistical basis and physical implications of the above criteria can be clarified in terms of probability theory. In a data set consisting of n faults, the misfit angle for each fault can

be considered as an independent rv, and there are in total n independent rv's (i.e, S_1, S_2, ···, S_n). From a probabilistic point of view, the best solution for stress inversion should be the one that maximizes the maximum likelihood function. Since we have only one observation for each rv S_i, the maximum likelihood function can be expressed as (Blom, 1989, pp. 198-199)

$$ML(z^*) = \prod_{i=1}^{n} f_i(s_i; z^*) \tag{4.29}$$

where the subscript i denotes the ith fault, f is the density function (depending on the probability models) and z^* represents the unknown values of the parameters and/or the arguments in the ML (maximum likelihood) function; here z^* includes the variance of measurement errors and the unknown stress tensor (i.e., the three principal stress directions and the stress ratio δ).

If there is no uncertainty in fault plane orientation (i.e., E_i is a fixed variable), the misfit angle results solely from the uncertainty in slip direction. In this case, the distribution of S_i is identical to the distribution of Ω_i but with zero mean, and the variance of S_i is independent of the stress tensor and constant for each slip Ω_i. Furthermore, if we assume that Ω_i follows the normal or the von Mises distribution, maximizing the ML function (equation (4.29)) is equivalent to criteria 1 and 2, respectively. If the absolute value of Ω_i is assumed to follow the exponential distribution, maximizing the ML function reduces to criterion 3. Alternatively, if the slip direction is perfectly known (Ω_i is a fixed variable), the misfit angle results solely from the uncertainty in fault plane orientation. In this case, the distribution of S_i is equal to the distribution of E_i but with zero mean. Assuming the fault plane orientation (Θ_i, Φ_i) obeys some distribution, maximizing the ML function reduces to criterion 4. However, no known distributions on the sphere lead exactly to the criterion 4. If (Θ_i,Φ_i) follows exactly the Fisher distribution, ζ_i should be replaced by $\cos(\zeta_i)$ in equation (4.27). In summary, the first three criteria all implicitly assume

that the orientation of fault plane is known without uncertainty, whereas Ω_i (slip direction) follows the normal distribution, the von Mises distribution, and the exponential distribution (for $|\Omega_i|$), respectively. On the other hand, criterion 4 implicitly assumes that the slip direction is known, whereas (Θ_i, Φ_i) (fault plane orientation) follows a distribution similar to the Fisher. Previous workers have recognized that criteria 1 and 2 give rise to nearly the same solution for stress inversion. The probabilistic and statistical basis behind this coincidence is the fact that the von Mises distribution is very close to the normal distribution, subject to the condition that the variance of measurement errors is small.

An inversion method that takes both the slip and the fault plane uncertainties simultaneously into account can be based on the maximization of the ML function given in equation (4.29). The advantage of using the ML function is that the inversion can be performed without knowledge of the distribution of the misfit angle, if a numerical method is used in which the continuous rv's (Θ_i, Φ_i), Ω_i, E_i and S_i are simulated by discrete variables. However, this involves the computation of the density of S_i for each datum and each step of iteration. This computation is usually cumbersome. The problem can be simplified by approximately modelling the misfit angle S_i by the von Mises distribution. This approximation is of high accuracy without losing generality. Consequently, a new criterion (criterion 5) can be derived from equations (4.21) and (4.29),

$$C_5 = \frac{1}{\prod_{i=1}^{n} I_0(\kappa_{si})} \exp\left[\sum_{i=1}^{n} \kappa_{si} \cos(s_i)\right] \tag{4.30}$$

where $\cos(s_i)$ is given by equation (4.23). Solutions for stress inversion can be obtained by maximizing C_5. Effects of both measurement errors on stress inversion are embodied in the

concentration parameter κ_{si} which is a function of κ and κ_{ei} (see equation (4.20)). The parameter κ (independent of the stress field) is constant, representing the effects of measurement errors in slip direction, and κ_{ei} (dependent of the stress field) is a variable for each fault, reflecting the effects of uncertainty in fault plane orientation. If either fault plane orientation or slip direction are taken as perfectly known, criterion 5 reduces either to criterion 2 or to one similar to criterion 4.

To maximize equation (4.30), not only the misfit angle but also the concentration parameter κ_{si} for each fault must be calculated. As discussed previously, the Fisher distribution of rv's (Θ, Φ) can be approximately modeled by the independent bivariate normal rv (Θ^*, Φ^*), where (Θ^*, Φ^*) denotes the direction of the normal to the fault plane in the local coordinate system (see Figure 3.3). Using Gauss's approximation formulae (Blom, 1989, pp. 123-125), I obtain for each fault

$$v_{ei} = v[E(\Theta_i^*,\Phi_i^*)] \approx v(\Theta_i^*)\left(\frac{\partial E(\theta_{0i}^*,\phi_{0i}^*)}{\partial \Theta_i^*}\right)^2 + v(\Phi_i^*)\left(\frac{\partial E(\theta_{0i}^*,\phi_{0i}^*)}{\partial \Phi_i^*}\right)^2 \tag{4.31}$$

where v_{ei} is the variance of rv E_i (maximum shear stress direction) on the line, and θ^*_{0i}, ϕ^*_{0i} and $v(\Theta_i^*)$, $v(\Phi_i^*)$ are the means and the variances of rv's Θ_i^* and Φ_i^*, respectively. The derivative $\partial E/\partial\Theta_i^*$ is identical to $\partial E/\partial\Theta_i$ which can be derived from equation (4.16), whereas $\partial E/\partial\Phi_i^*$ is different from $\partial E/\partial\Phi_i$. Although it is possible to rewrite equation (4.16) in terms of Θ^*, Φ^* and to obtain an analytical solution for the partial derivatives, the process involves the transformation between the local coordinate system and the geographical coordinate system for each fault plane. Using a numerical method to evaluate the derivatives is much easier. A condition for satisfactory accuracy of Gauss's approximation formulae is that $E(\Theta^*, \Phi^*)$ can be described approximately

by a plane in the region where the main part of the mass of the rv (Θ^*, Φ^*) is located (Blom 1989, pp. 123-125). Figure 4.7 shows an example of contour map of the direction of shear stress with respect to the strike. It can be seen that E is nearly linear locally along the Θ^* and Φ^* directions, except when the mean direction (θ_0, ϕ_0) is close to one of the principal stress axes. As the measurement errors are small and the mass of the distribution of rv's (Θ^*, Φ^*) is concentrated around the mean direction, application of Gauss's approximation formulae is acceptable. Replacing $v(\Theta_i^*)=v(\Phi_i^*)\approx 1/\kappa'$ in equation (4.31), we have

$$v_{\varepsilon i} \approx \frac{1}{\kappa'}\left[\left(\frac{\partial E(\theta_{0i}^*,\phi_{0i}^*)}{\partial \Theta_i^*}\right)^2 + \left(\frac{\partial E(\theta_{0i}^*,\phi_{0i}^*)}{\partial \Phi_i^*}\right)^2\right] \tag{4.32}$$

Calculation of the variance $v_{\varepsilon i}$ requires the mean direction (θ^*_{0i}, ϕ^*_{0i}) of each fault plane; since this is unknown, the measured fault plane orientation for each fault is substituted into the derivatives. The concentration parameter $\kappa_{\varepsilon i}$ is related to $v_{\varepsilon i}$ by (Mardia, 1972, p. 74)

$$A(\kappa_{\varepsilon i}) = \exp\left(-\frac{v_{\varepsilon i}}{2}\right) \tag{4.33}$$

where $A(\kappa_{\varepsilon i})=I_1(\kappa_{\varepsilon i})/I_0(\kappa_{\varepsilon i})$ is the ratio of modified Bessel functions. It is reasonable to assume that the measurement errors in slip direction and in fault plane orientation are of same order, i.e., the concentration parameter κ of rv Ω is approximately equal to the concentration parameter κ' of rv's (Θ, Φ). Assuming $\kappa'=\kappa$ simplifies the calculation of the concentration parameter κ_s of rv S. Since the measurement errors are usually small, $A(\kappa)\approx 1-1/(2\kappa)$ (Fisher et al., 1987, p. 82). Consequently, by recalling equation (4.20) the concentration parameter κ_{si} is obtained as

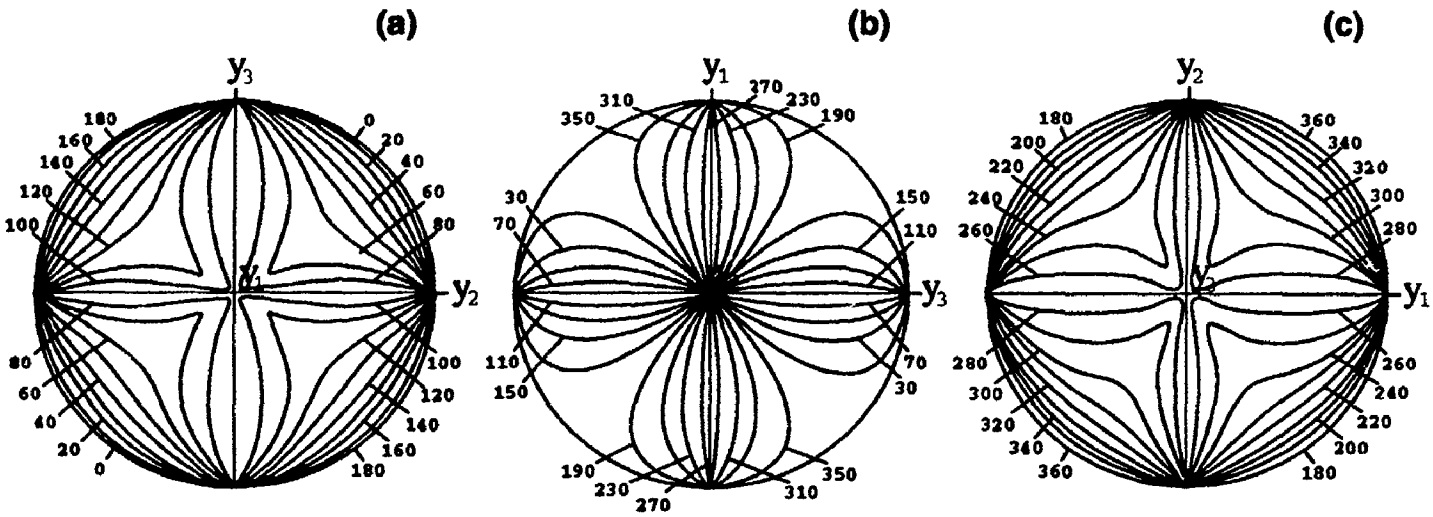

Figure 4.7. Upper hemisphere polar projection of the angle E between shear stress and strike direction (contour lines in degrees), as a function of orientation of the normal to the fault plane in y_i-coordinates. (a), (b), and (c) refer to vertical orientation of σ_1, σ_2, and σ_3, respectively. The stress ratio is δ=0.5.

$$A(\kappa_{si}) = (1-\frac{1}{2\kappa})\exp(-\frac{v_{\varepsilon i}}{2}) \tag{4.34}$$

where $v_{\varepsilon i}$ is given by equation (4.32). Expanding $A(\kappa_{si})$ in series and neglecting higher-order terms, the approximate solution for κ_{si} is

$$\begin{aligned} \kappa_{si} &= \frac{1}{2[1-A(\kappa_{si})]}, && \text{for } A(\kappa_{si}) \geq 0.5 \\ \kappa_{si} &= 2A(\kappa_{si}), && \text{for } A(\kappa_{si}) < 0.5 \end{aligned} \tag{4.35}$$

As mentioned previously, the von Mises distribution on the circle is very similar to the normal distribution on the line when the concentration parameter is relatively large. Since the dispersion of the distribution of rv E_i is usually small except when the mean direction (θ_{0i}, ϕ_{0i}) is close to one of the principal stress axes, modelling of rv E_i by the normal distribution gives rise to similar results as the von Mises distribution. Furthermore, as the difference of two independent normal variables is a normal random variable, the misfit angle S_i also approximately follows the normal distribution, truncated at $\pm\pi$ and with zero mean. Therefore, recalling equation (4.29), another new inversion criterion (criterion 6) can be written as

$$C_6 = \frac{1}{\prod_{i=1}^{n}\sqrt{v_{si}}}\exp(-\frac{1}{2}\sum_{i=1}^{n}\frac{s_i^2}{v_{si}}) \tag{4.36}$$

where $v_{si}=(1/\kappa)+v_{\varepsilon i}$ is the variance of rv S_i, and $v_{\varepsilon i}$ is given by equation (4.32). Solutions for stress inversion can be obtained by maximizing C_6. Equations (4.30) and (4.36) lead to similar solutions for stress field inversion. Criterion 6 can be considered as a fast and approximate algorithm for criterion 5. In addition, if there are no measurement errors in fault plane orientation, i.e., the fault plane orientation is taken as perfectly known, equation (4.36) reduces to criterion 1.

Unlike the previous criteria (equations (4.25)-(4.28)), which yield an inversion solution independent of the variance of measurement errors, the two criteria proposed here are affected by the variance, which is unknown. To deal with this problem, an objective approach is to use the estimated variance (i.e, the sample variance that maximizes the criteria). In the case of criterion 6, the variance can be estimated from equations (4.32) and (4.36) by solving $\partial C_6/\partial v=0$ and noting that $v=1/\kappa$

$$\hat{v} = \frac{1}{n}\sum_{i=1}^{n}\frac{s_i^2}{1+b_i} \tag{4.37}$$

where b_i is the sum of squares of the derivatives given in equation (4.32). Substituting equation (4.37) in (4.36), equation (4.36) reduces to 4-D inversion (i.e., the principal stress directions and the stress ratio δ). However, the estimated concentration parameter $\hat{\kappa}$ cannot be expressed in closed form for criterion 5, for which a 5-D inversion (i.e., the above unknowns plus the concentration parameter) has to be performed to obtain the solution for the stress field. In both cases, the procedure consists in a grid search of the combination of parameters that maximizes the criteria. In comparison with criterion 5, criterion 6 reduces significantly the computing time. The computer program for stress inversion is given in Appendix 1.

As mentioned previously, Angelier et al. (1982) were the first to develop a technique which takes both kinds of measurement errors simultaneously into consideration. In comparison with their method, the two inversion methods (criteria 5 and 6) proposed here lead to simpler computations.

HYPOTHESIS TESTING AND CONFIDENCE INTERVALS

1. Hypothesis Testing

The misfit angles between the predicted maximum shear stresses and the measured slip directions come mainly from two sources: (1) heterogeneous stress field, including the spatial and temporal variation of the principal stress directions, the ratio of stress difference, or both; (2) measurement errors in both slip direction and fault plane orientation, including smaller instrumental errors and larger observation errors. Other less known sources, such as fault interactions, block rotations and bias in data collection, may also result in misfit angles. In the previous section a uniform stress field was assumed; now I derive a test of the null hypothesis that the stress field is uniform against the alternative hypothesis that the stress field is nonuniform, in the sense of spatial and/or temporal variation in the principal stress directions and the stress ratio δ. The hypothesis test is in principle possible since the distribution of rv S_i is theoretically von Mises with zero mean and varying concentration parameter if the stress field is uniform. However, a transformation is required so that rv S_i will have a constant concentration parameter for each fault. Suppose that κ_{si} (where i denotes the ith fault) can be expressed as

$$\kappa_{si} = \frac{\hat{\kappa}}{a_i} \tag{4.38}$$

where $\hat{\kappa}$ is the estimated concentration parameter, and $a_i \geq 1.0$ (because κ_{si} is always smaller than $\hat{\kappa}$) is a factor associated with each fault. Let $S_i^* = S_i/(a_i)^{1/2}$ be a random variable with the distribution truncated at $\pm(\pi/(a_i)^{1/2})$. If κ_{si} is relatively large ($\kappa_{si} \geq 2$, which is the case for stress inversion), the truncated portion is negligible. The same transformation can be applied to the case where rv S_i is modelled by the normal distribution. The independent rv S_i^* follows approximately the von

Mises (or normal) distribution with zero mean direction and a constant concentration parameter $\hat{\kappa}$ for each fault, if the stress field is uniform. A significant deviation from a von Mises (or normal) distribution implies that the stress field is not uniform.

The χ^2-test can be used to check goodness of fit to a given distribution (Blom, 1989, pp. 270-271; DeGroot, 1986, pp. 519-531). It can be expressed as

$$Q = \sum_{j=1}^{k} \frac{(N_j - np_j)^2}{np_j} \tag{4.39}$$

where n is the sample size, and N_j and p_j are the number of data and the expected probability of the von Mises distribution with zero mean and concentration parameter $\hat{\kappa}$ in the jth interval (j=1, 2, 3, ···, k) respectively. As the sample size $n \rightarrow \infty$, Q converges to the χ^2 distribution with k-1-m degrees of freedom, where m is the number of unknown parameters. In the present case, the degrees of freedom are k-2 since the mean direction is known (i.e., zero) and the concentration parameter is unknown. Choosing a significance level α_1, the null hypothesis is rejected if $Q > \chi^2_{\alpha 1}(k-2)$. The significance level, usually chosen as $\alpha_1 \leq 0.05$, is the probability that the null hypothesis is rejected when true, and is related to the significance of deviations from the hypothesis. The smaller is α_1, the more strongly the hypothesis is rejected, that is, the deviations of stress field from uniformity are more significant.

2. Confidence Intervals

Determination of the confidence intervals for the four unknown parameters, i.e. the directions of the three principal stress axes and the stress ratio (δ) has been considered in some previous methods (Angelier et al., 1982; Gephart and Forsyth, 1984). A different approach for estimation of the confidence intervals is presented here. In the application of criteria 5 and 6, the

four unknown parameters are regarded as fixed variables. However, they cannot be inverted accurately even when the stress field is uniform. The reason is because the inversion solution depends on the variance of measurements in slip direction and in fault plane orientation, which is unknown. Instead of the true variance, the sample variance is used in stress inversion. Since the sample variance is a random variable, the confidence intervals for the three principal stress directions and the stress ratio (δ) can be estimated on the basis of consideration of the confidence interval for the variance of measurement errors.

As mentioned before, the normalized misfit angle $S_i^*=S_i/(a_i)^{1/2}$ (where a_i is defined in equation (4.38)) is an independent rv and follows approximately the von Mises distribution with zero mean direction and a constant concentration parameter for each fault. The rv S_i^* can also be approximately modelled by the normal distribution. When modelled by the normal distribution, $a_i=1+b_i$, where b_i is defined in equation (4.37). Using the theorem that the sum of the squares of normal variables follows the χ^2 distribution (Blom, 1989, p. 229), I obtain

$$\frac{1}{v}\sum_{i=1}^{n}(S_i^*)^2 \sim \chi^2(n) \tag{4.40}$$

where v is the variance of the measurements both of slip direction and of fault plane orientation, and the subscript denotes the ith fault. Choosing a confidence level $1-\alpha_2$, the confidence interval for v can be estimated by

$$\frac{1}{\chi^2_{\alpha/2}(n)}\sum_{i=1}^{n}(S_i^*)^2 < v < \frac{1}{\chi^2_{1-\alpha/2}(n)}\sum_{i=1}^{n}(S_i^*)^2 \tag{4.41}$$

Substituting equation (4.37) in inequality (4.41) yields

$$\frac{n\hat{v}}{\chi^2_{\alpha/2}(n)} < v < \frac{n\hat{v}}{\chi^2_{1-\alpha/2}(n)} \tag{4.42}$$

Since $\hat{v}$ (the measurement sample variance) is estimated, calculation of the confidence interval for v is straightforward.

According to criteria 5 and 6, the uncertainty in the four unknown parameters of stress field comes from the uncertainty in the measurement variance, provided that the stress field is uniform. Thus, the confidence intervals for the three principal stress directions and the stress ratio can be estimated by substituting the two limits for v given by inequality (4.42) into criterion 5 or 6 and repeating the inversion process. The confidence limits are represented by two vectors for each of the three principal directions, between which the inverted three principal directions lie. Unlike the previous approaches in which the confidence intervals for the three principal directions are presented by three ellipses in stereo-diagrams, the new approach gives rise to the confidence intervals for the three principal direction as three curves in stereo-diagrams because the solution of the three principal directions by criterion 5 or 6 is unique for a given variance.

EXAMPLES

The two new inversion methods, i.e., criteria 5 and 6 (equations (4.30) and (4.36)), are applied to three field examples. The three data sets, taken from field fault measurements, come from Angelier (1990). The data are listed in Table 4.1. The first data set consists of 33 faults, from Neogene reef limestone near Agia Vavara, central Crete, Greece (site AVB). The second dat set, composed of 38 faults, was collected in Neogene marly limestone near Tymbaki, southern Crete, Greece (site TYM). The third data set is composed of 50 faults, from the Mineoka

Table 4.1. Fault-slip data (angles in degrees) from sites AVB, TYM, and KAM. All the faults are normal or normal strike-slip, denoted by N. Retabulated from Angelier (1990).

Site	Fault Plane		Slip	Sense of slip	Site	Fault Plane		Slip	Sense of Slip
	Strike	Dip	Pitch of Stria			Strike	Dip	Pitch of Stria	
AVB	59	71N	74E	N	TYM	63	67S	81W	N
	45	65W	69N	N		30	58E	58S	N
	42	70W	68N	N		32	69E	85N	N
	47	63N	84E	N		43	63E	84S	N
	44	56E	83S	N		25	68E	87N	N
	72	65S	81E	N		71	48N	85E	N
	63	70S	81E	N		70	69N	88W	N
	46	61N	83E	N		17	68W	80N	N
	70	73N	85E	N		96	70N	72W	N
	72	72N	89W	N		89	71N	89E	N
	53	86N	72E	N					
	60	74N	71E	N	KAM	56	66S	64E	N
	47	77N	61E	N		59	67S	64E	N
	55	65N	60E	N		31	55E	63N	N
	75	52S	62E	N		60	52S	79E	N
	39	85W	71N	N		179	36E	85N	N
	42	71W	69N	N		142	70E	73N	N
	59	63N	71E	N		117	55N	72W	N
	49	58N	69E	N		60	67N	30E	N
	47	57N	78E	N		92	60N	87W	N
	84	56S	67E	N		124	64N	68W	N
	49	40N	68E	N		46	39S	20W	N
	69	51S	64E	N		58	40S	75E	N
	77	32S	67E	N		155	51E	64S	N
	52	54N	55E	N		121	73N	42E	N
	59	67S	73E	N		114	70N	74W	N
	47	65N	61E	N		64	28S	42W	N
	61	86S	67E	N		138	35E	85N	N
	47	74N	49E	N		160	40E	75N	N
	31	69W	45N	N		150	43E	76N	N
	59	65S	85W	N		96	50S	84E	N
	56	56S	79E	N		40	40E	46S	N
	70	80N	89W	N		116	29S	64E	N
						130	35N	83W	N
TYM	47	61S	80E	N		160	40E	76N	N
	38	59E	80S	N		136	82E	66N	N
	92	80N	58W	N		101	28S	77W	N
	54	68N	78W	N		51	52S	31W	N
	47	63N	78W	N		141	85E	80N	N
	112	88N	59W	N		145	78E	88N	N
	76	78N	65W	N		122	77N	88E	N
	48	60S	80W	N		168	76E	58N	N
	79	61N	86E	N		127	77N	67W	N
	69	56S	88E	N		52	23S	38W	N
	51	70S	69W	N		119	46N	89W	N
	38	50W	86N	N		80	77N	76E	N
	60	51S	79W	N		144	17E	43N	N
	81	62S	77W	N		144	17E	76S	N
	58	62N	84W	N		116	49N	79E	N
	36	61W	75S	N		103	68N	83E	N
	36	60E	76S	N		54	44S	68W	N
	39	63E	85S	N		69	50N	64E	N
	70	72S	63E	N		116	60N	89W	N
	51	53S	89E	N		89	57N	69E	N
	11	47W	79N	N		49	46N	40E	N
	59	45N	67W	N		59	51S	34W	N
	114	74S	66W	N		64	60S	60W	N
	27	42W	89N	N		67	42S	78W	N
	36	56W	87N	N		73	45S	81W	N
	39	77E	50S	N		60	43S	71W	N
	59	61S	62W	N		101	85N	56E	N
	70	58N	74E	N					

ophiolite of Kamogeawa, Boso Peninsula, Central Japan (site KAM). These three areas are characterized by extensional tectonics with predominant normal dip-slip and oblique-slip faulting. The fault planes of site KAM are more diverse in orientation than the other two (see Angelier, 1990 for detailed description).

In the search for the best solutions for the three data sets, a grid search technique is adopted. For each iterative step, the value of one of the four unknown parameters is changed, i.e., the Euler angles α, β, γ (representing the principal stress directions) and the stress ratio δ, and C_6 is calculated according to equation (4.36). For criterion 5, another unknown parameter, i.e. the concentration parameter κ, is added. The search proceeds in a wide range of the 4-D or 5-D space composed of the unknown parameters. The best solutions for the principal stress directions and the stress ratio are those that maximize the criteria. The length of each iterative step is regarded as the computing precision which is listed in the caption of Table 4.2 (see appendix 1.1 for the computer program).

Table 4.2 lists the results of the inversion for the three areas. In order to compare our results with the previous methods, the above three data sets are also inverted by criterion 2 (equation (4.26)) which is one of the most common procedures. Besides, the inversion results for the three data sets by other previous methods are also listed in Table 4.2 for comparison. Criterion A1 and criterion A2 in Table 4.2 refer to the method based on minimization of the sum of squares of tangents of misfit angles (Angelier, 1984, 1990) and the method proposed by Angelier et al. (1982) that takes both types of measurement errors into consideration, respectively. The principal stress directions inverted by criteria 5 and 2 are also shown in Figure 4.8. In all three data sets, criterion 6 gives nearly the same results as criterion 5. However, criterion 6 saves much computing time. The difference with criteria 2, A1 and A2 is not large, but noticeable. In

Table 4.2. Results of stress inversion for sites AVB, TYM and KAM with different methods (see text). The three principal stress axes are denoted by σ_1, σ_2 and σ_3, respectively. Stress ratio, estimated concentration parameter and standard deviation (in degrees) are denoted by δ, $\hat{\kappa}$ and $\hat{\phi}^{1/2}$. The computing precision is 1° for σ_1, σ_2 and σ_3, 0.01 for δ, 0.1 for $\hat{\kappa}$ and 0.1° for $\hat{\phi}^{1/2}$.

Site	Method	σ_1		σ_2		σ_3		δ	$\hat{\kappa}$	$\hat{\phi}^{1/2}$
		Plunge	Trend	Plunge	Trend	Plunge	Trend			
	criterion 5	75°	63°	15°	244°	0°	154°	0.26	62.1	7.3°
	criterion 6	75°	63°	15°	244°	0°	154°	0.26	60.4	7.4°
AVB	criterion 2	73°	72°	17°	240°	4°	331°	0.28	39.0	9.2°
	criterion A1	73°	73°	17°	240°	4°	331°	0.30		
	criterion A2	74°	69°	16°	241°	2°	331°	0.53		
	criterion 5	83°	202°	6°	57°	4°	327°	0.13	23.3	12.0°
TYM	criterion 6	83°	202°	6°	57°	4°	327°	0.13	23.0	12.1°
	criterion 2	81°	281°	6°	55°	7°	145°	0.06	17.8	13.6°
	criterion A1	82°	275°	6°	57°	5°	147°	0.07		
	criterion 5	82°	242°	3°	130°	7°	40°	0.31	8.9	19.8°
KAM	criterion 6	82°	242°	3°	131°	8°	41°	0.32	8.4	20.4°
	criterion 2	85°	254°	4°	120°	4°	30°	0.26	5.4	24.7°
	criterion A1	84°	246°	4°	118°	5°	28°	0.32		

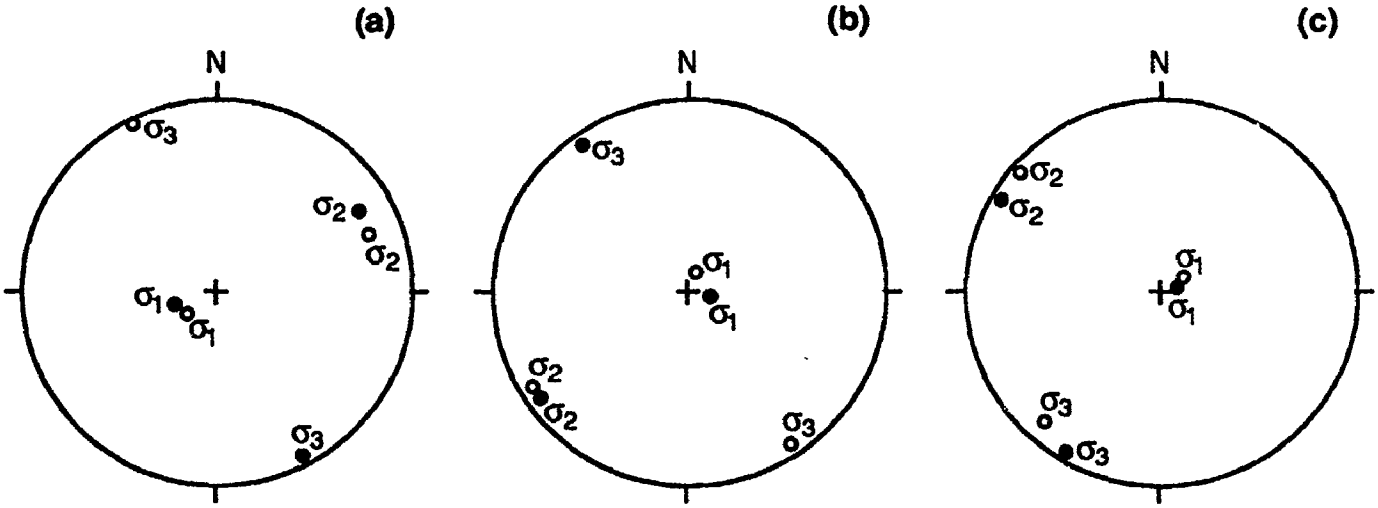

Figure 4.8. Results of stress inversion for principal stress directions using criterion 5 (open circles) and criterion 2 (solid circles). (a) site AVB; (b) site TYM; (c) site KAM. Upper hemisphere Schmidt's projection.

some cases, the difference in principal stress directions is more than 10° (angular distance on the sphere) and the difference in stress ratio is as large as 0.27. As mentioned before, criterion A1 is considered as a fast and approximate algorithm for criterion 2. It can be seen from Table 4.2 that these two criteria lead to similar results of stress inversion. Comparing the three data sets, I note that more diverse fault plane orientations result in a larger difference of results between the two new methods and criterion 2 or A1. This is not surprising since, if all fault planes have the same orientation, criteria 5 and 2 yield the same stress tensor but different estimated concentration parameter. Furthermore, since the dispersion of rv E (shear stress direction) is a function of both principal stress directions and stress difference ratio (see equations (4.32) and (4.33)), the effect of measurement errors in fault plane orientation on stress inversion also depends on the orientation of principal stress axes and δ. In all the three examples, σ_1 is almost vertical and the other two stress axes are nearly horizontal, and δ is small (see Table 4.2). Other cases should be investigated to test the difference in results where these conditions are not satisfied.

Table 4.3 lists the misfit angle, the concentration parameter, and the normalized misfit angle calculated by criterion 5 for each fault at sites AVB, TYM and KAM. It can be seen that nearly all concentration parameters κ_s for different faults are larger than 2. This implies that the linear transformation devised in equation (4.38) is quite adequate. The hypothesis that the stress fields in each of the three examples are uniform is tested using the χ^2 test and normalized misfit angles (i.e., $s_i^*=s_i/(a_i)^{1/2}$), according to the procedure described in the previous section. The results are shown in Figure 4.9. In all three cases, sample size is relatively small. Consequently, site AVB is divided only into five intervals, and sites TYM and KAM are divided into seven and nine intervals respectively. The values of Q (equation (4.39)) are 1.4589 for site AVB, 2.9901

Table 4.3. Results of calculated misfit angle (s), concentration parameter (κ_s), and normalized misfit angle (s*) for each of the faults from sites AVB, TYM, and KAM (angles in degrees). The faults are listed in the same sequence as for Table 4.1.

Site	s	κ_s	s*	Site	s	κ_s	s*
AVB	-0.31	37.391	-0.24	TYM	-6.70	17.926	-5.87
	1.44	50.469	1.30		-18.64	21.943	-18.09
	3.03	47.499	2.65		20.25	19.187	18.37
	15.30	50.392	13.78		4.54	20.360	4.24
	-9.31	37.662	-7.25		19.39	20.083	18.00
	-8.03	45.243	-6.86		-13.36	23.054	-13.29
	-1.93	35.002	-1.45		-6.37	22.291	-6.23
	14.48	51.615	13.20		-6.70	18.279	-5.94
	0.11	23.912	0.07		7.44	21.680	7.17
	4.37	23.567	2.69		-11.88	21.736	-11.48
	17.94	4.888	5.03				
	-3.72	32.523	-2.69	KAM	52.75	4.989	39.50
	-2.46	32.054	-1.77		55.39	4.889	41.05
	-12.35	45.028	-10.52		33.17	4.511	23.61
	9.27	49.212	8.25		36.09	7.586	33.32
	22.24	10.611	9.19		0.61	6.326	0.52
	4.44	46.129	3.82		8.05	6.726	6.99
	-3.69	43.852	-3.10		19.47	7.573	17.96
	-0.88	50.601	-0.79		-51.38	4.088	-34.83
	8.89	51.744	8.11		12.60	7.043	11.21
	1.20	53.907	1.12		22.16	7.093	19.78
	0.54	44.981	0.46		-49.04	5.537	-38.68
	9.63	46.598	8.35		39.84	7.852	37.42
	-2.24	35.575	-1.69		-35.28	8.351	-34.17
	-16.01	49.245	-14.25		-44.53	5.913	-36.29
	8.74	35.249	6.58		22.61	6.119	18.75
	-7.39	49.408	-6.59		-19.42	7.635	-17.99
	25.09	1.783	4.25		-0.74	8.374	-0.72
	-16.40	39.000	-13.00		6.95	8.706	6.87
	-17.40	53.333	-16.12		6.44	8.503	6.30
	-13.73	37.298	-10.64		27.94	6.679	24.20
	1.98	41.437	1.62		-26.57	4.692	-19.29
	0.67	8.273	0.24		36.78	4.386	25.82
					2.49	8.138	2.38
TYM	19.05	20.305	17.78		5.95	8.706	5.88
	1.61	21.188	1.54		15.42	4.255	10.66
	17.00	15.669	13.94		5.13	4.812	3.77
	7.12	21.714	6.87		-37.84	6.170	-31.51
	8.11	21.779	7.84		-6.05	2.824	-3.41
	7.84	3.929	3.22		-11.87	5.000	-8.90
	13.45	19.261	12.22		2.01	5.137	1.53
	-1.33	20.322	-1.24		9.37	4.685	6.80
	-12.81	23.067	-12.74		23.01	5.436	17.98
	3.58	19.629	3.29		-20.51	5.095	-15.52
	-12.79	18.104	-11.28		0.39	7.860	0.36
	-8.63	21.959	-8.38		13.25	2.435	6.93
	-5.90	19.995	-5.47		-23.24	4.237	-16.03
	-17.04	18.252	-15.08		37.76	4.237	26.05
	-0.10	22.354	-0.10		-10.34	7.789	-9.67
	12.84	21.456	12.32		3.86	6.050	3.18
	-1.77	21.272	-1.69		1.12	7.038	0.99
	6.79	20.659	6.39		-23.65	6.311	-19.91
	23.72	13.048	17.75		3.81	7.289	3.44
	8.75	20.415	8.19		-12.55	7.285	-11.35
	-14.23	21.796	-13.77		-59.21	5.260	-45.52
	15.21	22.512	14.95		-31.33	7.528	-28.82
	-46.93	4.094	-19.67		-1.60	6.843	-1.40
	-6.40	21.556	-6.16		13.89	8.844	13.85
	-6.20	21.807	-6.00		17.07	8.796	16.97
	-22.39	10.530	-15.05		5.93	8.120	5.66
	-23.34	19.510	-21.35		-0.45	1.230	-0.17
	-23.92	22.951	-23.74				

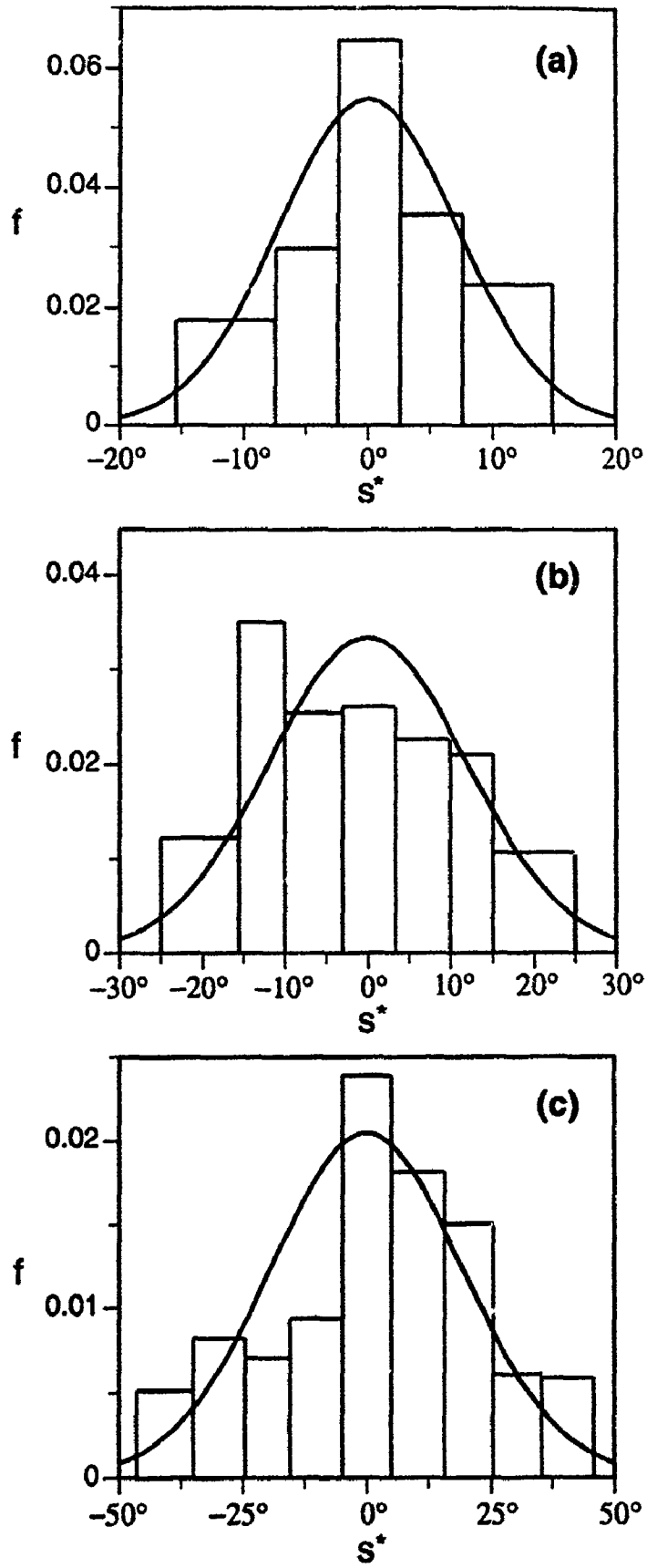

Figure 4.9. Histograms of the distribution of normalized misfit angle (S^*) compared with the von Mises distribution (curves) for the estimated concentration parameter $\hat{\kappa}$. (a) site AVB; (b) site TYM; (c) site KAM. The vertical axis (f) is the probability density.

for site TYM, and 5.6264 for site KAM, respectively. The corresponding significance level at which the null hypothesis is rejected is α_1=0.693 for site AVB, α_1=0.702 for site TYM and α_1=0.5626 for site KAM. Therefore, the null hypothesis that the stress field is uniform is acceptable for all the three examples at significance levels much higher than the conventional $\alpha_1 \leq 0.05$. The relatively small sample sizes limit the robustness of these conclusions; larger sample sizes would be necessary to more accurate hypothesis testing.

The 90% confidence intervals for the three principal stress directions and the ratio of stress difference are calculated based on the estimation of confidence interval for $v^{1/2}$ (see inequalities (4.41) and (4.42)) and the results are listed in Table 4.4. In comparison with the previous approaches (Angelier et al., 1982; Gephart and Forsyth, 1984), the present approach gives rise to much smaller confidence intervals for the principal directions, especially for the site AVB for which the 90% confidence intervals are nearly as the same order as the computing precision. The confidence interval for the ratio of stress difference is relatively large. This result suggests that the solution for the principal stress directions is not sensitive to the variance of measurement errors for the three examples studied.

The concentration parameter of measurement errors in both slip direction and fault plane orientation is not constrained in present analysis. Instead, I use the estimated concentration parameter (or variance) to test the hypothesis. The estimated standard deviation for site KAM is unexpectedly large. The test result for site KAM is valid only in the case where such a large concentration parameter is real, because the χ^2 method has no control over the sample concentration parameter. If the dispersion of measurement errors is constrained a priori, the result could be different. As more field examples are studied, it may be possible to estimate empirically the range of variation of the concentration parameter of measurement errors and

Table 4.4. Estimates of 90% confidence intervals for the standard deviation of measurement errors ($v^{1/2}$), the principal stress directions (σ_1, σ_2, σ_3), and the ratio of stress difference (δ). The computing precision is 0.1° for $v^{1/2}$, 1° for σ_1, σ_2, σ_3, and 0.01 for δ.

Site	$v^{1/2}$	σ_1 (Plunge, Trend)	σ_2 (Plunge, Trend)	σ_3 (Plunge, Trend)	δ
AVB	6.1° - 9.2°	(75°,63°) - (74°,63°)	(15°,243°) - (16°,244°)	(0°,153°) - (0°,154°)	0.32 - 0.19
TYM	10.1° - 14.8°	(83°,196°) - (84°,214°)	(5°,57°) - (6°,59°)	(5°,327°) - (3°,329°)	0.15 - 0.10
KAM	17.0° - 23.7°	(82°,263°) - (83°,238°)	(4°,134°) - (2°,128°)	(5°,44°) - (8°,38°)	0.37 - 0.26

consequently to constrain it. In addition, the sample size is another important factor affecting the hypothesis testing. The reliability of the conclusion improves with increasing sample size.

CONCLUSIONS

In the search of a probabilistic basis for the inversion of fault plane orientation and slip direction data to obtain the tectonic stress field, I have accepted the basic assumption that shear stress direction and slip direction coincide on any fault plane. The distributions of the random variables Ω (pitch angle of striation) and Θ, Φ (plunge and trend of the normal to the fault plane) for any given fault are taken to be the $VM(\omega_0, \kappa)$ and $F\{(\theta_0, \phi_0), \kappa'\}$, respectively. These can be approximated, subject to certain conditions, by the normal and bivariate normal distributions.

The distribution of shear stress direction E (angle between unit shear vector and fault strike) depends on the orientation of the fault plane, the principal stress axes, and the stress ratio. I have evaluated it numerically and found that it is approximately $VM(\varepsilon_0, \kappa_\varepsilon)$ with varying concentration parameter for each fault. It follows that the misfit angle S between observed and predicted shear stress direction is also approximately $VM(s_0, \kappa_s)$, with $s_0=0$ and κ_s a function of the concentration parameters of Ω and E.

I propose two new inversion criteria, named criterion 5 and criterion 6 in this chapter, taking into account uncertainties of both fault plane orientation and direction of slip, based on numerical maximization of the maximum likelihood (ML) function of the misfit angles of all faults of a given data set. The inversion can be four-dimensional (three principal stress directions and stress ratio) for criterion 6, or five-dimensional (the above four unknowns plus the concentration parameter) if criterion 5 is used. Criterion 6 can be considered as a fast and

approximate algorithm for criterion 5. Commonly used inversion procedures can be shown to be particular cases of the new general method.

After a linear transformation that makes the concentration parameter of rv S the same for each fault, the χ^2 goodness-of-fit test can be applied to the transformed data to check the null hypothesis that the observed set is accountable in terms of a homogeneous stress field (in which case S is a von Mises variable). A procedure is devised to calculate the confidence intervals for the four unknown parameters, i.e., the principal stress directions and the ratio of stress difference.

Inversion, goodness-of-fit test and estimation of the confidence intervals have been performed on three data sets taken from the literature available. The two new criteria give practically identical results in each case, but noticeable differences (although of limited magnitude) exist between the new criteria and the old criteria that I checked for comparison. The hypothesis of a homogeneous stress field is accepted in each case, although the test is weak due to the relatively small sample size and depends on the estimated concentration parameters. More data sets, with much larger size and taken from various tectonic settings, are needed to explore the power of the method.

REFERENCES

Angelier, J., Determination of the mean principal directions of stresses for a given fault population, *Tectonophysics, 56*, T17-T26, 1979.

Angelier, J., Tectonic analysis of fault slip data sets, *J. Geophys. Res., 89*, 5835-5848, 1984.

Angelier, J., From orientation to magnitudes in paleostress determinations using fault slip data, *J. Struct. Geol., 11*, 1/2, 37-50, 1989.

Angelier, J., Inversion of field data in fault tectonics to obtain the regional stress - III. A new rapid direct inversion method by analytical means, *Geophys. J. Int., 103*, 363-376, 1990.

Angelier, J., A. Tarantola, B. Valette, and S. Manoussis, Inversion of field data in fault tectonics to obtain the regional stress - I. Single phase fault populations: A new method of computing the stress tensor, *Geophys. J. R. Astr. Soc., 69*, 607-621, 1982.

Bergerat, F., J. Angelier and T. Villemin, Fault systems and stress patterns on emerged oceanic ridges: a case study in Iceland, *Tectonophysics., 179*, 183-197, 1990.

Blom, G., *Probability and Statistics: Theory and Application*, Springer-Verlag, New York, 1989.

Bott, M. H. P., The mechanism of oblique slip faulting, *Geol. Mag., 96*, 109-117, 1959.

Caldentey, C., and X. Lana, Implications of principal stress axes and eigenvalue ratios on critical orientation of fractures. Application to two tectonic regions in Alaska, *Pageoph, 133*, 87-102, 1990.

Carey, E., Analyse numérique d'un modèle mécanique élémemtaire appliqué à l'étude d'une population de failles: calcul d'un tenseur moyen des contraintes à partir des stries de glissement, *Thèse de 3ème Cycle,* Université de Paris Sud, 1976.

Carey, E., and B. Brunier, Analyse théorique et numérique d'un modèle mécanique élémentaire

appliqué à l'étude d'une population de failles, *C. R. Hebd. Seanc. Acad. Sci. Ser. D*, *279*, 891-894, 1974.

Carey-Gailhardis, E., and J. L. Mercier, A numerical method for determining the state of stress using focal mechanisms of earthquake populations: application to Tibetan teleseisms and microseismicity of Southern Peru, *Earth planet. Sci. Lett.*, *82*, 165-179, 1987.

Célérier, B., How much does slip on a reactivated fault plane constrain the stress tensor? *Tectonics*, *7*, 1257-1278, 1988.

DeGroot, M. H., *Probability and Statistics*, 2nd edn, Addison-Wesley, 1986.

Etchecopar, A., G. Vasseur, and M. Daignières, An inverse problem in microtectonics for the determination of stress tensors from fault striation analysis, *J. Struct. Geol.*, *3*, 51-56, 1981.

Fisher, N. I., T. Lewis, and B. J. J. Embleton, *Statistical Analysis of Spherical Data*, Cambridge University Press, London, 1987.

Fleischmann, K. H., and Nemcok, M., Paleostress inversion of fault-slip data using the shear stress solutions of Means, *Tectonophysics*, *196*, 195-202, 1991.

Gephart, J. W., Principal stress directions and the ambiguity in fault plane identification from focal mechanism, *Bull. Seismol. Soc. Am.*, *75*, 621-625, 1985.

Gephart, J. W., Stress and the direction of slip on fault planes, *Tectonics*, *9*, 845-858, 1990.

Gephart, J. W., and D. W. Forsyth, An improved method for determining the regional stress tensor using earthquake focal mechanism data: Application to the San Fernando earthquake sequence, *J. Geophys. Res*, *89*, 9305-9320, 1984.

Gephart, J. W., and D. W. Forsyth, On the state of stress in New England as determined from earthquake focal mechanisms, *Geology*, *13*, 70-72, 1985.

Huang, Q., and J. Angelier, Inversion of field data in fault tectonics to obtain the regional stress - II. Using conjugate sets within heterogeneous families for computing paleostress axes, *Geophys. J.*, *96*, 139-149, 1989.

Jaeger, J. C., and N. G. W. Cook. *Fundamentals of Rock Mechanics*, 3rd edn, Chapman and Hall, London, 1979.

Lana, X., and A. M. Correig, An example of stress tensor distribution deduced from the aftershocks of the November 23, 1980 southern Italy earthquake, *Tectonophysics, 135*, 289-296, 1987.

Mandl, G., *Mechanics of Tectonic Faulting*, Elsevier, Amsterdam, 1988.

Mardia, K. V., *Statistics of Directional Data*, Academic Press, London, 1972.

Michael, A. J., Determination of stress from slip data: Faults and folds, *J. Geophys. Res.*, *89*, 11517-11526, 1984.

Michael, A. J., Use of focal mechanisms to determine stress: a control study, *J. Geophys. Res.*, *92*, 357-368, 1987.

Reches, Z., Determination of the tectonic stress tensor from slip along faults that obey the Coulomb yield condition, *Tectonics, 6*, 849-861, 1987.

Vasseur, G., A. Etchecopar, and H. Philip, State of stress inferred from multiple focal mechanisms, *Annu. Geophys.*, *1*, 291-298, 1983.

Vetter, U. R., Variation of the regional stress tensor at the western Great Basin boundary from the inversion of earthquake focal mechanisms, *Tectonics.*, *9*, 63-79, 1990.

Will, T. M., and Powell, R., A robust approach to the calculation of paleostress field from fault plane data, *J. Struct. Geol.*, *13*, 813-821, 1991.

Chapter 5

Determination of the Frictional Strength of Faults from Inversion of Fault Slip Data: a New Method

ABSTRACT

Using the Coulomb-Navier failure criterion as the mechanical constraint, it is possible to determine the average coefficient of friction of faults. The friction coefficient is characterized by the normalized critical stress difference, i.e., the critical stress difference between the maximum and the minimum principal stress divided by the effective pressure. If the stress field is uniform, the normalized critical stress difference is the same for each fault. On the basis of the normalized critical stress difference, a new method is proposed to determine the average friction coefficient of faults and the normalized magnitudes of the principal stresses from inversion of a population of faults of measured orientations and slip directions. This method is applied to four fault-slip data sets taken from field fault measurements. For three of the four examples, an average friction coefficient $\overline{\mu}_0$=0.64, 0.70, and 0.88 is obtained. One example shows a relatively small average friction coefficient $\overline{\mu}_0$=0.22, but this value is of poor quality due to the effect of a possibly non-uniform stress field. These results are in agreement with the average value of friction coefficient (μ_0=0.75) determined from the laboratory experiments. Because the new method is based on the assumption of uniform stress field, the reliability of inversion results decreases with increase of heterogeneity both in the principal directions and in the magnitudes of principal stresses. The pore fluid pressure cannot be determined from inversion of fault-slip data and must

be determined by other independent methods. The results suggest that the long-lasting controversy of whether the deviatoric stress level in the crust is of the order of tens or hundreds of megapascals is mainly due to the uncertainty in the pore fluid pressure.

INTRODUCTION

The geometry of faulting, shown by the orientations of fault planes and associated slip directions, is a direct reflection of the state of stress in the crust. Following the assumptions that the slip direction coincides with the direction of maximum shear stress on the fault plane (Bott, 1959) and that the tectonic stress field in a region is uniform, Carey and Brunier (1974) first proposed a method to determine the tectonic stress field by inversion of a population of faults with known orientations and slip directions. Since then, the method has been greatly improved by many workers (Angelier, 1979; Etchecopar, 1981; Angelier et al., 1982; Angelier, 1984; Gephart and Forsyth, 1984; Michael, 1984; Gephart, 1985; Angelier, 1990). It has now become an economical and simple technique to quantitatively determine the paleostress field (using fault measurement data) and the contemporary stress field (using earthquake focal mechanisms) (Vasseur et al., 1983; Gephart and Forsyth, 1985; Carey-Gailhardis and Mercier, 1987; Lana and Correig, 1987; Michael, 1987; Huang and Angelier, 1989; Zoback, 1989; Bergerat et al., 1990; Caldentey and Lana, 1990; Vetter, 1990; Fleischmann and Nemcok, 1991; Will and Powell, 1991; Wysss et al., 1992).

Using the inversion method based on the geometrical constraint (i.e., the constraint imposed by slip directions), four of the six independent parameters of the stress tensor can be obtained, i.e., the three principal stress directions and the dimensionless stress ratio $\delta=(\sigma_2-\sigma_3)/(\sigma_1-\sigma_3)$. The other two parameters, the magnitudes of two of the three principal stresses, are related to the fault strength and the pore fluid pressure, and cannot be determined on the basis of the geometrical constraint alone. However, as some workers have suggested (Reches, 1987; Célérier, 1988; Gephart, 1988; Angelier, 1989; Gephart, 1992; Reches et al., 1992;), using the Coulomb-

Navier failure criterion as an additional constraint (the mechanical constraint), it is possible to determine the frictional strength of faults from inversion of fault-slip data, and consequently to obtain the fifth parameter of the tectonic stress tensor. Furthermore, introducing the mechanical constraint to stress inversion helps in clarifying the argument that the inversion method based on the geometrical constraint alone does not ensure that each of the observed faults is consistent with a reasonable failure criterion, since a few faults may have too small a shear stress and/or a ratio of the shear stress to normal stress to rupture (Gephart and Forsyth, 1984; Michael, 1984; Reches, 1987; Michael, 1987; Gephart, 1988; Célérier, 1988; Reches et al., 1992). A method based on the mechanical constraint was proposed by Reches et al. (1992). The method was applied to more than twenty areas of different tectonic setting to determine the average frictional coefficient of faults by inversion of fault-slip data. An average friction coefficient was obtained for each area, ranging from 0.0 to 1.3 (Reches et al., 1992). The dispersion of the friction coefficients obtained is much larger than that derived from rock friction experiments (Byerlee, 1978). Moreover, according to the Coulomb-Navier failure criterion, a zero friction coefficient implies that faulting can occur along a preexisting fault plane subject to zero or very small tectonic shear stress. Neither earthquake observations nor in situ stress measurements agree with this inference (Raleigh et al., 1972; Hanks, 1977; Zoback and Healy, 1984). Apparently, the results may be related to some underlying assumption or approximation in the method, rather than to the real strength of faults (Reches et al.'s method is discussed in detail in the sequel).

This chapter deals with the mechanical constraints on the stress field. Firstly, I examine the mathematical basis and physical implications of the previous method proposed by Reches et al. (1992) and discuss its applicability to stress inversion. Then, I propose a new method that incorporates both the geometrical constraint and the mechanical constraint to determine the

frictional strength of geological faults from inversion of fault-slip data.

THEORETICAL BASIS OF STRESS INVERSION

Faulting in the upper crust is usually described in terms of the Coulomb-Navier brittle failure criterion. According to the Coulomb-Navier criterion, two sets of conjugate faults are predicted to develop in homogeneous and isotropic rocks. Consequently, for conjugate fault sets, it is easy to determine the principal stress directions and the friction coefficient of rocks from measurements of the fault geometry (fault plane orientation, slip direction, and angle between the two fault planes). More often, however, faulting in rocks which are anisotropic with respect to strength occurs along preexisting fault planes. The conjugate faults predicted by the Coulomb-Navier failure criterion are no longer a valid concept in this case. Instead, multiple fault mechanisms (i.e., varied fault plane orientations and slip directions) are characteristic of the fault geometry. Obviously, determination of the stress field from the reactivation of preexisting faults is more complex than that from the conjugate faults. This problem is dealt with by various inversion methods.

All the previous inversion methods are based on the following assumptions: (1) The slip occurs along the direction of maximum resolved shear stress on the fault plane (Bott, 1959); (2) the shear and normal stress on the fault satisfy the Coulomb-Navier failure criterion; and (3) the tectonic stress field in a region is spatially and temporally uniform. Assumptions (1) and (2) are often termed the geometrical and the mechanical constraint respectively, which lead to the development of two different types of generalized methods (for example, Carey and Brunier, 1974; Angelier, 1984; Reches, 1987; Angelier, 1990; Gephart, 1990; Reches, 1992; also the

method proposed in Chapter 4 of this thesis). Assumption (3) is necessary for both generalized methods, by which the stress field is determined from inversion of a large population of faults rather than a single or a small number of faults.

In Chapters 3 and 4, two Cartesian coordinate systems were defined, that is, x_i (i=1, 2, 3) coincident with the geographic coordinate system and y_i (i=1, 2, 3) coincident with the principal stress coordinate system, respectively. I have derived in Chapter 4 the expression for the misfit angle between the maximum shear stress direction (**l**) and the slip direction (**p**). The expression is

$$\cos(s)=\mathbf{l}\cdot\mathbf{p}=\frac{-(n_{1y}p_{1y}+\delta n_{2y}p_{2y})}{[(n_{1y}^2+\delta^2 n_{2y}^2)-(n_{1y}^2+\delta n_{2y}^2)^2]^{1/2}} \tag{5.1}$$

In Chapter 3, the critical stress difference has been derived for arbitrarily oriented preexisting faults. Here, I rewrite equation (3.15) as

$$(\sigma_1-\sigma_3)=\frac{\mu_0\rho gz(1-\lambda)+S_0}{[(n_{1y}^2+\delta^2 n_{2y}^2)-(n_{1y}^2+\delta n_{2y}^2)^2]^{1/2}+\mu_0[(u_1^2+\delta v_1^2)-(n_{1y}^2+\delta n_{2y}^2)]} \tag{5.2}$$

where u_1 and v_1 are given in equation (4.4); u_1 and v_1 are identical to m_1 and m_2 in equation (3.15), and denote the cosines of the angles between the σ_1-axis or σ_2-axis and the vertical direction, respectively.

Equations (5.1) and (5.2) are the mathematical expressions for the geometrical constraint (assumption (1)) and the mechanical constraint (assumption (2)), respectively. They provide the mathematical basis for developing different methods of stress inversion. Because the geometrical constraint on the stress field has been studied in Chapter 4, in the following sections I focus on the mechanical constraint. I first discuss the previous inversion methods. Then a new method

based on equation (5.2) is proposed to determine the frictional strength of faults from inversion of a population of fault-slip data.

PREVIOUS INVERSION METHODS

A single or a limited number of faults provide little information about the stress field, but many faults with different orientations and slip directions are likely to impose constraints on the stress field. Therefore, all methods of stress inversion are based on the evaluation of a population of faults. Different inversion methods are characterized by different criteria, resulting in different algorithms. Since the geometrical constraint and the mechanical constraint are likely to constrain different parameters of the stress tensor, I discuss them separately.

1. The Geometrical Constraint

On the basis of the geometrical constraint (equation (5.1)), a number of methods have been proposed to determine the stress field from fault-slip data, in which the best solutions for the unknown parameters of the stress tensor are obtained by minimizing in some way the misfit angle between predicted maximum shear stress direction and observed slip direction. These methods differ mainly in their ways of minimization of the misfit angle (see Angelier (1990) and Chapter 4 of this thesis for a general discussion). In Chapter 4, by introducing probability and spherical statistics theory into the stress inversion problem, I have proven that the misfit angle between the predicted maximum shear stress and the slip direction follows approximately the von Mises or the normal distribution and proposed two new inversion methods, i.e., criterion 5 and

criterion 6. Because the two criteria give rise to nearly the same solutions to the stress field, criterion 6 will be used in this chapter to determine the principal stress directions and the stress ratio δ. Here, I rewrite the criterion 6 as

$$C_6 = \frac{1}{\prod_{i=1}^{n} \sqrt{v_{si}}} \exp\left(-\frac{1}{2}\sum_{i=1}^{n} \frac{s_i^2}{v_{si}}\right) \tag{5.3}$$

where s is the misfit angle given by equation (5.1), v is the variance of the misfit angle, and the subscript i denotes the ith fault. The inversion involves a grid search for solutions in the four dimensional space composed of the four unknown parameters, i.e., the three principal directions and the stress ratio δ. The best solutions for the four unknown parameters are those that maximize criterion 6 (see Chapter 4 for a discussion of the detailed inversion procedure). Hereafter, criterion 6 is called criterion C_6.

2. The Mechanical Constraint

As mentioned above, using the inversion method based on the geometrical constraint, four of the six independent parameters of the stress tensor can be obtained. The other two parameters, the magnitudes of two of the three principal stresses, are related to the fault frictional strength and to the pore fluid pressure and cannot be determined from the geometrical constraint, because the misfit angle (s) in equation (5.1) is not affected by the magnitude of the principal stresses. To overcome this limitation, the Coulomb-Navier failure criterion was introduced to stress inversion by several workers (Reches, 1987; Gephart, 1988; Angelier, 1989; Gephart, 1992; Reches et al., 1992). Reches et al. (1992) proposed a method to determine the in situ friction

coefficient of faults by inversion of fault-slip data. The method has been applied to more than 20 areas of different tectonic settings. An average friction coefficient was obtained for each area, ranging from 0.0 to 1.3 (Reches et al., 1992). As mentioned previously, this result shows an unexpectedly large dispersion in the friction coefficient and zero friction coefficients for some of the areas studied.

In Reches et al.'s model (1992), an ideal local stress tensor is devised to be associated with each fault (here, I use unit vectors $\mathbf{P}^*$, $\mathbf{B}^*$, and $\mathbf{T}^*$ to denote the maximum, the intermediate, and the minimum principal stress direction of this ideal local stress tensor). The ideal local stress tensor is defined as follows: the $\mathbf{P}^*$-$\mathbf{T}^*$ plane coincides with the plane common to the slip $\mathbf{p}$ and the normal $\mathbf{n}$ to the fault plane, and $\mathbf{P}^*$ makes an angle ψ^* with $\mathbf{p}$ and an angle $\psi^*+90°$ with $\mathbf{n}$, where $\psi^*=(1/2)\tan^{-1}(1/\mu_0)$, μ_0 being the friction coefficient (Figure 5.1). Under the ideal local stress, the maximum shear stress coincides with the slip direction on the fault plane and the critical stress difference between the maximum and the minimum principal stress is minimized for each fault according to the Coulomb-Navier failure criterion. Reches et al.'s method consists of searching for a general uniform stress field and an average friction coefficient which are responsible for all faults. The best solutions are those that minimize the sum of the angles between the principal stress axes of the general stress tensor and the corresponding principal stress axes of the ideal local stress tensor for each fault. The criterion or algorithm of this method can be written as (Reches et al., 1992)

$$MC_1 = \sum_{i=1}^{n} (\mathbf{P}_i^* \wedge y_1 + \mathbf{B}_i^* \wedge y_2 + \mathbf{T}_i^* \wedge y_3) \tag{5.4}$$

where y_1, y_2 and y_3 denote the three principal stress directions of the general stress tensor (see Figure 5.1), $\mathbf{P}^*$, $\mathbf{B}^*$, and $\mathbf{T}^*$ the principal stress directions of the ideal local stress tensor, i the ith

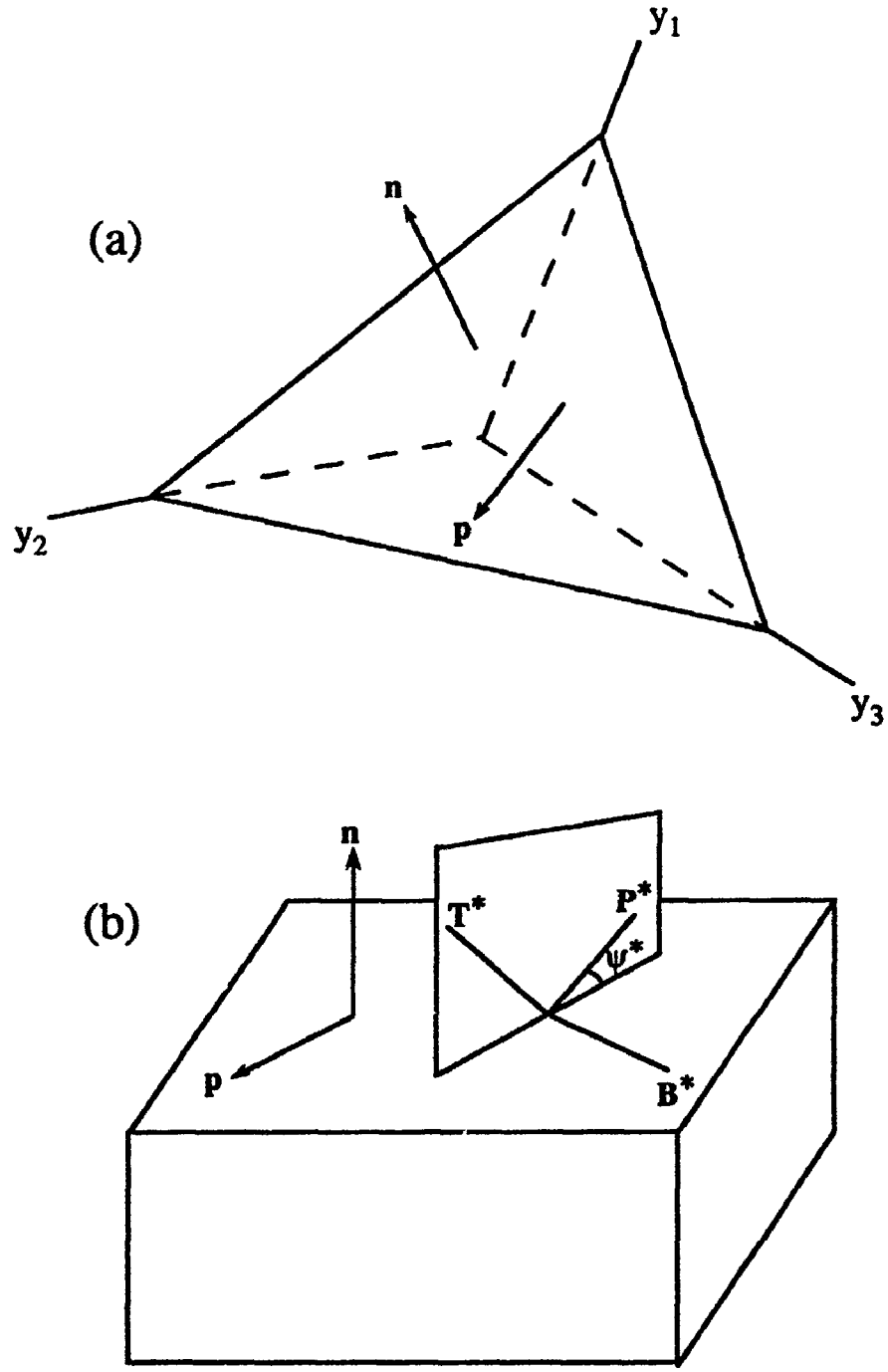

Figure 5.1. Relationship between the general stress field with principal directions y_1, y_2, y_3 and the local stress field with principal directions $\mathbf{P}^*$, $\mathbf{B}^*$, $\mathbf{T}^*$. (a) A fault plane with respect to the general principal stress directions; (b) the same fault plane with respect to the local principal stress directions. The unit vectors **n** and **p** denote the normal to the fault plane and the slip direction, respectively.

fault, and ^ indicates the angle between the two axes. Reches et al., (1992) also proposed another criterion

$$MC_2 = \sum_{i=1}^{n} [(1-\delta)\mathbf{P}_i^{*}\wedge y_1 + \delta \mathbf{T}_i^{*}\wedge y_3] \tag{5.5}$$

where δ is the stress ratio. In equations (5.4) and (5.5), I omit the constant denominators 3n and 2n (n is the total number of faults) which appeared in Reches et al.'s original formulations. These constant denominators do not affect the results of stress inversion.

Now I examine these two criteria. According to the definition of the ideal local stress tensor, the intermediate principal stress direction $\mathbf{B}^{*} = \mathbf{n} \times \mathbf{p}$. Therefore, the components of the unit vector $\mathbf{B}^{*}$ in the x_i-coordinate system (i.e., the geographical coordinate system) can be expressed as

$$\begin{pmatrix} B_{1x}^{*} \\ B_{2x}^{*} \\ B_{3x}^{*} \end{pmatrix} = \begin{pmatrix} n_{2x}p_{3x} - n_{3x}p_{2x} \\ n_{3x}p_{1x} - n_{1x}p_{3x} \\ n_{1x}p_{2x} - n_{2x}p_{1x} \end{pmatrix} \tag{5.6}$$

where n_{ix} and p_{ix} (i=1, 2, 3) are the direction cosines of the normal (**n**) to the fault plane and the slip direction (**p**), respectively. The unit vector $\mathbf{P}^{*}$, indicating the maximum principal direction of the ideal local stress tensor, is related to **p**, **n**, and $\mathbf{B}^{*}$ as follows

$$\begin{aligned} P_{1x}^{*}p_{1x} + P_{2x}^{*}p_{2x} + P_{3x}^{*}p_{3x} &= \cos\psi^{*} \\ P_{1x}^{*}n_{1x} + P_{2x}^{*}n_{2x} + P_{3x}^{*}n_{3x} &= -\sin\psi^{*} \\ P_{1x}^{*}B_{1x}^{*} + P_{2x}^{*}B_{2x} + P_{3x}^{*}B_{3x} &= 0 \end{aligned} \tag{5.7}$$

where $\psi^{*}=(1/2)\tan^{-1}(1/\mu_0)$ is the angle between $\mathbf{P}^{*}$ and **p**. Substituting equatic (5.6) in equation (5.7), the direction cosines of $\mathbf{P}^{*}$ in the x_i-coordinate system can be obtained

$$
\begin{aligned}
P^*_{1x} &= p_{1x}\cos\psi^* - n_{1x}\sin\psi^* \\
P^*_{2x} &= p_{2x}\cos\psi^* - n_{2x}\sin\psi^* \\
P^*_{3x} &= p_{3x}\cos\psi^* - n_{3x}\sin\psi^*
\end{aligned}
\tag{5.8}
$$

Similarly, the components of $\mathbf{T}^*$ in the x_i-coordinate system can be derived by vector multiplication of $\mathbf{B}^*$ and $\mathbf{P}^*$

$$
\begin{aligned}
T^*_{1x} &= -p_{1x}\sin\psi^* - n_{1x}\cos\psi^* \\
T^*_{2x} &= -p_{2x}\sin\psi^* - n_{2x}\cos\psi^* \\
T^*_{3x} &= -p_{3x}\sin\psi^* - n_{3x}\cos\psi^*
\end{aligned}
\tag{5.9}
$$

Equations (5.6), (5.8), and (5.9) show that the angles $\mathbf{P}^*\hat{}\,y_1$ and $\mathbf{T}^*\hat{}\,y_3$ are functions of the slip direction (**p**), the fault plane orientation (**n**), and the coefficient of friction (μ_0), whereas the angle $\mathbf{B}^*\hat{}\,y_2$ is a function of the slip direction and fault plane orientation only.

The cosines of the angles between $\mathbf{P}^*$ and y_1, $\mathbf{B}^*$ and y_2, and $\mathbf{T}^*$ and y_3 can be expressed as

$$
\begin{aligned}
\cos(\mathbf{P}^*\hat{}\,y_1) &= P^*_{1x}u_1 + P^*_{2x}u_2 + P^*_{3x}u_3 \\
\cos(\mathbf{B}^*\hat{}\,y_2) &= B^*_{1x}v_1 + B^*_{2x}v_2 + B^*_{3x}v_3 \\
\cos(\mathbf{T}^*\hat{}\,y_3) &= T^*_{1x}w_1 + T^*_{2x}w_2 + T^*_{3x}w_3
\end{aligned}
\tag{5.10}
$$

where u_i, v_i, and w_i (i=1, 2, 3) are the direction cosines of the three principal stress axes y_1, y_2, and y_3 of the general stress tensor in the x_i-coordinate systems (see the transformation matrix in Chapter 4). Substituting equations (5.6), (5.8), and (5.9) in equation (5.10), one can derive the angles $\mathbf{P}^*\hat{}\,y_1$, $\mathbf{B}^*\hat{}\,y_2$, and $\mathbf{T}^*\hat{}\,y_3$ which constitute the criteria MC_1 and MC_2 (see equations (5.4) and (5.5)) as

$$\begin{aligned}
\mathbf{P}^{*}\wedge y_1 &= \cos^{-1}\left|\cos\psi^{*}(u_1p_{1x}+u_2p_{2x}+u_3p_{3x})-\sin\psi^{*}(u_1n_{1x}+u_2n_{2x}+u_3n_{3x})\right| \\
\mathbf{B}^{*}\wedge y_2 &= \cos^{-1}\left|v_1(n_{2x}p_{3x}-n_{3x}p_{2x})+v_2(n_{3x}p_{1x}-n_{1x}p_{3x})+v_3(n_{1x}p_{2x}-n_{2x}p_{1x})\right| \\
\mathbf{T}^{*}\wedge y_3 &= \cos^{-1}\left|-\sin\psi^{*}(w_1p_{1x}+w_2p_{2x}+w_3p_{3x})-\cos\psi^{*}(w_1n_{1x}+w_2n_{2x}+w_3n_{3x})\right|
\end{aligned} \tag{5.11}$$

The absolute value sign is applied to the terms on the right side of equation (5.11) to denote the fact that each angle in criteria MC_1 and MC_2 (equations (5.4) and (5.5)) refers to the acute angle between two stress axes.

From equation (5.11), one can see that criterion MC_1 (equation (5.4)) does not constrain the stress ratio $\delta=(\sigma_2-\sigma_3)/(\sigma_1-\sigma_3)$, because the angles $\mathbf{P}^{*}\wedge y_1$, $\mathbf{B}^{*}\wedge y_2$, and $\mathbf{T}^{*}\wedge y_3$ are independent of δ. Similarly, it can be proven that criterion MC_2 (equation (5.5)) does not constrain the stress ratio either, although it is introduced into criterion MC_2. Criterion MC_2 can be rewritten as (noting that δ is independent of $\mathbf{P}\wedge y_1$ and $\mathbf{T}\wedge y_3$)

$$MC_2=\sum_{i=1}^{n}\mathbf{P}_i^{*}\wedge y_1+\delta\sum_{i=1}^{n}(\mathbf{T}_i^{*}\wedge y_3-\mathbf{P}_i^{*}\wedge y_1) \tag{5.12}$$

Equation (5.12) shows that MC_2 is a linear function of the stress ratio δ, with a slope equal to $\sum(\mathbf{T}_i^{*}\wedge y_3-\mathbf{P}_i^{*}\wedge y_1)$. Obviously, MC_2 can be a minimum only when that $\delta=0$ or 1 (depending on the quantity $\sum(\mathbf{T}_i^{*}\wedge y_3-\mathbf{P}_i^{*}\wedge y_1)$). In other words, no matter what a data set is, criterion MC_2 always gives rise to either $\delta=0$ or 1 for the stress inversion.

The above analysis shows that the criteria MC_1 and MC_2 proposed by Reches et al. (1992) can be used to determine the three principal stress directions, but not the stress ratio (δ). However, the principal stress directions inverted by Reches' method are less accurate than the methods based on the geometrical constraint, such as the method which I have developed in Chapter 4, because the slip direction on each fault is determined not only by the principal stress directions, but also by the stress ratio δ. This is reflected in the fact that the average misfit angle

(between maximum shear stress and slip direction) calculated by Reches et al.'s method is unexpectedly large for most data sets studied (Reches et al., 1992).

One of the main purposes of Reches' method is to determine the coefficient of friction of faults. Now I examine how much the frictional coefficient is constrained by the criteria MC_1 and MC_2. Here, I consider a special case, i.e., $\mathbf{B}^{*}\wedge y_2=0$ for each fault. Let ψ denote the angle between the maximum principal stress direction (y_1) and the fault plane. The angles between y_1 and **p** (the slip direction), y_1 and **n** (the normal to the fault plane), y_3 and **p**, and y_3 and **n** are therefore equal to ψ, $90°+\psi$, $90°+\psi$, and $180°-\psi$, respectively. Substituting these parameters in equation (5.11) yields

$$\begin{aligned} \mathbf{P}^{*}\wedge y_1 &= \cos^{-1}|\cos\psi^{*}\cos\psi+\sin\psi^{*}\sin\psi| \\ \mathbf{B}^{*}\wedge y_2 &= 0 \\ \mathbf{T}^{*}\wedge y_3 &= \cos^{-1}|\sin\psi^{*}\sin\psi+\cos\psi^{*}\cos\psi| \end{aligned} \tag{5.13}$$

It is reasonable to assume that the best solution of the general stress tensor should be among the many possible candidates which satisfy the conditions that $0\le\mathbf{P}\wedge y_1\le 90°$ and $0\le\mathbf{T}\wedge y_3\le 90°$ for each fault. Therefore, the absolute value signs in equation (5.13) can be removed. Consequently, substituting equation (5.13) in (5.4) gives

$$\begin{aligned} MC_1 &= 2\sum_{i=1}^{n}\cos^{-1}(\cos\psi^{*}\cos\psi_i+\sin\psi^{*}\sin\psi_i) \\ &= 2n\psi^{*}-2\sum_{i=1}^{n}\psi_i \end{aligned} \tag{5.14}$$

Equation (5.14) shows that MC_1 is minimized when ψ^{*} equals to $(1/n)\sum\psi_i$, i.e, the average value of the angle ψ_i (i=1, 2, ..., n) between the maximum principal stress direction y_1 and each fault plane. From the relation $\psi^{*}=(1/2)\tan^{-1}(1/\mu_0)$, one can see that the friction coefficient μ_0 decreases with increasing $(1/n)\sum\psi_i$. Thus, for $(1/n)\sum\psi_i<45°$, $\mu_0>0$ is obtained; for $(1/n)\sum\psi_i\ge 45°$,

$\mu_0 \leq 0$ is the solution for the average friction coefficient. These results show that the average friction coefficient determined by criteria MC_1 and MC_2 is closely related to the average value of angles between the maximum principal stress axis and each fault plane. The above proof, although derived for the special case where the intermediate axes of the local and the general stress tensor coincide, can be extended to the general case where **B**^y does not equal to zero simultaneously for all faults. but the proof has to proceed by a numerical approach.

The above analysis shows that Reches et al.'s method is applicable to new faults developed in homogeneous and isotropic rocks, whose orientation with respect to the principal stress axes is determined by the friction coefficient. Its applicability to reactivated preexisting faults in anisotropic rocks is questionable. For the reactivation of preexisting faults, there is no simple relation between the fault plane orientation with respect to the principal stress axes and the friction coefficient. This is because the preexisting planes of weakness, although randomly distributed, are not uniformly distributed in all directions in three-dimensional space. Consequently, the reactivated faults are often not the most favourably oriented faults satisfying the conditions that the intermediate principal stress axis is parallel to the fault plane and the maximum principal stress axis makes an angle $\psi=(1/2)\tan^{-1}(1/\mu_0)$ with the fault plane, simply because planes of weakness with this orientation do not occur. Both theoretical analysis and well documented field evidence demonstrate that reactivated preexisting faults may deviate by as much as 45° (or more) and as little as 15° (or less) from the maximum principal stress axis (for example, Ivins et al., 1990, and the analysis in Chapter 2 and 3 of this thesis). Therefore, the "friction coefficient" obtained from criteria MC_1 and MC_2 reflects the average value of the angles between the maximum principal stress axis and the fault planes rather than the real strength of faults. The zero "friction coefficient" and the "friction coefficient" larger than 1.3 obtained by

Reches (1992) imply that the angle between the principal stress axis and each fault plane is on the average equal to or larger than 45° and equal to or smaller than 18.8° for the study areas, respectively.

A NEW INVERSION METHOD

The Coulomb-Navier failure criterion is adequate to describe both the formation of new faults and the reactivation of preexisting faults. Based on the Coulomb-Navier criterion, the critical stress difference for arbitrarily oriented preexisting faults can be expressed as a function of material parameters, depth, principal stress direction, stress ratio, and orientation of fault planes (see equation (5.2)). Here, on the basis of the critical stress difference, I propose a new method to determine the average friction coefficient of preexisting faults from inversion of fault-slip data. Using the critical stress difference to develop a inversion technique has also been considered by Angelier (1989) and by Gephart (1992), but the present method is different from theirs.

1. Criterion for Inversion of the Average Friction Coefficient

As shown by equation (5.2), the critical stress difference (σ_1-σ_3) increases with depth and decreases with increase of the pore fluid pressure, which implies that faults at different depths and/or with different pore pressures, though subject to a given tectonic stress field, fail at different magnitudes of the principal stress difference. However, all faults can be brought to the same normalized stress field ($\sigma_{1(n)}$, $\sigma_{2(n)}$, $\sigma_{3(n)}$) by dividing the magnitudes of the original principal

stresses σ_1, σ_2, and σ_3 by $\rho gz(1-\lambda)$ (Figure 5.2). Consequently, from equation (5.2), the dimensionless normalized critical stress difference at faulting can be written as

$$(\sigma_{1(n)}-\sigma_{3(n)}) = \frac{(\sigma_1-\sigma_3)}{\rho gz(1-\lambda)} = \frac{\mu_0 + S_0/[\rho gz(1-\lambda)]}{[(n_{1y}^2+\delta^2 n_{2y}^2)-(n_{1y}^2+\delta n_{2y}^2)^2]^{1/2}+\mu_0[(u_1^2+\delta v_1^2)-(n_{1y}^2+\delta n_{2y}^2)]} \tag{5.15}$$

According to assumption (3), all the faults have the same normalized critical stress difference $(\sigma_{1(n)}-\sigma_{3(n)})$. Byerlee's (1978) experimental results show that the cohesion of a preexisting fault is, on the average, about S_0=0 MPa for $3<\sigma_n<200$ MPa and S_0=60 MPa for $\sigma_n \geq 200$ MPa, where σ_n is the normal stress acting on the fault plane. For both cases, the second term of the numerator on the right side of equation (5.15) is negligible, and thus equation (5.15) can be simplified as

$$(\sigma_{1(n)}-\sigma_{3(n)}) = \frac{\mu_0}{[(n_{1y}^2+\delta^2 n_{2y}^2)-(n_{1y}^2+\delta n_{2y}^2)^2]^{1/2}+\mu_0[(u_1^2+\delta v_1^2)-(n_{1y}^2+\delta n_{2y}^2)]} \tag{5.16}$$

Equation (5.16) expresses the normalized critical stress difference $(\sigma_{1(n)}-\sigma_{3(n)})$ as a function of the friction coefficient, the fault plane orientation, the principal stress directions, and the stress ratio, while effectively neglecting cohesion. The fault plane orientation is known, and the principal stress directions and the stress ratio (δ) can be obtained from stress inversion (such as by criterion C_6, Chapter 4). Therefore, the average friction coefficient can be determined by an inversion method. Suppose that $\overline{\mu}_0$ is the average friction coefficient, and the dispersion of the friction coefficient from the average value if small for each fault. From equation (5.16), the average normalized critical stress difference can be expressed as

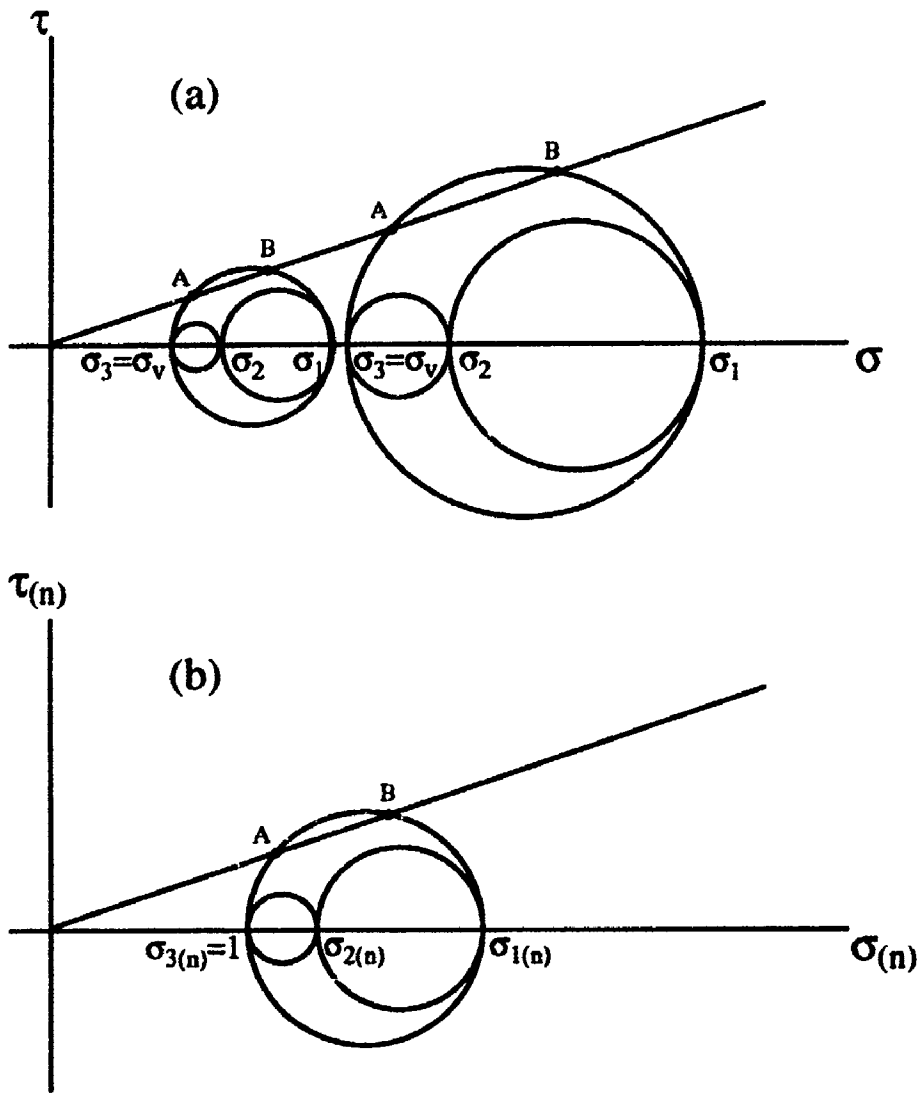

Figure 5.2. The critical stress states of faults A and B subject to two different effective overburden pressures indicated by $\sigma_v=\rho gz(1-\lambda)$. (a) Before normalization of the principal stresses; (b) after normalization of the principal stresses. (It is assumed that $\sigma_3=\sigma_v$ and ratio $\delta=0.3$).

$$(\overline{\sigma}_{1(n)} - \overline{\sigma}_{3(n)}) = \frac{1}{n}\sum_{i=1}^{n}(\sigma_{1(n)} - \sigma_{3(n)})_i \tag{5.17}$$

where the subscript i denotes the ith fault, n the total number of faults, and the normalized critical stress difference $(\sigma_{1(n)}\text{-}\sigma_{3(n)})$ is given by equation (5.16) with replacement of μ_0 by the constant average friction coefficient $\overline{\mu}_0$ for each fault. Thus, for each fault, there is a misfit between normalized critical stress difference and average normalized critical stress difference

$$\Delta(\sigma_{1(n)} - \sigma_{3(n)}) = (\sigma_{1(n)} - \sigma_{3(n)}) - (\overline{\sigma}_{1(n)} - \overline{\sigma}_{3(n)}) \tag{5.18}$$

where $(\overline{\sigma}_{1(n)}\text{-}\overline{\sigma}_{3(n)})$ is given by equation (5.17) and $(\sigma_{1(n)}\text{-}\sigma_{3(n)})$ is given by equation (5.16) with substitution of μ_0 with $\overline{\mu}_0$.

Treatment of the misfit stress differences $\Delta(\sigma_{1(n)}\text{-}\sigma_{3(n)})$ is of primary importance to develop a inversion criterion and algorithm. If the stress field is uniform and each fault has the same frictional properties, the ideal solution for the friction coefficient is the one that makes the sum of the absolute values of misfits zero (Figure 5.3)

$$\sum_{i=1}^{n} |\Delta(\sigma_{1(n)} - \sigma_{3(n)})_i| = 0 \tag{5.19}$$

Equation (5.19) is usually not satisfied, because the average friction coefficient $\overline{\mu}_0$ is used to calculate the misfit stress difference for each fault, whereas different faults may have different friction coefficients. Besides, the misfit stress difference $\Delta(\sigma_{1(n)}\text{-}\sigma_{3(n)})$ also results from other sources, such as measurement errors in fault plane orientation, uncertainties in three principal directions and stress ratio δ, local stress concentrations, and so on. In other words, the misfit stress difference $\Delta(\sigma_{1(n)}\text{-}\sigma_{3(n)})$ is a random variable, affected by many uncertainties and random factors. From a probabilistic point of view, a criterion for inversion of the average friction coefficient should be devised on the basis of the probability distribution of the misfit stress

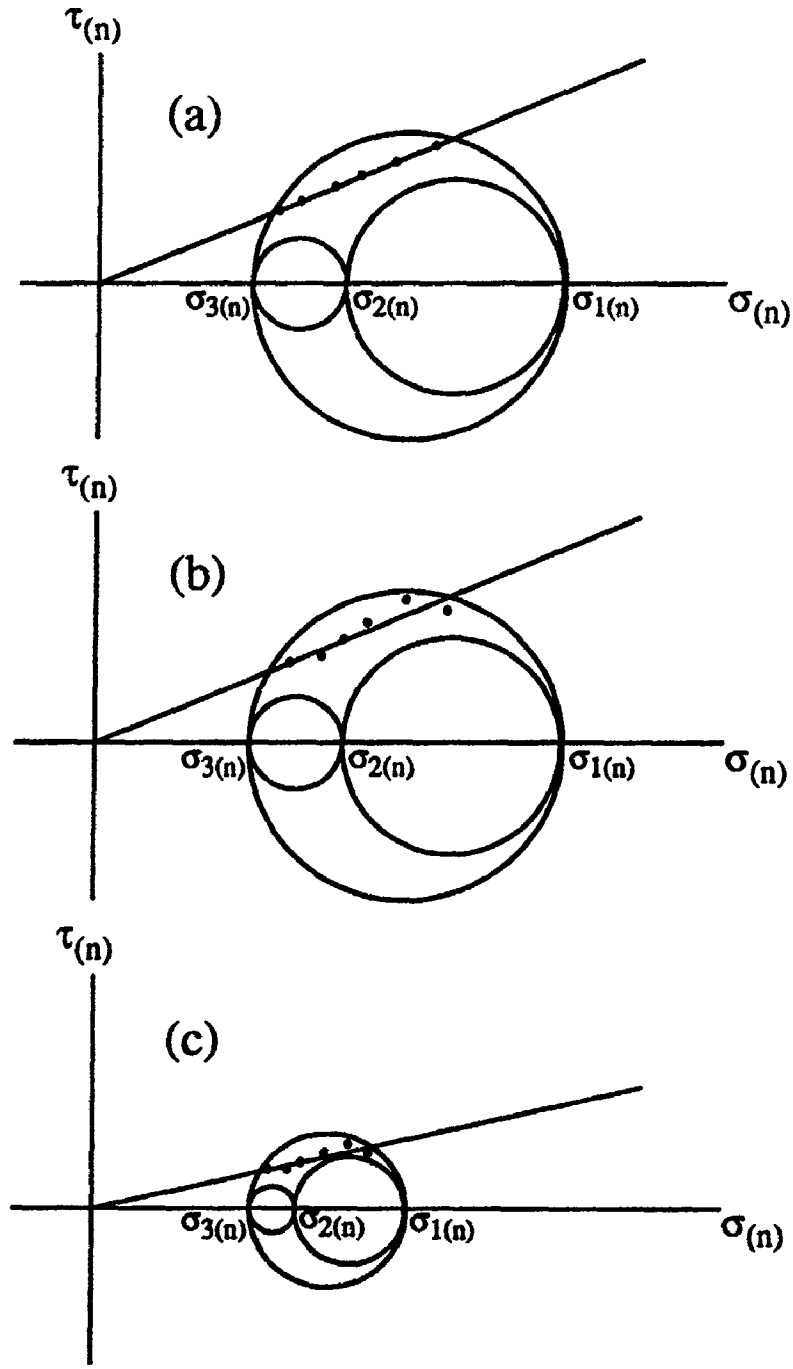

Figure 5.3. Simulated orientations of faults with respect to the principal stress axes. (a) The ideal case where all faults have the same average normalized critical stress difference; (b) and (c) where there is a dispersion in the average normalized critical stress difference, and the distribution of fault orientations indicates a large average friction coefficient for (b) and a small one for (c). The average friction coefficient and the average normalized critical stress difference are denoted by the straight lines and the largest Mohr circles; the stress ratio is δ=0.3.

difference. However, it is difficult to evaluate its distribution because many the above mentioned factors (for instance, the variation of the coefficient of friction and disturbances of local stresses) are unknown. Any a priori assumption about these unknown factors is likely to detract from the physical significance of any inversion criterion. Therefore, I use the method of least squares, which is widely used as empirical criterion (Blom, 1989, pp. 201-202).

Equation (5.16) shows that the normalized critical stress difference is a decreasing function of the coefficient of friction and it goes to zero when the coefficient of friction is equal to zero. Thus, if the search for the average friction coefficient were based on minimization of the sum of squares of misfit stress differences, $\overline{\mu}_0$=0 would always be obtained. This criterion is obviously invalid. To overcome this difficulty, I introduce a parameter $\Delta\sigma_i$

$$\Delta\sigma_i = \frac{\Delta(\sigma_{1(n)} - \sigma_{3(n)})_i}{(\overline{\sigma}_{1(n)} - \overline{\sigma}_{3(n)})} \tag{5.20}$$

$\Delta\sigma_i$ is the misfit ratio for the ith fault, that is, the ratio of the misfit stress difference $\Delta(\sigma_{1(n)}-\sigma_{3(n)})_i$ to the average normalized critical stress difference $(\overline{\sigma}_{1(n)}-\overline{\sigma}_{3(n)})$, given by equations (5.18) and (5.17) respectively. The criterion based on minimizing the sum of squares of the misfit ratios ($\Delta\sigma_i$) can be expressed as

$$MC_3 = \sum_{i=1}^{n} \Delta\sigma_i^2 \tag{5.21}$$

where the subscript i denotes the ith fault. The inversion consists of a search for the best solution for the average friction coefficient $\overline{\mu}_0$ by minimizing criterion MC_3. The basic physical assumption behind this new inversion method is that the normalized critical stress difference at faulting is identical for each fault (see Figure 5.3).

2. Inversion Procedure and Confidence Intervals

Criterion MC_3 is not suitable for the determination of the three principal directions and the stress ratio δ, although it is also a function of these four parameters. This is because the fault slip direction is irrelevant to criterion MC_3, whereas it imposes strong constraints on the principal stress directions and the stress ratio. The three principal stress directions and the stress ratio δ can be determined by criterion C_6 (see equation (5.3)) which is based on the geometrical constraint. Criterion MC_3 is used to determine the average coefficient of friction only.

The inversion procedure is as follows: (1) Criterion C_6 is used to determine the three principal stress directions and the stress ratio δ, and the hypothesis that the data set represents a uniform stress field is tested (see Chapter 4 for detailed procedures); (2) an average friction coefficient, invariant for each fault is chosen; I select a wide range from 0.01 to 1.5; (3) in each step of the iteration, the value of the selected average friction coefficient is changed and the value of MC_3 is calculated according to equation (5.21); the increment in each iterative step is 0.01, i.e., the selected average friction coefficient is increased by 0.01 in each calculation of the value of MC_3; (4) the values of MC_3 for various values of $\overline{\mu}_0$ are compared; the best solution for the average coefficient of friction is the one that minimizes MC_3. A FORTRAN program for this algorithm is listed in Appendix 2.

As mentioned previously, the inversion method based on the geometrical constraint can determine only four of the six independent parameters of the stress field. The other two parameters, which are the magnitudes of two principal stresses (the third can be obtained from δ), are related to the coefficient of friction of faults and the pore fluid pressure. Using the method proposed above, we can determine the average friction coefficient of faults and consequently the

fifth parameter of the stress field. The fifth parameter is characterized by the average normalized critical stress difference. Substituting the inverted average coefficient of friction in equation (5.17), the average normalized critical stress difference ($\overline{\sigma}_{1(n)}$-$\overline{\sigma}_{3(n)}$) can be calculated. Once ($\overline{\sigma}_{1(n)}$-$\overline{\sigma}_{3(n)}$) is determined, the three average normalized principal stresses can be obtained. From equation (3.7) of Chapter 3 and the relation $\sigma_2=\sigma_3+\delta(\sigma_1-\sigma_3)$, the three average normalized principal stresses can be expressed as

$$\begin{aligned}
\overline{\sigma}_{1(n)} &= \frac{\overline{\sigma}_1}{\rho g z(1-\lambda)} = 1-(\overline{\sigma}_{1(n)}-\overline{\sigma}_{3(n)})(u_1^2+\delta v_1^2-1) \\
\overline{\sigma}_{2(n)} &= \frac{\overline{\sigma}_2}{\rho g z(1-\lambda)} = 1-(\overline{\sigma}_{1(n)}-\overline{\sigma}_{3(n)})(u_1^2+\delta v_1^2-\delta) \\
\overline{\sigma}_{3(n)} &= \frac{\overline{\sigma}_3}{\rho g z(1-\lambda)} = 1-(\overline{\sigma}_{1(n)}-\overline{\sigma}_{3(n)})(u_1^2+\delta v_1^2)
\end{aligned} \tag{5.22}$$

where u_1 and v_1 are the cosines of angles between y_1 (σ_1-axis) and x_1 (the vertical) and between y_2 (σ_2-axis) and x_1, respectively.

The precision of inversion of the average friction coefficient is described by the confidence interval. If the probability distribution of the misfit stress difference $\Delta(\sigma_{1(n)}$-$\sigma_{3(n)})$ were known, the confidence interval for the average friction coefficient could be readily determined. However, because the theoretical distribution of $\Delta(\sigma_{1(n)}$-$\sigma_{3(n)})$ is unknown, it is difficult to precisely determine the confidence interval for the average friction coefficient. As addressed above, the method of least squares is used as a empirical criterion to construct criterion MC_3 (see equation (5.21)). Because the least squares method implicitly assumes that the misfit ratio $\Delta\sigma$ for each fault follows the normal distribution, the confidence interval for the average friction coefficient can be estimated based on this assumption. Since $\Delta\sigma$ can be considered as an independent random variable for each fault, using the theorem that the sum of the squares of

independent normal variables follows the χ^2 distribution (Blom, 1989, p. 235), I obtain

$$\frac{1}{v_{\Delta\sigma}}\sum_{i=1}^{n}\Delta\sigma_i^2 \sim \chi^2(n-1) \tag{5.23}$$

where $v_{\Delta\sigma}$ is the variance of $\Delta\sigma$. The estimated (or sample) variance of the misfit ratios can be expressed as

$$\hat{v}_{\Delta\sigma}=\frac{1}{(n-1)}\sum_{i=1}^{n}\Delta\sigma_i^2 \tag{5.24}$$

The solution for the average friction coefficient is one that minimizes the criterion MC_3. This implies that $\hat{v}_{\Delta\sigma}$ is the minimal one among all possible values, each of which corresponds to a selected average friction coefficient. Therefore, choosing a confidence level $1-\alpha_2$, the confidence interval for the inverted average friction coefficient can be estimated by constructing a one-sided confidence interval for $v_{\Delta\sigma}$. From equation (5.23), the one-sided $1-\alpha_2$ confidence interval for $v_{\Delta\sigma}$ is

$$v_{\Delta\sigma}<\frac{1}{\chi^2_{1-\alpha_2}(n-1)}\sum_{i=1}^{n}\Delta\sigma_i^2 \tag{5.25}$$

i.e.,

$$v_{\Delta\sigma}<\frac{(n-1)\hat{v}_{\Delta\sigma}}{\chi^2_{1-\alpha_2}(n-1)} \tag{5.26}$$

where the sample variance $\hat{v}_{\Delta\sigma}$ is given by equation (5.24). The confidence limits for the average friction coefficient are those that yield the two values of MC_3 equal to the confidence limit for $v_{\Delta\sigma}$ times (n-1), where n is the sample size. Following the same procedure, the confidence intervals for the normalized three principal stresses (equations (5.22)) can be estimated.

In summary, incorporating both the geometrical constraint (fault slip) and the mechanical constraint (the Coulomb-Navier failure criterion) in the inversion of fault data allows the determination of five of the six independent parameters of the tectonic stress field. The only parameter which cannot be determined by the present method is the pore fluid pressure. The stress analysis (see equation (5.2)) shows that the role played by pore fluid pressure in faulting is analogous to that of depth. Since depth does not affect fault orientations and slip directions (for a given stress field), the pore fluid pressure is unlikely to be relevant to fault plane orientations and slip directions. Consequently, the pore fluid pressure cannot be determined by a method based on inversion of fault-slip data. It must be determined by other independent approaches, such as in situ measurements.

EXAMPLES

The new inversion method (equation (5.21)) is applied to four field examples. All the four examples are taken from field fault measurements. The first three data sets (sites AVB, TYM, and KAM) have been used in Chapter 4 to determine the principal stress directions and the stress ratio δ (see Table 4.1 in Chapter 4 for listing of the data). Those results (i.e., the principal stress directions and the stress ratio) for sites AVB, TYM, and KAM will be used here to determine the average coefficient of friction and the three normalized principal stresses. The fourth data set comes from Etchecopar et al. (1981). The data set, composed of 38 faults, was collected in the Permian basin of Lodève, Hérault, France (site LOD). This area is characterized by extensional tectonics with predominant normal dip-slip and oblique-slip (Etchecopar et al., 1981). The data from site LOD are listed in Table 5.1.

Table 5.1. Fault-slip data from site LOD. All the faults are normal or normal strike-slip, denoted by N. Retabulated from Etchecopar et al. (1981).

Site	Fault Plane		Slip		Sense of Slip
	Strike	Dip	Pitch of Striae	Azimuth	
LOD	150	85E	55N		N
	85	58N	90E		N
	97	75N	90E		N
	120	70N	75W		N
	125	70N	80W		N
	90	85N	85E		N
	5	75E	90N		N
	110	65N	85W		N
	100	60N	90E		N
	100	70S	90E		N
	85	70S	90E		N
	120	62S		09	N
	100	55N	90E		N
	129	45S		35	N
	122	70N	75W		N
	125	70N	75W		N
	125	46S		25	N
	84	75S	82W		N
	120	80N	70W		N
	2	72E	75N		N
	106	74S	90E		N
	136	65E	70N		N
	10	86W	85N		N
	37	85W	70N		N
	20	70W	90N		N
	0	85E	85S		N
	85	55N	75E		N
	130	75N	80W		N
	15	86W	80N		N
	30	38W		114	N
	95	60S	75W		N
	105	86N	60W		N
	105	75N	90E		N
	130	75N	80W		N
	110	80N	70W		N
	90	48N	80W		N
	100	49N	85E		N
	20	45W		95	N

Following the inversion procedure described in the above section, the four sets of data are inverted to obtain the three principal stress directions, the stress ratio δ, the average friction coefficient, and the three average normalized principal stresses. In order to compare results with the previous methods, the four data sets are also inverted by criterion MC_1 proposed by Reches (1992), in which the selected range of the average friction coefficient is 0.0-1.5, and the increment in each iterative step is 0.01 for the friction coefficient and 1° for the principal stress directions. Table 5.2 lists the three principal stress directions inverted by criterion C_6 and criterion MC_1, and the stress ratio δ inverted by criterion C_6 (because the stress ratio cannot be determined by criterion MC_1) for the four areas, i.e., sites AVB, TYM, KAM, and LOD. The inversion results for the principal stress directions by the two methods are also plotted in Figure 5.4.

Reches et al. (1992) argued that methods based on the geometrical constraint, such as criterion C_6, are less powerful than criterion MC_1 because the misfit angle between the predicted maximum shear stress and slip direction may vanish for large numbers of general stress tensors (or fields). For instance, when the plane common to the σ_1-axis and σ_3-axis coincides with the plane defined by the slip and the normal to the fault plane, the misfit angle S vanishes for $0°<\psi<90°$, but the misfit angles between the principal stress directions of the ideal local stress tensor and those of the general stress tensor vanish only for a unique orientation $\psi^*=(1/2)\tan^{-1}(1/\mu_0)$, where ψ and ψ^* are the angles between the σ_1-axis and the fault plane, and $\mathbf{P}^*$ and the fault plane, respectively (see Figure 5.1). This argument is certainly valid for conjugate faults. If all faults belong to exact conjugate sets, criterion C_6 must fail. However, faulting in anisotropic rocks is characterized by reactivation of preexisting faults. Usually, the distribution of fault plane orientations deviate from the conjugate sets to some extent, and the distribution of slip direction is more or less asymmetrical. The above argument is no longer valid

Table 5.2. Results of stress inversion for sites AVB, TYM, KAM, and LOD with different methods. The three principal stress axes are denoted by σ_1, σ_2 and σ_3, respectively. Stress ratio and estimated standard deviation for the measurement errors in both fault plane orientation and slip direction are denoted by δ and $\Phi^{1/2}$. The computing precision is 1° for σ_1, σ_2 and σ_3, 0.01 for δ and 0.1° for $\Phi^{1/2}$.

Site	Method	σ_1		σ_2		σ_3		δ	$\Phi^{1/2}$
		Plunge	Trend	Plunge	Trend	Plunge	Trend		
AVB	Criterion C_6	75°	63°	15°	244°	0°	154°	0.26	7.4
	Criterion MC_1	73°	71°	17°	238°	4°	330°		
TYM	Criterion C_6	83°	202°	6°	57°	4°	327°	0.13	12.1
	Criterion MC_1	83°	236°	7°	53°	0°	143°		
KAM	Criterion C_6	82°	242°	3°	131°	8°	41°	0.32	20.4
	Criterion MC_1	78°	229°	6°	108°	10°	16°		
LOD	Criterion C_6	90°	na	0°	99°	0°	189°	0.14	5.8
	Criterion MC_1	82°	279°	8°	113°	2°	23°		

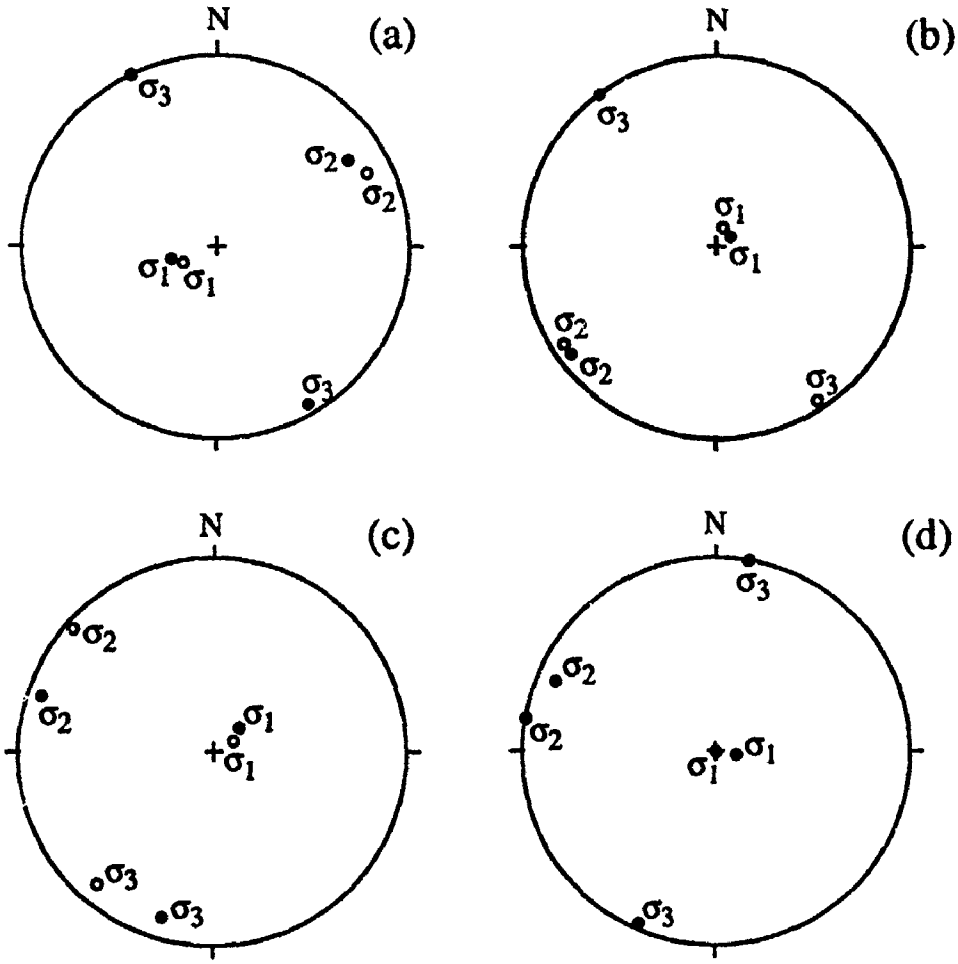

Figure 5.4. Principal stress directions determined by criterion 6 (open circles) and criterion MC_1 (solid circles). (a) Site AVB; (b) site TYM; (c) site KAM; (d) site LOD. Upper hemisphere Schmidt's projection.

in this case. As a matter of fact, criterion C_6 is more powerful than criterion MC_1 in the determination of the principal stress directions when the distribution of fault plane orientations has higher dispersion. This point is well supported by the four examples studied. Having compared the results obtained by the two different methods, I find that when the distribution of both fault plane orientations and slip directions is less scattered, such as in the cases of sites AVB and TYM where fault planes are close to the conjugate sets and slips are relatively symmetric, the two methods (criteria C_6 and MC_1) give rise to similar results for the principal stress directions. However, when the distribution of fault plane orientations and slip directions is more scattered, such as for site KAM and LOD, the difference between criteria C_6 and MC_1 becomes larger.

The misfit angle, variance, and normalized misfit angle for each fault from site LOD are listed in Table 5.3. The normalized misfit angles are used to test the hypothesis that the stress field is uniform for site LOD, according to the χ^2 procedure described in Chapter 4. The result of hypothesis testing is shown in Figure 5.5. For site LOD, the value of Q (see equation (4.39)) is 7.606 and the corresponding significance level at which the null hypothesis is rejected is α_1=0.369. Therefore, the hypothesis that the stress field is uniform is accepted for site LOD at a significance level much higher than the conventional $\alpha_1 \leq 0.05$. The hypothesis testing for sites AVB, TYM, and KAM has been performed in Chapter 4. Note, however, that the size of the population for site LOD is not very large, and therefore the test is not very robust.

In the inversion of fault-slip data to determine the average friction coefficient, three faults, whose normals are very close to the σ_1-axis, are omitted and 47 of 50 faults are used for site KAM. For the other three examples, all faults are used. Table 5.4 lists the average friction coefficient of faults inverted by criteria MC_1 and MC_3 for sites AVB, TYM, KAM, and LOD.

Table 5.3. Results for calculated misfit angle (s), variance (v), and normalized misfit angle (s*) for each of the faults from site LOD (angles in degrees). The faults are listed in the same sequence as for Table 5.1.

Site	s	v	s*
LOD	-5.64	1090.1143	-0.98
	3.58	36.0190	3.43
	1.08	43.5541	0.94
	7.06	41.5080	6.30
	0.59	42.3107	0.52
	8.98	341.7477	2.79
	-2.50	47.5732	-2.09
	1.43	37.5519	1.34
	-0.28	36.5330	-0.27
	-0.41	39.3496	-0.37
	5.53	40.4261	5.01
	4.20	36.5644	4.00
	-0.24	36.0093	-0.23
	-2.08	34.1782	-2.04
	6.44	41.8332	5.73
	5.59	42.3107	4.94
	2.33	34.4909	2.28
	-1.08	49.3009	-0.88
	4.64	114.4571	2.50
	11.36	43.6668	9.89
	-3.52	43.3236	-3.08
	10.48	37.6768	9.82
	-2.67	224.3037	-1.02
	16.78	1039.3395	2.99
	5.06	41.9216	4.50
	-21.04	426.0445	-5.86
	-11.69	35.6930	-11.26
	-3.93	60.9842	-2.89
	3.62	541.4027	0.89
	8.88	34.9424	8.64
	-13.89	36.5163	-13.22
	18.20	424.1057	5.08
	-3.22	44.4712	-2.78
	-3.93	60.9842	-2.89
	11.37	75.2847	7.54
	11.86	35.5372	11.44
	-5.22	35.7200	-5.02
	13.45	36.0306	12.89

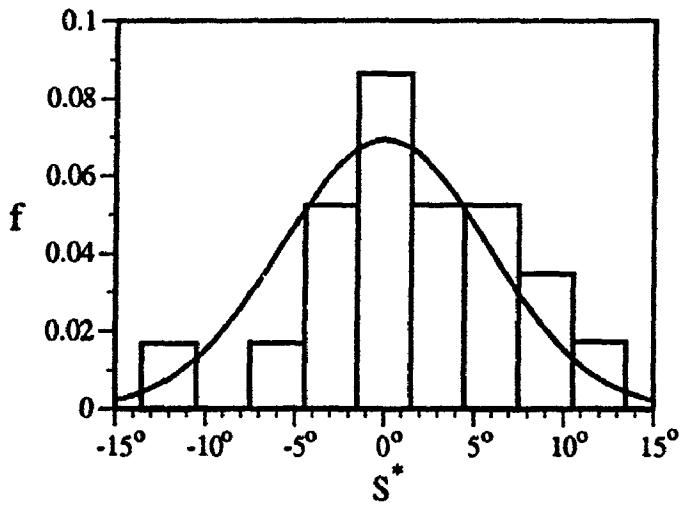

Figure 5.5. Histograms of the distribution of normalized misfit angle (S^*) compared with the normal distribution (curve) for the estimated variance $\Diamond$ for site LOD.

Table 5.4. Inversion results for the average friction coefficient ($\overline{\mu}_0$), average normalized critical stress difference ($\overline{\sigma}_{1(n)}$-$\overline{\sigma}_{3(n)}$), average normalized principal stresses ($\overline{\sigma}_{1(n)}$, $\overline{\sigma}_{2(n)}$, $\overline{\sigma}_{3(n)}$) for sites AVB, TYM, KAM, and LOD with different methods.

Site	Method	$\overline{\mu}_0$	$(\overline{\sigma}_{1(n)}-\overline{\sigma}_{3(n)})$	$\overline{\sigma}_{1(n)}$	$\overline{\sigma}_{2(n)}$	$\overline{\sigma}_{3(n)}$
AVB	Criterion MC_1	0.68				
	Criterion MC_3	0.64	0.78	1.04	0.45	0.26
TYM	Criterion MC_1	0.63				
	Criterion MC_3	0.70	0.78	1.01	0.33	0.23
KAM	Criterion MC_1	0.0				
	Criterion MC_3	0.22	0.46	1.01	0.70	0.55
LOD	Criterion MC_1	0.96				
	Criterion MC_3	0.88	0.89	1.00	0.23	0.11

The average normalized critical stress difference and average normalized magnitudes of principal stresses are calculated according to equations (5.17) and (5.22). The results obtained by criterion MC_3 are also plotted in Figures 5.6 and 5.7. It is interesting to note that, as in the case of principal stress directions, criteria MC_1 and MC_3 yield similar average friction coefficients for sites AVB and TYM, but noticeably different results for sites KAM and LOD. As mentioned before, the dispersion both in fault plane orientations and in slip directions is small for sites AVB and TYM and relatively large for sites KAM and LOD. The above results suggest that the difference between criterion MC_3 and criterion MC_1 increases with the increase of the dispersion in fault plane orientations and slip directions. In three of the four examples, the new method (criterion MC_3) yields an average friction coefficient ranging from 0.64 to 0.88. These results are coincident with the average value of friction coefficient μ_0=0.75 derived from laboratory experiments (Byerlee, 1978). For site KAM, a relatively small average friction coefficient μ_0=0.22 is obtained. However, because the new method is based on the assumption that the stress field is uniform, this result could be affected by an inhomogeneous stress field. As discussed in Chapter 4, the estimated standard deviation ($\Phi^{1/2}$=20.4°) of measurement errors for site KAM is large, which may indicate a non-uniform stress field, because the χ^2 method tests only the shape of distribution of a random variable but not its variance. When a population of faults which actually come from different stress fields is forced into a uniform stress field, their orientations with respect to the principal stress axes of this uniform field are greatly biased and some of the faults may be perpendicular to the principal stress axes. In this case, a small average friction coefficient is always obtained by the present method. Therefore, the average coefficient of friction for site KAM is less significant than those for sites AVB, TYM, and LOD because of the possible effect of inhomogeneous stress field.

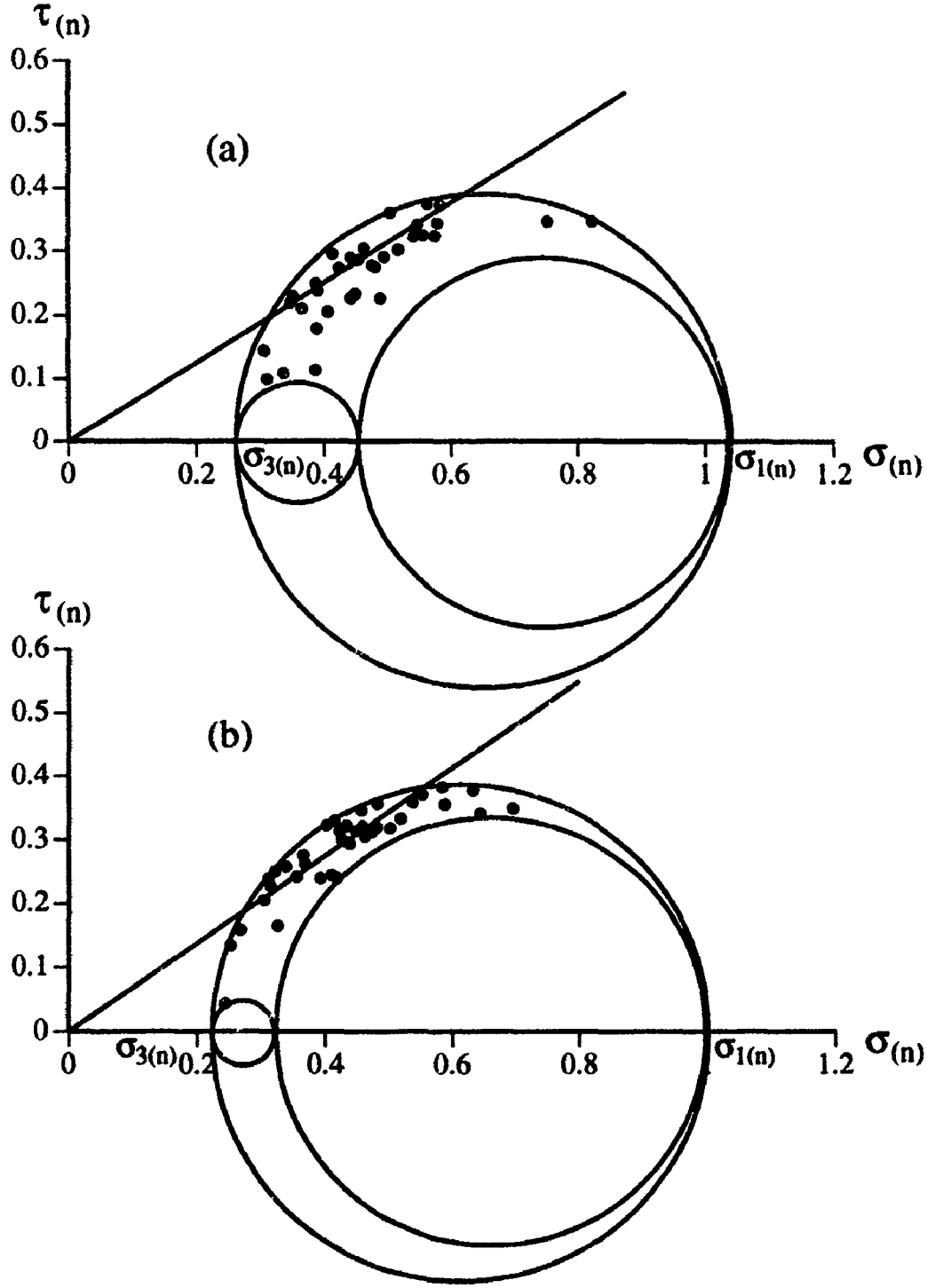

Figure 5.6. Distribution of fault plane orientations, inverted average friction coefficient (straight lines), and normalized critical stress difference (circles). (a) Site AVB; (b) site TYM.

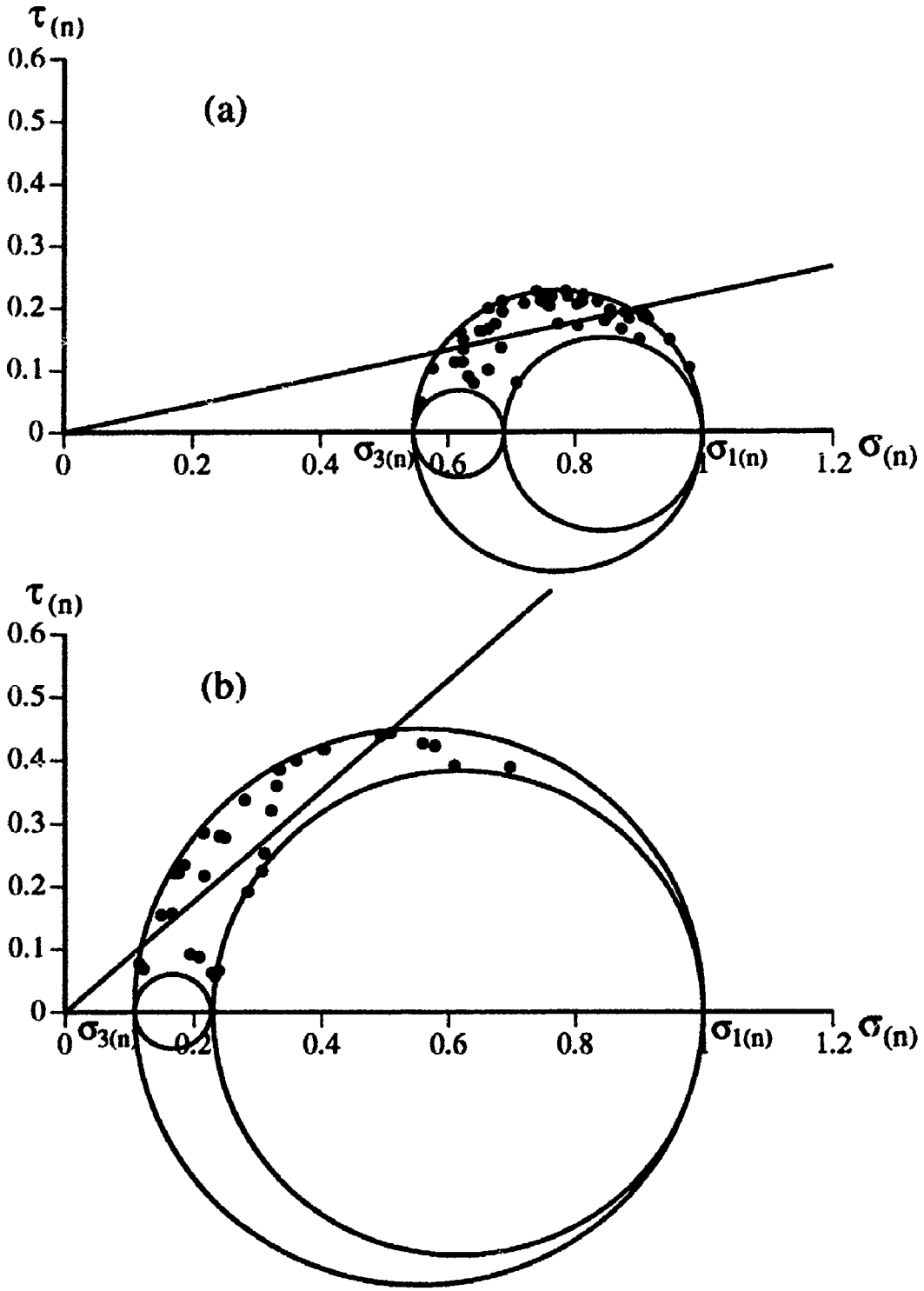

Figure 5.7. Distribution of fault plane orientations, inverted average friction coefficient (straight lines), and normalized critical stress difference (circles). (a) Site KAM; (b) site LOD.

The 90% confidence intervals for the average friction coefficient, average normalized critical stress difference, and average normalized magnitudes of the principal stresses inverted by criterion MC_3 are calculated based on the assumption that the misfit ratio $\Delta\sigma$ follows the normal distribution, and the results are listed in Table 5.5. Comparing Table 5.5 with Table 4.4 in Chapter 4, one finds that the 90% confidence interval for the average friction coefficient is much larger than those for the principal stress directions. This result suggests that the geometry of faulting, i.e., fault plane orientations and slip directions, imposes stronger constraints on the orientation of the stress field than on the magnitude of stresses and frictional strength.

Although the above examples are not sufficient to draw a definite conclusion, they help to clarify some of the arguments on whether inversion methods based on the geometrical constraint alone ensure that each of the observed fault planes is consistent with a reasonable failure criterion (Gephart and Forsyth 1984; Michael 1984; Reches 1987; Michael 1987; Gephart 1988; Célérier 1988). Of the four examples, three data sets (sites AVB, TYM, and LOD), which are well characterized by uniform stress fields, give rise to large ratios of the shear stress to the normal stress for most faults except for a number of faults which require a small coefficient of friction so that faulting can occur along them. For site KAM, the ratio between shear stress and normal stress is small on most faults. However, as discussed above, this may result from a non-uniform stress field rather than from the inversion method itself. In addition, it should be pointed out that even for sites AVB, TYM, and LOD, the "uniform stress fields" are the first-order approximations. They may be non-uniform to some extent. Consequently, a few faults with small shear stress-normal stress ratios are not necessarily significant.

Table 5.5. Estimates of 90% confidence intervals for the average friction coefficient ($\overline{\mu}_0$), average normalized critical stress difference ($\overline{\sigma}_{1(n)}$-$\overline{\sigma}_{3(n)}$), and average normalized principal stresses ($\overline{\sigma}_{1(n)}$, $\overline{\sigma}_{2(n)}$, $\overline{\sigma}_{3(n)}$) obtained by criterion MC_3 (see Table 5.4).

Site	$\overline{\mu}_0$	$(\overline{\sigma}_{1(n)}-\overline{\sigma}_{3(n)})$	$\overline{\sigma}_{1(n)}$	$\overline{\sigma}_{2(n)}$	$\overline{\sigma}_{3(n)}$
AVB	0.45 - 0.94	0.66 - 0.91	1.03 - 1.05	0.36 - 0.53	0.14 - 0.37
TYM	0.50 - 1.00	0.67 - 0.90	1.01 - 1.01	0.23 - 0.42	0.11 - 0.34
KAM	0.10 - 0.41	0.24 - 0.72	1.01 - 1.02	0.53 - 0.84	0.30 - 0.77
LOD	0.60 - 1.38	0.79 - 1.01	1.00 - 1.00	0.13 - 0.32	-0.01 - 0.21

DISCUSSION AND CONCLUSIONS

The common stress inversion methods which are based on the geometrical constraint allow the determination of four of the six independent parameters of the tectonic stress field, i.e., the three principal stress directions and the stress ratio δ. Using the Coulomb-Navier failure criterion as an additional constraint (the mechanical constraint), it is possible to determine the frictional strength of faults, and consequently to determine the fifth parameter of the stress field. The fifth parameter is characterized by the normalized critical stress difference, i.e., the critical stress difference (σ_1-σ_3) divided by the effective overburden pressure ($\rho gz(1-\lambda)$). The pore fluid pressure that constrains the sixth parameter of the stress field cannot be determined from inversion of fault-slip data, because it is irrelevant to the geometry (as opposed to the occurrence) of faulting. Therefore, the pore fluid pressure must be determined by other independent methods.

In this chapter, the inversion method proposed by Reches et al. (1992) to determine the average friction coefficient of faults has been examined. It has been found that the applicability of their method is restricted to conjugate faults developed in homogeneous and isotropic rocks, where fault plane orientations with respect to the maximum principal stress axis are directly related to the friction coefficient of rocks. The method is problematic when applied to reactivation of preexisting faults in anisotropic rocks, where faulting geometry is characterized by various orientations of fault planes and asymmetric slip directions.

By combining the geometrical and the mechanical constraint, a new method has been proposed to determine the average friction coefficient of faults from inversion of a population of faults of measured orientations and slip directions. The new method is based on the assumption that the normalized critical stress difference is constant for each fault, which is

consistent with the general assumption that the stress field is uniform. The inversion procedure of the new method comprises two steps: (1) using criterion C_6 to obtain the principal stress directions and the stress ratio; and (2) regarding these four parameters of stress field as known, using criterion MC_3 to determine the average friction coefficient and the normalized magnitudes of the principal stresses.

The new method has been applied to four data sets taken from field fault measurements. An average friction coefficient ranging from 0.64 to 0.88 has been obtained for three of the four data sets. One data set shows a relatively small average coefficient of friction ($\overline{\mu}_0$=0.22), but the quality of this value is poor because of the possible effect of a non-uniform stress field. The inversion results are coincident with the average value of friction coefficient μ_0=0.75 obtained from laboratory experiments. These results suggest that the uncertainty in the level of tectonic stresses in upper crust (for instance, the controversy of whether the deviatoric stress in the deep upper crust is of the order of tens or hundreds of megapascals) is mainly due to the uncertainty in the pore fluid pressure.

Because a probabilistic basis to the distribution of the misfit ratio $\Delta\sigma$ is lacking, the new method is based on an empirical criterion (least squares). This prevents the development of a procedure to test whether the magnitudes of the stress field are uniform. Further work, introducing probability theory into the inversion of the average friction coefficient, is necessary to improve the present method. Furthermore, because the model is established on the basis of the assumption that the stress field is uniform, inversion results for the average friction coefficient are of significance only in the case where the tectonic stress field is relatively uniform both in the principal directions and in the magnitudes of the principal stresses, that is, the effects of heterogeneous stresses are small.

REFERENCES

Angelier, J., Determination of the mean principal directions of stresses for a given fault population, *Tectonophysics, 56*, T17-T26, 1979.

Angelier, J., Tectonic analysis of fault slip data sets, *J. Geophys. Res., 89*, 5835-5848, 1984.

Angelier, J., From orientation to magnitudes in paleostress determinations using fault slip data, *J. Struct. Geol., 11*, 1/2, 37-50, 1989.

Angelier, J., Inversion of field data in fault tectonics to obtain the regional stress - III. A new rapid direct inversion method by analytical means, *Geophys. J. Int., 103*, 363-376, 1990.

Angelier, J., A. Tarantola, B. Valette, and S. Manoussis, Inversion of field data in fault tectonics to obtain the regional stress - I. Single phase fault populations: A new method of computing the stress tensor, *Geophys. J. R. Astr. Soc., 69*, 607-621, 1982.

Bergerat, F., J. Angelier and T. Villemin, Fault systems and stress patterns on emerged oceanic ridges: a case study in Iceland, *Tectonophysics., 179*, 183-197, 1990.

Blom, G., *Probability and Statistics: Theory and Application*, Springer-Verlag, New York, 1989.

Bott, M. H. P., The mechanism of oblique slip faulting, *Geol. Mag., 96*, 109-117, 1959.

Byerlee, J. D., Friction of rocks, *Pure Appl. Geophys., 116*, 615-626, 1987.

Caldentey, C., and X. Lana, Implications of principal stress axes and eigenvalue ratios on critical orientation of fractures. Application to two tectonic regions in Alaska, *Pageoph, 133*, 87-102, 1990.

Carey, E., and B. Brunier, Analyse théorique et numérique d'un modèle mécanique élémentaire appliqué à l'étude d'une population de failles, *C. R. Hebd. Seanc. Acad. Sci. Ser. D, 279*, 891-894, 1974.

Carey-Gailhardis, E., and J. L. Mercier, A numerical method for determining the state of stress using focal mechanisms of earthquake populations: application to Tibetan teleseisms and microseismicity of Southern Peru, *Earth planet. Sci. Lett., 82*, 165-179, 1987.

Célérier, B., How much does slip on a reactivated fault plane constrain the stress tensor? *Tectonics, 7*, 1257-1278, 1988.

Etchecopar, A., G. Vasseur, and M. Daignières, An inverse problem in microtectonics for the determination of stress tensors from fault striation analysis, *J. Struct. Geol., 3*, 51-56, 1981.

Fleischmann, K. H., and Nemcok, M., Paleostress inversion of fault-slip data using the shear stress solutions of Means, *Tectonophysics, 196*, 195-202, 1991.

Gephart, J. W., Principal stress directions and the ambiguity in fault plane identification from focal mechanism, *Bull. Seismol. Soc. Am., 75*, 621-625, 1985.

Gephart, J. W., Stress and the direction of slip on fault planes, *Tectonics, 9*, 845-858, 1990.

Gephart, J. W., On the use of stress inversion of fault-slip data to infer the frictional strength of rocks (abstract), *Eos Trans. AGU, 69*, 1462, 1988.

Gephart, J. W., Fault geometries as constraints on the stress tensor (abstract), *Eos Trans. AGU, 73*, 298, 1992.

Gephart, J. W., and D. W. Forsyth, An improved method for determining the regional stress tensor using earthquake focal mechanism data: Application to the San Fernando earthquake sequence, *J. Geophys. Res, 89*, 9305-9320, 1984.

Gephart, J. W., and D. W. Forsyth, On the state of stress in New England as determined from earthquake focal mechanisms, *Geology, 13*, 70-72, 1985.

Hanks, T. C., Earthquake stress drops, ambient tectonic stresses, and stresses that drive plates,

Pure Appl. Geophys., *115*, 441-458, 1977.

Huang, Q., and J. Angelier, Inversion of field data in fault tectonics to obtain the regional stress - II. Using conjugate sets within heterogeneous families for computing paleostress axes, *Geophys. J.*, *96*, 139-149, 1989.

Ivins, E. R., T. H. Dixon, and M. P. Golombek, Extensional reactivation of an abandoned thrust: a bound on shallowing in the brittle regime, *J. Struct. Geol.*, *12*, 303-314, 1990.

Lana, X., and A. M. Correig, An example of stress tensor distribution deduced from the aftershocks of the November 23, 1980 southern Italy earthquake, *Tectonophysics*, *135*, 289-296, 1987.

Michael, A. J., Determination of stress from slip data: Faults and folds, *J. Geophys. Res.*, *89*,11517-11526, 1984.

Michael, A. J., Use of focal mechanisms to determine stress: a control study, *J. Geophys. Res.*, *92*, 357-368, 1987.

Raleigh, C. B., J. H. Healy, and J. D. Bredehoeft, Faulting and crustal stress at Rangely, Colorado, in *Flow and Fracture of Rocks, Geophys. Monog. Ser.*, vol. 16, edited by Heard H. C., I. Y. Borg, N. L. Carter, and C. B. Raleigh, pp. 275-284, AGU, Washington D. C., 1972.

Reches, Z., Determination of the tectonic stress tensor from slip along faults that obey the Coulomb yield condition, *Tectonics*, *6*, 849-861, 1987.

Reches, Z., G. Baer, and Y. Hatzor, Constraints on the strength of the upper crust from stress inversion of fault slip data, *J. Geophys. Res.*, *97*, 12481-12493, 1992.

Vasseur, G., A. Etchecopar, and H. Philip, State of stress inferred from multiple focal mechanisms, *Ann. Geophys.*, *1*, 291-298, 1983.

Vetter, U. R., Variation of the regional stress tensor at the western Great Basin boundary from the inversion of earthquake focal mechanisms, *Tectonics.*, *9*, 63-79, 1990.

Will, T. M., and Powell, R., A robust approach to the calculation of paleostress field from fault plane data, *J. Struct. Geol.*, *13*, 813-821, 1991.

Wyss, M., B. Liang, W. R. Tanigawa, and X. Wu, Comparison of orientations of stress and strain tensors based on fault plane solutions in Kaoiki, Hawaii, *J. Geophys. Res.*, *97*, 4769-4790, 1992.

Zoback, M. L., State of stress and modern deformation of the northern Basin and Range province, *J. Geophys. Res.*, *94*, 7105-7128, 1989.

Zoback, M. D., and J. H. Healy, Friction, faulting and in situ stress, *Annu. Geophys.*, *2*, 689-698, 1984.

Chapter 6

Modelling of Earthquake Rupturing as a Stochastic Process and Estimation of its Distribution Function from Earthquake Observations

ABSTRACT

The effect on earthquake rupturing of heterogeneities in tectonic stress and in material strength along a large fault zone is incorporated in the potential dynamic stress drop, defined as the difference between the tectonic shear stress and the dynamic frictional strength according to a slip-weakening model. The distribution of the potential dynamic stress drop $\Delta\tau_d(x)$ along the strike of the fault is modelled as a one-dimensional stochastic process. Using a simple dynamic fracture criterion, a relation is established between earthquake rupturing and potential dynamic stress drop, by which any earthquake rupture process can be regarded as a segment of a realization of the process $\Delta\tau_d(x)$, i.e., a segment where $\Delta\tau_d(x)>0$. Since dynamic slip varies approximately linearly with dynamic stress drop, it has the same distribution function as $\Delta\tau_d(x)$, provided that $\Delta\tau_d(x)$ is a Gaussian process.

Three independent earthquake observations, i.e., the average stress drop, the Gutenberg-Richter magnitude-frequency relation, and the surface slip along earthquake faults, are used to estimate the distribution function of $\Delta\tau_d(x)$. An analytical solution is derived for the distribution function of $\Delta\tau_d(x)$, which shows that among all known distributions, only the fractional Brownian process with index $H\rightarrow 0$ (fractal dimension D=2 in the one-dimensional case) can give rise to

the observed approximately constant stress drop independent of earthquake size. The probability distribution of the size of zerosets of the fractional Brownian process shows a power law relation with the frequency, which resembles the frequency-seismic moment relation. Using an average b-value of 1.0 for small earthquakes, an index $H \rightarrow 0$ for the fractional Brownian process is obtained. The model predicts that the b-value for large earthquakes is smaller than that for small earthquakes along the same fault zone, which is in agreement with observations. The surface slip data of two strike-slip dominated earthquake faults with rupture lengths larger than 100 km are inverted using power spectral analysis. Both data sets display a power-law relation between the sample power spectrum and the spatial frequency, which implies a fractional Brownian distribution. The index H is approximately zero for both earthquake faults. Stress drops, b-values, and surface slips all independently suggest that the earthquake rupturing process can be modelled stochastically as a fractional Brownian motion with index $H \rightarrow 0$.

INTRODUCTION

Earthquake sequences are complex dynamic processes associated with brittle faulting. The spatial and temporal distribution of earthquakes has a significant random component. This is reflected in the fact that many physical properties of earthquakes have been formulated through statistical approaches, such as the frequency-magnitude relation, the average stress drop-earthquake size relation and the recurrence times of large events (Wyss, 1973; Kanamori and Anderson, 1975; Caputo, 1977; Hanks, 1977; Wesnousky et al., 1983; Singh et al., 1983; Hanks and Boore, 1984). It has also been recognized that the heterogeneities in tectonic stress and in rock strength along active fault zones may play an important role in earthquake mechanics (Das and Aki, 1977; Aki, 1979; Lay and Kanamori, 1981; Lay et al., 1982; Aki, 1984, 1992; Dmowska and Lovison; 1992; Ruff, 1992). Consequently, understanding the distribution characteristics of stress-strength heterogeneities may clarify the earthquake mechanism.

Two empirical statistical relations seem to hold universally. One is the Gutenberg-Richter (frequency-magnitude) relation (1954). The other is the constancy of average stress drop (e.g., Aki, 1972; Thatcher and Hanks, 1973; Kanamori and Anderson, 1975; Hanks, 1977). As the logarithm of seismic moment has statistically a linear relation with the magnitude, assuming a constant stress drop, earthquake frequency can be related to seismic moment by a power law (Brune and King, 1967; Wyss and Brune, 1968; Kanamori and Anderson, 1975). This power law relation has led to the conclusion that the distribution of earthquakes is fractal (Hanks, 1979; von Seggern, 1980; Andrews, 1980; Aki, 1981; Huang and Turcotte, 1988; Knopoff, 1992). Using different b-values, different fractal dimensions have been obtained, which nearly cover the permissible range from 2 to 3 in the two-dimensional case (Hanks, 1979; von Seggern, 1980;

Andrews, 1980; Huang and Turcotte, 1988). Thus, the variation in b-value is thought to be a consequence of the spatial and temporal variation of the fractal dimension D (von Seggern, 1980; Huang and Turcotte, 1988). Investigations have also been carried out into the spectral properties of stress-strength heterogeneities based on the constancy of average stress drop (Hanks, 1979; Andrews, 1980). In spite of the same assumptions that (1) average stress drop is constant and (2) stress-strength heterogeneities follow a fractal distribution (specifically, a power law dependence of the spectrum of potential stress drop on wave number by Hanks (1979) and a power law dependence of the frequency of ruptures on size by Andrews (1980)), Hanks (1979) infers the fractal dimension D=2, while D=3 is given by Andrews (1980) for the two-dimensional case. Theoretically, the physical properties of the fractal distribution of stress-strength heterogeneities are quite different for different D. It appears that the physical significance of the b-value and the constancy of average stress drop are still imperfectly understood.

The measured surface slips of large earthquake ruptures show heterogeneous features (Sharp et al., 1982; Crone and Machette, 1984; Deng et al., 1986; Zhang et al., 1987; Nakata et al., 1990; Yoshida and Abe, 1992). The variation of slip along the strike of an earthquake fault is very irregular. This irregularity cannot be interpreted solely in terms of variation of surface lithology and fault geometry, but it must reflect complex physical processes along the fault. Since slip is directly related to stress drop, measured surface slips are particularly useful to infer the distribution of stress-strength heterogeneities.

In this chapter, effects of heterogeneity in stress and strength on earthquake rupturing are incorporated in the potential dynamic stress drop, defined as the difference between the tectonic shear stress and the dynamic frictional strength according to a slip-weakening model. The potential dynamic stress drop is modelled as a stochastic process. The analysis differs from

previous ones mainly in three aspects: (1) the basis of the model is the stick-slip weakening model (Scholz and Aviles, 1986), which is physically more realistic; (2) the analysis proceeds in the stochastic domain and follows the fundamentals of stochastic processes; (3) in two of the three lines of study, no assumption is made on the distribution of stress-strength heterogeneities, whereas a fractal (fractional Brownian process) distribution of the heterogeneities is assumed in all previous models. Three independent earthquake observations, i.e., the constancy of average stress drops, the frequency-magnitude relation and the surface slips of earthquake faults, are used to explore tne characteristics of the potential dynamic stress drop distribution. Throughout the chapter, I focus my attention on the spatial variation of the potential dynamic stress drop. The effect of the time factor on the occurrence of earthquakes is discussed only briefly. Further investigation into the time variation of the dynamic stress drop is needed.

EARTHQUAKE RUPTURING AS A STOCHASTIC PROCESS

Assume a planar fault with area A_{max} that can generate earthquakes of all sizes; the maximum magnitude corresponds to rupture of the entire area. All earthquakes nucleate at some point on the fault plane, and the earthquake size (magnitude or seismic moment) depends on the ultimate rupture area (Hanks, 1979; Andrews, 1980; von Seggern, 1980; Huang and Turcotte, 1988). When an earthquake nucleates, the stress at the nucleation point must satisfy the Coulomb-Navier static fracture criterion

$$\tau_s(x_0,y_0) - \tau_f(x_0,y_0) \geq 0 \tag{6.1}$$

where $\tau_s(x_0,y_0)$, $\tau_f(x_0,y_0)$ are static shear stress and static frictional strength respectively, and (x_0,y_0) are the coordinates of the nucleation point in a Cartesian system on the fault plane with

x-axis and y-axis parallel to the strike and the dip direction, respectively. Once the rupture has nucleated, dynamic fracture criteria govern the propagation of rupture. A simple dynamic criterion can be expressed as (Richards, 1976; von Seggern, 1980)

$$a\tau_s(x,y) - \tau_f(x,y) \geq 0 \tag{6.2}$$

where $a \geq 1$ is a factor that brings the static stress up to a dynamic stress due to the stress concentration at the crack tips. The rupture will propagate if the dynamic criterion is satisfied in the area around the nucleation point. The magnitude of stress concentration at the crack tips is approximately equal to the dynamic stress drop of the adjacent ruptured area (Nur, 1978). Therefore, inequality (6.2) can be written also as

$$\tau_s(x,y) + \Delta\tau_d(x_0,y_0) - \tau_f(x,y) \geq 0 \tag{6.3}$$

where $\Delta\tau_d(x_0,y_0)$ is the dynamic stress drop of the adjacent ruptured area. Note that $\Delta\tau_d(x,y)$ is not the average stress drop, but a function of position.

A slip-weakening model is assumed here (see Figure 6.1). Thus, $\Delta\tau_d(x,y)$ is related to the static shear stress and the dynamic frictional strength as (Scholz and Aviles, 1986)

$$\Delta\tau_d(x,y) = \tau_s(x,y) - \tau_d(x,y) \tag{6.4}$$

I term $\Delta\tau_d(x,y)$ the potential dynamic stress drop, since before any earthquake occurs $\Delta\tau_d(x,y)$ exists potentially on the fault surface. $\Delta\tau_d(x,y)$ incorporates the effects of both heterogeneity in stress and in strength on rupture propagation.

If either $\tau_s(x,y)$ or $\tau_d(x,y)$ (or both) are stochastic processes, $\Delta\tau_d(x,y)$ will be a two-dimensional stochastic process. Detailed discussion of the physical genesis of random distributions of $\tau_s(x,y)$ and $\tau_d(x,y)$ is beyond the scope of this chapter. It is apparent, however, that $\tau_s(x,y)$ and $\tau_d(x,y)$ are not only a function of position but also of time since earthquake

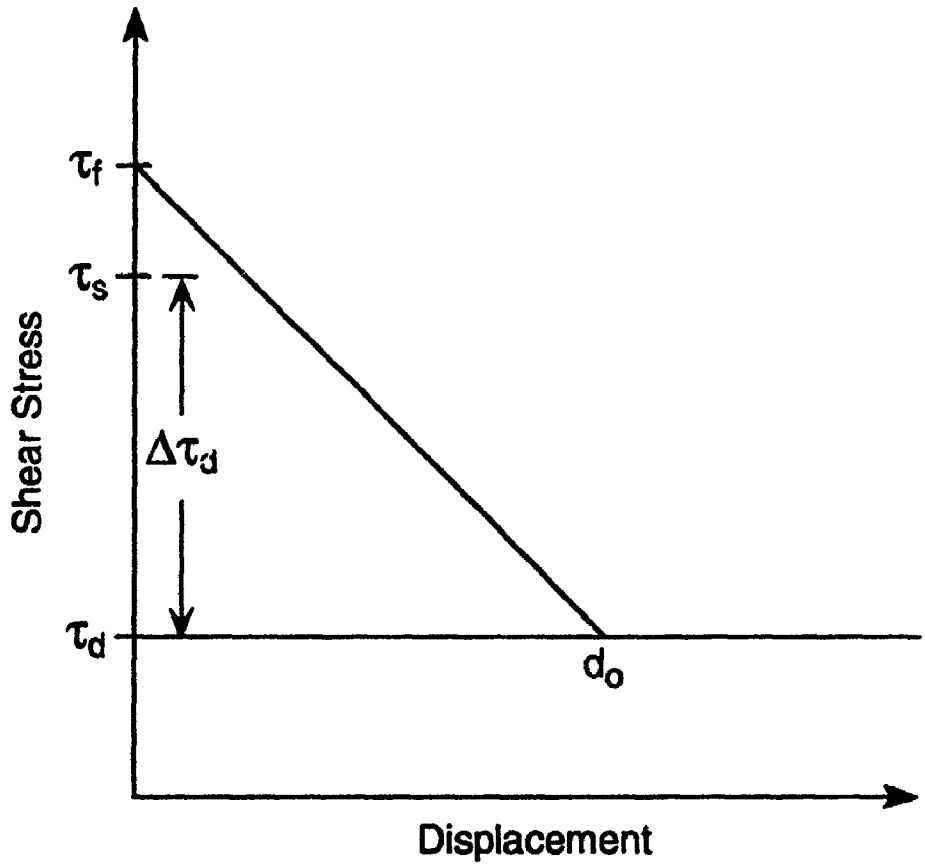

Figure 6.1. Slip weakening model. τ_f, τ_s, and τ_d are static frictional strength, static shear stress, and dynamic frictional strength, respectively. $\Delta\tau_d$ denotes dynamic stress drop, and d_0 is the characteristic slip.

sequences involve the time scale. Several lines of evidence favour the stochastic nature of $\tau_s(x,y)$ and $\tau_d(x,y)$: (1) spatial and temporal variations in principal stress directions and magnitudes may result in a random distribution in shear stress on the fault plane (Lana and Correig, 1987; Reches et al., 1992); (2) the friction coefficient shows a time-dependent behaviour (Dieterich, 1972, 1978; Dieterich and Conrad, 1984); (3) the occurrence of small earthquakes causes random redistributions of the shear stress along the fault plane (Andrews, 1980); and (4) irregular variations of pore pressure and stress corrosion give rise to randomness in time-dependence of the strength (e.g., Scholz, 1990, pp. 29-35).

Here, I consider only the variation of $\Delta\tau_d(x,y)$ along the strike direction, i.e. $\Delta\tau_d(x)$ is modelled by a one-dimensional stochastic process, as a profile of the two-dimensional process $\Delta\tau_d(x,y)$. When an earthquake nucleates at a point, the inequality $\tau_s(x,y)-\tau_f(x,y)<0$ must hold everywhere except at the nucleation point. The rupture terminates at points where the potential stress drop $\Delta\tau_d(x)\leq 0$, according to inequality (6.3). However, $\Delta\tau_d(x)\leq 0$ is a sufficient but not necessary condition for the termination of the rupture. The rupture can also stop at points where $\Delta\tau_d(x)$ is small and the state of stress does not satisfy the dynamic criterion (inequality (6.3)). Consequently, under this simple dynamic criterion, earthquake rupturing is connected with the potential stress drop. Any earthquake faulting process can be regarded as a segment of a realization of the stochastic process $\Delta\tau_d(x)$, i.e., a segment where $\Delta\tau_d(x)>0$. Different spectra (or distribution functions) of $\Delta\tau_d(x)$ will give rise to different patterns of earthquake distributions.

Many physical processes in nature can be modelled by Gaussian (normal) processes (Priestley, 1981). If both $\tau_s(x)$ and $\tau_d(x)$ are stationary up to order one, i.e. have a constant mean, $\Delta\tau_d(x)$ also has a constant mean $E\{\Delta\tau_d(x)\}=E\{\tau_s(x)\}-E\{\tau_d(x)\}$ because $\tau_s(x)$ and $\tau_d(x)$ are independent. Furthermore, if both $\tau_s(x)$ and $\tau_d(x)$ are Gaussian processes, it can be proven that

$\Delta\tau_d(x)$ is also a Gaussian process. Earthquake observation suggests that during a seismic cycle the regional tectonic stress increases with time, and rock strength decreases with time due to stress corrosion and wearing-out of asperities. Both effects will cause an increase of the mean of $\Delta\tau_d(x)$ with time. Because a larger segment of $\Delta\tau_d(x)$ will be shifted above zero due to the increase of the mean, the probability of large earthquakes increases with time. Seismic cycles have been interpreted in terms of variation of the spectrum of stress and strength from roughness to smoothness (von Seggern, 1980; Huang and Turcotte, 1988). They could also result from a stationary process (usually with rough paths) coupled with a time-varying (increasing) mean of the potential dynamic stress drop.

In the next section, I first introduce briefly the procedure of spectral analysis which is a common method for estimation of the distribution function of stochastic processes. Then the method is applied to some examples of simulated stochastic processes.

SPECTRAL ANALYSIS OF STOCHASTIC PROCESSES

Many models of stochastic processes are based on the Gaussian (normal) probability distribution. A stochastic process $Z(x)$ is Gaussian if, for any x, the joint probability distribution of $\{Z(x_1), Z(x_2), ..., Z(x_n)\}$ is multivariate normal (Priestley, 1981, pp. 113-114). Many Gaussian processes are constructed on the basis of Gaussian "white noise" (i.e., a purely random process), such as the autoregressive process, the moving average process, the general linear process and the fractional Brownian motion (for general discussion, see Priestley, 1981, pp. 100-183; Feder, 1988, pp. 163-183). Figure 6.2 shows a discrete parameter Gaussian white noise with zero mean and unit variance.

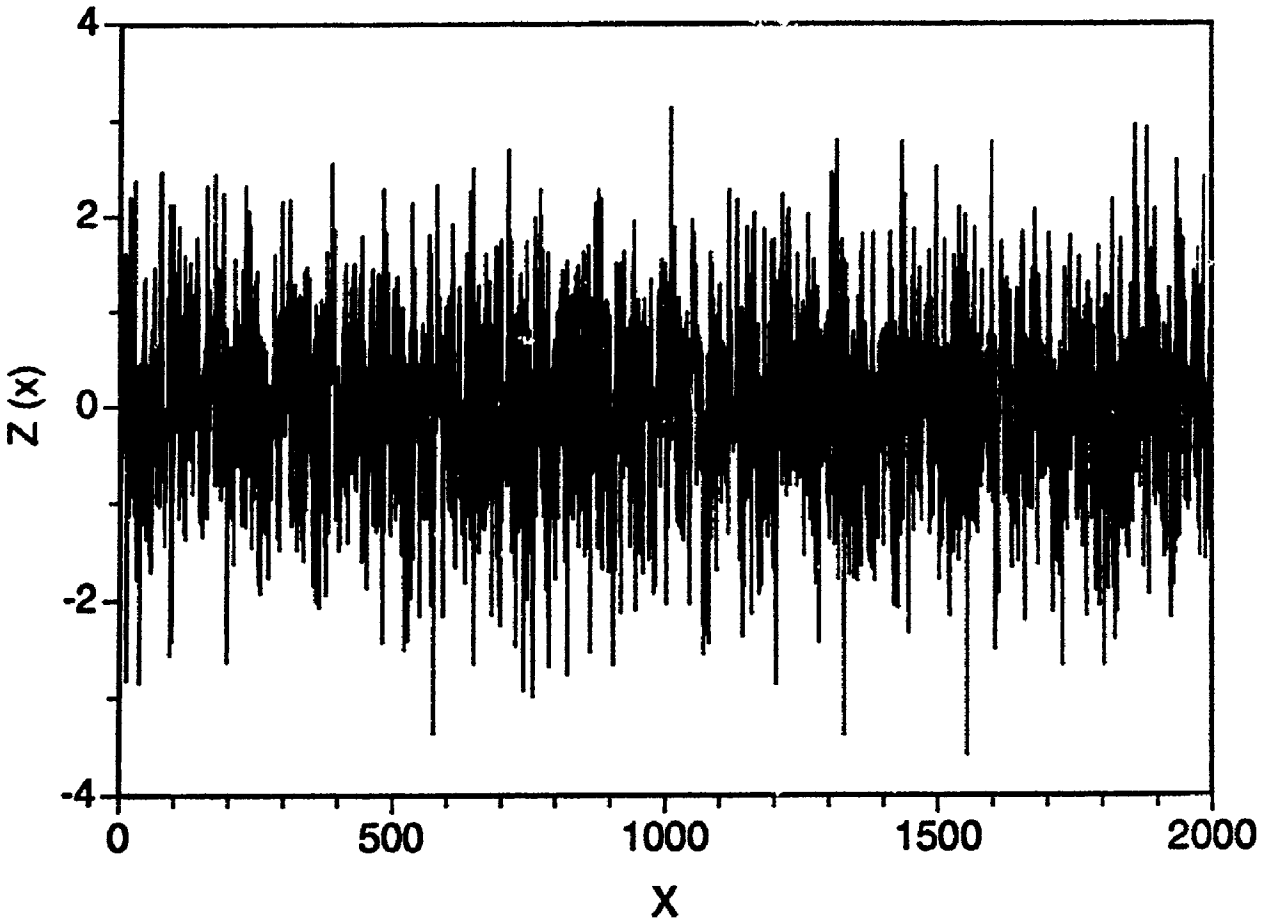

Figure 6.2. Simulated Gaussian white noise (purely random process), with zero mean and unit variance.

Stochastic processes can be divided into two classes: stationary and non-stationary. Stationary processes describe stable systems, which are characterized by the constancy of the mean, the variance and the covariance, i.e., the mean, the variance and the covariance are independent of position if the horizontal axis x represents spatial position. The above mentioned autoregressive, moving average and general linear process belong to this class. By contrast, systems that are evolving with position are described by non-stationary processes, in which the mean, and/or the variance or the covariance are dependent of position. Among non-stationary processes, the fractional Brownian process (or motion) is of particular importance, and has found geophysical applications, such as simulation of landscape evolution and seafloor topography (Mandelbrot, 1983, pp. 247-276; Fox and Hayes, 1985; Goodchild, 1988; Huang and Turcotte, 1989). Fractional Brownian motion with index H ($0<H<1$) is defined as follows (Mandelbrot, 1983, pp. 350-352; Feder, 1988, p. 170; Falconer, 1990, p. 246; Turcotte, 1992, p. 75): (1) $Z(x)$ is continuous and $Z(0)=0$ with probability $P=1$; (2) for any $x\geq 0$ and $s>0$, the increment $Z(x+s)-Z(x)$ follows the normal distribution with zero mean and variance $s_0 s^{2H}$, that is

$$P\{Z(x+s)-Z(x)\leq z\}=\frac{1}{\sqrt{2\pi s_0}\, s^{H}}\int_{-\infty}^{z}\exp\left(-\frac{u^2}{2s_0 s^{2H}}\right)du \qquad (6.5)$$

where s_0 is a factor identical to the variance of the increment $Z(x+s)-Z(x)$ when $s=1$. This definition can be extended to processes with constant mean (m) by changing the definition (1) from $Z(0)=0$ to $Z(0)=m$.

When $H=1/2$, the fractional Brownian motion reduces to the Brownian motion. Hereafter the notations $H\rightarrow 0$ and $H\rightarrow 1$ are used to denote the two end members of the fractional Brownian family. Figure 6.3 shows examples of the fractional Brownian process with $m=0$ and different indexes H, simulated using the method proposed by Feder (1988, pp. 172-174) and the white

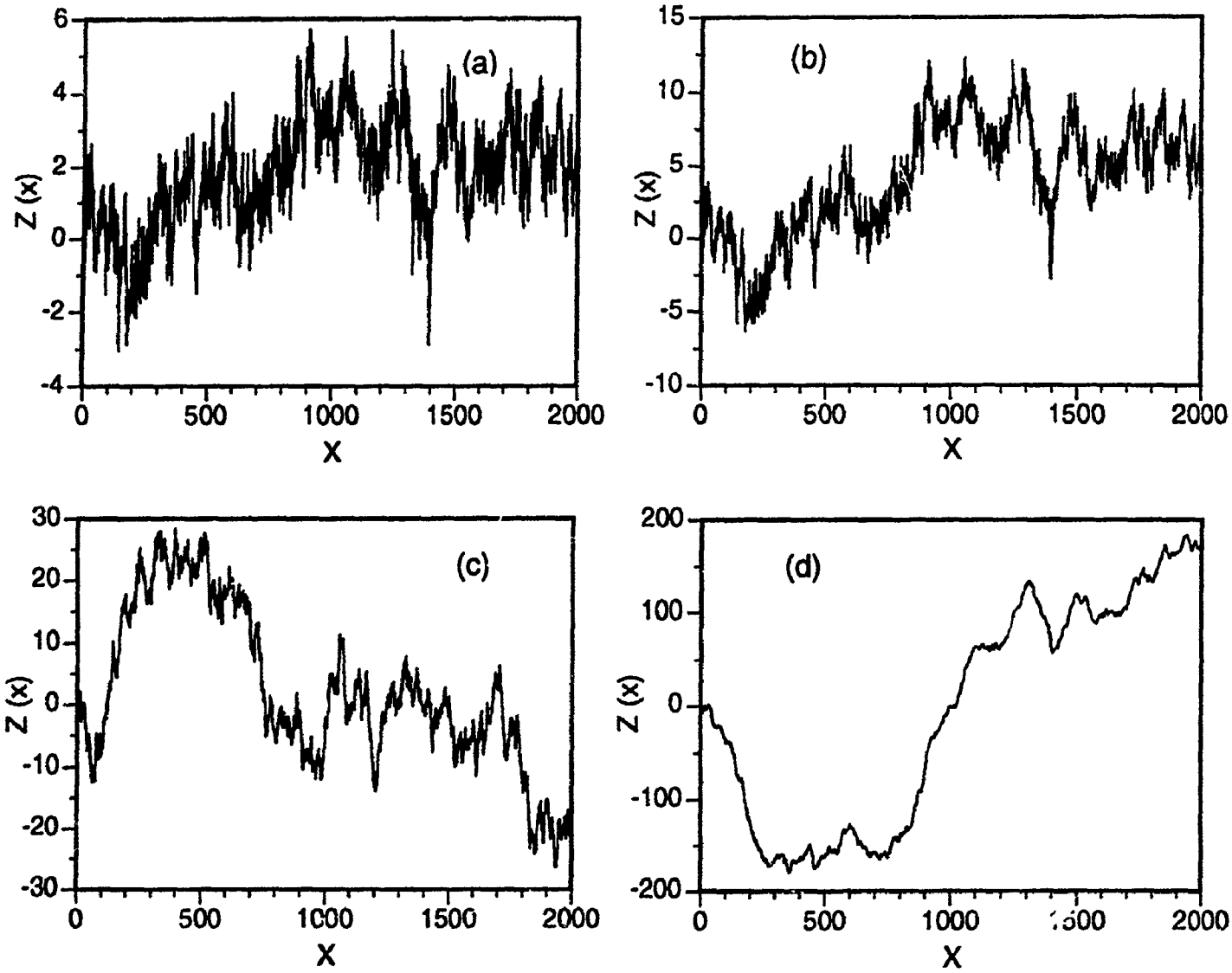

Figure 6.3. Simulated one-dimensional fractional Brownian processes for different indice 'H), with zero mean and variance equal to x^{2H} (a) H=0.01; (b) H=0.2; (c) H=0.5; and (d) H=0.8.

noise shown in Figure 6.2. The spectral properties of the processes are quite different for different H. The smaller H, the more conspicuous is the high frequency component of the process, and the process tends to be stationary for $H \rightarrow 0$. The path (graph) of a fractional Brownian motion has approximate fractal (Hausdorff) dimension $D \approx 2-H$ for the one-dimensional case and $D \approx 3-H$ for the two-dimensional case, respectively (Falconer, 1990, pp. 246-247).

The spatial positions of a stochastic process are random; one realization (record) is different from another. However, the characteristics of the ensemble (i.e. all possible realizations) can be described in terms of the power spectral density function. For a real-valued stationary process, the power spectral density is the Fourier cosine transform of its autocovariance function (Priestley, 1981, pp. 211-214)

$$h(k) = \frac{1}{2\pi} \int_{-\infty}^{\infty} R(s) \cos(ks)\, ds \tag{6.6}$$

where k is wave number. Since the theoretical power spectral density functions are known for different stochastic processes, the distribution function of an observed process can be inferred by estimating its sample power spectral density function.

Assume Z(x) to be a continuous record of a process over the interval $0 \le x \le X_0$. When sampled at small intervals Δx, $2\Delta x$, ..., $N\Delta x$, this gives the discrete set of values $Z(\Delta x)$, $Z(2\Delta x)$, ..., $Z(N\Delta x)$, where $N = X_0/\Delta x$. The sample mean and the sample autocovariance function are, respectively

$$\hat{m} = \frac{1}{N} \sum_{i=1}^{N} Z(i\Delta x) \tag{6.7}$$

$$\hat{R}(s) = \frac{1}{N} \sum_{i=1}^{N-|s|} [Z(i\Delta x) - \hat{m}][Z(i\Delta x + |s|) - \hat{m}] \tag{6.8}$$

Consequently, the estimate of the power spectral density function ($\hat{h}(k)$) can be expressed as (Priestley, 1981, p. 433)

$$\hat{h}(k) = \frac{1}{2\pi} \sum_{s=-(N-1)}^{(N-1)} \lambda(s)\, \hat{R}(s) \cos(ks) \tag{6.9}$$

where $\lambda(s)$ is the lag window which acts as a weighting function to eliminate the "tail effect" of the sample autocovariance function (for a general discussion, see Priestley, 1981, pp. 432-449). Because of the aliasing effect, only the sample spectral density function for the interval $-\pi/\Delta x \leq k \leq \pi/\Delta x$ can be obtained, where Δx is the interval of sampling.

In theory, the above estimation is applicable to stationary processes only. It is interesting to note, however, that application of the procedure to the fractional Brownian process yields an approximate power law dependence of the power spectrum on the wavenumber k, provided that k is relatively large,

$$\hat{h}(k) \approx c_s k^{-(1+2H)} \tag{6.10}$$

where c_s is a constant and H is the index (Mandelbrot, 1983, p. 388; Falconer, 1990, pp. 155-158, p. 247). Independently of the physical meaning of the power spectra, therefore, equations (6.7)–(6.9) can be applied to infer whether a given record originates in a particular stationary process or in one of the fractional Brownian family, by comparing the sample power spectral density function with theoretical ones. Figures 6.4 and 6.5 show the sample power spectral densities for the records of white noise and fractional Brownian motion with different index H shown in Figures 6.2 and 6.3, respectively, calculated using the Parzen window with window parameter M=40%N, where N is the total sample size (Priestley, 1981, pp. 443-444). As the

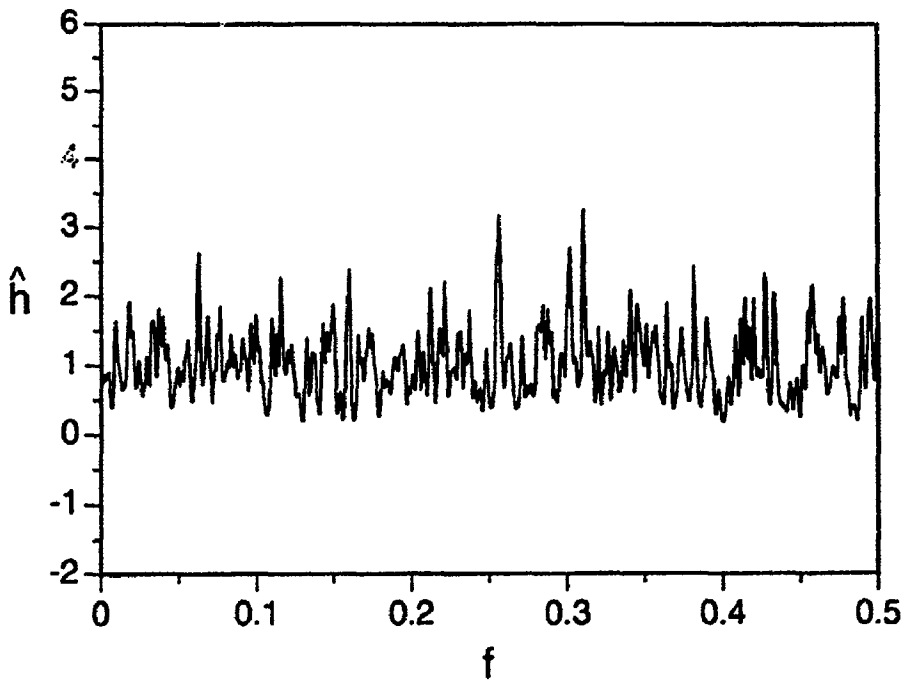

Figure 6.4. Calculated power spectral density versus spatial frequency for the white noise shown in Figure 6.2.

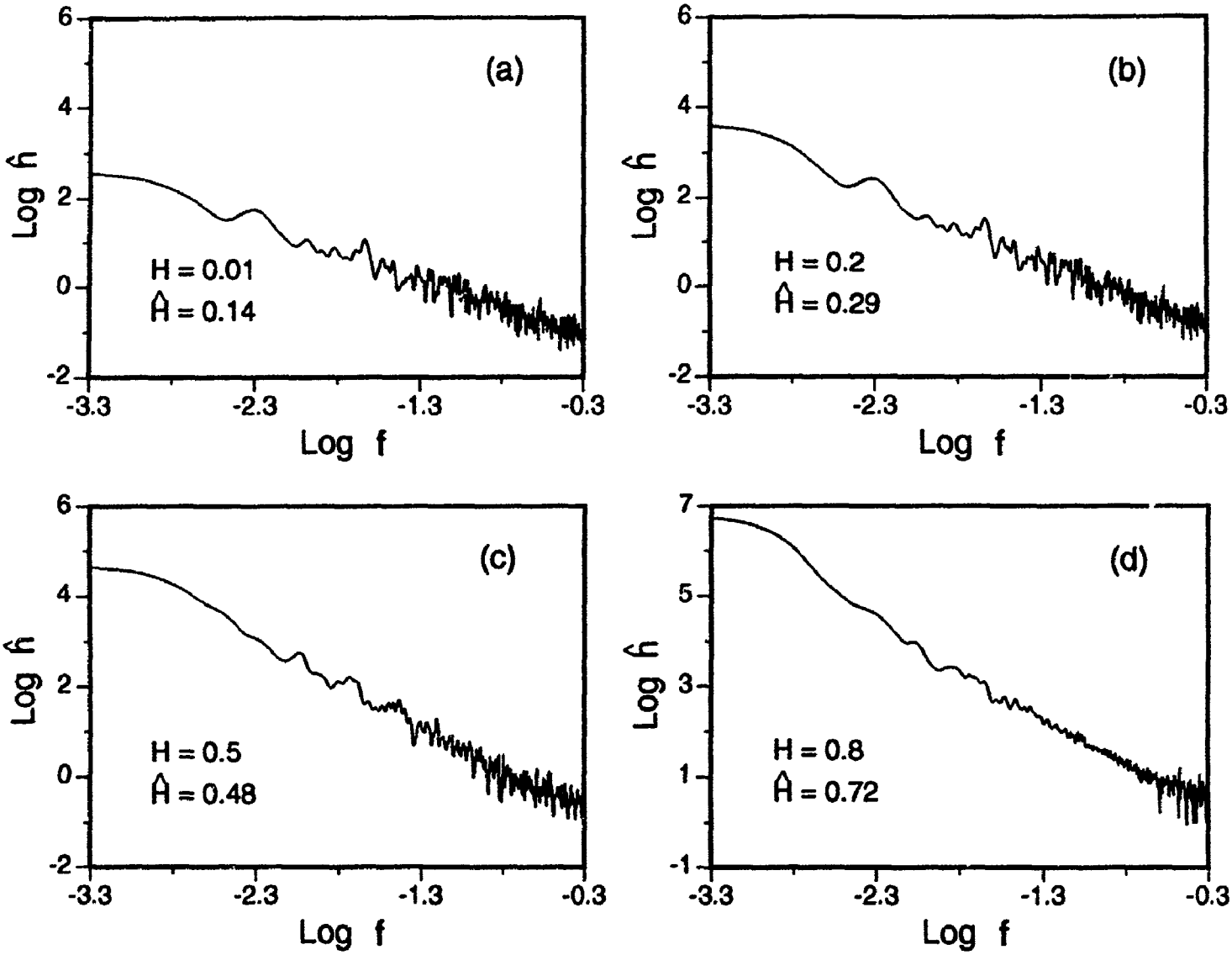

Figure 6.5. Calculated logarithmic power spectral density versus logarithmic spatial frequency for fractional Brownian processes with different indices H. (a), ..., (d) correspond to (a), ..., (d) in Figure 6.3. H and $\hat{H}$ are the theoretical index and the estimated index by least squares linear fit, respectively.

theoretical spectral density function is known to be constant for all k for the white noise and a power law with exponential 1+2H for the fractional Brownian motion, it can be seen that the estimates are consistent with the theory, except that the index H is slightly overestimated when $H<1/2$ and underestimated when $H>1/2$.

The method of spectral analysis described above will be applied to measured surface slip along earthquake faults to infer the distribution function of $\Delta\tau_d(x)$ in the next section, and compared with inferences from the constraints posed by the average stress drop and the magnitude-frequency relation.

ESTIMATION OF THE DISTRIBUTION FUNCTION OF $\Delta\tau_d(x)$ FROM EARTHQUAKE OBSERVATIONS

Having established the relation between the earthquake rupture process and the potential dynamic stress drop $\Delta\tau_d(x)$, the distribution function of $\Delta\tau_d(x)$ must now be estimated from observation. For this purpose, the most useful earthquake parameters are the stress drop, the magnitude (or moment), and the surface slip of earthquake ruptures.

1. Average Stress Drop

One of the most remarkable features of the earthquake process is that average stress drops are statistically constant, independent of source dimension and of geographic location over twelve orders of magnitude in seismic moment (e.g., Aki, 1972; Thatcher and Hanks, 1973; Kanamori and Anderson, 1975; Hanks, 1977). Some investigations have been carried out into the spectral

properties of stress-strength heterogeneities based on this observation. Assuming either a power law dependence of the spectrum of potential stress drop on wave number (Hanks, 1979) or a power law dependence of the frequency of ruptures on size (Andrews, 1980; note that both assumptions are equivalent to the fractional Brownian motion), Hanks (1979) infers the fractal dimension D=2, whereas D=3 is obtained by Andrews (1980), for the two-dimensional case.

As mentioned previously, an earthquake rupture process can be regarded as a segment of a realization of the stochastic process $\Delta\tau_d(x,y)$, i.e., a segment where $\Delta\tau_d(x,y)>0$. Thus the average stress drop is the integral of $\Delta\tau_d(x,y)$ over the rupture area, divided by the area. In the one-dimensional case, the average stress drop can be expressed accordingly as

$$\overline{\Delta\tau_d}(L) = \frac{1}{L}\int_L \Delta\tau_d(x)\,dx, \qquad (\Delta\tau_d(x) \geq 0) \tag{6.11}$$

For the average stress drop to be constant, the mean value of $\overline{\Delta\tau_d}(L)$ must be independent of L, where L is the rupture length. Here, I examine how constancy of average stress drop may arise from a stochastic process.

First of all, consider a special case, that is, assume a fractional Brownian distribution of $\Delta\tau_d(x)$. The paths (graphs) of the fractional Brownian motion are self-affine fractals, i.e., they look the same upon changing scales $X \rightarrow pX$ and $\Delta\tau_d(x) \rightarrow p^H\Delta\tau_d(x)$, where p is a factor and H is the index (Wong and Lin, 1988). However, this scale invariant property of fractional Brownian motion is only valid for the statistical average of ensembles. For any given finite realization the two records can be quite different and the vertical scale will not be changed by the expected factor p^H. This means that the spatial position of $\Delta\tau_d(px)$ is not equal to that of $p^H\Delta\tau_d(x)$ for any finite records, but their mean values are identical. Using this scale invariant property and recalling equation (6.11), the mean value of average stress drop over a rupture length pL is

$$E[\overline{\Delta\tau_d}(pL)] = \frac{1}{pL}\int_{pL} E[\Delta\tau_d(px)]\,d(px), \qquad (\Delta\tau_d(px) \geq 0) \tag{6.12}$$

Changing the integral variable from px to x and noting that $E[\Delta\tau_d(px)]=p^H E[\Delta\tau_d(x)]$, we have

$$\begin{aligned} E[\overline{\Delta\tau_d}(pL)] &= \frac{1}{L}\int_L p^{\,H} E[\Delta\tau_d(x)]\,dx \\ &= p^{\,H} E[\overline{\Delta\tau_d}(L)], \qquad (\Delta\tau_d(x) \geq 0) \end{aligned} \tag{6.13}$$

Equation (6.13) shows that if $\Delta\tau_d(x)$ follows a fractional Brownian distribution, ruptures with different length (or earthquakes with different magnitude) can have a constant average stress drop only if $H \rightarrow 0$; otherwise, the mean value of average stress drops would increase systematically with rupture size. Since $H \rightarrow 0$ corresponds to the fractal dimension D=2 for the one-dimensional case, this result coincides with that of Andrews (1980). Furthermore, equation (6.13) also agrees with the observation that average earthquake stress drops, although having a constant mean value, vary within a finite dispersion (Hanks, 1977).

Now take the general case, i.e., without any assumption about the probability distribution of $\Delta\tau_d(x)$. As $\Delta\tau_d(x)$ is a continuous stochastic process, its sample mean is

$$\hat{m}_\tau = \frac{1}{x_1 - x_0}\int_{x_0}^{x_1} \Delta\tau_d(x)\,dx \tag{6.14}$$

Note that $\hat{m}_\tau$ is different from $\overline{\Delta\tau_d}(L)$ given in equation (6.11). The former is the sample mean of a segment of a realization of the process $\Delta\tau_d(x)$, which can take either a positive or a negative value. The latter is the sample mean of a portion of a realization where $\Delta\tau_d(x) \geq 0$. Since $\Delta\tau_d(x)$ is a random variable for any fixed x, it follows that $\hat{m}_\tau$ is also a random variable. Its mean can be derived from equation (6.14) as

$$E(\hat{m}_\tau) = \frac{1}{x_1 - x_0} \int_{x_0}^{x_1} E[\Delta\tau_d(x)]dx \tag{6.15}$$

where $E[\Delta\tau_d(x)]$ is the mean of $\Delta\tau_d(x)$ at a point x, and its variance is

$$\begin{aligned} V(\hat{m}_\tau) &= E[(\hat{m}_\tau - E(\hat{m}_\tau))^2] \\ &= E\{[\frac{1}{x_1 - x_0} \int_{x_0}^{x_1} (\Delta\tau_d(x) - E(\Delta\tau_d(x)))dx]^2\} \end{aligned} \tag{6.16}$$

Consequently, any $\overline{\Delta\tau_d}(L)$ (the average earthquake stress drop) can be considered as a sample of all positive values taken by the random variable $\hat{m}_\tau$.

Taking a Gaussian process as an example, $\hat{m}_\tau$ follows the normal distribution with mean and variance given by equations (6.15) and (6.16), respectively (Priestley, 1981, p. 91). Because $\overline{\Delta\tau_d}(L)$ takes only positive values, its mean value is always larger than the mean of $\hat{m}_\tau$, and it also increases as the mean of $\hat{m}_\tau$ increases (Figure 6.6). Therefore, for the average stress drop to have a constant mean, the mean of $\hat{m}_\tau$ must be constant. Equation (6.15) shows that this condition is satisfied only if $\Delta\tau_d(x)$ has a constant mean, i.e., $E[\Delta\tau_d(x)]=m_\tau$, independent of position. Equation (6.15) is thus reduced to

$$E(\hat{m}_\tau) = m_\tau \tag{6.17}$$

where m_τ is the mean of the process $\Delta\tau_d(x)$. However, the constant mean is a necessary but not a sufficient condition for $\Delta\tau_d(x)$ to give rise to the constancy of average stress drops. This point can be seen clearly by considering the variance of $\hat{m}_\tau$.

Figure 6.7 shows two distributions of $\hat{m}_\tau$ with same mean and different variances. The mean value of the average stress drop increases with the variance of the sample mean. Consequently, for the average stress drop to maintain a constant mean value, $\hat{m}_\tau$ must have a constant mean and a constant variance. Substituting equation (6.17) into equation (6.16) gives

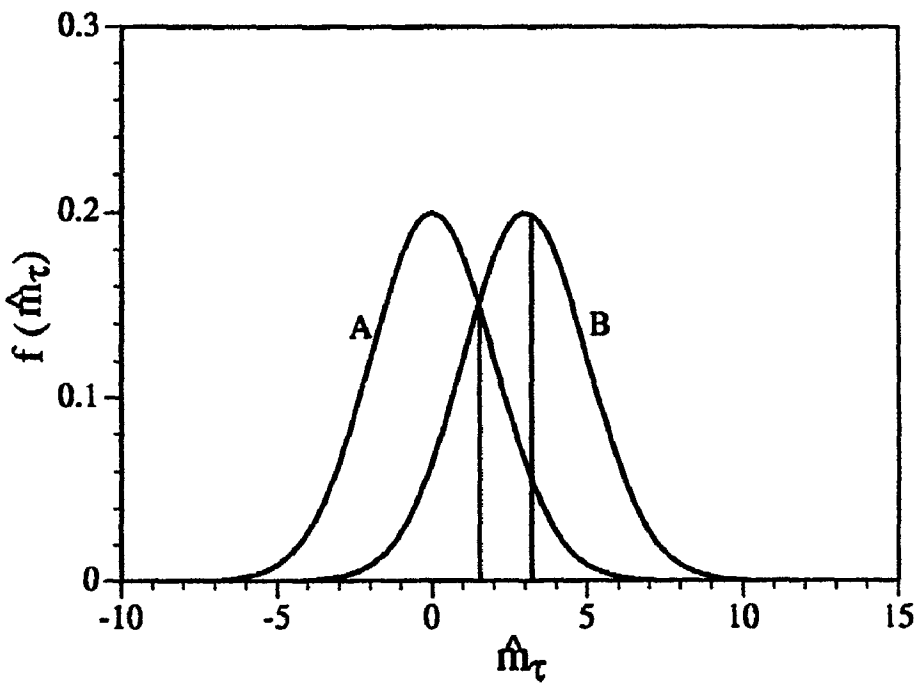

Figure 6.6. Schematic diagram of two normal distributions of $\hat{m}_\tau$, with same variance V=4 and different means (A) $E(\hat{m}_\tau)=0$ and (B) $E(\hat{m}_\tau)=3$. The two vertical lines show the positions of the mean of $\overline{\Delta\tau_d}(L)$ for the two distributions.

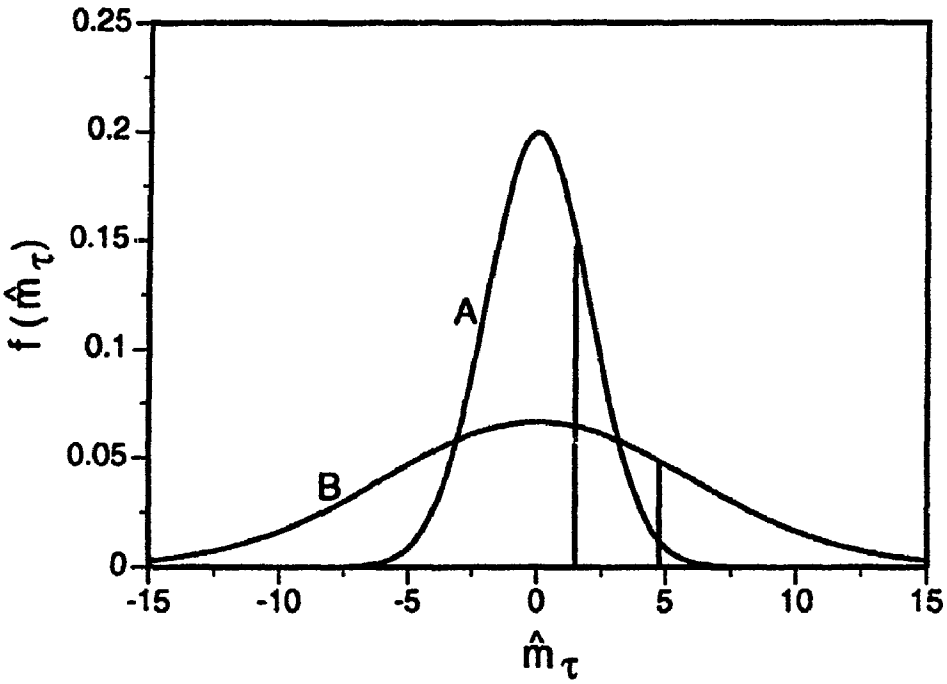

Figure 6.7. Schematic diagram of two normal distributions of $\hat{m}_\tau$, with same mean (zero) and different variance (A) V=4 and (B) V=36. The two vertical lines show the positions of the mean of $\overline{\Delta\tau_d}(L)$ for the two distributions.

$$V(\hat{m}_\tau) = E[(\hat{m}_\tau - m_\tau)^2]$$
$$= E[\frac{1}{(x_1 - x_0)^2}\int_{x_0}^{x_1}(\Delta\tau_d(x) - m_\tau)dx \int_{x_0}^{x_1}(\Delta\tau_d(t) - m_\tau)dt] \tag{6.18}$$

Changing the integral variables from x, t to x, s=t-x, I thus obtain

$$V(\hat{m}_\tau) = \frac{1}{(x_1 - x_0)^2}\int_{-(x_1-x_0)}^{x_1-x_0} ds \int_{x_0}^{x_1-s} cov(\Delta\tau_d(x), \Delta\tau_d(x+s))dx, \qquad (s \geq 0)$$
$$V(\hat{m}_\tau) = \frac{1}{(x_1 - x_0)^2}\int_{-(x_1-x_0)}^{x_1-x_0} ds \int_{x_0+|s|}^{x_1} cov(\Delta\tau_d(x), \Delta\tau_d(x+s))dx, \qquad (s < 0) \tag{6.19}$$

where $cov(\Delta\tau_d(x), \Delta\tau_d(x+s))$ is the autocovariance function of $\Delta\tau_d(x)$. Equation (6.19) shows that a necessary condition for $V(\hat{m}_\tau)$ to be constant is that the autocovariance function be independent of position. This result demonstrates that $\Delta\tau_d(x)$ must be stationary up to order two. If the fractional Brownian motion is used to model the process $\Delta\tau_d(x)$, only one member in this family can become a candidate, i.e. that with $H \rightarrow 0$, because fractional Brownian motions with other indexes are non-stationary. This conclusion is consistent with that based on the scale invariance.

Stationarity is not a sufficient condition for $\Delta\tau_d(x)$ to produce a constant earthquake stress drop. By taking the autocovariance function, which is now a function of s only, out of the second integral, equation (6.19) reduces to

$$V(\hat{m}_\tau) = \frac{1}{x_1 - x_0}\int_{-(x_1-x_0)}^{x_1-x_0} cov(\Delta\tau_d(x), \Delta\tau_d(x+s))(1 - \frac{|s|}{x_1 - x_0})ds \tag{6.20}$$

For most stationary processes, as $cov(\Delta\tau_d(x), \Delta\tau_d(x+s))$ is an even and decreasing function of $|s|$, $V(\hat{m}_\tau)$ (the variance of the sample mean) is also a decreasing function of the sample size, and usually $V(\hat{m}_\tau) \rightarrow 0$ as the sample size (x_1-x_0) goes to infinity (Priestley, 1981, p. 320). Since the mean value of average stress drop increases slowly with increase of $V(\hat{m}_\tau)$ (see Figure 6.6), small

earthquakes should have a mean value of average stress drop slightly larger than that of large earthquakes. Besides, the dispersion of average stress drops should decrease as earthquake size increases. Statistical results on earthquake stress drop show that neither of these predictions is fulfilled (Hanks, 1977). This excludes stationary processes whose autocovariance function is a decreasing function of $|s|$. However, a stationary process exists which can lead both to a constant mean and a constant variance of $V(\hat{m}_\tau)$, i.e., give rise to a constant mean value of earthquake stress drop, independent of earthquake size. This is the fractional Brownian process with index $H \to 0$. Since the autocovariance function can be expressed as

$$\begin{aligned} \mathrm{cov}[\Delta\tau_d(x), \Delta\tau_d(x+s)] &= E[(\Delta\tau_d(x) - m_\tau)(\Delta\tau_d(x+s) - m_\tau)] \\ &= \frac{1}{2}\{V[\Delta\tau_d(x)] + V[\Delta\tau_d(x+s)] - V[\Delta\tau_d(s+x) - \Delta\tau_d(x)]\} \end{aligned} \tag{6.21}$$

where V denotes the variance, recalling the definition of fractional Brownian motion (equation (6.5)), the autocovariance function is

$$\begin{aligned} \mathrm{cov}[\Delta\tau_d(x), \Delta\tau_d(x+s)] &= \frac{s_0}{2}[(x^{2H} + (x+s)^{2H} - s^{2H}], \qquad (s \geq 0) \\ \mathrm{cov}[\Delta\tau_d(x), \Delta\tau_d(x+s)] &= \frac{s_0}{2}[(x - |s|)^{2H} + x^{2H} - |s|^{2H}], \qquad (s < 0) \end{aligned} \tag{6.22}$$

When $H \to 0$, the autocovariance function is approximately independent of both x and s, and s_0 becomes the variance of the process $\Delta\tau_d(x)$. Thus, $V(\hat{m}_\tau)$ can be obtained from equations (6.20) and (6.22) as

$$V(\hat{m}_\tau) \approx \frac{s_0}{2(x_1 - x_0)} \int_{-(x_1 - x_0)}^{x_1 - x_0} \left(1 - \frac{|s|}{x_1 - x_0}\right) ds \approx \frac{s_0}{2} \tag{6.23}$$

The variance of $V(\hat{m}_\tau)$ (sample mean), which is approximately equal to half the variance of the process, is constant and independent of sample size. Consequently, the mean value of $\overline{\Delta\tau_d}(L)$

(average earthquake stress drop) is also constant and independent of rupture length.

In summary, the observed constancy of average stress drop requires that $\Delta\tau_d(x)$ be a stationary process. This implies that the earthquake process is a stable physical system, the statistical properties of which do not change over position. However, the constancy of average stress drop implies rather more than this. Many stationary processes whose autocovariance function is characterized by a decreasing dependence of $|s|$ cannot give rise to a constant average stress drop independent of rupture size. Of the known models, only the fractional Brownian motion with $H \rightarrow 0$ can reproduce the observations. The fractional Brownian motion with $H \rightarrow 0$ differs from other stationary processes mainly in its correlation function. It has a long-run correlation between positions of $\Delta\tau_d(x)$ in the "past" and in the "future" along the x-axis, whereas other stationary processes are either "memoryless", such as the white noise, or of "poor memory".

2. The Gutenberg-Richter Relation

The Gutenberg-Richter (frequency-magnitude) relation is one of the most important statistical properties of earthquakes. Statistics of seismicity show that the exponential relation between the cumulative number of earthquakes and the magnitude holds universally over a broad range of magnitudes, although the parameters in the function may vary from one area to another (e.g., von Seggern, 1980; Rydelek and Sacks, 1989; Pacheco et al., 1992). As the logarithm of seismic moment has a statistically linear relation with the magnitude, assuming a constant stress drop leads to a power law relation between the cumulative number of earthquakes and the seismic moment (Brune and King, 1967; Wyss and Brune, 1968; Kanamori and Anderson, 1975)

3 of/de 3

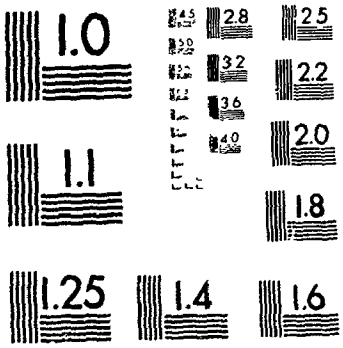

MICROCOPY RESOLUTION TEST CHART
NATIONAL BUREAU OF STANDARDS
STANDARD REFERENCE MATERIAL 1010a
(ANSI and ISO TEST CHART No 2)

$$N(M_0) = c_1 M_0^{-\frac{b}{c}} \tag{6.24}$$

where M_0 is seismic moment, c_1 is a constant, and b and c are the slopes of the logarithmic magnitude-frequency relation and of the logarithmic seismic moment-magnitude relation, respectively. This power law scaling relation has led to the proposal that earthquakes are manifestations of a fractal physical process (Hanks, 1979; von Seggern, 1980; Andrews, 1980; Aki, 1981; Huang and Turcotte, 1988).

Investigations into the statistical behaviour of earthquake occurrence have followed two different directions, namely (a) the Gutenberg-Richter relation is interpreted in terms of the random spatial distribution of active fault sizes, i.e., it is a consequence of the seismicity along an ensemble of faults (Turcotte, 1986; Hirata, 1989; Sornette et al., 1990; Sornette et al., 1991; Sornette and Davy, 1991; Knopoff, 1992); or (b) the Gutenberg-Richter relation is the consequence of the random distribution of inhomogeneous stress and strength along a single large fault zone (Hanks, 1979; von Seggern, 1980; Andrews, 1980; Huang and Turcotte, 1988). My analysis follows the second line. The problem of the relation between the b-values and the spatial distribution of an ensemble of faults will not be discussed here.

Although the frequency-magnitude relation is usually derived from statistics of regional or global seismicity, a few studies of seismicity along a single fault zone suggest that it is also applicable in this case (Wesnousky et al., 1983; Singh et al., 1983; Schwartz and Coppersmith, 1984; Davison and Scholz, 1985). Assuming a circular rupture model and an average c-value equal to 1.5, equation (6.24) can be expressed in terms of the rupture area

$$N(A) = c_2 A^{-b} \tag{6.25}$$

for small earthquakes with rupture radius $r \leq h_0/2\sin\theta_d$, where h_0 is the thickness of the

seismogenic layer and θ_d is the dip of the fault plane, and c_2 is a constant (von Seggern, 1980; Scholz, 1982; Huang and Turcotte, 1988). Several models of the distribution of inhomogeneous stress and strength along a large fault zone as a two-dimensional fractional Brownian process to account for the Gutenberg-Richter relation are available (von Seggern, 1980; Huang and Turcotte, 1988). Assuming $b \approx 1.0$, von Seggern (1980) obtained D=3 (fractal dimension for the graph of the two-dimensional fractional Brownian motion). Huang and Turcotte (1988) obtained $b \approx 0.77$-1.11 by numerical simulation of the two-dimensional fractional Brownian motion with fractal dimension $D \approx 2.2$-2.4. In both cases, the spatial and temporal variation in b-value were considered as a reflection of the variation in the fractal dimension. Here, I discuss the physical implications of the Gutenberg-Richter relation from the stochastic properties of the potential dynamic stress drop.

In the two-dimensional case, the propagation of earthquake rupture in principle stops at positions where $\Delta\tau_d(x,y)=0$. Therefore, the study of the earthquake size distribution is approximately equivalent to the study of the size distribution of zerosets of the stochastic process $\Delta\tau_d(x,y)$. The zerosets are defined as sets of intersections between $\Delta\tau_d(x,y)$ and the plane $\Delta\tau_d(x,y)=0$, and their size is the area within the intersection line. For two-dimensional fractional Brownian motion, the number of zerosets with size larger than A is given as (Adler, 1981, p. 215; Mandelbrot, 1983, p. 260 and p. 272)

$$N(A) = c_3 A^{-\frac{2-H}{2}} \tag{6.26}$$

where c_3 is a constant and H is the index. $D_z=2-H$ is often called the fractal (or Hausdorff) dimension of the zerosets; the relation between the fractal dimension of the zerosets and the fractal dimension of the path of fractional Brownian motion is $D_z=D-1$. Equation (6.26) is derived

under the condition that the process has zero mean, whereas the mean of $\Delta\tau_d(x,y)$ is likely to increase during a seismic cycle and may not be zero. It has been proven, however, that equation (6.26) is still valid for any level sets defined as sets of intersections between $\Delta\tau_d(x,y)$ and the plane $\Delta\tau_d(x,y)=B$, where B is any given value, as long as the level sets are not empty (Adler, 1981, p. 251). This implies that equation (6.26) can be applied to $\Delta\tau_d(x,y)$ with non-zero mean as well.

Equation (6.26) shows that the fractional Brownian motion gives rise to a power law relation between the cumulative number and the size of zerosets similar to the frequency-rupture area relation given in equation (6.25). Comparison of the two equations yields

$$H = 2 - 2b \tag{6.27}$$

Based on equation (6.27), the spatial and temporal variation in b-value can be interpreted in terms of the variation of fractal dimension D of $\Delta\tau_d(x,y)$ (von Seggern, 1980; Huang and Turcotte, 1988). However, since the cumulative number of zerosets with size larger than A is a random variable, equation (6.26) refers to its mean value (Adler, 1981, p. 215; Karatzas, 1988, pp. 400-417). Consequently, for a given H or D, two records of any given finite realization of $\Delta\tau_d(x,y)$ do not give rise to the same number-size relation, but the mean value of the cumulative number of zerosets for all realizations is related to the size by a power law relation (equation (6.26)). Since each realization of the process $\Delta\tau_d(x,y)$ corresponds to an instant on the time-axis, the mean value of the cumulative number of zerosets is equivalent to the cumulative number of earthquakes during a long period of time. Therefore, the variation in b-values can arise from a dispersion from the mean value due to the randomness of zerosets, rather than from a one-to-one relation between the b-value and the fractal dimension D. This inference is supported by the observation that the average b-value over long time periods is stable and approximately equal to 1.0, although

over short times it varies from 0.5 to 1.5 (Shi and Bolt, 1982; Scholz, 1990, pp. 188-189). Taking on the average $b \approx 1.0$, it follows that $H \rightarrow 0$. This result is consistent with that based on the observation of constant average stress drop.

For larger earthquakes, i.e. earthquakes with rupture length $L \geq h_0/\sin\theta_d$, where h_0 and θ_d have the same meanings as in equation (6.25), a model has been proposed by Scholz (1982; 1990, pp. 180-189). This model (termed L-model), assuming an average c-value equal to 1.5 and a constant fault width, expresses the cumulative number of large earthquakes with rupture length $\geq L$ as

$$N(L) = c_4 L^{-\frac{4b}{3}} \tag{6.28}$$

where c_4 is a constant.

The ultimate rupture sizes of large intraplate earthquakes depend predominantly on how far the rupture can propagate along the strike direction, since the rupture width is constrained by the thickness of seismogenic layer. Therefore, their frequency-size relation is equivalent to the distribution of zerosets of the one-dimensional process $\Delta\tau_d(x)$. The mean value of the cumulative number of zerosets with length larger than L is given by (Adler, 1981, p. 215; Mandelbrot, 1983, p. 354)

$$N(L) = c_5 L^{-(1-H)} \tag{6.29}$$

where c_5 is a constant and H is the index ($D_z = 1-H$ is the fractal or Hausdorff dimension of the zerosets for the one-dimensional fractional Brownian motion). Comparing equation (6.27) with (6.28), one obtains

$$H = 1 - \frac{4b}{3} \tag{6.30}$$

The average b-value for large earthquakes along a single fault zone is not available because the historical record is not sufficient to do meaningful statistics for a single fault. Using $H \rightarrow 0$, I predict that on the average $b \approx 0.75$, i.e., the b-value for large earthquakes is less than that for small earthquakes along a single fault zone. A few case studies have suggested that the maximum earthquake size is greatly underestimated by the extrapolation of the size distribution of small earthquakes for the same fault, which implies a smaller b-value for large earthquakes (Wesnousky et al., 1983; Singh et al., 1983; Schwartz and Coppersmith, 1984; Davison and Scholz, 1985). This result is in agreement with the theoretical prediction based on the fractional Brownian process.

3. Surface Slip of Earthquake Faults

Investigation of large earthquake ruptures has shown that the variation of surface slip along the strike of faults is very irregular (Sharp et al., 1982; Crone and Machette, 1984; Deng et al., 1986; Zhang et al., 1987; Nakata et al., 1990; Yoshida and Abe, 1992). This irregularity cannot be interpreted in terms of the variation of surface lithology and fault geometry alone, but must reflect a complex physical process along the fault.

On the basis of the circular rupture model and/or the rectangular L-model, a linear relation is obtained between the average stress drop and the mean slip (Scholz, 1990, p. 181)

$$\overline{\Delta\tau_d} = c_6 \overline{\Delta u_d} \tag{31}$$

where c_6, for a given rupture, is a constant that depends on the rupture model and material

parameters. Assuming that this relation is valid as a function of position, I rewrite equation (6.31) as

$$\Delta\tau_d(x) = c_6 \Delta u_d(x), \qquad (\Delta\tau_d(x) \geq 0) \tag{6.32}$$

For a given rupture, integration of equation (6.32) yields equation (6.31). Since $\Delta\tau_d(x)$ is a stochastic process, $\Delta u_d(x)$ is also a stochastic process. Its mean is

$$E[\Delta u_d(x)] = c_7 E[\Delta\tau_d(x)], \qquad (\Delta\tau_d(x) \geq 0) \tag{6.33}$$

where $c_7 = 1/c_6$ is a constant for a given earthquake. Its autocovariance function is

$$\mathrm{cov}[\Delta u_d(x), \Delta u_d(x+s)] = c_7^2 \,\mathrm{cov}\,[\Delta\tau_d(x), \Delta\tau_d(x+s)], \qquad (\Delta\tau_d(x) \geq 0) \tag{6.34}$$

Equation (6.34) shows that the process $\Delta u_d(x)$ has the same distribution function as $\Delta\tau_d(x)$, but with a different mean and variance, provided that $\Delta\tau_d(x)$ is a Gaussian process. This can be seen clearly from their autocorrelation functions. Equation (6.34) gives

$$\rho_u(s) = \frac{\mathrm{cov}[\Delta u_d(x), \Delta u_d(x+s)]}{[V(\Delta u_d(x))\, V(\Delta u_d(x+s))]^{1/2}} = \rho_\tau(s) \tag{6.35}$$

where $\rho_u(s)$ and $\rho_\tau(s)$ are the autocorrelation functions of the two processes. Since their autocorrelation functions are identical, $\Delta u_d(x)$ and $\Delta\tau_d(x)$ have the same normalized power spectrum. Therefore, the distribution function of the potential dynamic stress drop $\Delta\tau_d(x)$ can be estimated by power spectral analysis of surface slip data. However, in order to make the estimation rigorous, slip data sets should satisfy the following conditions: (1) the earthquake fault is large; (2) there exist no or little surface unconsolidated sediments; and (3) the size of the data set is large, i.e., there are many measurements of slip along the earthquake fault.

Although there are many earthquake ruptures whose slips have been measured, the data

sets that satisfy the above three conditions are rare. I analyze two earthquake ruptures reasonably suitable for this purpose. One is the 1920 Haiyuan earthquake (M=8.7) in northwest China (36.7°N, 105.3°E) (Deng et al., 1986; Zhang et al., 1987). The other is the 1990 Luzon earthquake (M_s=7.8) in the Philippines (15.679°N, 121.172°E) (Nakata et al., 1990; Yoshida and Abe, 1992). The Haiyuan earthquake caused a surface breakage about 220 km long. The fault is predominantly strike-slip with a relatively small dip-slip component. Although the earthquake occurred several decades ago, the displacements are still visible in most places along the fault trace. Deng et al. (1986) and Zhang et al. (1987) did detailed measurements of the horizontal component of displacement associated with this earthquake, for a total of 168 slip measurements along the 220 km long surface fault (the maximum measured horizontal displacement is about 12 m). The surface fault associated with the Luzon, Philippines earthquake is about 120 km long, with a predominant strike-slip component. The surface ruptures are impressive, offsetting roads, foot-paths, streams, paddy dikes and so on (Nakata et al., 1990; Yoshida and Abe, 1992). The displacements were measured in detail along the fault (Nakata et al., 1990; Yoshida and Abe, 1992). There are in total 111 separate measurements and the measured maximum amount of slip is about 6 m. The data for the two faults are shown in Figures 6.8 and 6.9.

I have applied power spectral analysis (see equations (6.7), (6.8), and (6.9)) to the measured surface slips of the two earthquake faults to estimate the distribution function of $\Delta\tau_d(x)$. The analysis proceeds according to the following steps. (1) The minimum distance between any two measured slips is used as the basic unit of sampling interval, i.e., Δx=0.1 km for the Haiyuan earthquake fault and Δx=0.25 km for the Luzon earthquake fault. Measurements not taken at the interval limits are attributed to their closest sampling position. (2) Since many sampling positions are empty, the sample mean is interpolated at these positions in the calculation of the sample

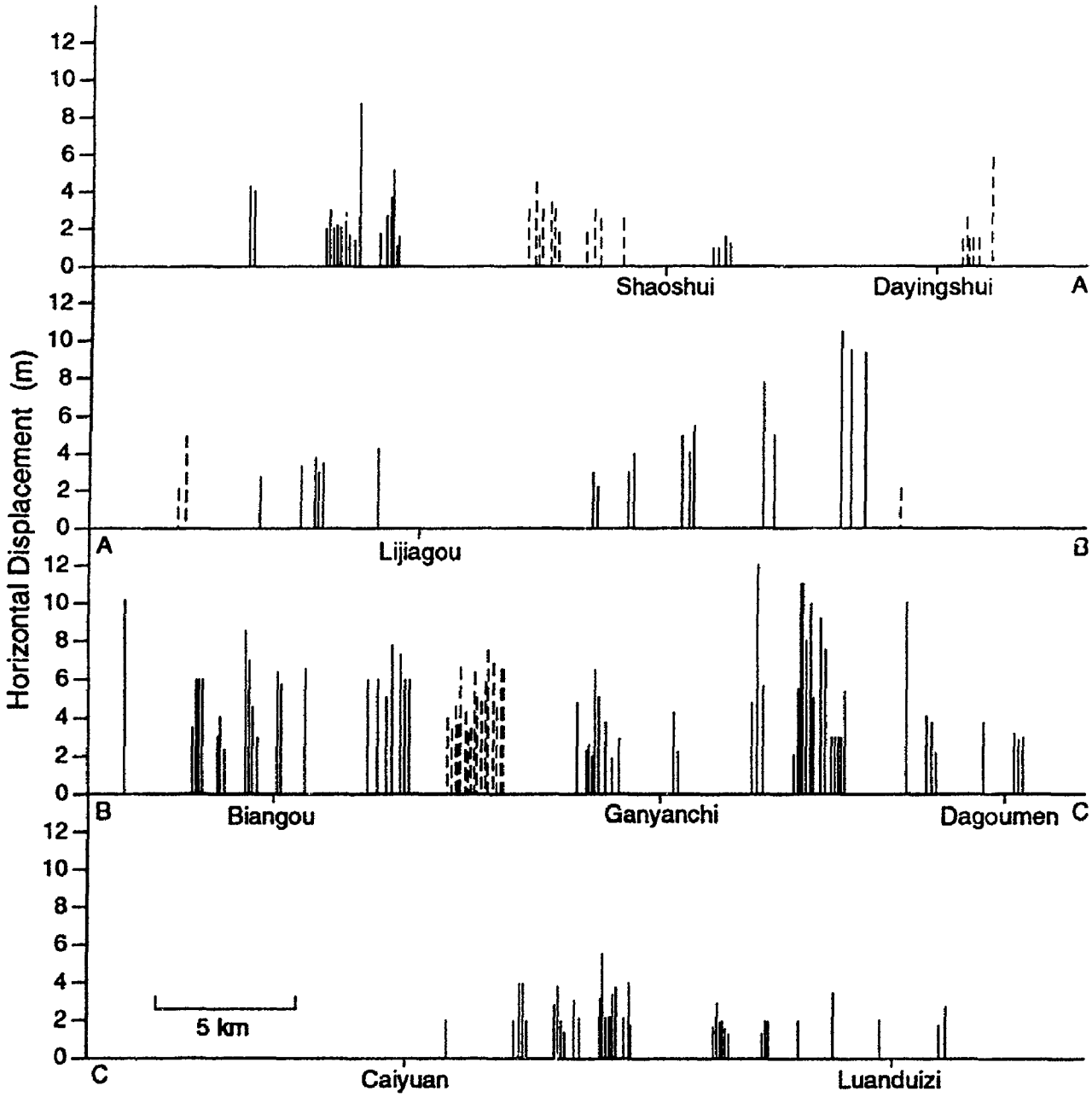

Figure 6.8. The distribution of the measured horizontal displacements associated with the Haiyuan earthquake in northwest China. From Deng et al. (1986).

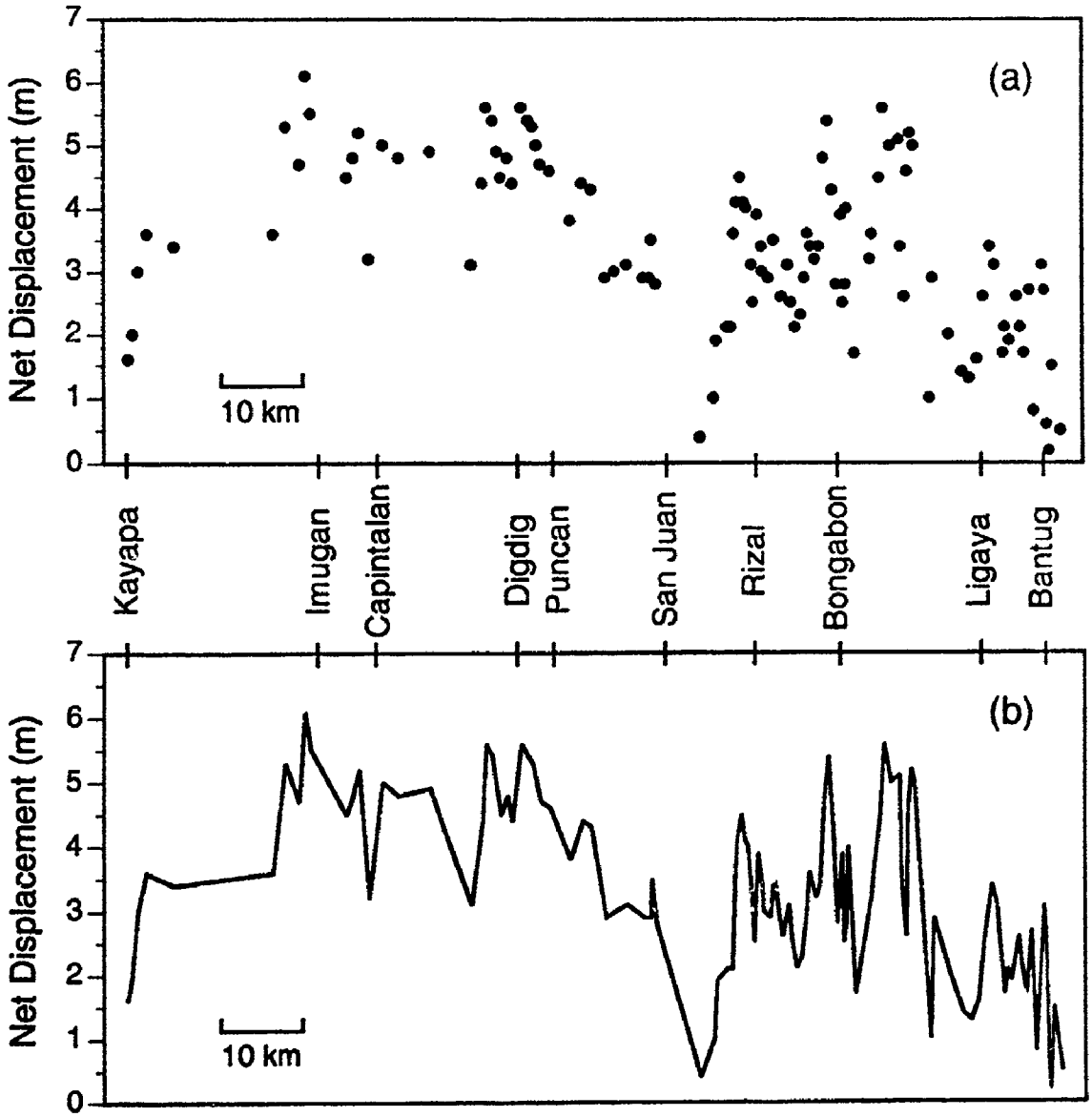

Figure 6.9. The distribution of the measured surface displacements associated with the Luzon earthquake, Philippines. (a) The measurements and their locations; (b) the graphic expression of the variation of displacements.

autocovariance function. This ensures that the interpolated values make no contribution to the sample autocovariance function (see equation (6.8)). (3) The Parzen window with window parameter M=40%N (where N is the total number of samples) is chosen, which is the same as that used in Figures 6.4 and 6.5.

The estimated power spectra of surface slips for the two earthquake faults are shown in Figure 6.10. The estimation is not robust due to the small sample size of both data sets, and the graphs of power spectral density are more fluctuating than the theoretical ones (see Figure 6.5). However, the sample power spectral density shows clearly a power law dependence on the spatial frequency f (wavelength is 1/f) for both data sets. These results confirm that the process $\Delta\tau_d(x)$ follows the fractional Brownian distribution. The estimated index, calculated using the method of least squares, is $\hat{H}=0.13$ for the Haiyuan earthquake and $\hat{H}=0.27$ for the Luzon earthquake. As mentioned before, the index H is slightly overestimated by spectral analysis when it is small (refer to Figure 6.5). Consequently, this result does not contradict the conclusion $H \rightarrow 0$ obtained from the observation of constant average stress drop and from the Gutenberg-Richter relation. It also shows that, even just before the two large earthquakes occurred, the spectra of the potential dynamic stress drop were very rough, contrary to the hypothesis (von Seggern, 1979; Huang and Turcotte, 1988) of a gradual change from roughness to smoothness of the stress-strength difference during the earthquake cycle.

CONCLUSIONS

All previous stochastic models of the earthquake process assume a priori a fractal distribution of stress and strength heterogeneities along the seismic fault. This assumption is

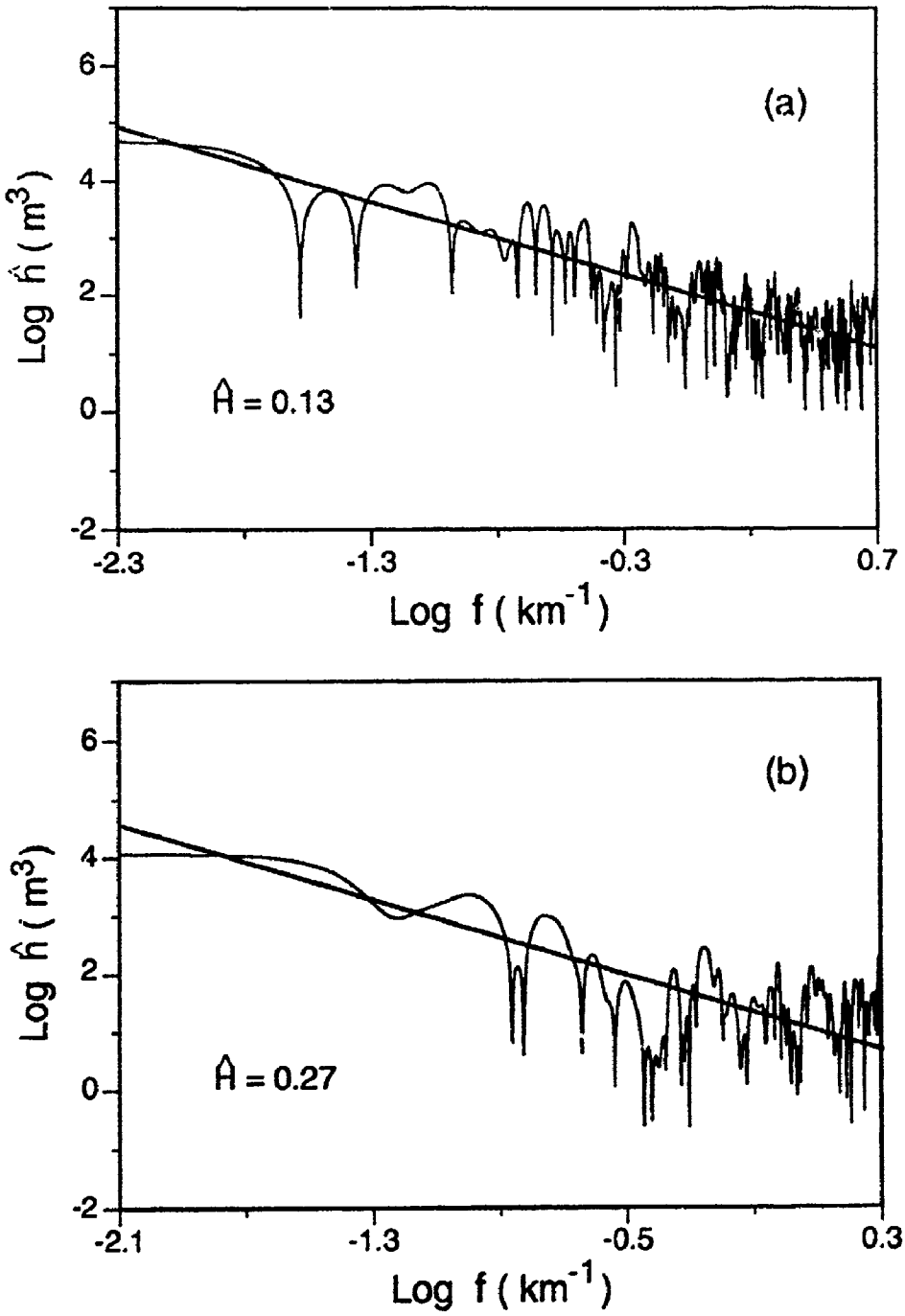

Figure 6.10. Logarithmic power spectral density of surface slips versus logarithmic spatial frequency. (a) Haiyuan earthquake fault; (b) Luzon earthquake fault. The linear least squares best fits are denoted by the straight lines. $\hat{H}$ is the estimated index.

dropped in this chapter. Assuming a stick-slip weakening model, a relation is established between heterogeneities in stress and strength and the potential dynamic stress drop (and, consequently, fault slip). The variation of the potential dynamic stress drop $\Delta\tau_d(x)$ along the strike of the fault plane is modelled as a one-dimensional stochastic process. Thus, any seismic rupture can be regarded as a segment of a realization of $\Delta\tau_d(x)$ where $\Delta\tau_d(x)>0$.

Three sets of independent observations (average stress drop, Gutenberg-Richter magnitude-frequency relation, and surface slip along a seismic fault) are used to infer the properties of $\Delta\tau_d(x)$. The constancy of the observed average stress drop places important constraints on the distribution function of $\Delta\tau_d(x)$. The property of scale invariance shows that, if the distribution of $\Delta\tau_d(x)$ is of fractional Brownian type, only the member of the Brownian family with index $H\rightarrow 0$ can give rise to a constant mean value of average stress drop. The result for the general case, i.e., without the assumption of fractal distribution, is the same as that based on the property of scale invariance. Among several possible stochastic models, it appears that only the fractional Brownian motion with $H\rightarrow 0$ (fractal dimension D=2 in the one-dimensional case) can produce an approximately constant mean value of seismic stress drop, and so fit the observations.

The distribution of zerosets in the fractional Brownian motion has the same power law dependence on frequency as the earthquake rupture size, and therefore the fractal dimension D can be related to the b-value in the magnitude-frequency law. However, the spatial and temporal variations of b-value can be interpreted as a consequence of the randomness of the zerosets, rather than as a consequence of the variation of D. Using an average value $b\approx 1.0$, the result $H\rightarrow 0$ is obtained for the case of small earthquakes, which is in agreement with that based on the constancy of average stress drop. I also infer that the b-value for large earthquakes is somewhat lower than that for small earthquakes along the same fault. This inference seems to be confirmed

by observation, and is potentially of importance for the estimation of the maximum magnitude.

Using the relation between the average stress drop and the average slip, the dynamic slip can be expressed as a linear function of the dynamic stress drop both of which are a function of position along the seismic fault. The dynamic slip follows the same distribution as the dynamic stress drop, provided that the latter is a Gaussian process. Consequently, the distribution function of the potential dynamic stress drop can be inferred using earthquake fault slip data. The slip data of two large predominantly strike-slip earthquake faults have been analyzed by power spectral analysis; the 1920 Haiyuan earthquake (M=8.7) in northwest China, and the 1990 Luzon earthquake (M_s=7.8) in the Philippines. Both faults show clearly a power law relation between the power spectrum and the spatial frequency, which confirms that the process $\Delta\tau_d(x)$ follows the fractional Brownian distribution. The estimated index, calculated using the method of least squares, is $\hat{H}$=0.13 for the Haiyuan earthquake and $\hat{H}$=0.27 for the Luzon earthquake. As the index H is slightly overestimated by spectral analysis when it is small, this result is in agreement with the conclusion $H \rightarrow 0$ obtained from the observation of constant average stress drop and from the Gutenberg-Richter relation.

Further work is required to confirm the fractional Brownian distribution (with $H \rightarrow 0$) of the earthquake process, using other lines of evidence, based for instance on records of strong ground motion. My analysis suggests that many earthquake parameters, such as the b-value and the average stress drop, are random variables. The dispersions as well as the central values of these variables are likely to pose additional constraints on the distribution function of $\Delta\tau_d(x)$. In addition, the model presented in this chapter is purely stochastic and does not consider the deterministic properties of the seismic occurrence. Models combining stochastic and deterministic analyses will improve our understanding of the earthquake process.

With respect to earthquake prediction, the model is pessimistic about the relevance of the variation of b-values to the likelihood of large earthquakes, because the b-value is a random variable and is unstable over short time periods. The model also suggests that understanding the variation of $\Delta\tau_d(x)$ along a single large fault zone is of primary importance for earthquake prediction. Any workable approach to earthquake prediction should incorporate the stochastic analysis of seismicity the distribution pattern of small earthquakes, and space-time correlations between earthquakes along a single fault.

REFERENCES

Adler, R. J., *The Geometry of Random Fields*, John Wiley and Sons, Chichester, 1981.

Aki, K., Earthquake mechanism, *Tectonophysics, 13*, 423-446, 1972.

Aki, K., Characterization of barriers on an earthquake fault, *J. Geophys. Res, 84*, 6140-6148, 1979.

Aki, K., A probabilistic synthesis of precursory phenomena, in *Earthquake Prediction, an International Review. M. Ewing Ser. 4*, edited by D. Simpson and P. Richards, Washington, D.C., American Geophysical Union, pp. 566-574, 1981.

Aki, K., Asperities, barriers and characteristics of earthquakes, *J. Geophys. Res., 89*, 5867-5872, 1984.

Aki, K., Higher-order interrelations between seismogenic structures and earthquake processes, *Tectonophysics, 211*, 1-12, 1992.

Andrews, D. J., A stochastic fault model, 1. static case, *J. Geophys. Res., 85*, 3867-3877, 1980.

Brune, J. N., and C. Y. King, Excitations of mantle Rayleigh waves of period 100 sec. as a function of magnitude, *Bull. Seismol. Soc. Am., 57*, 1355-1366, 1967.

Caputo, M., A mechanical model for the statistics of earthquakes, magnitude, moment, and fault distribution, *Bull.Seismol. Soc. Am, 67*, 849-861, 1977.

Crone, A., and M. Machette, Surface faulting accompanying the Borah Peak earthquake, central Idaho, *Geology, 12*, 664-667, 1984.

Das, S., and K. Aki, Fault plane with barrier: a versatile earthquake model, *J. Geophys. Res., 82*, 5658-5670, 1977.

Davison, F., and C. Scholz, Frequency-moment distribution of earthquakes in the Aleutian Arc:

a test of the characteristic earthquake model, *Bull. Seismol. Soc. Am.*, *75*, 1349-1362, 1985.

Deng, Q., S. Chen, F. Song, S. Zhu, Y. Wang, W. Zhang, D. Jiao, B. C. Burchfiel, P. Molnar, L. Royden, and P. Zhang, Variation in the geometry and amount of slip on the Haiyuan (Nanxihaushan) fault zone, China and the surface rupture of the 1920 Haiyuan earthquake, in *Earthquake Source Mechanics, AGU Geophys. Mono. 37, M. Ewing Ser. 6*, edited by S. Das, J. Boatwright and C. H. Scholz, Washington, D.C., American Geophysical Union, pp. 169-182, 1986.

Dieterich, J., Time-dependent friction in rocks, *J. Geophys. Res.*, *77*, 3690-3697, 1972.

Dieterich, J., Time-dependent friction and the mechanics of stick slip, *Pure Appl. Geophys.*, *116*, 790-806, 1978.

Dieterich, J., and G. Conrad, Effect of humidity on time- and velocity-dependent friction in rocks, *J. Geophys. Res.*, *89*, 4196-4202, 1984.

Dmowska, R., and L. C. Lovison, Influence of asperities along subduction interfaces on the stressing and seismicity of adjacent areas, *Tectonophysics, 211*, 23-43, 1992.

Falconer, K., *Fractal Geometry, Mathematical Foundations and Applications*, John Wiley and Sons, Chichester, 1990.

Feder, J., *Fractals*, Plenum Press, New York, 1988.

Fox, C. G., and D. E. Hayes, Quantitative methods for analyzing the roughness of the seafloor, *Reviews of Geophys.*, *23*, 1-48, 1985.

Goodchild, M. F., Lakes on fractal surfaces: a null hypothesis for lake-rich landscapes, *Mathematical Geology, 20*, 615-630, 1988.

Gutenberg, B., and C. F. Richter, *Seismicity of the Earth and Associated Phenomena*, Princeton

University Press, N.J., 1954.

Hanks, T. C., Earthquake stress drops, ambient tectonic stresses, and stresses that drive plates, *Pure Appl. Geophys.*, *115*, 441-58, 1977.

Hanks, T. C., b values and ω^{γ} seismic source models: Implications for tectonic stress variation along active crustal fault zones and the estimation of high-frequency strong ground motion, *J. Geophys. Res.*, *84*, 2235-2242, 1979.

Hanks, T. C., and D. M. Boore, Moment- magnitude relation in theory and practice, *J. Geophys. Res.*, *89*, 6226-6235, 1984.

Hirata, T., A correlation between the b value and the fractal dimension of earthquakes, *J. Geophys. Res.*, *94*, 7507-7514, 1989.

Huang, J., and D. L. Turcotte, Fractal distribution of stress and strength and variations of b-value, *Earth and Planet. Sci. Lett.*, *91*, 223-230, 1988.

Huang, J., and D. L. Turcotte, Fractal mapping of digitized images: application to the topography of Arizona and comparison with synthetic images, *J. Geophys. Res.*, *94*, 7491-7495, 1989.

Kanamori, H., and D. L. Anderson, Theoretical basis of some empirical relations in seismology, *Bull. Seismol. Soc. Am.*, *65*, 1077-1095, 1975.

Karatzas, I., *Brownian Motion and Stochastic Calculus*, Springer-Verlag, New York, 1988.

Knopoff, L., Modelling the physics of earthquakes (abstract), *Eos Trans.*, *73*, 197, the 1992 AGU spring meeting in Montreal, Canada, 1992.

Lana, X., and A. M. Correig, An example of stress tensor distribution deduced from the aftershocks of the November 23, 1980 southern Italy earthquake, *Tectonophysics*, *135*, 289-296, 1987.

Lay, T., and H. Karamori, An asperity model of great earthquake sequences, in *Earthquake*

Prediction, an International Review. M. Ewing Ser. 4, edited by D. Simpson and P. Richards, Washington, D.C., American Geophysical Union, pp. 579-592, 1981.

Lay, T., H. Kanamori, and L. Ruff, The asperity model and the nature of large subduction zone earthquakes, *Earthquake Pred. Res., 1*, 3-71, 1982.

Mandelbrot, B. B., *The Fractal Geometry of Nature*, W. H. Freeman and Company, New York, 1983.

Nakata, T., H. Tsutsumi, R. S. Punongbayan, R. E. Rimando, J. Daligdig, and A. Daag, Surface faulting associated with the Philippine earthquake of 1990 (in Japanese), *J. Geography, 99*, 515-532, 1990.

Nur, A., Nonuniform friction as physical basis for earthquake mechanics, *Pure Appl. Geophys., 116*, 964-989, 1987.

Pacheco, J. F., C. H. Scholz, and L. R. Sykes, Change in frequency-size relationship from small to large earthquakes, *Nature, 355*, 71-73, 1992.

Priestley, M. B., *Spectral Analysis and Time Series*, Academic Press, London, 1981.

Reches, Z., G. Bear, and Y. Hatzor, Constraints on the strength of the upper crust from stress inversion of fault slip data, *J. Geophys. Res., 97*, 12481-12493, 1992.

Richards, P. G., Dynamic motion near an earthquake fault: a three- dimensional solution, *Bull. Seismol. Soc. Am., 66*, 1-32, 1976.

Ruff, L. J., Asperity distribution and large earthquake occurrences in subduction zones, *Tectonophysics, 211*, 61-84, 1992.

Rydelek, P. A., and I. S. Sacks, Testing the completeness of earthquake catalogues and the hypothesis of self-similarity, *Nature, 337*, 251-253, 1989.

Scholz, C. H., Scaling law for large earthquakes: consequences for physical models, *Bull.*

Seismol. Soc. Am., *72*, 1-14, 1982.

Scholz, C. H., *The mechanics of earthquake and faulting*, Cambridge University Press, Cambridge, 1990.

Scholz, C. H., and C. Aviles, The fractal geometry of faults and faulting, in *Earthquake Source Mechanics, AGU Geophys. Mono. 37, M. Ewing Ser. 6*, edited by S. Das, J. Boatwright and C. H. Scholz, Washington, D.C., American Geophysical Union, pp. 147-155, 1986.

Schwartz, D., and K. Coppersmith, Fault behavior and characteristic earthquakes: Examples from the Wasatch and San Andreas fault zones. *J. Geophys. Res.*, *89*, 5681-5698, 1984.

Sharp, R., J. Lienkaemper, M. Bonilla, D. Burke, B. Fox, D. Herd, D. Miller, D. Morton, D. Ponti, M. Rymer, J. Tionsley, J. Yount, J. Kahle, E. Hart, and K. Sieh, Surface faulting in the central Imperial Valley, in *The Imperial Valley, California, Earthquake of October 15, 1979, U.S. Geol. Surv. Prof. Paper*, vol. 1254, pp. 119-144, 1982.

Shi, Y., and A. Bolt, The standard error of the magnitude-frequency b value, *Bull. Seismol. Soc. Am.*, *72*, 1677-1687, 1982.

Singh, S., M. Rodriguez, and L. Esteva, Statistics of small earthquakes and frequency of occurrence of large earthquakes along the Mexican subduction zone, *Bull. Seismol. Soc. Am.*, *73*, 1779-1796, 1983.

Sornette, A., P. Davy, and D. Sornette, Growth of fractal fault patterns, *Phys. Rev. Lett.*, *65*, 2266-2269, 1990.

Sornette, D., C. Vanneste, and A. Sornette, Dispersion of b-values in Gutenberg-Richter law as a consequence of a proposed fractal nature of continental faulting, *Geophys. Res. Lett.*, *18*, 897-900, 1991.

Sornette, D., and P. Davy, Fault growth model and the universal fault length distribution,

Geophys. Res. Lett., 18, 1079-1081, 1991.

Thatcher, W., and T. C. Hanks, Source parameters of southern California earthquakes, *J. Geophys. Res., 78*, 8547-8576, 1973.

Turcotte, D. L., A fractal model for crustal deformation, *Tectonophysics, 132*, 261-269, 1986.

Turcotte, D. L., *Fractals and Chaos in Geology and Geophysics*, Cambridge University Press, Cambridge, 1992.

von Seggern, D., A random stress model for seismicity statistics and earthquake prediction, *Geophys. Res. Lett., 7*, 637-640, 1980.

Wesnousky, S., C. Scholz, and K. Shimazaki, Earthquake frequency distribution and the mechanics of faulting, *J. Geophys. Res., 88*, 9331-9340, 1983.

Wong, P.-Z., and J.-S. Lin, Studying fractal geometry on submicron length scales by small-angle scattering, *Mathematical Geology, 20*, 655-665, 1988.

Wyss, M., Towards a physical understanding of the earthquake frequency distribution, *Geophys. J. R. astr. Soc., 31*, 341-359, 1973.

Wyss, M., and J. N. Brune,Seismic moment, stress and source dimensions for earthquakes in the California-Navada regions, *J. Geophys. Res., 73*, 4681-4694, 1968.

Yoshida, Y., and K. Abe, Source mechanism of the Luzon, Philippine earthquake of July 16, 1990, *Geophys. Res. Lett., 19*, 545-548, 1992.

Zhang, W., D. Jiao, P. Zhang, P. Molnar, B. C. Burchfiel, Q. Deng, Y. Wang, and F. Song, Displacement along the Haiyuan fault associated with the great 1920 Haiyuan, China, earthquake, *Bull. Seismol. Soc. Am., 77*, 117-131, 1987.

Chapter 7

Summary

This thesis covers three topics concerning the mechanics of faulting and earthquakes, in which five problems have been solved. The main results are summarized as follows:

1. Faulting in Anisotropic Rocks: the Two-Dimensional Case

(1) Sibson's formulations for the critical stress difference for sliding on most favourably oriented cohesionless thrust, normal, and strike-slip faults have been extended to faults with finite cohesion. Explicit expressions for the critical stress difference have been derived for faulting in homogeneous, isotropic rocks and along most favourably oriented preexisting anisotropies with finite cohesion in terms of material parameters, pore fluid pressure, and depth.

(2) Expressions for the critical stress difference for faulting along an arbitrarily oriented strength anisotropy in the three different faulting regimes have been derived as a function of material parameters, pore fluid pressure, depth, and orientation of the strength anisotropy.

(3) The ranges of orientations for which sliding occurs along a preexisting plane of weakness rather than along a fresh plane have been derived for different faulting regimes as a function of material parameters, pore fluid pressure, and depth.

2. Faulting in Anisotropic Rocks: the Three-Dimensional Case

(1) The critical stress difference for faulting along arbitrarily oriented preexisting strength anisotropies under an arbitrarily oriented stress field has been expressed as a function of material parameters, pore fluid pressure, depth, orientation of the strength anisotropies, and orientation of

the stress field.

(2) An expression has been given for calculating the limiting range of orientations of strength anisotropies (within which faulting occurs along preexisting strength anisotropies rather than along fresh planes in homogeneous, isotropic rocks) as a function of material parameters, pore fluid pressure, depth, and orientations of the stress field.

(3) Expressions have been derived for calculating the maximum shear stress, the normal stress, and the slip direction on the fault plane. Based on the slip direction, a kinematic classification of faulting has been given.

(4) Triangular diagrams have been used to graphically present the results, where expected type of faulting is given as a function of stress orientations (for new faults), or as a function of orientations of strength anisotropies (for reactivation of preexisting faults).

3. Inversion for the Principal Stress Directions and the Stress Ratio

(1) The probability distribution of the direction of predicted maximum shear stress on the fault plane has been evaluated and has been found to follow approximately the von Mises distribution. Consequently, the misfit angle between observed slip and predicted maximum shear stress direction can also be modelled approximately by the von Mises distribution with mean zero and concentration parameter depending on the variance of measurement errors both in slip directions and in fault plane orientations, and on principal stress directions and stress ratio. Subject to certain conditions, both the predicted maximum shear stress direction and the misfit angle can be modelled approximately by the normal distribution.

(2) Two new inversion criteria, named C_5 and C_6, have been proposed to determine the principal stress directions and the stress ratio from inversion of a population of faults of measured

orientations and slip directions. Both criteria take into account simultaneously uncertainties in fault plane orientation and slip direction, and are based on numerical maximization of the maximum likelihood function of the misfit angles on all faults of a given data set.

(3) A procedure has been proposed to test whether the data set is compatible with a uniform stress field, and a new method has been presented to evaluate the precision of the inversion results (i.e., the confidence intervals) for the principal stress directions and the stress ratio.

(4) Inversion, hypothesis testing, and estimation of the confidence intervals have been performed on three data sets taken from the available literature, and the results have been compared with those obtained from previous methods.

4. Inversion of the Friction Coefficient of Faults and the Normalized Magnitudes of Principal Stresses

(1) It has been shown that, using the Coulomb-Navier failure criterion as an mechanical constraint, it is possible to determine the average coefficient of friction of faults, and consequently to obtain the fifth parameter of the stress field from inversion of a population of faults of measured orientations and slip directions. The pore fluid pressure, which determines the sixth parameter of the stress field, cannot be determined by inversion of fault-slip data and must be determined by other independent methods, such as in situ measurements.

(2) Reches et al.'s inversion method for the determination of the average coefficient of friction has been analyzed, and has been found to be applicable only to conjugate faults developed in homogeneous, isotropic rock. The method is unreliable when applied to reactivation of preexisting faults in anisotropic rocks.

(3) According to the Coulomb-Navier failure criterion, the normalized critical stress difference is the same for each fault if the stress field is uniform. On the basis of the normalized critical stress difference, a new method has been proposed to determine the average coefficient of friction, the average normalized critical stress difference, and the average normalized magnitudes of the principal stresses from inversion of fault-slip data.

(4) The new method has been applied to four sets of data taken from field fault measurements available in the literature. Of the four examples, three yield an average coefficient of friction ranging from 0.64 to 0.88 (one example gives rise to a relatively small average friction coefficient). These inversion results are in agreement with the average value (μ_0=0.75) of friction coefficient obtained from laboratory experiments.

5. Modelling of Earthquake Rupturing as a Stochastic Process

(1) All previous stochastic models of the earthquake process assume a priori a fractal distribution of stress and strength heterogeneities along the seismic fault. This assumption is dropped in this thesis. Assuming a stick-slip weakening model, a relation has been established between heterogeneities in stress and strength and the potential dynamic stress drop. The variation of the potential dynamic stress drop along the strike of the fault has been modelled as a one-dimensional stochastic process. Three independent observations (average stress drop, Gutenberg-Richter magnitude-frequency relation, and surface slip along a seismic fault) have been used to infer the distribution properties of the potential dynamic stress drop.

(2) Based on the constancy of average stress drop, a analytical solution has been derived for the distribution function of the potential dynamic stress drop. The result shows that among many known models, only the fractional Brownian process with index $H \rightarrow 0$ can give rise to the

observed constant average stress drop.

(3) The distribution of zerosets in the fractional Brownian process has the same power law dependence on frequency as the earthquake rupture size, and therefore the fractal dimension D can be related to the b-value in the magnitude-frequency law. Using an average $b \approx 1.0$, the result $H \rightarrow 0$ has been obtained for the case of small earthquakes. The b-value for large earthquake along a single fault or fault zone has been inferred to be smaller than that for small earthquakes along the same fault zone.

(4) The surface slip data of two large predominantly strike-slip earthquake faults (the 1920 Haiyuan earthquake in northwest China, and the 1990 Luzon earthquake in the Philippines) have been analyzed by power spectral analysis. Both faults show clearly a power law relation between the power spectrum and the spatial frequency, which confirms that the potential dynamic stress drop follows the fractional Brownian distribution. The estimated index is 0.13 for the Haiyuan earthquake and 0.27 for the Luzon earthquake, which do not contradict the result $H \rightarrow 0$ obtained from the observation of constant average stress drop and from the Gutenberg-Richter relation.

Appendices

FORTRAN Programs for Stress Inversion

INTRODUCTION

In order to simplify the use of the new methods proposed in this thesis to determine the tectonic stress field from inversion of fault-slip data, two FORTRAN programs are listed in appendices 1, 2. Appendix 1 is a FORTRAN program for the determination of the three principal stress directions and the stress ratio. Because criterion C_5 and criterion C_o in Chapter 4 give rise to nearly the same inversion results, and criterion C_6 saves much computing time, the program provided here is written for criterion C_6. Appendix 2 lists a FORTRAN program for determination of the average friction coefficient, average normalized critical stress difference, and normalized magnitudes of the three principal stresses, based on criterion MC_3 (see Chapter 5). Both these programs have been tested on a SUN STATION computer. Although most notations for variables defined in the programs are consistent with the notations in the context of Chapter 4 and Chapter 5, some are different. The reader is advised to follow the definitions of variables within the programs.

APPENDIX 1

```
      PROGRAM STRESS INVERSION
C
C
C     THIS PROGRAM IS WRITTEN FOR DETERMINATION OF THE
C     PRINCIPAL STRESS DIRECTIONS AND STRESS RATIO, BASED ON
C     CRITERION C6 (SEE CHAPTER 4). IT COMPRISES A MAIN PROGRAM
C     CALLED "STRESS INVERSION" AND TWO SUBROUTINES CALLED
C     "VARIANCE" AND "MISFIT" RESPECTIVELY. THE SUBROUTINE
C     "VARIANCE" IS TO CALCULATE THE VARIANCE OF RANDOM
C     VARIABLE MISFIT ANGLE FOR EACH FAULT. THE SUBROUTINE
C     "MISFIT" IS TO CALCULATE THE VALUE OF MISFIT ANGLE
C     FOR EACH FAULT.
C
C
C     THE THREE PRINCIPAL STRESS DIRECTIONS ARE DESCRIBED BY
C     THE EULER ANGLES: ALPHA, BETA, AND GAMMA, AND THE STRESS
C     RATIO IS DENOTED BY DELTA (SEE THE CONTEXT OF CHAPTER 4).
C
C
C     MAXIMUM --- THE MAXIMUM VALUE OF CRITERION C6 WITHIN THE
C           RANGE OF BETA AND GAMMA SELECTED (OR SEARCHED).
C     MBETA --- THE EULER ANGLE BETA THAT YIELDS THE "MAXIMUM"
C           VALUE OF C6 WITHIN THE RANGE SELECTED.
C     MGAMMA --- THE EULER ANGLE GAMMA THAT YIELDS THE
C           "MAXIMUM" VALUE OF C6 WITHIN THE RANGE SELECTED.
C     NUM --- TOTAL NUMBER OF FAULTS (IN INTEGER FORM) USED IN
C           STRESS INVERSION.
C     ANUM --- TOTAL NUMBER OF FAULTS (IN DECIMAL FORM) USED IN
C           STRESS INVERSION.
C     I1, I2, AND I3 --- THE RANGE OF STRESS RATIO "DELTA"
C           SELECTED, AND THE INCREMENT OF EACH ITERATIVE STEP.
C     J1, J2, AND J3 --- THE RANGE OF THE EULER ANGLE ALPHA
C           SELECTED, AND THE INCREMENT OF EACH ITERATIVE STEP.
C     K1, K2, AND K3 --- THE RANGE OF THE EULER ANGLE BETA
C           SELECTED, AND THE INCREMENT OF EACH ITERATIVE STEP.
C     L1, L2, AND L3 --- THE RANGE OF THE EULER ANGLE GAMMA
C           SELECTED, AND THE INCREMENT OF EACH ITERATIVE STEP.
C
C
      REAL MAXIMUM,MBETA,MGAMMA
      PARAMETER(PI=3.14159265359,NUM=50,ANUM=50.0)
```

```
      PARAMETER(I1=27,I2=37,I3=1,J1=3,J2=13,J3=1)
      PARAMETER(K1=153,K2=163,K3=1,L1=59,L2=69,L3=1)
C
      DIMENSION PLANE1(NUM)
      DIMENSION PLANE2(NUM)
      DIMENSION PITCH1(NUM)
      DIMENSION PITCH2(NUM)
      DIMENSION W1(3)
C
      COMMON U1,U2,U3,V1,V2,V3,DELTA
C
      SI(X)=SIN(X*PI/180.0)
      CO(X)=COS(X*PI/180.0)
      DIFFER(X,Y)=(X-Y)/0.4
C
C
C     THE OUTPUT DATA FILE IS NAMED "C6.DAT". THE INPUT DATA
C     FILES ARE NAMED "PLANE1.XXX", "PLANE2.XXX", "PITCH1.XXX",
C     AND "PITCH2.XXX". THE FILES "PLANE1.XXX" AND "PLANE2.XXX"
C     CONTAIN FAULT PLANE ORIENTATION DATA. THE FILES
C     "PITHCH1.XXX" AND "PITCH2.XXX" CONTAIN SLIP DIRECTION
C     DATA. SEE NEXT COMMENTS FOR DETAILED DESCRIPTION OF THE
C     INPUT DATA.
C
C
      OPEN(10,FILE='C6.DAT')
      OPEN(11,FILE='PLANE1.XXX')
      OPEN(12,FILE='PLANE2.XXX')
      OPEN(13,FILE='PITCH1.XXX')
      OPEN(14,FILE='PITCH2.XXX')
C
      READ(11,*) PLANE1
      READ(12,*) PLANE2
      READ(13,*) PITCH1
      READ(14,*) PITCH2
C
      DO 1000 I=I1,I2,I3
      DELTA=0.01*I
C
      WRITE(10,1100) DELTA
C
      DO 900 J=J1,J2,J3
      ALPHA=J
C
```

```
      WRITE(10,1200) ALPHA
C
      MAXIMUM=-50000.0
C
      DO 800 K=K1,K2,K3
      BETA=K
C
      DO 700 L=L1,L2,L3
      GAMMA=L
C
C
C     U1, U2, U3, V1, V2, V3 --- THE ELEMENTS OF TRANSFORMATION
C           MATRIX (SEE THE CONTEXT OF CHAPTER 4).
C
C
      U1=CO(ALPHA)
      U2=SI(ALPHA)*SI(GAMMA)
      U3=SI(ALPHA)*CO(GAMMA)
      V1=SI(ALPHA)*SI(BETA)
      V2=CO(BETA)*CO(GAMMA)-CO(ALPHA)*SI(BETA)*SI(GAMMA)
      V3=-CO(BETA)*SI(GAMMA)-CO(ALPHA)*SI(BETA)*CO(GAMMA)
C
      SUM1=0.0
      SUM2=0.0
C
C
C     SUPPOSE X1, X2, AND X3 BE UNIT VECTORS COINCIDENT WITH
C     THE VERTICAL, THE EAST, AND THE NORTH DIRECTION OF THE
C     GEOGRAPHICAL COORDINATE SYSTEM, RESPECTIVELY, AND P BE A
C     UNIT VECTOR COINCIDENT WITH THE SLIP DIRECTION (SEE
C     CHAPTER 4). THE INPUT DATA ARE DEFINED AS FOLLOWS:
C
C     THETA --- THE ANGLE BETWEEN THE NORMAL TO THE FAULT PLANE
C           AND THE UNIT VECTOR X1 (0°≤ THETA ≤90°). THETA IS
C           IDENTICAL TO THE DIP ANGLE OF FAULT PLANE.
C     PHI --- THE AZIMUTH OF THE NORMAL TO THE FAULT PLANE
C           (0°≤ PHI ≤360°). PHI IS IDENTICAL TO THE AZIMUTH OF
C           THE DIP OF FAULT PLANE.
C     PLUNGE --- THE ANGLE BETWEEN UNIT SLIP VECTOR P AND UNIT
C           VECTOR X1 (0°≤ PLUNGE ≤180°). IF FAULTING IS
C           NORMAL OR NORMAL STRIKE-SLIP, 0°≤ PLUNGE ≤90°. IF
C           FAULTING IS THRUST OR THRUST STRIKE-SLIP,
C           90°≤ PLUNGE ≤180°.
C     TREND --- THE AZIMUTH OF THE UNIT SLIP VECTOR P
```

```
C             (0°≤ TREND ≤360°).
C
C       ALL THE ANGLES THETA, PHI, PLUNGE, AND TREND ARE IN
C       DEGREES. FOR EACH FAULT, THETA IS CONTAINED IN INPUT FILE
C       "PLANE1.XXX", PHI IS IN FILE "PLANE2.XXX", PLUNGE IS IN
C       FILE "PITCH1.XXX", AND TREND IS IN INPUT FILE
C       "PITCH.XXX", RESPECTIVELY.
C
C
        DO 600 M=1,NUM
        THETA=PLANE1(M)
        PHI=PLANE2(M)
        PLUNGE=PITCH1(M)
        TREND=PITCH2(M)
C
C
C       FROM LINE 10 TO LINE 20, A NUMERICAL TECHNIQUE IS USED TO
C       CALCULATE THE VARIANCE OF RANDOM VARIABLE MISFIT ANGLE
C       FOR EACH FAULT.
C
C
10      DO 500 N=-1,1
        ATHETA=THETA+0.2*N
        RR=0.0
        CALL VARIANCE(ATHETA,PHI,RR,D)
        W1(N+2)=D
500     CONTINUE
C
        ATHETA=THETA
        RR=-0.2
        CALL VARIANCE(ATHETA,PHI,RR,D)
        W2=D
C
        RR=0.2
        CALL VARIANCE(ATHETA,PHI,RR,D)
        W3=D
C
        IF(W1(2).GE.2.0.AND.W1(2).LE.178.0) THEN
        FX1=DIFFER(W1(3),W1(1))
        FY1=DIFFER(W2,W3)
C
        ELSE
C
        FA1=2.0*DIFFER(W1(2),W1(1))
```

```
      FA2=2.0*DIFFER(W1(3),W1(2))
      FA3=ABS(FA1)-ABS(FA2)
      IF(FA3.GE.0.0) THEN
      FX1=FA1
      ELSE
      FX1=FA2
      END IF
C
      FB1=2.0*DIFFER(W1(2),W3)
      FB2=2.0*DIFFER(W2,W1(2))
      FB3=ABS(FB1)-ABS(FB2)
      IF(FB3.GE.0.0) THEN
      FY1=FB1
      ELSE
      FY1=FB2
      END IF
C
      END IF
C
C
C     VAR --- THE VARIANCE OF RANDOM VARIABLE MISFIT ANGLE.
C
C
20    VAR=1.0+FX1*FX1+FY1*FY1
C
C
C     DD --- THE VALUE OF MISFIT ANGLE.
C
C
      CALL MISFIT(THETA,PHI,PLUNGE,TREND,DD)
C
      SUM1=SUM1+DD*DD/VAR
      SUM2=SUM2+LOG(VAR)
C
600   CONTINUE
C
C
C     SUM --- THE VALUE OF CRITERION C6.
C     HERE, IN CALCULATION OF THE VALUE OF CRITERION C6, A
C     FACTOR 2π WHICH APPEARS IN THE NORMAL DISTRIBUTION IS
C     USED. THIS CONSTANT FACTOR IS OMITTED IN THE ORIGINAL
C     CRITERION C6 OF CHAPTER 4, BECAUSE IT DOES NOT AFFECT
C     THE INVERSION RESULTS.
C
```

```
C
      SUM=-ANUM/2.0*(1.0+LOG(2.0*PI)+LOG(SUM1/ANUM))-SUM2/2.0
C
      IF(SUM.GT.MAXIMUM) THEN
      MAXIMUM=SUM
      MBETA=BETA
      MGAMMA=GAMMA
      END IF
C
700   CONTINUE
C
800   CONTINUE
C
      WRITE(10,1300) MBETA,MGAMMA,MAXIMUM
C
900   CONTINUE
C
1000  CONTINUE
C
1100  FORMAT(3X,'DELTA=',F4.2)
1200  FORMAT(3X,'ALPHA=',F5.1)
1300  FORMAT(2X,'MBETA=',F5.1,2X,'MGAMMA=',F5.1,2X,'MAXIMUM=',F12.6)
C
      STOP
      END
C
C
C
C
      SUBROUTINE VARIANCE(ATHETA,PHI,RR,D)
C
C
C     N1, N2 --- THE DIRECTIONAL COSINES OF THE UNIT
C            NORMAL TO THE FAULT PLANE IN THE STRESS
C            COORDINATE SYSTEM.
C
C
      REAL N1,N2
      PARAMETER(PI=3.14159265359)
      COMMON U1,U2,U3,V1,V2,V3,DELTA
C
      SI(X)=SIN(X*PI/180.0)
      CO(X)=COS(X*PI/180.0)
      TRANS1(X1,X2,X3)=X1*U1+X2*U2+X3*U3
```

```
      TRANS2(X1,X2,X3)=X1*V1+X2*V2+X3*V3
C
      F1=CO(ATHETA)*CO(ATHETA)
      F2=SI(ATHETA)*SI(ATHETA)
C
      IF(F2.GE.0.00001) THEN
      F3=(CO(RR)-F1)/F2
      IF(F3.GE.1.0) F3=1.0
      IF(F3.LE.-1.0) F3=-1.0
      F4=ACOS(F3)*180.0/PI
      APHI=PHI-SIGN(F4,RR)
C
      ELSE
      F5=90.0
      APHI=PHI-SIGN(F5,RR)
      END IF
C
      A1=CO(ATHETA)
      A2=SI(ATHETA)*SI(APHI)
      A3=SI(ATHETA)*CO(APHI)
      B1=0.0
      B2=-CO(APHI)
      B3=SI(APHI)
C
      N1=TRANS1(A1,A2,A3)
      N2=TRANS2(A1,A2,A3)
      S1=TRANS1(B1,B2,B3)
      S2=TRANS2(B1,B2,B3)
C
      FACT1=N1*N1
      FACT2=N2*N2
      FACT3=FACT1+DELTA*DELTA*FACT2-(FACT1+DELTA*FACT2)**2
      IF(FACT3.LE.0.0) FACT3=0.0
      CC=SQRT(FACT3)
C
      IF(CC.GE.0.001) THEN
      DD=(-N1*S1-DELTA*N2*S2)/CC
      IF(DD.GE.1.0) DD=1.0
      IF(DD.LE.-1.0) DD=-1.0
      D=ACOS(DD)*180.0/PI
      ELSE
      D=0.0
      END IF
C
```

```
      END
C
C
C
C
      SUBROUTINE MISFIT(THETA,PHI,PLUNGE,TREND,D)
C
C
      REAL N1,N2
      PARAMETER(PI=3.14159265359)
      COMMON U1,U2,U3,V1,V2,V3,DELTA
C
      SI(X)=SIN(X*PI/180.0)
      CO(X)=COS(X*PI/180.0)
      TRANS1(X1,X2,X3)=X1*U1+X2*U2+X3*U3
      TRANS2(X1,X2,X3)=X1*V1+X2*V2+X3*V3
C
C
C     A1, A2, A3 --- THE COORDINATES OF THE UNIT NORMAL TO THE
C           FAULT PLANE IN THE GEOGRAPHICAL COORDINATES SYSTEM.
C     B1, B2, B3 --- THE COORDINATES OF THE UNIT SLIP IN THE
C           GEOGRAPHICAL COORDINATES SYSTEM.
C
C
      A1=CO(THETA)
      A2=SI(THETA)*SI(PHI)
      A3=SI(THETA)*CO(PHI)
      B1=CO(PLUNGE)
      B2=SI(PLUNGE)*SI(TREND)
      B3=SI(PLUNGE)*CO(TREND)
C
C
C     N1, N2 --- THE COORDINATES OF THE UNIT NORMAL TO THE
C           FAULT PLANE IN THE STRESS COORDINATE SYSTEM.
C     E1, E2 --- THE COORDINATES OF THE UNIT SLIP IN THE
C           STRESS COORDINATES SYSTEM.
C
C
      N1=TRANS1(A1,A2,A3)
      N2=TRANS2(A1,A2,A3)
      E1=TRANS1(B1,B2,B3)
      E2=TRANS2(B1,B2,B3)
C
      FACT1=N1*N1
```

```
      FACT2=N2*N2
      FACT3=FACT1+DELTA*DELTA*FACT2-(FACT1+DELTA*FACT2)**2
      IF(FACT3.LE.0.0) FACT3=0.0
      CC=SQRT(FACT3)
C
      IF(CC.GE.0.001) THEN
      DD=(-N1*E1-DELTA*N2*E2)/CC
      IF(DD.GE.1.0) DD=1.0
      IF(DD.LE.-1.0) DD=-1.0
      D=ACOS(DD)*180.0/PI
      ELSE
      D=180.0
      END IF
C
      END
```

APPENDIX 2

```
      PROGRAM FRICTION INVERSION
C
C
C     THIS PROGRAM IS USED TO DETERMINE THE AVERAGE COEFFICIENT
C     OF FRICTION OF PREEXISTING FAULTS FROM INVERSION OF A
C     POPULATION OF FAULTS OF MEASURED ORIENTATIONS AND SLIP
C     DIRECTIONS.
C
C     MU0 ---  THE SELECTED AVERAGE COEFFICIENT OF FRICTION.
C     NUM --- THE TOTAL NUMBER (IN INTEGER FORM) OF FAULTS USED
C           IN FRICTION INVERSION.
C     ANUM --- THE TOTAL NUMBER (IN DECIMAL FORM) OF FAULTS
C           USED IN FRICTION INVERSION.
C     ALPHA, BETA, GAMMA --- THE EULER ANGLES INDICATING THE
C           PRINCIPAL STRESS DIRECTIONS OBTAINED FROM STRESS
C           INVERSION (SEE CHAPTER 4 AND APPENDIX 1).
C     DELTA --- THE STRESS RATIO OBTAINED FROM STRESS INVERSION
C           (SEE CHAPTER 4 AND APPENDIX 1).
C     I1, I2, AND I3 --- THE RANGE OF AVERAGE FRICTION
C           COEFFICIENT SELECTED, AND THE INCREMENT OF EACH
C           ITERATIVE STEP.
C
C
      REAL MU0,N1X,N2X,N3X,N1Y,N2Y
      PARAMETER(PI=3.14159265359,NUM=24,ANUM=24.0)
      PARAMETER(ALPHA=88.0,BETA=0.0,GAMMA=209.0,DELTA=0.06)
      PARAMETER(I1=1,I2=150,I3=1)
C
      DIMENSION PLANE1(NUM)
      DIMENSION PLANE2(NUM)
      DIMENSION CSD(NUM)
C
      SI(X)=SIN(X*PI/180.0)
      CO(X)=COS(X*PI/180.0)
C
C
C     THE OUTPUT FILE IS NAMED "MC3.DAT". THE INPUT FILES ARE
C     NAMED "PLANE1.XXX" AND "PLANE2.XXX", WHICH CONTAIN THE
C     FAULT PLANE ORIENTATION DATA. SEE NEXT COMMENTS FOR
C     DETAILED DESCRIPTION OF THE INPUT DATA.
C
```

```
C
      OPEN(10,FILE='MC3.DAT')
      OPEN(11,FILE='PLANE1.XXX')
      OPEN(12,FILE='PLANE2.XXX')
C
      READ(11,*) PLANE1
      READ(12,*) PLANE2
C
C
C     U1, U2, U3, V1, V2, V3 --- THE ELEMENTS OF TRANSFORMATION
C           MATRIX (SEE THE CONTEXT OF CHAPTER 4).
C
C
      U1=CO(ALPHA)
      U2=SI(ALPHA)*SI(GAMMA)
      U3=SI(ALPHA)*CO(GAMMA)
      V1=SI(ALPHA)*SI(BETA)
      V2=CO(BETA)*CO(GAMMA)-CO(ALPHA)*SI(BETA)*SI(GAMMA)
      V3=-CO(BETA)*SI(GAMMA)-CO(ALPHA)*SI(BETA)*CO(GAMMA)
C
      DO 300 I=I1,I2,I3
      MU0=0.01*I
C
      SUM1=0.0
      DO 100 J=1,NUM
C
C
C     THETA --- THE ANGLE BETWEEN THE NORMAL TO THE FAULT PLANE
C           AND THE VERTICAL DIRECTION (0°≤ THETA ≤90°). THETA
C           IS IDENTICAL TO THE DIP ANGLE OF FAULT PLANE.
C     PHI --- THE AZIMUTH OF THE NORMAL TO THE FAULT PLANE
C           (0°≤ PHI ≤360°). PHI IS IDENTICAL TO THE AZIMUTH OF
C           THE DIP OF FAULT PLANE.
C
C     BOTH THETA AND PHI ARE IN DEGREES. FOR EACH FAULT, THETA
C           IS CONTAINED IN THE INPUT FILE "PLANE1.XXX" AND PHI
C           IS IN THE FILE "PLANE2.XXX".
C
C
      THETA=PLANE1(J)
      PHI=PLANE2(J)
C
C
C     N1X, N2X, N3X --- THE COORDINATES OF THE UNIT NORMAL TO
```

```
C             THE FAULT PLANE IN THE GEOGRAPHICAL COORDINATE
C             SYSTEM.
C       N1Y, N2Y --- THE COORDINATES OF THE UNIT NORMAL TO THE
C             FAULT PLANE IN THE STRESS COORDINATE SYSTEM.
C
        N1X=CO(THETA)
        N2X=SI(THETA)*SI(PHI)
        N3X=SI(THETA)*CO(PHI)
C
        N1Y=U1*N1X+U2*N2X+U3*N3X
        N2Y=V1*N1X+V2*N2X+V3*N3X
C
        A=N1Y*N1Y+DELTA*DELTA*N2Y*N2Y
        B=N1Y*N1Y+DELTA*N2Y*N2Y
        C=U1*U1+DELTA*V1*V1
        D=A-B*B
        IF(D.LE.0.0) D=0.0
        E=SQRT(D)+MU0*(C-B)
        IF(E.LE.0.001) E=0.001
C
C
C       CSD(J) --- THE NORMALIZED CRITICAL STRESS DIFFERENCE FOR
C             EACH FAULT.
C
C
        CSD(J)=MU0/E
C
C
C       SUM1 --- THE AVERAGE NORMALIZED CRITICAL STRESS
C             DIFFERENCE.
C
C
        SUM1=SUM1+CSD(J)/ANUM
C
100     CONTINUE
C
        SUM=0.0
        DO 200 K=1,NUM
C
C
C       SUM --- THE MISFIT RATIO (SEE CHAPTER 5 FOR DETAILS).
C
C
        SUM=SUM+(CSD(K)/SUM1-1.0)**2
```

```
C
200     CONTINUE
C
        WRITE(10,400) MU0,SUM,SUM1
C
300     CONTINUE
C
        WRITE(10,500) U1,U2,U3,V1,V2,V3
400     FORMAT(3X,'MU0=',F5.2,3X,'SUM=',G16.8,2X,'SUM1=',G16.8)
500     FORMAT(2X,'U1=',F6.4,2X,'U2=',F6.4,2X,'U3=',F6.4,
     *          2X,'V1=',F6.4,2X,'V2=',F6.4,2X,'V3=',F6.4)
C
        STOP
        END
```

END

19-07-94

FIN